

Conception and Experimental Investigation of Thermal Switches

by

John Novak

Submitted to the Departments of Mechanical Engineering and Nuclear Engineering
in Partial Fulfillment of the Requirements for the Degrees of

Master of Science
in Mechanical Engineering

and

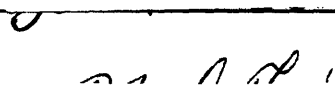
Master of Science
in Nuclear Engineering

at the
Massachusetts Institute of Technology

May 1995

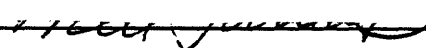
© MIT 1995

Signature of Author



Department of Nuclear Engineering
May 12, 1995

Certified by



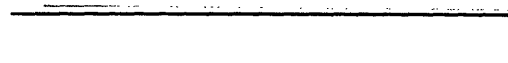
Neil Todreas
Department of Nuclear Engineering
Thesis Advisor

Certified by




Michael Driscoll
Department of Nuclear Engineering
Thesis Advisor

Certified by



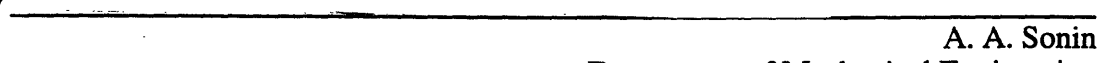
Borivoje Mikic
Department of Mechanical Engineering
Thesis Advisor

Accepted by



A. F. Henry
Department of Nuclear Engineering
Chairman, Department Committee on Graduate Students

Accepted by



A. A. Sonin
Department of Mechanical Engineering
Chairman, Department Committee on Graduate Students

MASSACHUSETTS INSTITUTE
OF TECHNOLOGY

JUN 07 1995

Eng.

Conception and Experimental Investigation of Thermal Switches

by

John Novak

Submitted to the Departments of Mechanical Engineering and Nuclear Engineering in May 1995 in partial fulfillment of the requirements for the Degrees of Master of Science in Mechanical Engineering and Master of Science in Nuclear Engineering

Thesis Abstract

A thermal switch is a device that can thermally couple and decouple a heat source and a heat sink. The research described in this thesis involved conceiving new thermal switch concepts, and experimentally investigating and developing some of them. Specifically, eighteen new thermal switch concepts were conceived, and the four most technologically feasible and economically affordable concepts were experimentally investigated and developed. The four thermal switch concepts chosen were:

1. Dissociation thermal switch
2. Particle Bed thermal switch
3. Wick thermal switch
4. Water (Evaporation-Condensation) thermal switch

These four thermal switch concepts were developed and tested via three different experimental setups. The first two experimental setups built were used to develop a dissociation and recombination algorithm for the chemicals that might be used for the dissociation and particle bed thermal switch. (Dissociation is the decomposition of a chemical into its constituents via thermal energy addition, and recombination is the recombining of these constituents to form the original chemical.) The third experimental setup built was used to investigate the heat transferring capability of the particle bed thermal switch, the wick thermal switch, and the water thermal switch for various on-mode (i.e., thermal-couple mode) setups and off-mode (i.e., thermal-decouple mode) setups. A successful dissociation and recombination algorithm was developed, and successful on-mode setups and off-mode setups were discovered for the wick thermal switch and the water thermal switch. The particle bed thermal switch was also able to thermally couple and decouple a heat source and a heat sink, but not as effectively as the wick thermal switch and the water thermal switch.

Thesis Supervisor: Dr. Neil Todreas

Title: Professor of Nuclear Engineering

Acknowledgments

The author wishes to express his sincere gratitude to his sponsor and faculty advisers. The sponsor, EPRI, provided solid, unwavering, financial funding while at the same time allowing the author and the faculty advisers research freedom to meet the objectives of the project. The two key faculty advisers, Professor Neil Todreas and Professor Michael Driscoll, provided a wealth of ideas and information and very insightful comments and criticisms. Lastly, the author wishes to thank Professor Borivoje Mikic for all the heat transfer theory he imparted to the author through his courses which enabled the successful design, performance, and completion of the research project.

Conception and Experimental Investigation of Thermal Switches

Abstract	2
Acknowledgement	3
Table of Contents	4
List of Tables	6
List of Figures	7
Chapter 1: Introduction	10
Chapter 2: Contemporary Passive Thermal Switches	17
2.1 Introduction.....	17
2.2 High-Temperature Gas-Gap Thermal Switch	17
2.3 Electrolytic Thermal Switch.....	19
2.4 Material-Type Thermal Switches	21
2.5 Axial Heat Pipes.....	25
2.6 Radial Heat Pipe.....	44
2.7 Other Types of Heat Pipes	44
2.8 Thermal Syphon.....	46
2.9 Bistable Passive Thermal Switch	46
2.10 Temperature-Initiated Passive Cooling System.....	51
2.11 Chapter Summary.....	56
Chapter 3: Conceived Passive Thermal Switches	62
3.1 Introduction.....	62
3.2 Categorization and Description of Thermal Switches.....	62
3.3 Chapter Summary.....	82
Chapter 4: Dissociation and Recombination Experiments	83
4.1 Introduction.....	83
4.2 Preliminary Experiments	84
4.3 Recombination Experiments.....	89
4.4 Chapter Summary.....	104
Chapter 5: The Heat Transfer Coefficient Experiment	106
5.1 Introduction.....	106
5.2 Experimental Setup.....	106
5.3 Experimental Procedure and Raw Data Reduction Algorithm.....	130
5.4 Description of Thermal Switches and Reduced Results.....	137
5.4.1 Particle Bed Thermal Switch.....	137
5.4.2 Wick Thermal Switch	142
5.4.3 Water Thermal Switch	150
5.5 Chapter Summary.....	160

Chapter 6: Summary and Recommendations for Future Work.....163
6.1 Introduction.....163
6.2 Summary and Recommendations for Future Work.....163

Appendix A Raw and Reduced Data of Dissociation and Recombination Experiments.....A1
Appendix B Components and Vendors EmployedB1
Appendix C Mass Calculations for Dissociation Experiments..... C1
Appendix D Computer Program.....D1
Appendix E Raw and Reduced Data of Heat Transfer Coefficient Experiments.....E1

List of Tables

Table 2.1	Types of Thermal Switches.....	58
Table 3.1	Heat Conduction Types of Thermal Switches	66
Table 3.2	Heat Convection Types of Thermal Switches.....	68
Table 3.3	Thermal Radiation Types of Thermal Switches.....	72
Table 6.1	Summary of Results.....	164

List of Figures

Figure 1.1	Categorization of Existing and Conceived Thermal Switches	14
Figure 2.1	High Temperature Gas-Gap Thermal Switch.....	18
Figure 2.2	Electrolytic Thermal Switch	20
Figure 2.3	Shape-memory Thermal Switch.....	22
Figure 2.4	Metal-impregnated Porous Ceramic Thermal Switch.....	24
Figure 2.5	Axial Heat Pipe.....	26
Figure 2.6	Axial Heat Pipe with Inert Gas in On-Mode	28
Figure 2.7	Axial Heat Pipe with Inert Gas in Off-Mode.....	28
Figure 2.8	Axial Heat Pipe with Inert Gas and Rigid-Wall Reservoir in On-Mode.....	29
Figure 2.9	Axial Heat Pipe with Inert Gas and Rigid-Wall Reservoir in Off-Mode.....	29
Figure 2.10	Axial Heat Pipe with Inert Gas and Bellowed-Wall Reservoir in On-Mode	31
Figure 2.11	Axial Heat Pipe with Inert Gas and Bellowed-Wall Reservoir in Off-Mode	31
Figure 2.12	Axial Heat Pipe with Bellowed Adiabatic Section in On-Mode	32
Figure 2.13	Axial Heat Pipe with Bellowed Adiabatic Section in Off-Mode.....	32
Figure 2.14	Axial Heat Pipe with Inert Gas and Temperature Controlled Rigid-Wall Reservoir in On-Mode.....	33
Figure 2.15	Axial Heat Pipe with Inert Gas and Temperature Controlled Rigid-Wall Reservoir in Off-Mode	33
Figure 2.16	Axial Heat Pipe with Inert Gas and Bellowed-Hollow-Wall Reservoir in On-Mode.....	35
Figure 2.17	Axial Heat Pipe with Inert Gas and Bellowed-Hollow-Wall Reservoir in Off-Mode.....	36
Figure 2.18	Axial Heat Pipe Utilizing Liquid Inventory Control	38
Figure 2.19	Axial Heat Pipe with Bendable Adiabatic Section	39
Figure 2.20	Axial Heat Pipe with Throttle Valve.....	40
Figure 2.21	Axial Heat Pipe with Expanding/Contracting Wick	42
Figure 2.22	Axial Heat Pipe with Magnetic Wick	43
Figure 2.23	Radial Heat Pipe	45
Figure 2.24	Thermal Syphon.....	47
Figure 2.25	Loop Thermal Syphon.....	48
Figure 2.26	Thermal Syphon with Inert Gas	49
Figure 2.27	Bistable Passive Thermal Switch Without Air in the Cylindrical Shell	50
Figure 2.28	Bistable Passive Thermal Switch With Air in the Cylindrical Shell	52

Figure 2.29	Temperature-Initiated Passive Cooling System.....	53
Figure 2.30	Categorization of Thermal Switches.....	57
Figure 3.1	Particle Bed Thermal Switch.....	75
Figure 3.2	Dissociation Thermal Switch.....	75
Figure 3.3	Change of Solid-Phase Structure Bar.....	75
Figure 3.4	Phase Change Thermal Switch.....	76
Figure 3.5	Variable Cross-Sectional Area Bar.....	76
Figure 3.6	Evaporation-Condensation Thermal Switch (with Fins).....	76
Figure 3.7	Liquid-Vapor Thermal Switch.....	77
Figure 3.8	Chamber Thermal Switch.....	77
Figure 3.9	Wick Thermal Switch.....	77
Figure 3.10A	Chemical Thermal Switch.....	78
Figure 3.10B	Chemical Thermal Switch.....	78
Figure 3.11	Grain Growth on Hot Component Surface.....	79
Figure 3.12	Attachment of Grooved Wall to the Heat Source.....	79
Figure 3.13	Surface Spectral Characteristics (Temperature Increase).....	80
Figure 3.14	Surface Spectral Characteristics (Chemical Reaction).....	80
Figure 3.15	Low Thermally Conducting Liquid or Gas Between the Components Whose Transmissivity (τ) Increases with Temperature.....	80
Figure 3.16	Double-Mesh Screen Covering the Hot Component Surface.....	81
Figure 3.17	Finned Components.....	81
Figure 4.1	Dissociation/Recombination Experimental Setup.....	85
Figure 4.2	Dissociation/Recombination Experimental Results for Magnesium Carbonate.....	90
Figure 4.3	Dissociation/Recombination Experimental Results for Lead Carbonate.....	91
Figure 4.4	Recombination Experimental Results with Increased Surface Area of MgO and a Nineteen-Hour Hold at 300 Celsius.....	93
Figure 4.5	Recombination Experimental Results with Increased Recombination Sites and a Nineteen-Hour Hold at 300 Celsius.....	95
Figure 4.6	Recombination-Pressurization Experimental Setup.....	96
Figure 4.7	Apparatus for Combining Moist CO ₂ with MgO.....	99
Figure 4.8	Dissociation Results Reconstituted Magnesium Carbonate.....	103
Figure 5.1	Partial Experimental Setup of Heat Transfer Coefficient Experiment.....	107
Figure 5.2	Macor Spacers.....	109
Figure 5.3	Stainless Steel Ring for Heater Flange.....	111
Figure 5.4	Stainless Steel Ring for Stainless Steel Pipe Flanges.....	112

Figure 5.5	Teflon Ring for Heater Flange	113
Figure 5.6	Teflon Ring for Stainless Steel Pipe Flanges	114
Figure 5.7	Location of Clamping Flanges (inches)	115
Figure 5.8	Complete Insulation System Design	118
Figure 5.9	Thermocouple Locations (inches)	119
Figure 5.10	Heater Control Panel	124
Figure 5.11	Circuit to Power Heater	125
Figure 5.12	Vacuum Pumping System	127
Figure 5.13	Particle Bed Thermal Switch	131
Figure 5.14	View AA of Figure 5.13—Cross-sectional View of Particle Bed	138
Figure 5.15	Particle Bed On-Mode and Off-Mode Heat Transfer Coefficients as a Function of Temperature Difference	140
Figure 5.16	Particle Bed Thermal Switch heat Transfer Coefficient Ratio	141
Figure 5.17	Wick Thermal Switch	143
Figure 5.18	Cross-sectional View of Wick Setup	144
Figure 5.19	Wick Thermal Switch On-Mode and Off-Mode Heat Transfer Coefficients	146
Figure 5.20	Wick Thermal Switch heat Transfer Coefficient Ratio. Off-Mode is Wick + Vacuum	148
Figure 5.21	Wick Thermal Switch Heat Transfer Coefficient Ratio. Off-Mode is Wick + Air	149
Figure 5.22	Water Thermal Switch—Water Height = 0.88 Inches	151
Figure 5.23	View AA of Figure 5.22—Water Thermal Switch	152
Figure 5.24	Water Thermal Switch—Water Height = 1.75 Inches	153
Figure 5.25	View AA of Figure 5.24—Water Thermal Switch	154
Figure 5.26	Water Thermal Switch On-Mode and Off-Mode Heat Transfer Coefficients	156
Figure 5.27	Water Thermal Switch Heat Transfer Coefficient Ratio. Off-Mode is a Vacuum at 1.65 torr	158
Figure 5.28	Water Thermal Switch Heat Transfer Coefficient Ratio. Off-Mode is Air at 1.0 atm	159
Figure 6.1	Best Performance Characteristics of Some of the Thermal Switches Investigated	166
Figure 6.2	Potential Water Thermal Switch in CANDU Reactor	173

Chapter One

Introduction

The need for temperature control permeates many different technological areas. This, of course, is not surprising, since key parameters such as material integrity, component performance, and system efficiency are all functions of temperature. Consequently, proper regulation of heat transfer and transport is of paramount importance. During the last three decades, research work in the area of temperature control has focussed primarily on temperature detection. Different materials have been investigated which have a property (such as electrical resistance, magnetic permeability, and electromagnetic transmissivity) that changes as a function of temperature. These thermometers are typically used to control various types of heat transferring systems which are electrically activated once a prespecified change in the monitored material property is detected. The one disadvantage of these types of temperature-control systems is the ever-present danger of mechanical failure. A minor malfunction in the detection and/or heat transferring system could result in complete loss of functional capability. This can be particularly critical for nuclear power plants, where loss of temperature control can result in material failure, allowing for the release of radioactive material.

Thus, this concern of mechanical failure in contemporary temperature control systems has recently motivated new research and development on devices known as thermal switches. A thermal switch is a passive device (i.e., nonelectro-mechanical) which thermally decouples a component from a heat sink when the component is at a temperature which is acceptable to the overall performance of the system of which it is a part, and strongly thermally couples the two (via the passive mechanisms of heat conduction, heat convection, and thermal radiation) when the component reaches a temperature which compromises the safety or reduces the efficiency of the

system (with safety taking precedence over efficiency when a choice must be made). A thermal switch is thus a passive device whose function is to prevent large heat loss between the component and heat sink when the temperature of the component is at its prespecified normal temperature range, and to enhance the transport of thermal energy from the component to the heat sink when the component reaches an unacceptable temperature (from a safety or efficiency point of view). It is the objective of this research to conceive and experimentally investigate new thermal switch concepts.

As implied above, thermal switches can be categorized into three types by their key operating mechanism for heat transfer. The three categories are: heat-conduction type, heat-convection type, and thermal-radiation type. Within each of these three categories are subcategories, depending on what parameter is being altered to create the switching action. For the heat-conduction type, the parameters that can be altered are the thermal conductivity of the thermal switch and the cross-sectional area of the thermal switch; for the heat-convection type it is the heat transfer coefficient of the thermal switch at the interface with the heat source, contact area between the thermal switch and heat source, heat transfer coefficient of the thermal switch at the interface with the heat sink, and contact area between the thermal switch and heat sink; and for the thermal-radiation type, the parameters that can be varied are the surface area and surface emissivity of the heat source, surface area and surface absorptivity of the heat sink, and view factor between the heat source and heat sink. The corresponding heat transport equation for each type of thermal switch is (definition of the terms in the equations immediately follows):

$$\text{heat-conduction type } q = kA_{CS}(\Delta T/\Delta x) \quad (1.1)$$

$$\text{heat-convection type } q = hA\Delta T \quad (1.2)$$

$$\text{thermal-radiation type } q = [A_h\sigma(T_h^4 - T_c^4)] / [((1 - \epsilon_h)/\epsilon_h) + (1/F_{h-c}) + (A_h/A_c)((1/\alpha_c) - 1)] \quad (1.3)$$

In all of these equations q is the heat transfer rate between the heat source (i.e., the component to which temperature control is being applied) and the heat sink. In the first equation, k is the thermal conductivity of the thermal switch, A_{CS} is the cross-sectional area of the thermal switch, ΔT is the

temperature difference between the end of the thermal switch in contact with the heat source and the end of the thermal switch in contact with the heat sink, and Δx is the length of the thermal switch from heat source to heat sink. In the second equation, hA is either the product of the heat transfer coefficient of the thermal switch while in contact with the heat source and the contact area between the thermal switch and heat source, or the heat transfer coefficient of the thermal switch while in contact with the heat sink and the contact area between the thermal switch and heat sink. If it is the former, then ΔT is the temperature difference between the surface of the heat source and the bulk temperature of the thermal switch. If it is the latter, then ΔT is the temperature difference between the bulk temperature of the thermal switch and the surface temperature of the heat sink. Lastly, in the third equation, A_h is the surface area of the heat source, σ is the Stefan-Boltzmann constant, T_h is the surface temperature of the heat source, T_c is the surface temperature of the heat sink, ϵ_h is the surface emissivity of the heat source, F_{h-c} is the view (or configuration) factor from the heat source to the heat sink, A_c is the surface area of the heat sink, and α_c is the surface absorptivity of the heat sink. As one can see by inspection of the equations, decreasing these parameters thermally decouples the heat source from the heat sink, and increasing the parameters thermally couples the two. It is this variation in parameters that creates the switching effect of the thermal switches.

The thermal switches that have been developed in the last thirty years are discussed in Chapter 2. (In comparison to the work done on temperature detection, it is substantially less.) The first part of the chapter narratively describes these thermal switches. This is followed by a table which categorizes the thermal switches according to what parameter is varied to achieve the thermal switching action. Lastly, schematics of the different thermal switches are given. The various thermal switches were identified by a search through the international patent database, and the scientific and engineering databases INSPEC and NTIS.

The thermal switch concepts conceived under the auspices of this project are discussed in Chapter 3. Eighteen different thermal switches were conceived. In this chapter, they are categorized and described narratively together, followed by schematics. Note that the schematics

show the thermal switches as applied in a pressure-tube type nuclear reactor, with the pressure tube as the component whose temperature is being controlled, and the calandria tube as the heat sink. This use of the thermal switches was chosen as a representative application of substantial interest, but one having a simple configuration which facilitates transferring the device to a variety of other situations. (Figure 1.1 gives a succinct categorization of both existing and conceived thermal switches, as well as the figures in which they are contained.)

Chapter 4 and Chapter 5 discuss the experimental aspects of the project. Chapter 4 is concerned with the experimental investigation of a dissociation/recombination chemical thermal switch, and Chapter 5 is concerned with the experimental investigation of a particle-bed thermal switch, a wick thermal switch, and a water thermal switch. Both chapters describe the experimental setups built, the method of data reduction utilized, and the results obtained. In addition, explanations are given for the trends observed in the data obtained. Chapter 6 reiterates the key experimental results obtained and provides recommendations for future work.

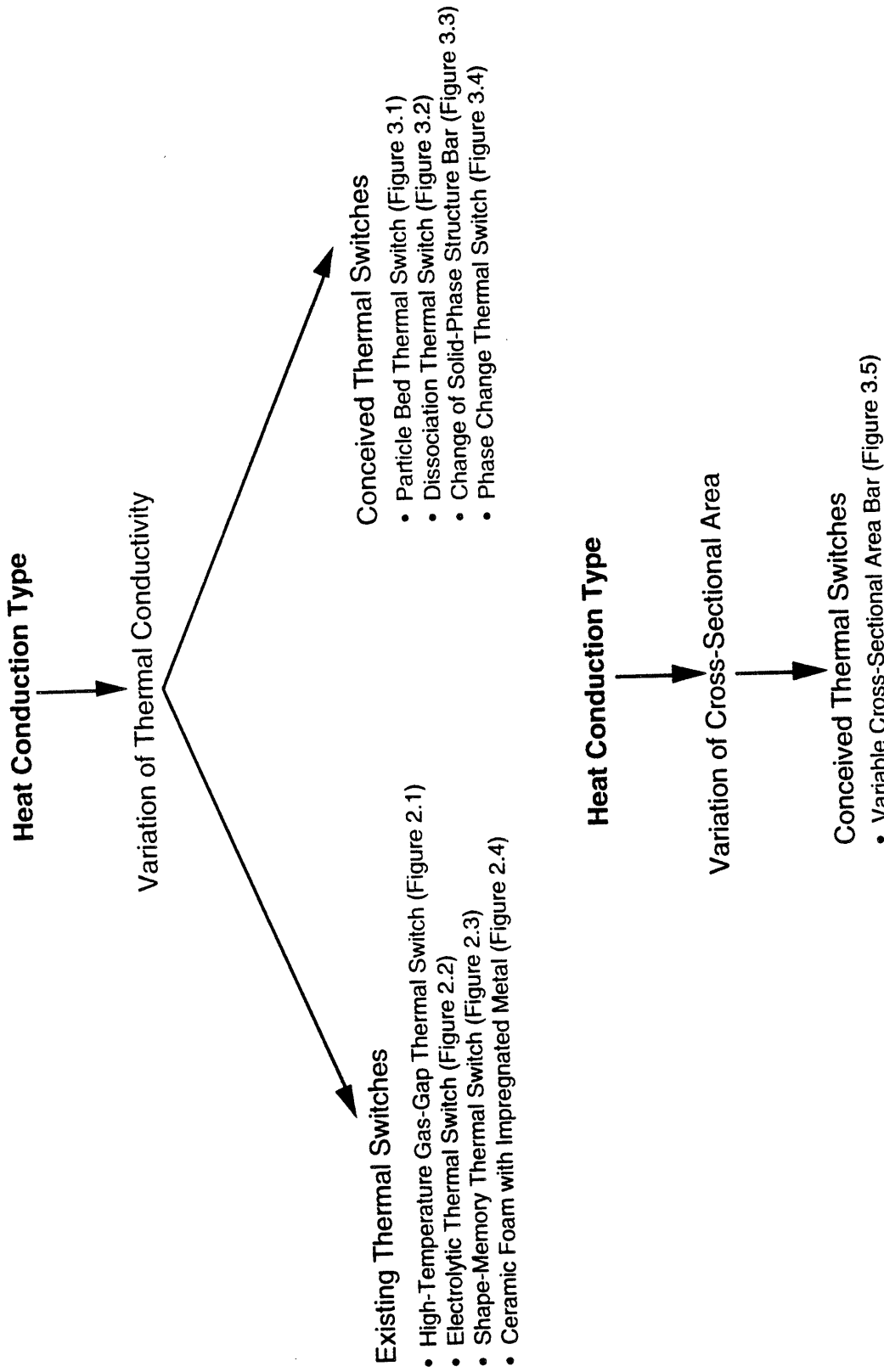


Figure 1.1. Categorization of Existing and Conceived Thermal Switches

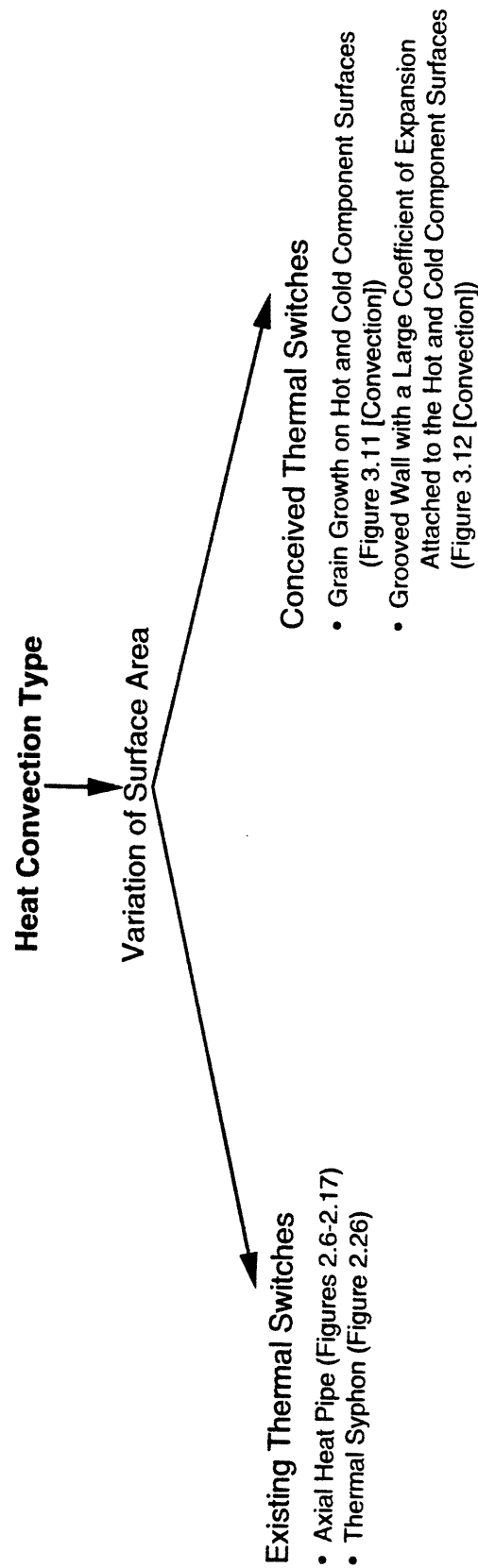
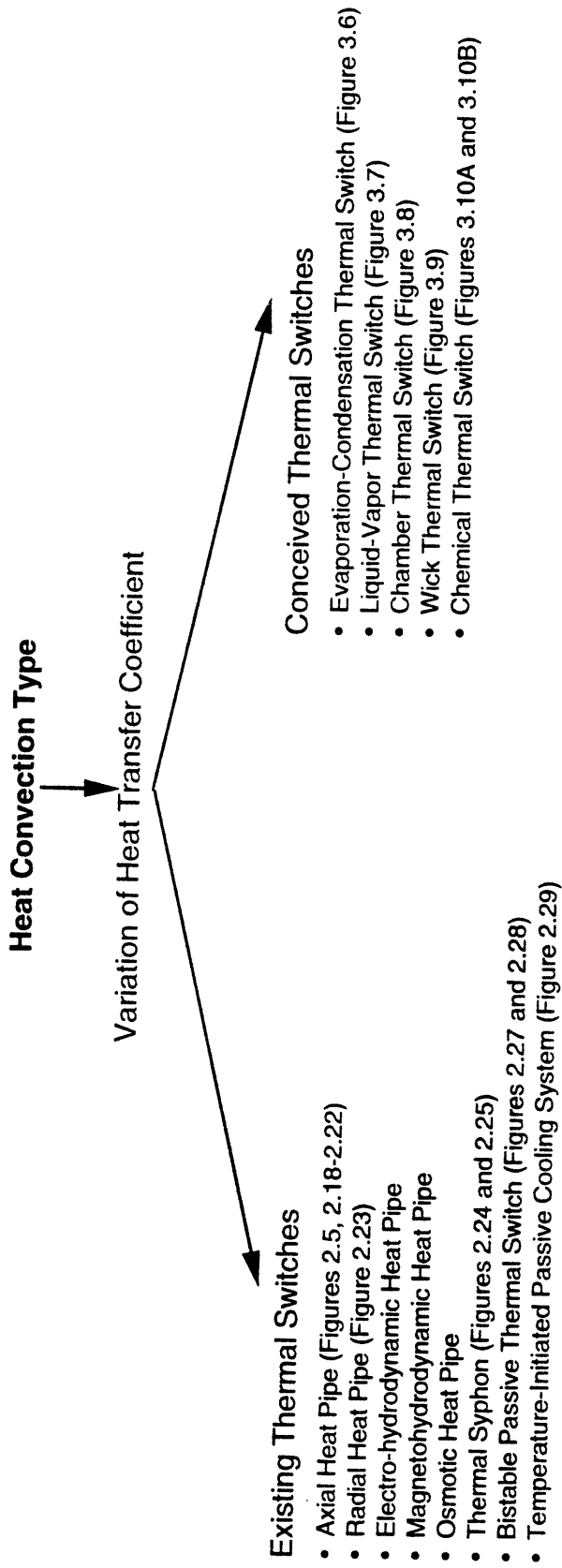


Figure 1.1 Continued

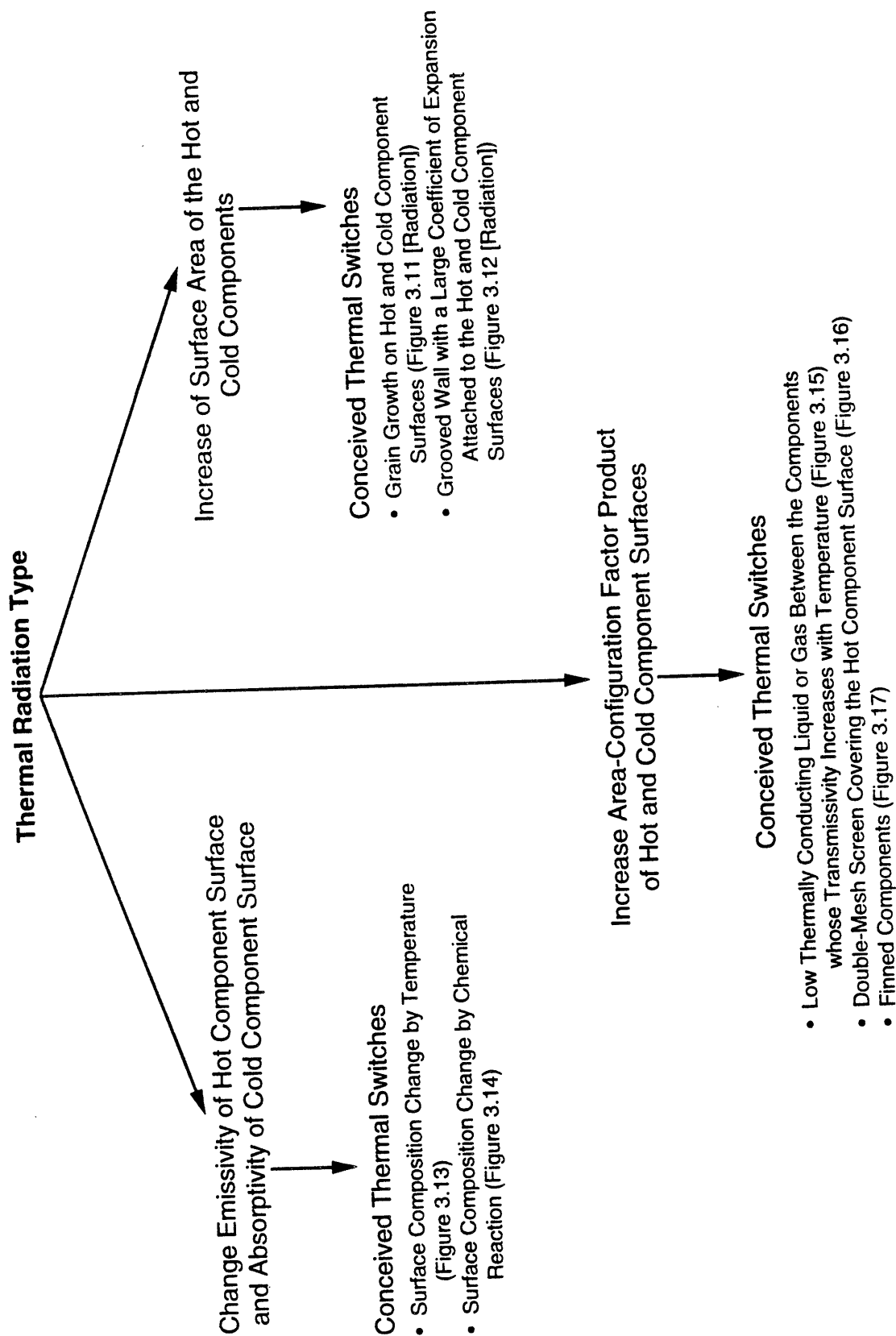


Figure 1.1 Continued

Chapter Two

Contemporary Passive Thermal Switches

2.1 Introduction

The thermal switches described in this chapter are those that have been conceived and developed over the last several decades. They have originated from a variety of sources, and have found application in many different areas. As mentioned in the introduction, these thermal switches were identified by a literature search through the international patent database, and the scientific and engineering databases INSPEC and NTIS. The superscripts found below refer to the references listed at the end of the chapter.

2.2 High-Temperature Gas-Gap Thermal Switch¹

One such passive temperature control device is the high-temperature gas-gap thermal switch. Conceived at NASA's Jet Propulsion Laboratory, the thermal switch operates at temperatures in the approximate range of 100°C to 1500°C. The principle of operation is illustrated in Figure 2.1, which shows a cylindrical version of the switch surrounding a cylindrical heat source that is to be thermally coupled or decoupled from a heat sink. The gap between the heat source and heat sink is filled with layers of low-emissivity and low-absorptivity nickel, molybdenum, or zirconium foil to suppress the radiative transfer of thermal energy across the gap. The spaces between the layers of foil are filled with woven quartz fibers to prevent the layers from touching, thereby reducing thermal conduction. With no gas present in the spaces between the layers of foil to provide a conducting pathway from the heat source to the heat sink, the thermal switch is off. To turn the thermal switch on (i.e., to thermally couple the heat source to the heat sink), the gap of the thermal switch is filled with a gas. Any of a large number of gases will

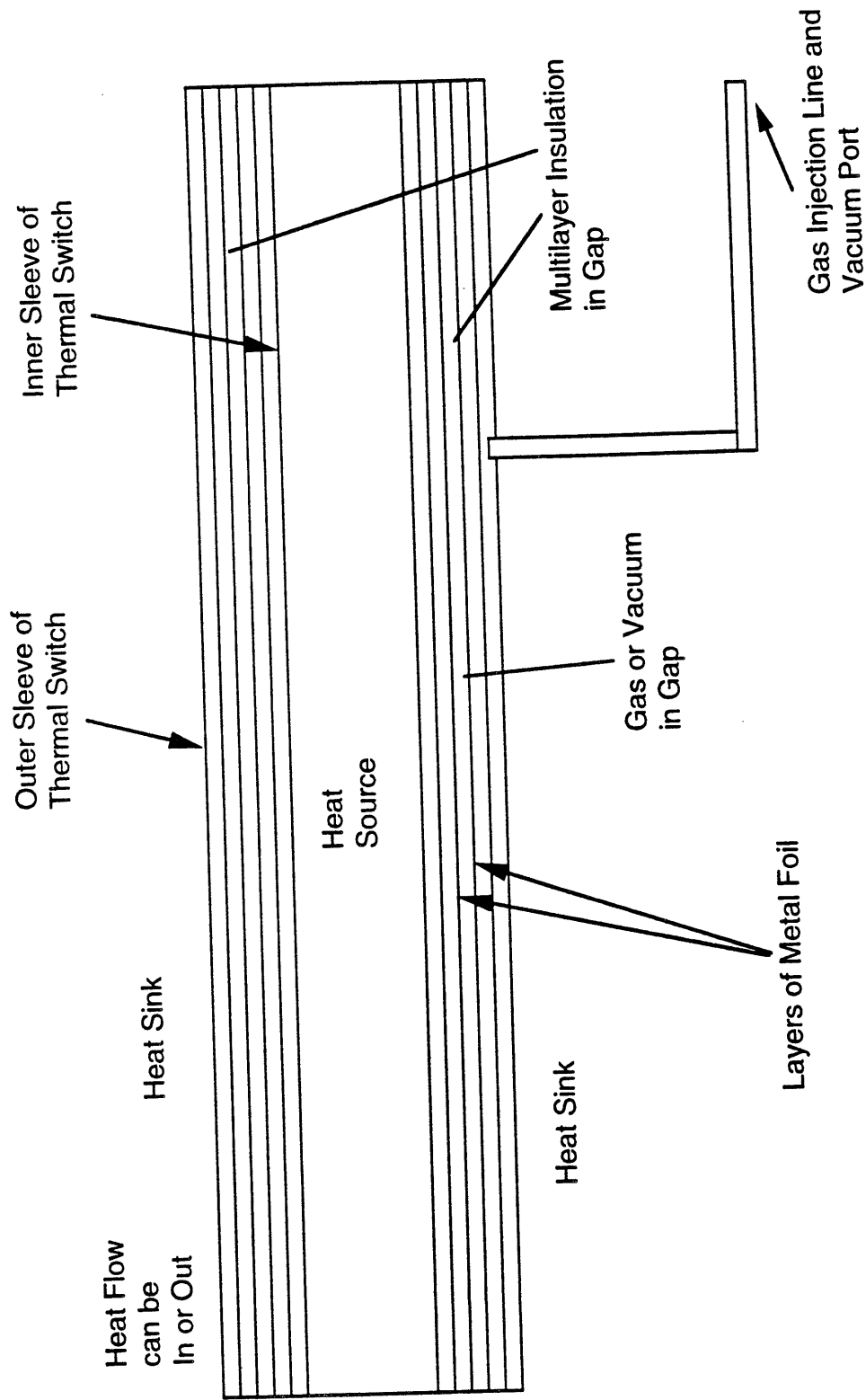


Figure 2.1. High Temperature Gas-Gap Thermal Switch

suffice, such as helium, hydrogen, nitrogen, or argon. Final selection should be made based on which gas is least reactive to the materials comprising the walls of the heat source and heat sink. The pressure of the gas in the gap has to be only about 1 torr (about 130 Pa) to provide substantial conduction of heat across the gap. To turn the switch back off, one merely pumps the gas out of the gap. Calculations indicate that the ratio of heat transfer rate for the thermal switch in the on mode to the heat transfer rate for the thermal switch in the off mode can be as high as 400.

The vacuum required to shut the thermal switch off is approximately 25 microns of Hg, and this can be provided in one of two ways. One method is to use a conventional piston vacuum pump. This type of pump is capable of providing a vacuum down to 15 microns of Hg. A second method, which is more novel, involves the usage of a sorption pump. Specifically, a bed of sorbent material such as charcoal, zeolite, hydrides, or oxides are cooled below the condensation temperature of the gas in the gap. The gas then condenses on the sorbent material yielding the vacuum desired. This second method provides a purer vacuum, but has the disadvantage of having to operate at cryogenic temperatures.

2.3 Electrolytic Thermal Switch²

Another type of thermal switch is the electrolytic thermal switch. This kind of thermal switch alters thermal conduction electrically. The device is composed of an inner electrically conductive (ionomeric) layer of low thermal conductivity sandwiched between two metal-foil electrodes (see Figure 2.2). The inner layer is a polymer such as polyaniline. In essence, the device is a metal/conductive-polymer electrical cell. The electrical charging of the device via the two metal-foil electrodes causes metal dendrites to grow from the electrodes into the electrically conductive polymer by deposition of ions from the polymer. Because the thermal conductivity of the metal is much greater than that of the polymer, the overall thermal conductance of the electrolytic thermal switch, and thus the heat transfer rate across the device, increases as the dendrites grow across the inner layer. When the electrical potential across the electrodes is removed, the metal dendrites electrochemically dissolve, yielding a low thermal conductance

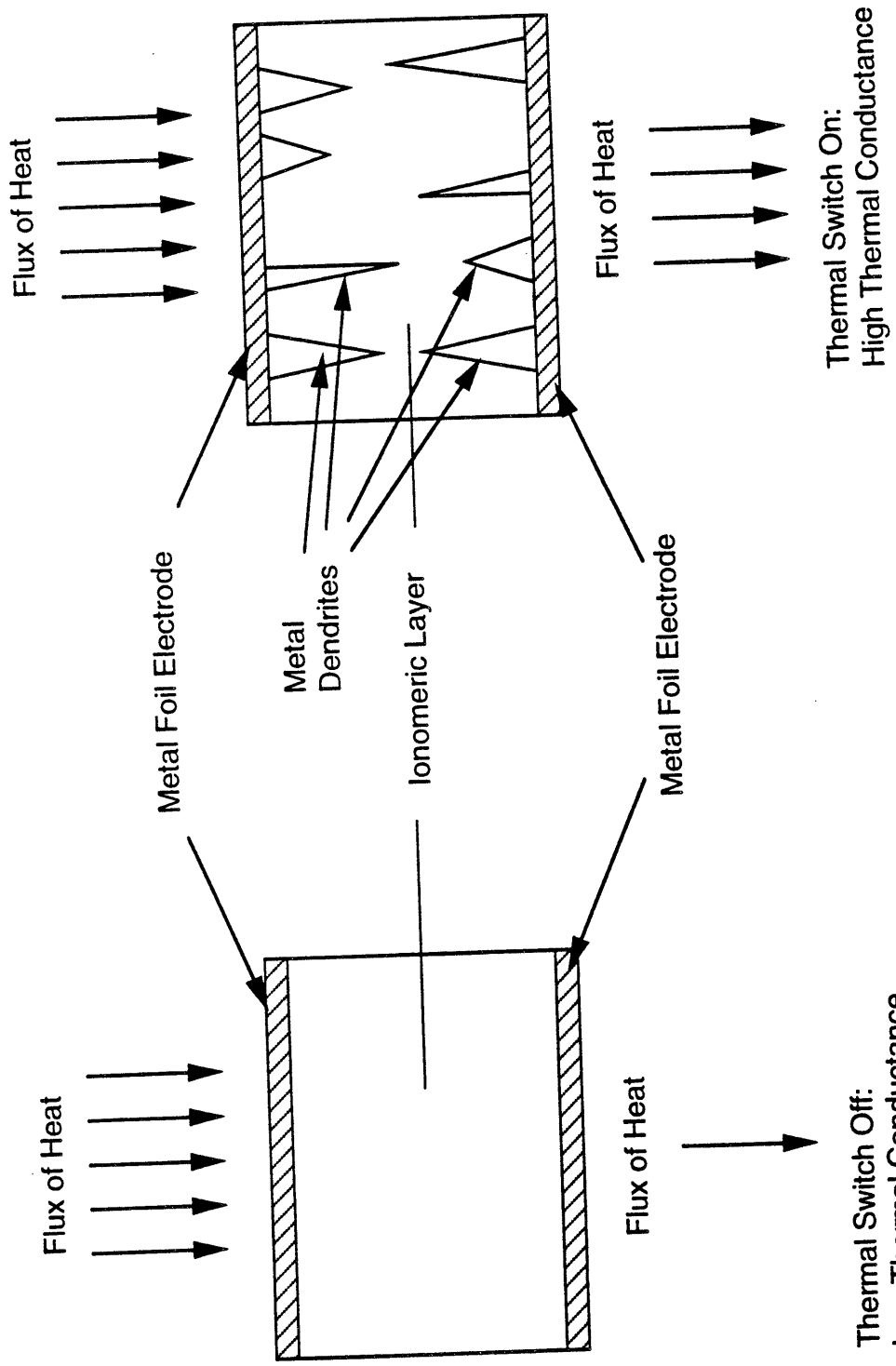


Figure 2.2. Electrolytic Thermal Switch

device. Experimental investigation by the developers is continuing in an effort to develop a device whose "on" state thermal conductance is 10 times greater than its "off" state thermal conductance. Presently, the ratio of "on" state thermal conductance to "off" state thermal conductance is 1.21.

The useful lifetime and operating characteristics of the electrolytic thermal switch depend on many parameters. Of greatest concern is that the metal deposits formed during the "on" mode of the thermal switch be dendritic rather than spongy or densely-packed, smooth layers of crystals. The properties of the metal deposits are affected by the temperature, current density, type of polymer, and the size, shape and material of the electrodes. With more experimental investigation, however, it is believed that metal dendrite formation and growth to achieve the required parameters will be worked out.

2.4 Material-Type Thermal Switches

Material-type passive thermal switches have also been developed. One kind is the shape-memory thermal switch³. The shape-memory thermal switch is a device which alters its shape with temperature. Specifically, as the temperature is increased through a particular temperature interval, the shape-memory thermal switch expands linearly, bringing into thermal contact the heat source with the heat sink (see Figure 2.3). Conversely, as the temperature is decreased through a particular temperature interval (not necessarily the same temperature interval as the expansion temperature interval), the shape-memory thermal switch reverts back to its original shape. The shape-memory thermal switch can be comprised of one of three alloys. The three shape-memory alloys are NiTi (Nickel and Titanium), Cu-Zn-Al (Copper, Zinc and Aluminum) and Cu-Al-Ni (Copper, Aluminum and Nickel). All three of these alloys change shape as they are heated through a particular temperature interval, and return to their original shape when cooled through another temperature interval. The temperature interval at which these shape changes take place depend on the alloy being used, the proportion of each metal present in the alloy, and the method of alloy processing. The alloys NiTi and Cu-Zn-Al change shape at temperatures well below 100°C no matter what proportions of the metals comprising them are used, or what alloy

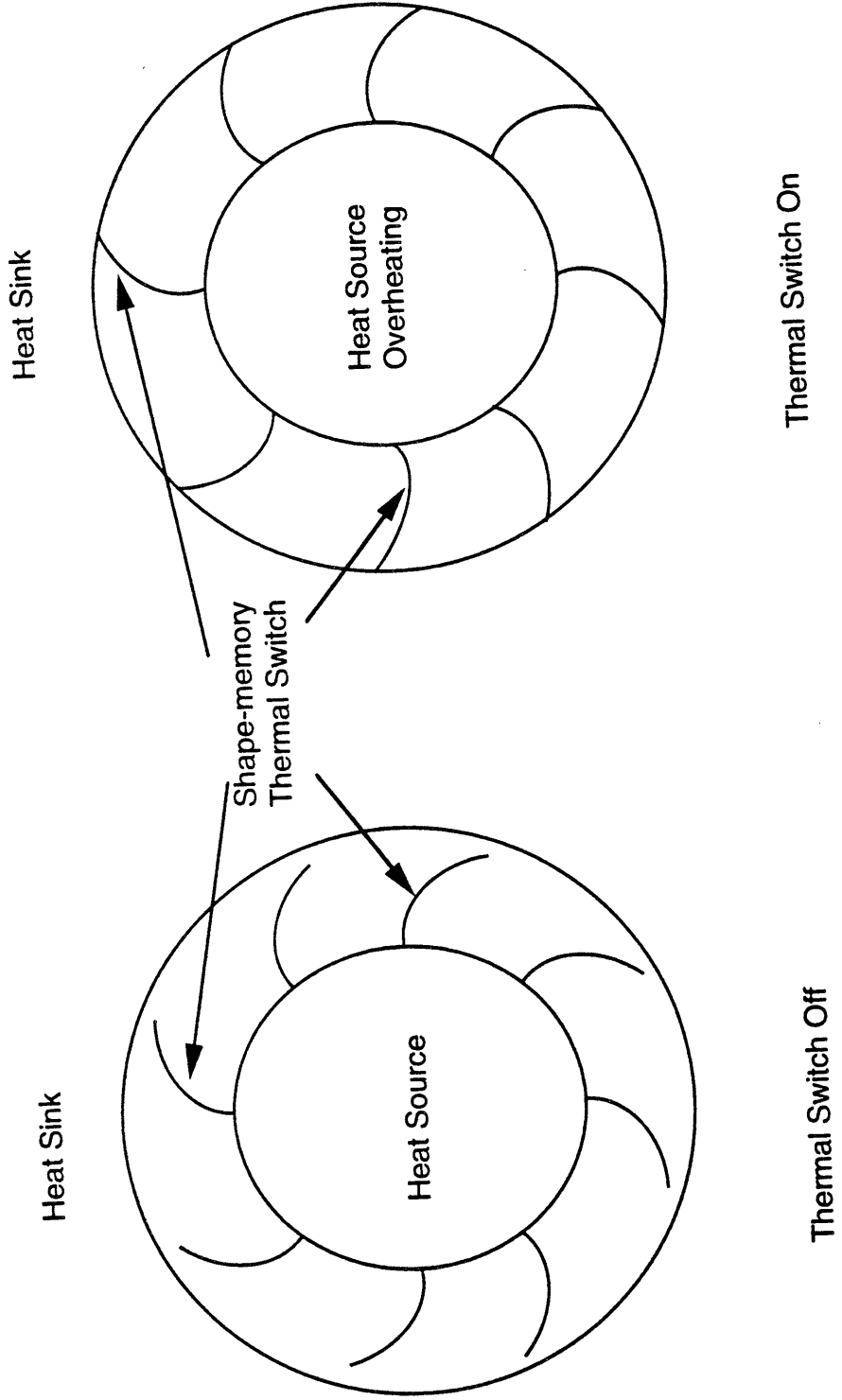


Figure 2.3. Shape-memory Thermal Switch

processing method is used. Consequently, these two alloys have limited commercial application. However, the third alloy listed, Cu-Al-Ni, provides a fully reversible shape memory effect at significantly higher temperatures. Indeed, for the proportions 82.5 wt. % copper, 14.2 wt % aluminum, and 3.3 wt % nickel, and isothermally aging the alloy in the temperature interval 250°C to 400°C, a change in original shape is observed while heating the alloy through the temperature interval from 175°C to 190°C, and a return to original shape is observed while cooling the alloy through the temperature interval from 155°C to 125°C. In addition, the memory effects in this alloy are unaffected by short overheating to temperatures as high as 300°C.

Another kind of a material-type thermal switch is a ceramic foam which is uniformly impregnated with a metal which coats the ceramic foam structure⁴. This thermal switch is constructed in the on-mode and upon temperature excursion moves to the off-mode (see Figure 2.4). Specifically, the impregnating of a porous ceramic with a thermally conductive metal results in a composite with an effective thermal conductivity many times higher than the unimpregnated, porous ceramic. The thermal switch remains a good conductor until the temperature reaches the melting point of the metal impregnates. At this point, the metal balls up, forming spherical droplets (due to non-wetting). This interrupts the thermal path through the material, drastically reducing the thermal conductivity of the composite. This then results in a composite which is a good thermal insulator. Thus the thermal switch is activated at the melting temperature of the metal impregnants. Obviously, the thermal switching effect is irreversible.

Ceramic foam materials investigated to date have been alumina, zirconia, and silica, although it is conceivable that any open porous ceramic would be acceptable. Ceramic foam densities corresponding to 15 to 40 per cent of their theoretical density have been found to be the most practicable, since below 15% theoretical density the ceramic ordinarily has poor mechanical properties, and above 40% theoretical density it becomes difficult to achieve uniform impregnation.

To date, silver and copper have been used as the metal impregnants. This has yielded thermal switches which are activated at 1762°F (the melting temperature of silver) and 1982°F (the

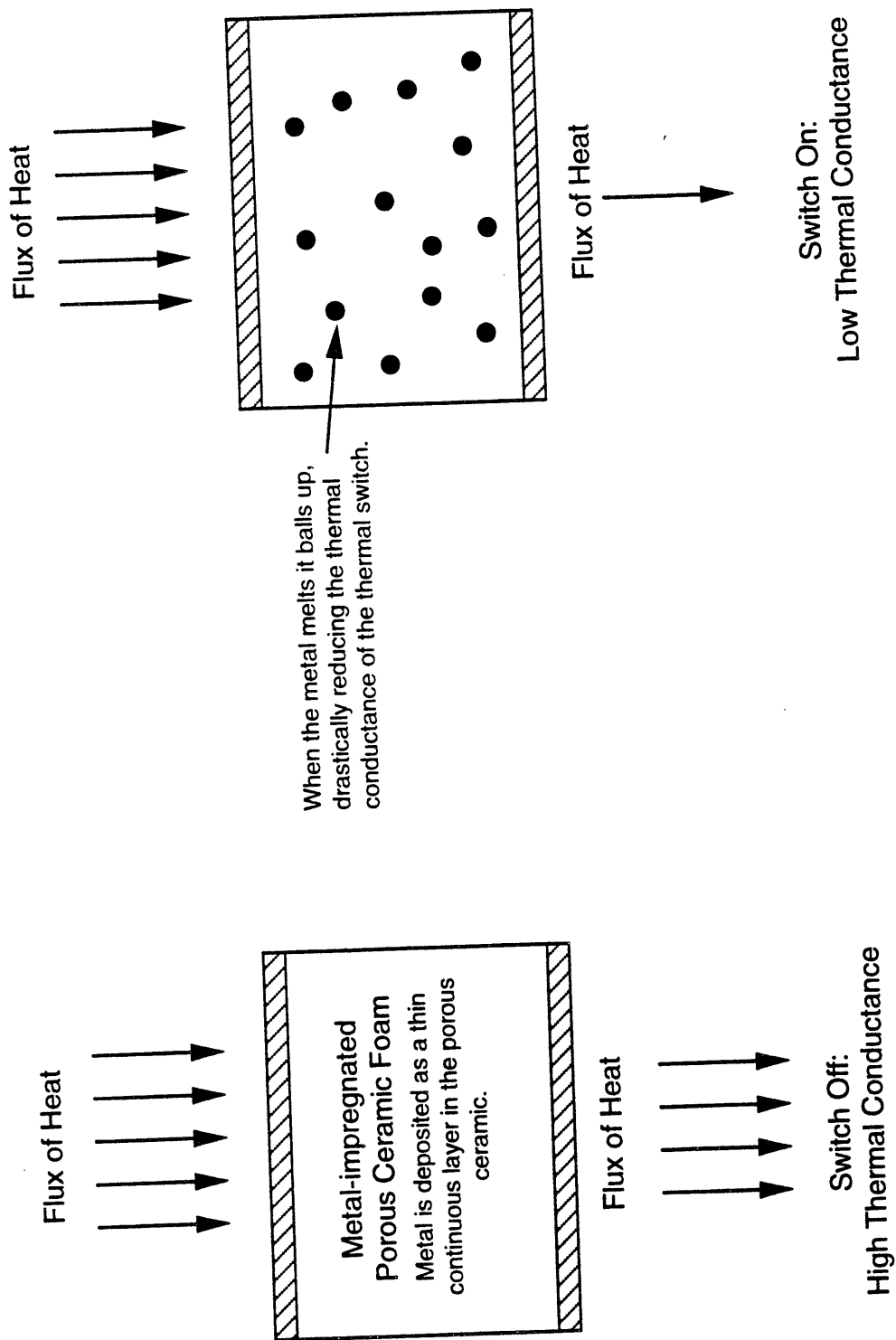


Figure 2.4. Metal-impregnated Porous Ceramic Thermal Switch

melting temperature of copper). Other metals can also be used as impregnants to increase or decrease the switching temperature of the thermal switch.

2.5 Axial Heat Pipes⁵

Perhaps the best known passive temperature control device is the heat pipe (see Figure 2.5). It is comprised of an enclosed container (which is usually cylindrical in shape) which contains a wick and a working fluid. One end of the cylindrical container is the evaporator section, the other end is the condenser section. In between the evaporator section and the condenser section is the adiabatic section. The heat pipe functions as follows.

Thermal energy is introduced at the evaporator section. This thermal energy is absorbed by the working fluid inside the evaporator section and the fluid is vaporized. This creates an axial vapor pressure gradient which causes the vapor to flow from the evaporator section to the condenser section. At the condenser section, the vapor condenses, releasing thermal energy and converting back to liquid. The liquid is then pumped by the wick, via capillary action, back to the evaporator section. The temperature range within which the heat pipe functions is determined by the working fluid. The higher the boiling point of the working fluid, the higher the working temperature range of the heat pipe. It is thus the selection of the working fluid which determines when the heat pipe turns on and when it turns off.

The temperature range over which a heat pipe with a particular fluid functions can be modified in several ways, although virtually all the methods involve utilizing a noncondensable, inert gas. The simplest method is merely to introduce a noncondensable, inert gas into the heat pipe in the condenser section with no modification in the physical geometry of the heat pipe. Visual observations and temperature measurements show that the working fluid vapor and the noncondensable, inert gas remain, for the most part, segregated, and that a definitive interface exists between them no matter what the orientation of the heat pipe. There is some diffusion of the vapor into the inert gas, but it is only a minimal amount. Thus, the active condenser length varies in accordance with temperature changes in the evaporator section and, hence, temperature changes

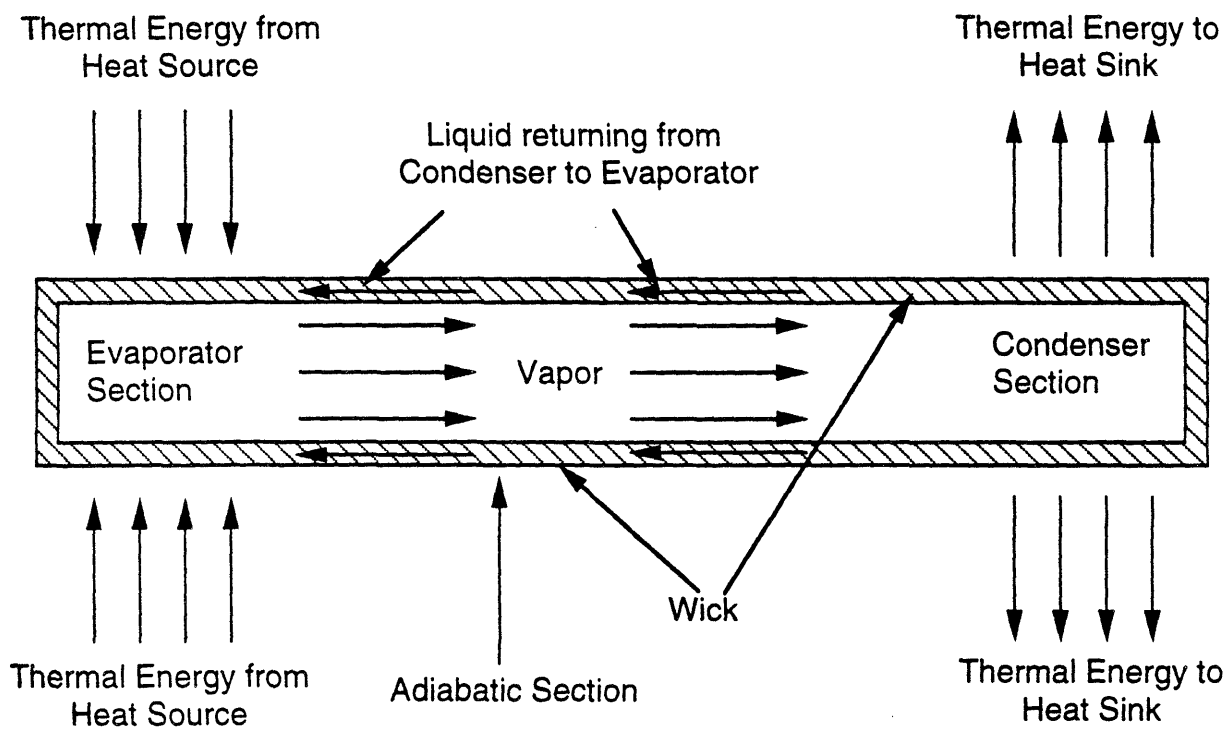


Figure 2.5. Axial Heat Pipe

in the heat source. An increase in evaporator temperature causes an increase in vapor pressure of the working fluid, which causes the gas to compress into a small volume, releasing a larger amount of active condenser length for heat rejection (see Figure 2.6). Conversely, a drop in evaporator temperature results in a lower vapor pressure, which allows the gas to expand, shutting off active condenser surface area (see Figure 2.7). Thus for a given amount of noncondensable, inert gas and a constant heat-sink temperature, the position of the gas/vapor interface is a function of the thermal energy being transported by the working fluid vapor. Hence, since the presence of the gas raises the lower limit at which the temperature of the heat pipe turns on (i.e., becomes thermally conductive) without altering the upper temperature limit of operation (at which wick dry-out occurs), suitable positioning of the gas/vapor interface can be used to control, within close limits, the temperature of the heat source (which is in contact with the evaporator section of the heat pipe).

However, one major drawback to this type of heat pipe is that the effective length of the condenser section is reduced with the presence of an inert gas. Indeed, no matter how hot the evaporator section becomes, a portion of the condenser section is always blocked off by the inert gas (with the exception of the small amount of vapor that diffuses into the inert gas.) This then results in a decrease in the rate of thermal energy transport by the heat pipe. One solution put forth to remedy this problem is to add a rigid wall reservoir downstream of the condenser section (see Figures 2.8 and 2.9). This reservoir provides a cavity for the inert gas to occupy as the vapor pressure increases due to the increase in heat source temperature. Hence, at the maximum operating temperature of the heat pipe, the maximum thermal energy transport rate of the heat pipe is realized. The reservoir area must be lined with wick material like the rest of the heat pipe to transport back to the evaporator section any working fluid which diffuses (in vapor form) into the reservoir area and condenses. This type of heat pipe also provides more precise control of the heat-source temperature than the gas-loaded heat pipe without a reservoir, since, for the same mass of gas, the change in compressibility of the gas with respect to temperature is greater with the larger volume.

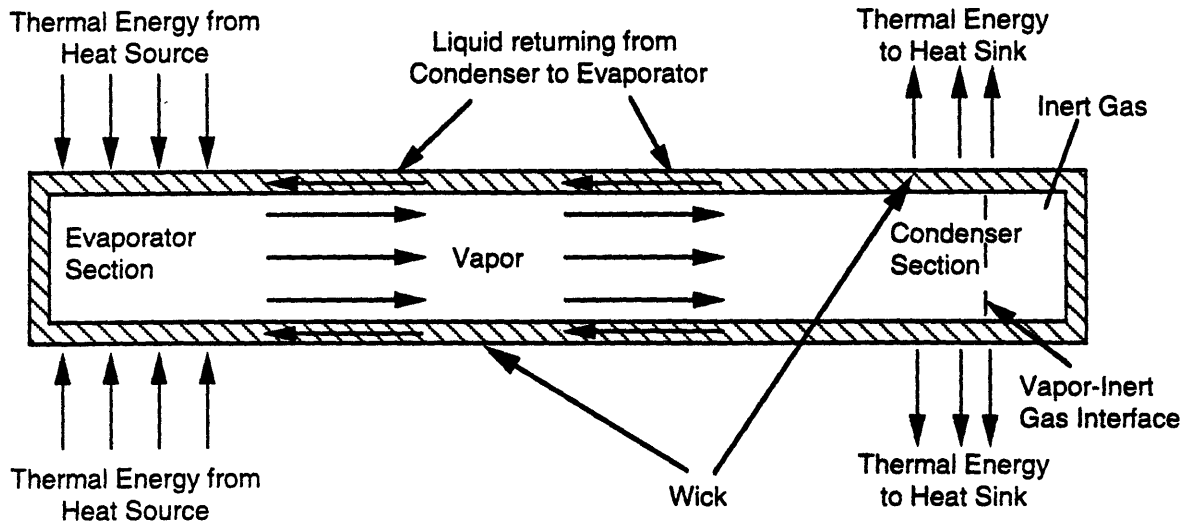


Figure 2.6. Axial Heat Pipe with Inert Gas in On-Mode

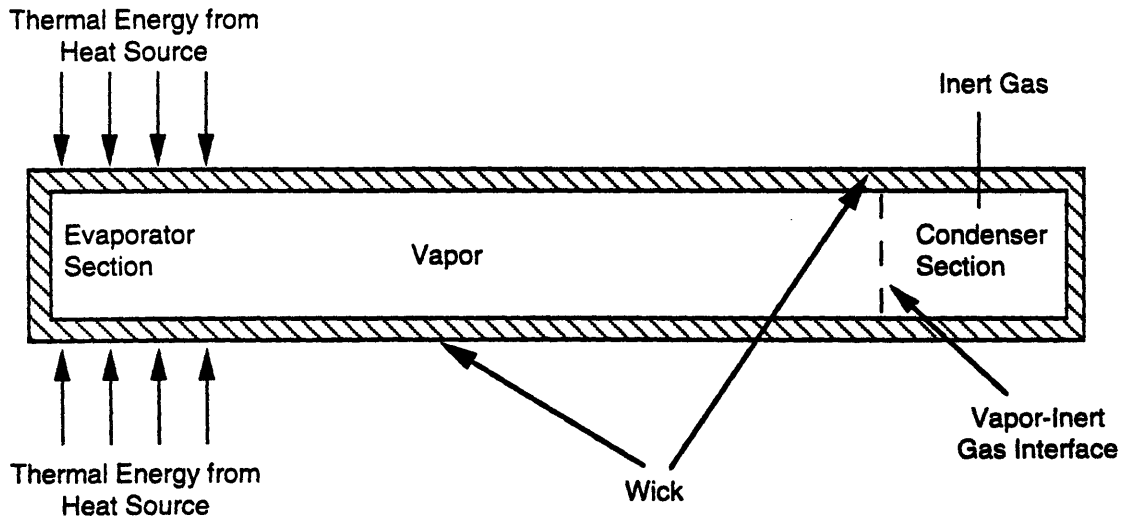


Figure 2.7. Axial Heat Pipe with Inert Gas in Off-Mode

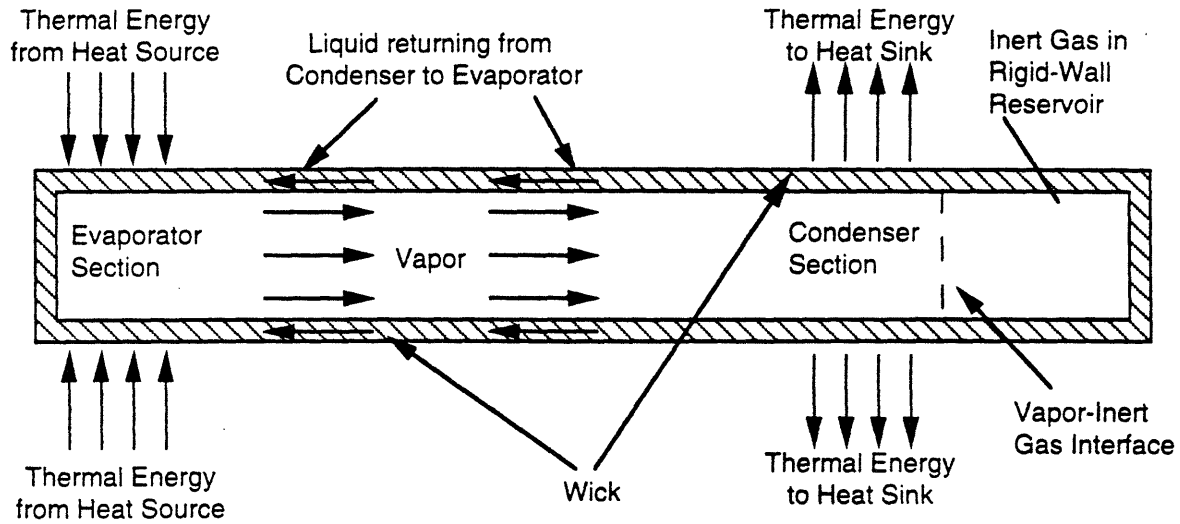


Figure 2.8. Axial Heat Pipe with Inert Gas and Rigid-Wall Reservoir in On-Mode. Rigid-Wall Reservoir is an Extension of the Condenser Section

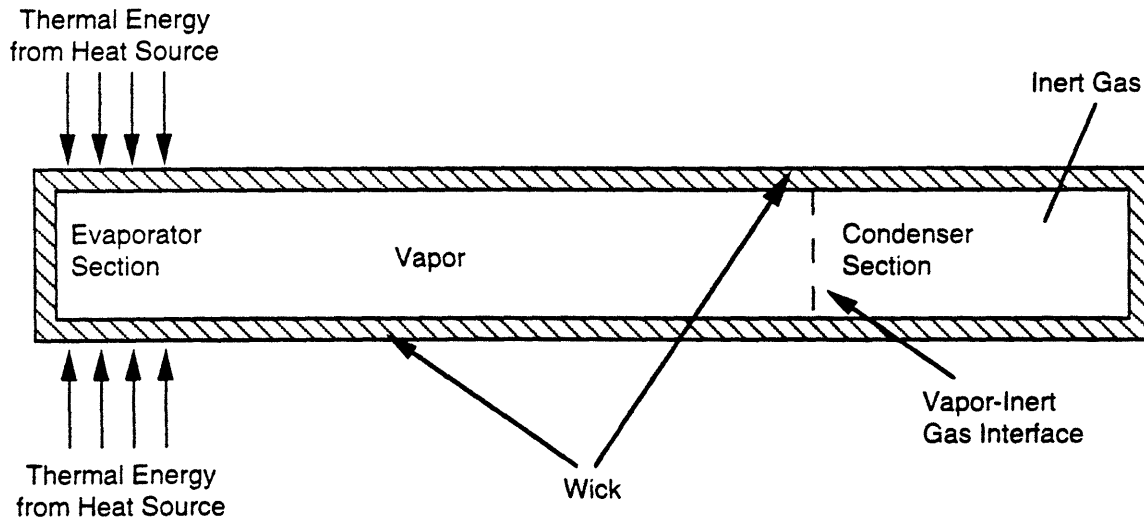


Figure 2.9. Axial Heat Pipe with Inert Gas and Rigid-Wall Reservoir in Off-Mode

Another variation of this type of heat pipe is a reservoir comprised of bellows. The bellows allow control of the inert gas volume. They expand, increasing the reservoir's length, as the vapor pressure increases (due to the increasing temperature of the heat source) and contract as the temperature of the heat source decreases (see Figures 2.10 and 2.11). This variation in reservoir length with the heat source temperature, coupled with the compressibility of the gas, allows even greater precision in controlling the temperature of the heat source than the heat pipe with a fixed rigid wall reservoir. The only disadvantage of this kind of heat pipe over a heat pipe with a fixed-wall reservoir is that the bellows add extra structural complexity to the heat pipe.

Heat pipes have also been constructed in which the adiabatic section of the heat pipe is comprised of bellows (see Figures 2.12 and 2.13). For this type of heat pipe, no inert gas or reservoir is present, and the condenser section is the flat face of the heat pipe opposite the evaporator section. The outside face of the condenser has a low emissivity. At a predetermined temperature of the heat source, the adiabatic section expands, bringing the condenser section into contact with a heat sink. As long as the heat source is at or above this predetermined temperature it remains in contact with the heat sink. Heat source and heat sink are thermally decoupled when the source temperature falls below this predetermined temperature, causing contraction of the bellows.

Each of the forms of heat pipe described above are non-feedback heat pipes. They operate on the principle that the thermal coupling between the heat source and the evaporator section of the heat pipe is strong. Hence, if the thermal impedance between the heat source and the heat pipe's evaporator section is large, control of the heat source temperature will, at best, be poor. The development of feedback-controlled heat pipes has enabled precise temperature control of the heat source to be obtained. Two forms of feedback control are feasible: active (electrical) and passive (mechanical).

The electric feedback controlled heat pipe consists of a temperature sensor, electronic controller, and a heat pipe with a heated reservoir containing inert gas (see Figures 2.14 and 2.15). Internal or external heaters are used to provide thermal energy to the reservoir. Heating the inert gas causes it to expand, decreasing the amount of condenser surface available to the vapor and,

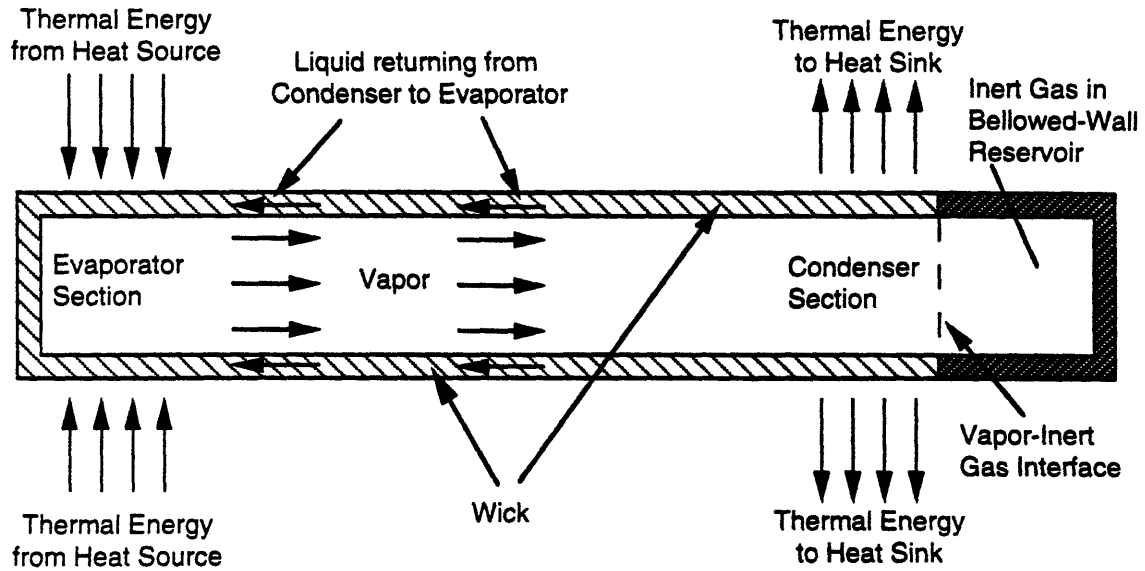


Figure 2.10. Axial Heat Pipe with Inert Gas and Bellowed-Wall Reservoir in On-Mode

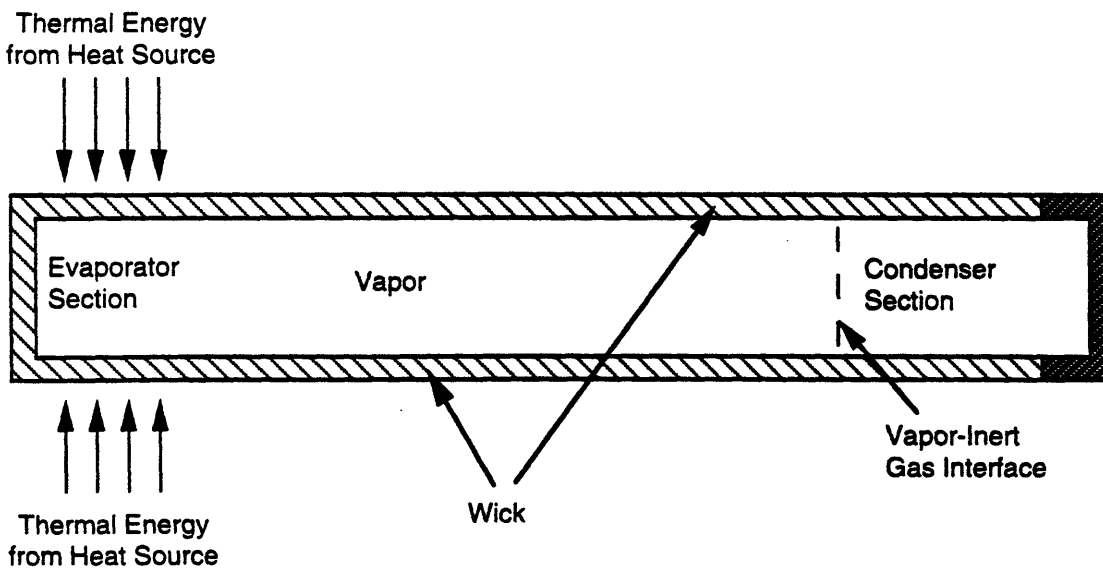


Figure 2.11. Axial Heat Pipe with Inert Gas and Bellowed-Wall Reservoir in Off-Mode

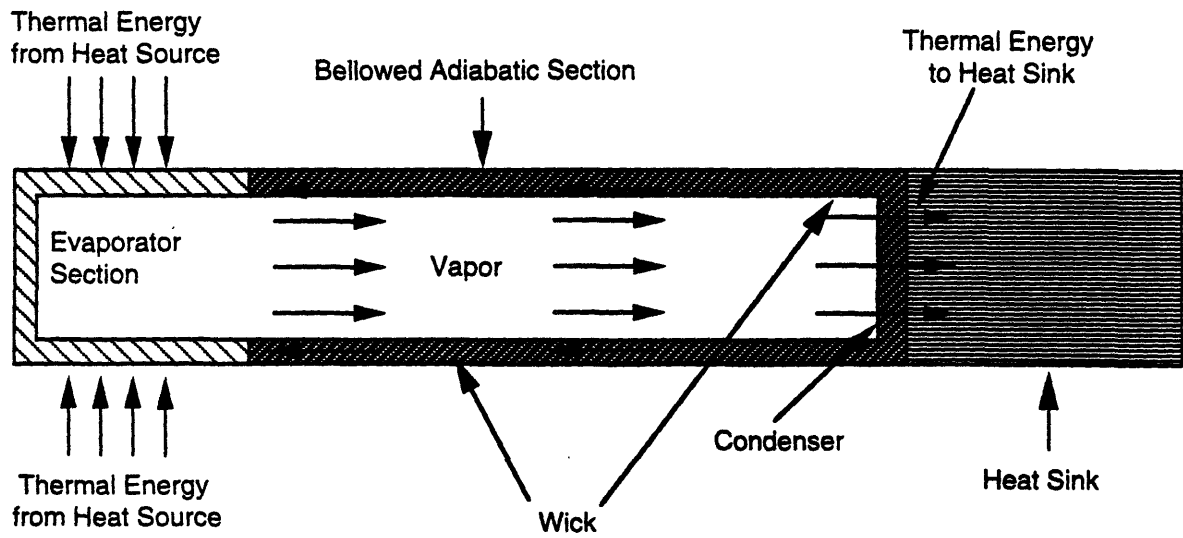


Figure 2.12. Axial Heat Pipe with Bellowed Adiabatic Section in On-Mode

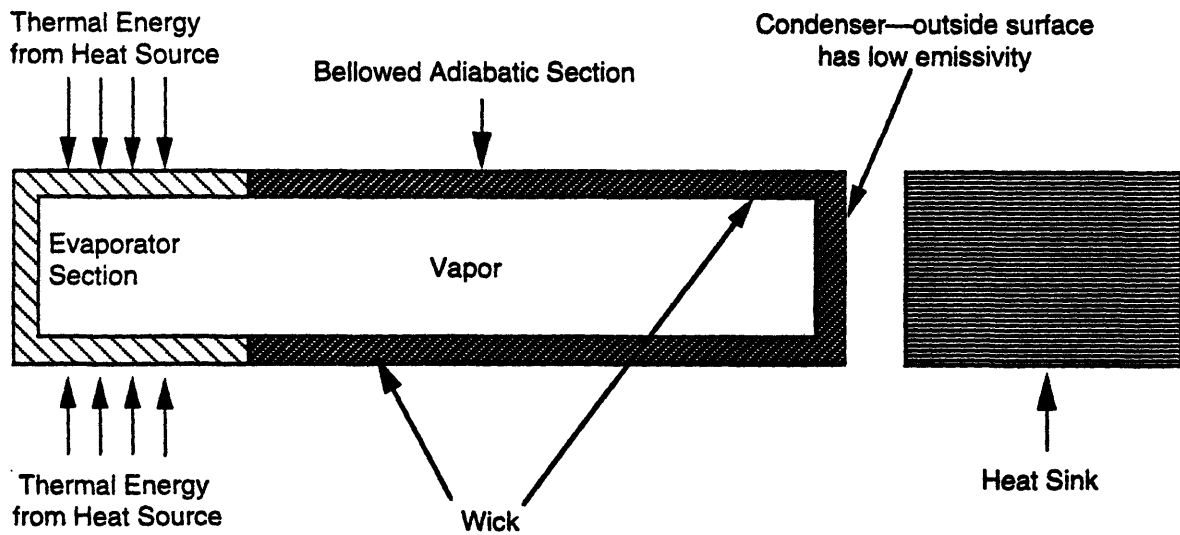


Figure 2.13. Axial Heat Pipe with Bellowed Adiabatic Section in Off-Mode

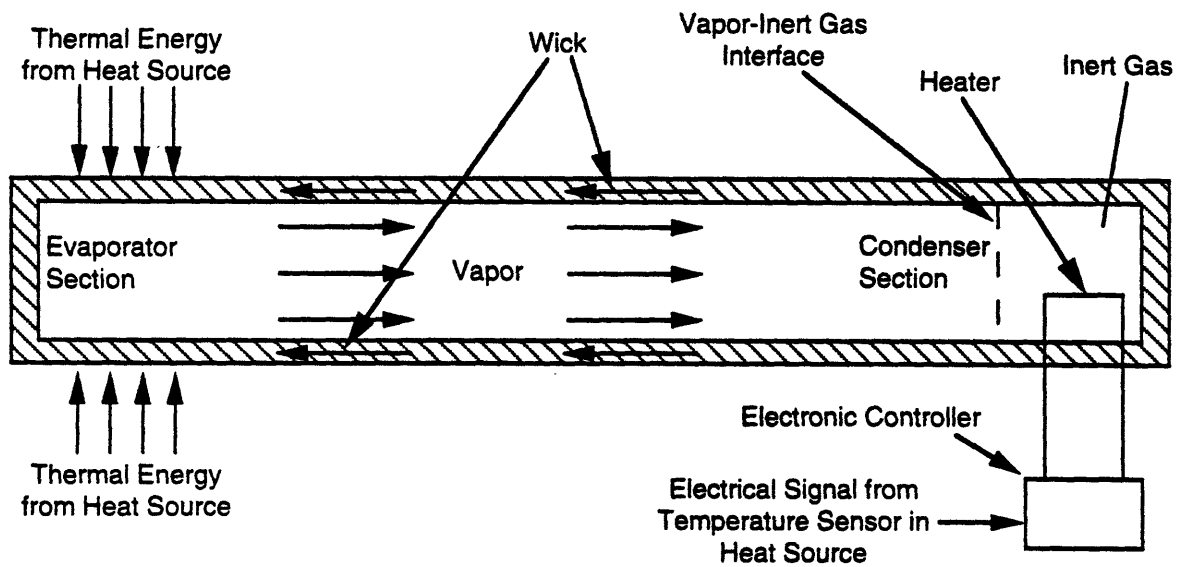


Figure 2.14. Axial Heat Pipe with Inert Gas and Temperature Controlled Rigid-Wall Reservoir. Heater is off and Heat Pipe is in On-Mode.

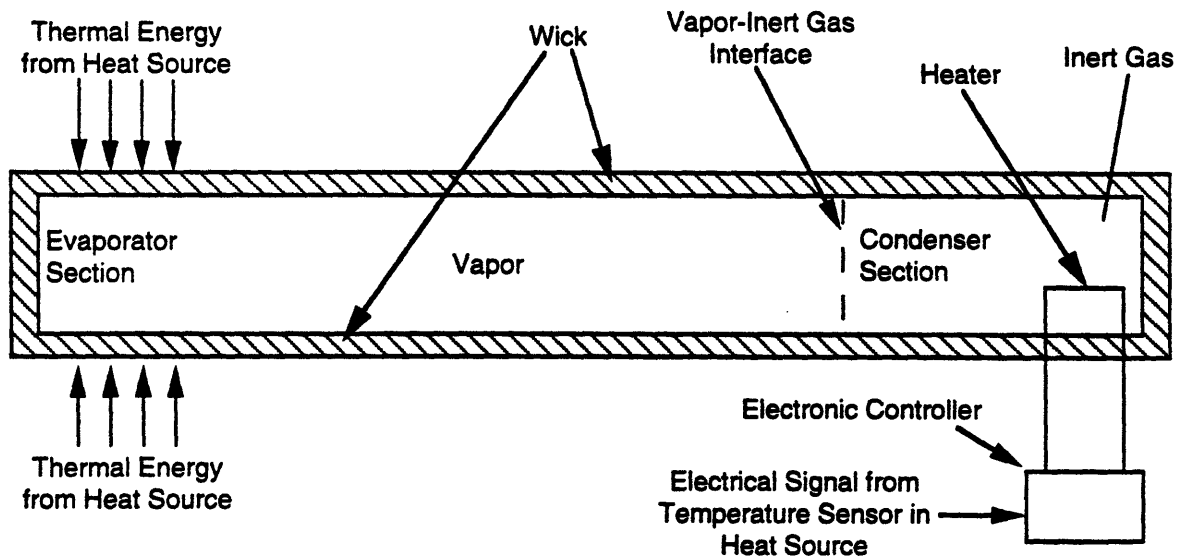


Figure 2.15. Axial Heat Pipe with Inert Gas and Temperature Controlled Rigid-Wall Reservoir. Heater is on and Heat Pipe is in Off-Mode.

hence, reducing thermal energy transport from the heat source. Similarly, allowing the gas to cool increases the amount of condenser surface available to the vapor and, hence, increases thermal energy transport from the heat source. Thus, by using a temperature sensing device at the heat source, and connecting this via a controller to the heater at the reservoir, the reservoir temperature can be regulated so that precise control of the vapor-inert gas interface occurs, maintaining the desired source temperature within precise bounds.

The mechanical feedback control of a heat pipe involves the use of a bellowed-hollow-wall reservoir and a sensing bulb located adjacent to the heat source (see Figures 2.16 and 2.17.). The cavity in the wall of the reservoir contains an auxiliary fluid, usually an incompressible liquid, and is connected to the sensory bulb by a capillary tube. Variations in the source temperature will cause a change in the pressure of the auxiliary fluid, resulting in a displacement of the bellows. This displacement causes the reservoir volume to change and, thus, the location of the vapor-inert gas interface. By relating the displacement of the bellows and, therefore, the vapor-gas interface in the heat pipe, to the temperature of the heat source, a feedback controlled system which regulates the heat-source temperature is obtained.

Comparing the active feedback control (electrical) with the passive feedback control (mechanical), better temperature control of the heat source is obtained using the active feedback control system. In the active system, the location of the vapor-inert gas interface can be more precisely controlled with the heater. However, with the passive feedback control system, there are fewer components, and they are exposed to less severe conditions (i.e., they do not get hot). Consequently, there is less likelihood of system failure. Thus, when selecting a temperature control system, temperature control capability must be weighed against system reliability.

All the control methods discussed above use a vapor/gas interface to vary the heat condenser area available for heat rejection from the heat pipe. Other techniques involving liquid inventory control, vapor flow control, and wick modification are also available.

For heat pipes employing liquid inventory control, it can be achieved in two different ways. One method is to remove and reintroduce the working fluid as needed. Specifically, as the

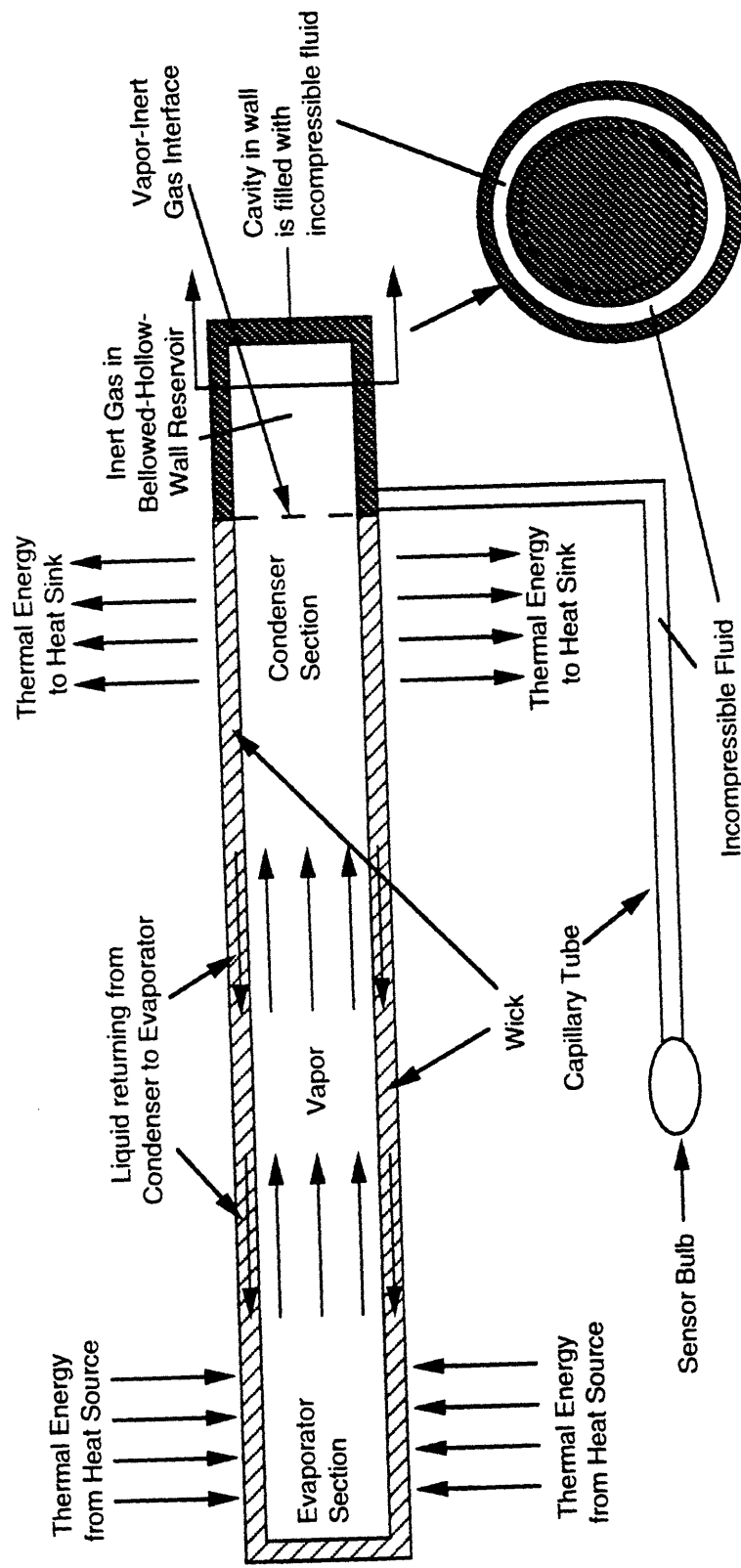


Figure 2.16. Axial Heat Pipe with Inert Gas and Bellowed-Hollow-Wall Reservoir in On-Mode

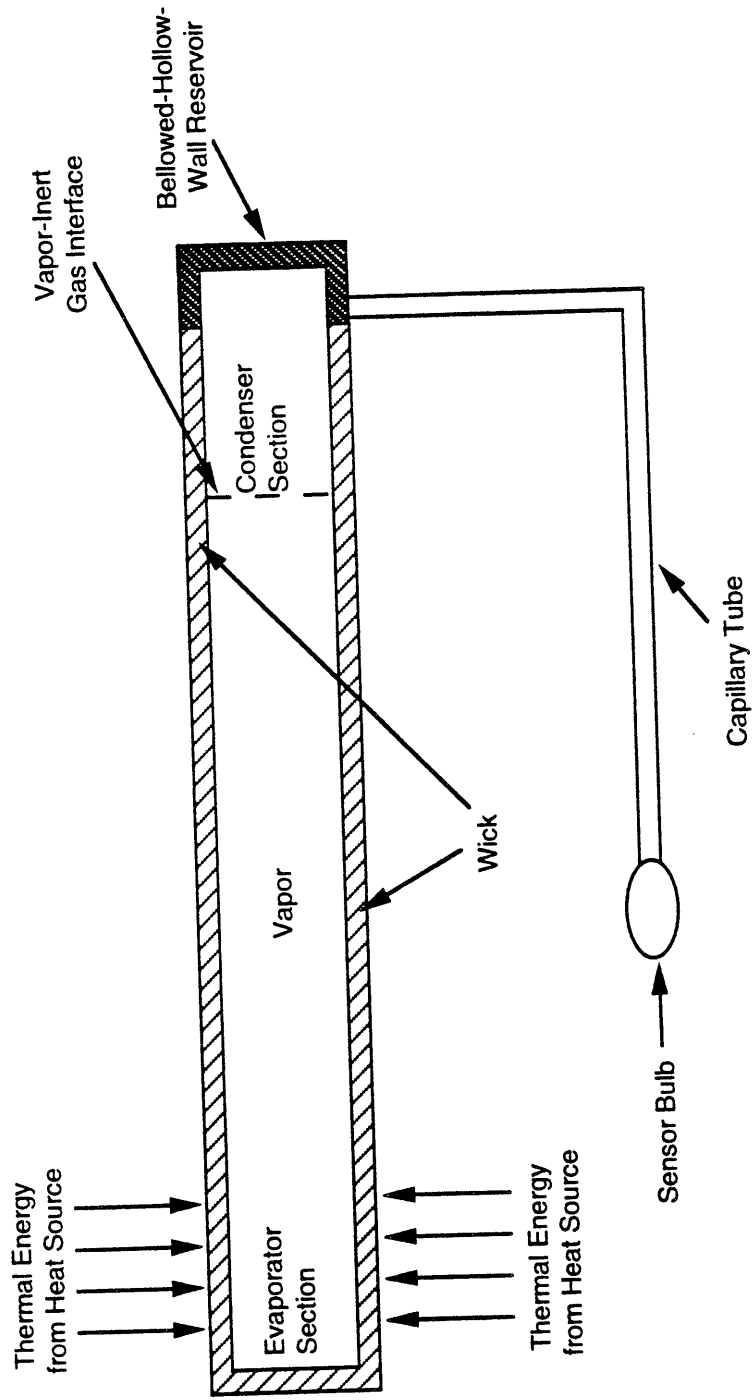


Figure 2.17. Axial Heat Pipe with Inert Gas and Bellowed-Hollow-Wall Reservoir in Off-Mode

working fluid condenses at the condenser section, it is removed from the heat pipe via an exit port located at the lowest point of the condenser section (see Figure 2.18). This working fluid is then recirculated into the heat pipe in discrete quantities by vapor bubble injection under the control of a heater which monitors the temperature of the heat source. If no fluid is injected into the heat pipe, the thermal conductance of the heat pipe will decrease as the condensate is removed. If fluid is injected into the heat pipe, thermal conductance will increase as fluid is supplied to the heat pipe.

Another way of achieving liquid inventory control is to manufacture a heat pipe with a bendable adiabatic section (see Figure 2.19). The amount of curvature in the bendable adiabatic section controls how much liquid returns to the evaporator section of the heat pipe. (The exact physical mechanism is that the static pressure head is increased due to the curvature by creating a longer return path from the condenser to the evaporator for the working fluid. The wick is designed such that the capillary pressure is less than the maximum static pressure head that can be imposed.) As returning liquid condensate is trapped in the center of the deformed tube, less liquid is available for evaporation in the evaporator. This results in a low liquid level that saturates only a portion of the evaporator wick, which yields a high heat pipe thermal impedance. If the heat pipe bendable section is deformed so that all the working fluid is completely trapped in the bendable portion, no liquid is available in the evaporator, and, hence, the heat pipe is completely off (i.e., no thermal energy is transported from the heat source). An external device linked to a heat source temperature sensor controls the amount of bend in the heat pipe, and thus the heat transfer rate of the heat pipe.

Concerning vapor flow control, it can be achieved using an electronic throttle valve located in the adiabatic section of the heat pipe (see Figure 2.20). A heat source temperature sensor and an electronic controller adjust the throttle valve aperture to control the flow of vapor through the pipe. Hence, to decrease the thermal conductance of the heat pipe, the throttle valve aperture is decreased. Conversely, to increase the heat pipe conductance, the throttle valve aperture is increased.

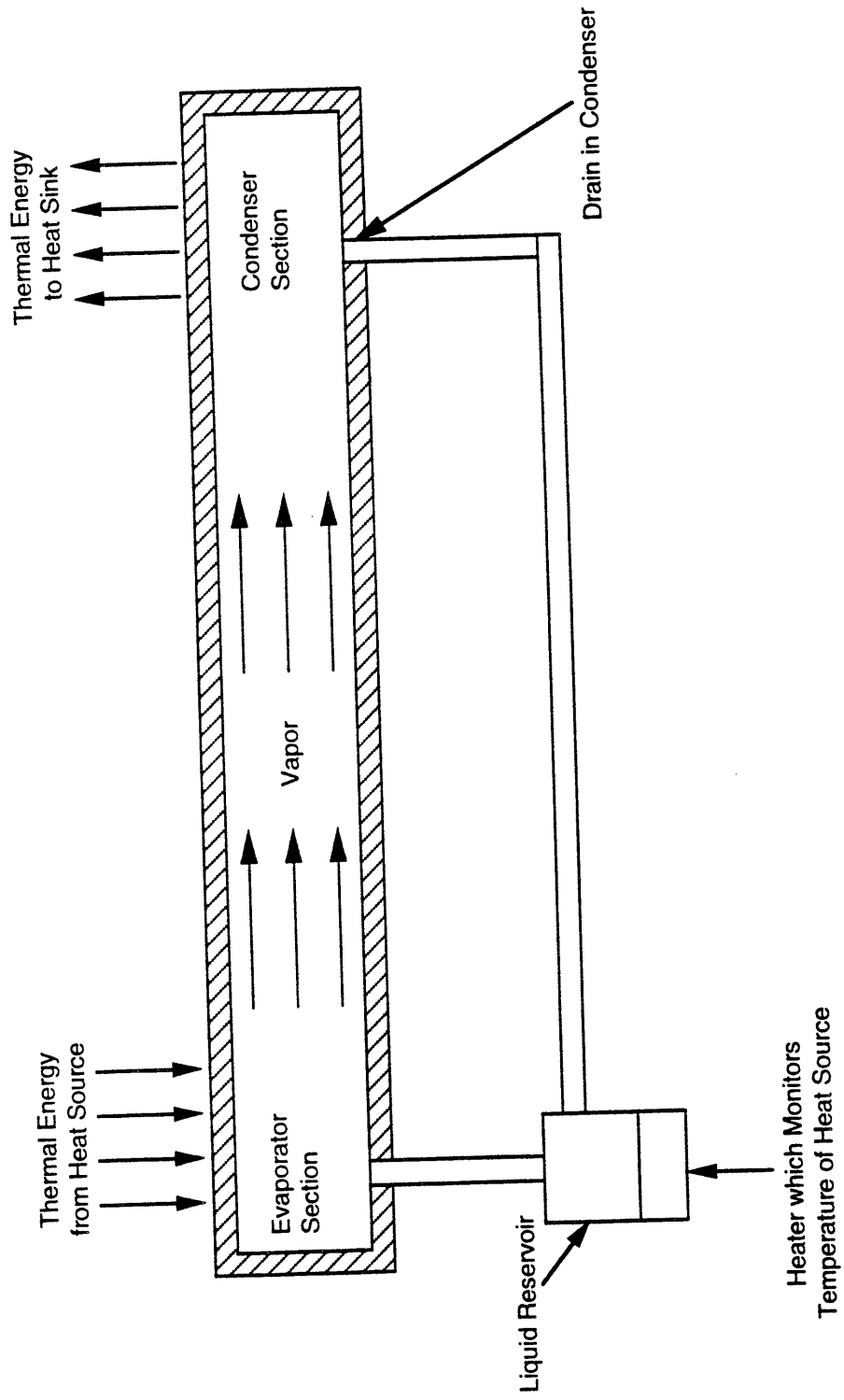


Figure 2.18. Axial Heat Pipe Utilizing Liquid Inventory Control

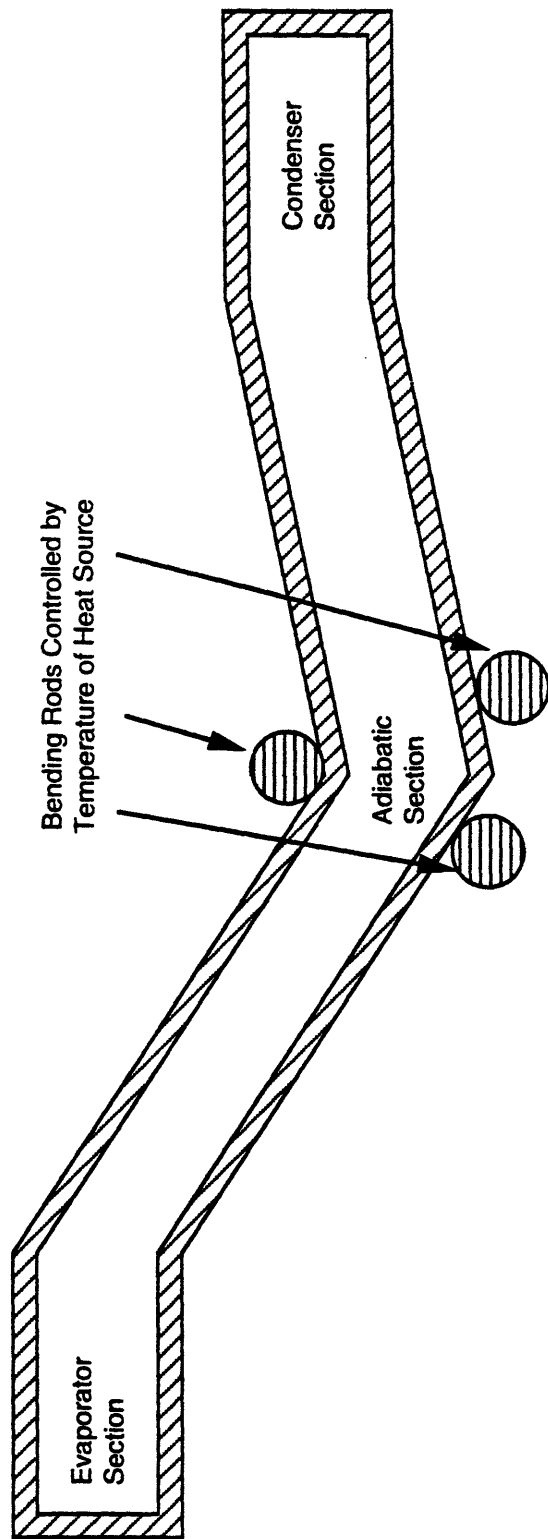


Figure 2.19. Axial Heat Pipe with Bendable Adiabatic Section

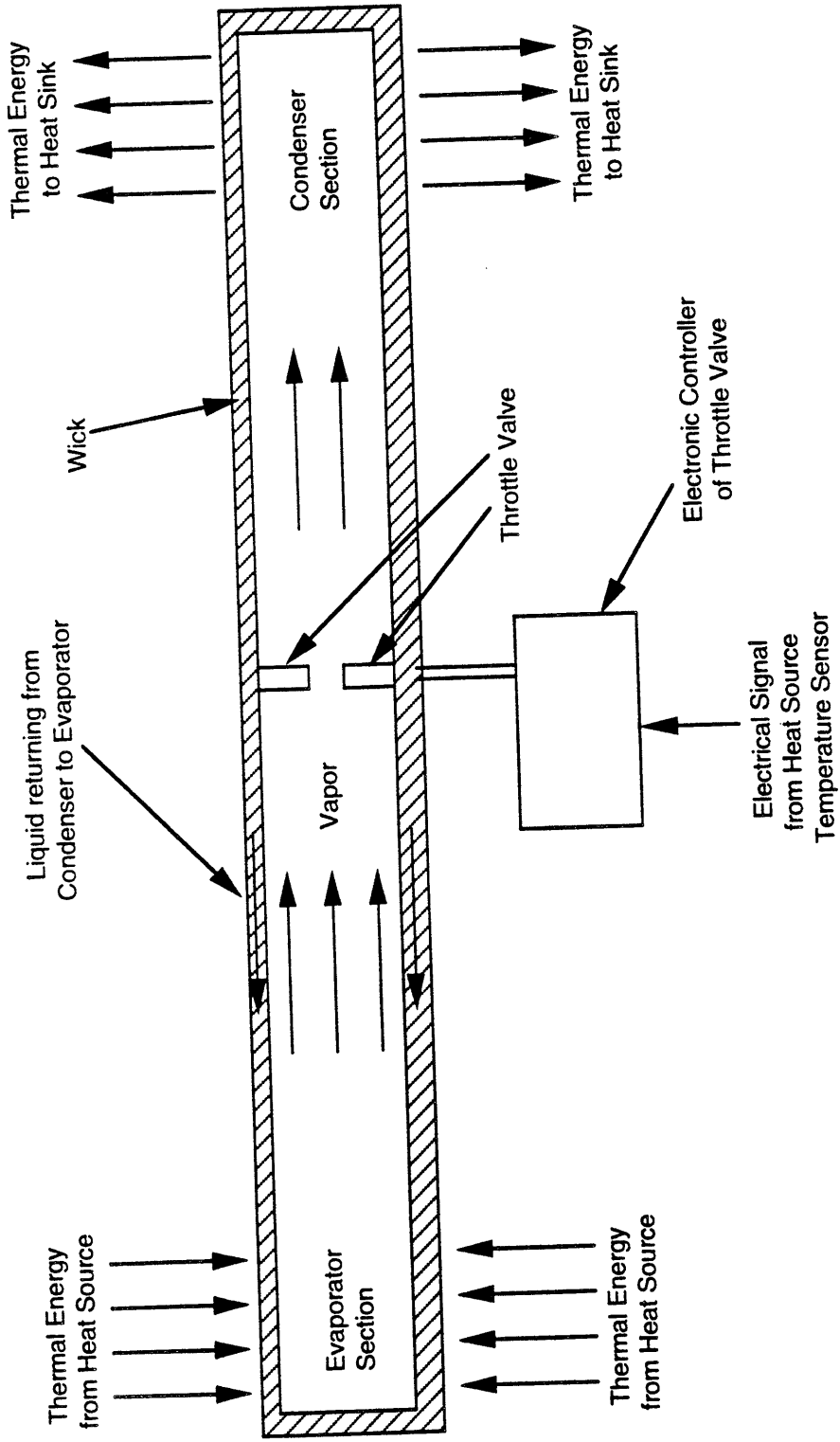


Figure 2.20. Axial Heat Pipe with Throttle Valve

Lastly, heat pipe control can be achieved by wick modification. Thus far, two different ways of wick modification have achieved successful results. One method involves using a wick material which shrinks as its temperature decreases and expands as its temperature increases. Half the axial length of the heat pipe, from the evaporator section to the midpoint of the adiabatic section, utilizes the expanding/contracting wick material. The other axial half of the heat pipe has wick material which maintains a constant axial length (see Figure 2.21). Thus, as the heat source cools off, the expanding/contracting wick material contracts, creating a discontinuity in the wick return path from the condenser to the evaporator section for the working fluid and, hence, turning the heat pipe off. Conversely, as the heat source becomes too hot, the wick material expands completing the wick return path for the working fluids and, hence, turning the heat pipe on. This expanding/contracting wick material has been developed by Hitachi.

The other method of achieving heat pipe control by wick modification also involves using two different wick materials which are separated to turn off the heat pipe, and brought back into contact with one another to turn on the heat pipe. However, the method of creating and removing the discontinuity in the pumping path of the liquid is different. Specifically, the wick material lining the heat pipe from the evaporator section to the midpoint of the adiabatic section is comprised of magnetic material, and the other axial half of the heat pipe is lined with nonmagnetic wick material (see Figure 2.22). An electromagnet is positioned at the point of contact between the two different wick materials (i.e., at the adiabatic section midpoint.) The electromagnet is interfaced with an electronic controller and a temperature sensing unit situated at the heat source. Hence, when the heat source becomes too hot, the electromagnet is activated and moved, bringing into contact at the adiabatic section midpoint the magnetic wick with the nonmagnetic wick. Conversely, when the heat source is at or below its proper temperature, the electromagnetic is used to create a discontinuity at the interfacing point of the two wicks, turning off the heat pipe.

Thus, the heat pipes discussed above represent the major types of axial heat pipes in existence today. They are thermal switches that can be used over a very wide temperature range, from low, cryogenic temperatures (starting from 1K), to molten metal temperatures (2,500-

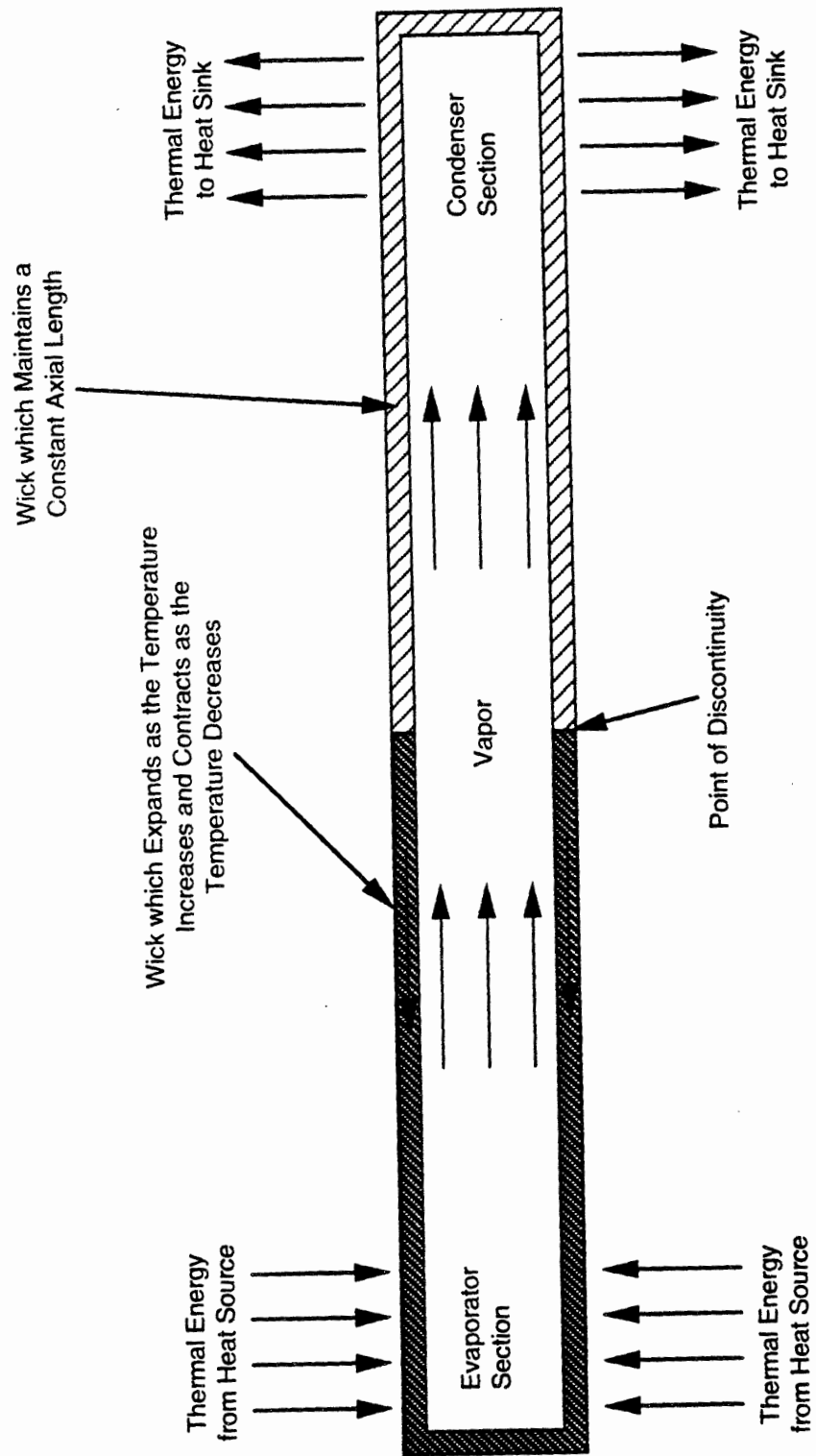


Figure 2.21. Axial Heat Pipe with Expanding/Contracting Wick

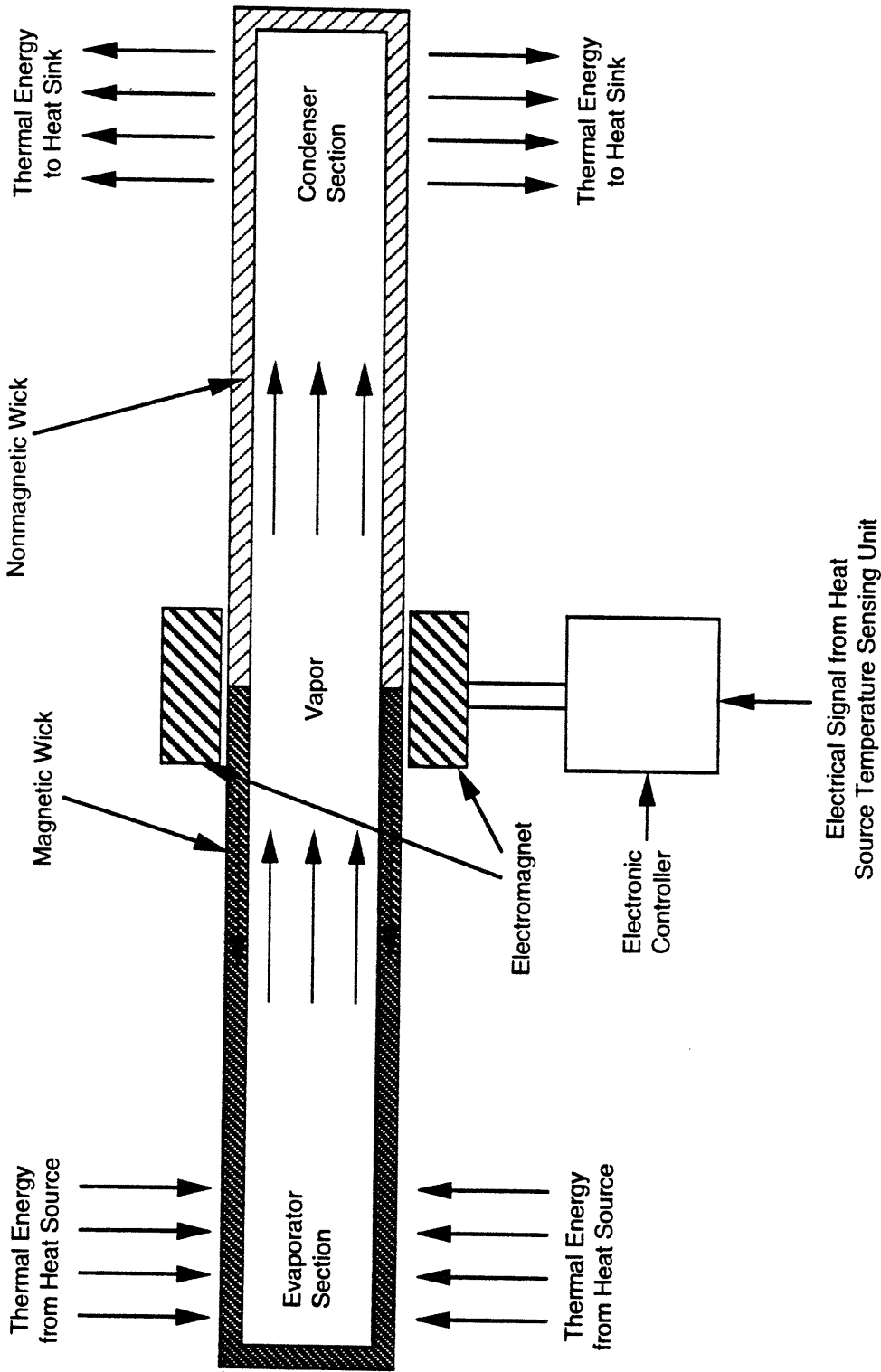


Figure 2.22. Axial Heat Pipe with Magnetic Wick

3,000K). Needless to say, they have found innumerable applications. Indeed, so successful has been this concept of thermal energy transport by vapor convection of latent heat, that variations of the axial heat pipe concept have arisen.

2.6 Radial Heat Pipe⁶

One variation that has proven successful is the radial heat pipe. It is similar to the axial heat pipe in that it is comprised of a container, a wick, and a working fluid. However, its cross-sectional configuration is annular, not circular and its direction of heat transfer is radial, not axial (see Figure 2.23). The evaporator section is usually the small radius surface of the annulus, although it can be the larger radius surface as well. Whichever surface it is, the other surface comprises the condenser section of the radial heat pipe. A wick lines the evaporator section. (If the evaporation section is the smaller-radius surface of the annulus, and the radial heat pipe will not be operating in a directly vertical, position, then care must be taken to ensure that the wick extends far enough radially at some circumferential point to contact and absorb the condensate.) As with the axial heat pipe, thermal energy is absorbed at the evaporation section and released at the condenser section. However, as mentioned above, the direction of vapor travel (and hence heat transfer) is radial, not axial.

2.7 Other Types of Heat Pipes⁵

Other types of heat pipes are electro-hydrodynamic heat pipes, magnetohydrodynamic heat pipes, and osmotic heat pipes. These devices also operate on the evaporation/condensation principle, with the difference arising in the method of condensate return. Electrohydrodynamic heat pipes use electrostatic volume forces to return the condensate to the evaporator section; magnetohydrodynamic heat pipes use magnetic volume forces, and osmotic heat pipes use osmotic forces for condensate return.

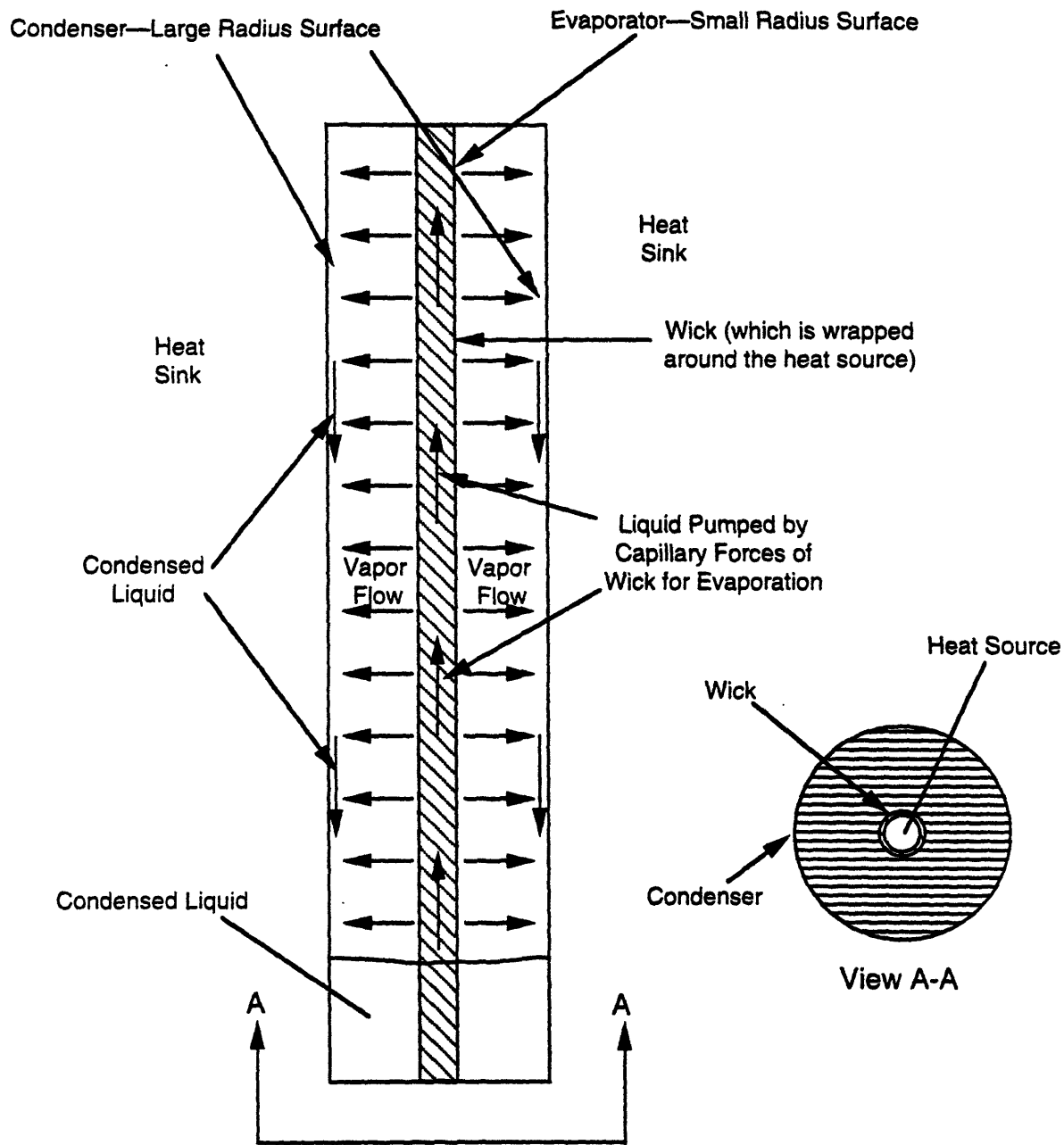


Figure 2.23. Radial Heat Pipe

2.8 Thermal Syphon^{7,8,9}

Another variation of the heat pipe concept is the thermal syphon. There are two different kinds of thermal syphons. One is basically an axial heat pipe without a wick (Figure 2.24), while the other is a loop without a wick (Figure 2.25). For both types of thermal syphons, like the heat pipes, the section between the evaporator and condenser is insulated. However, unlike the heat pipes, since no wick is present, the condenser section must be at a higher elevation than the evaporator section to return the working fluid from the condenser to the evaporator. Thermal syphons would be used instead of heat pipes in situations where the working fluid chosen is reactive with all wick materials available.

A third variation of the heat pipe concepts discussed earlier is the controllable thermal syphon. This device is similar to the axial-like thermal syphon described above, except that an noncondensable, inert gas is also present in the device (see Figure 2.26). Like the gas buffered heat pipes discussed earlier, the inert gas prevents any heat transfer by the thermal syphon until the vapor pressure of the working fluid is high enough to push the gas/vapor interface into the condenser region, allowing exposure of the working fluid vapor to the condenser walls. Suitable initial positioning of the gas/vapor interface yields the desired temperature control of the heat source. It should be noted that this gas-buffered thermal syphon is also known in the heat transfer field as a high conductance vapor thermal switch.

2.9 Bistable Passive Thermal Switch¹⁰

Another kind of thermal switch discovered in the literature survey is the bistable passive thermal switch. The bistable passive thermal switch can be visualized as a metallic cylindrical shell with two pipes running axially through it and linked to an accumulator (see Figure 2.27). One of the pipes runs axially along the bottom of the shell, while the other runs axially along the top of the shell. The lower pipe has hot fluid or gas flowing through it that acquired its thermal energy from a heat source. The upper pipe has cold fluid or gas flowing through it that leads to a heat sink such as a heat exchanger. The entire volume of the metallic cylindrical shell is filled with pressurized

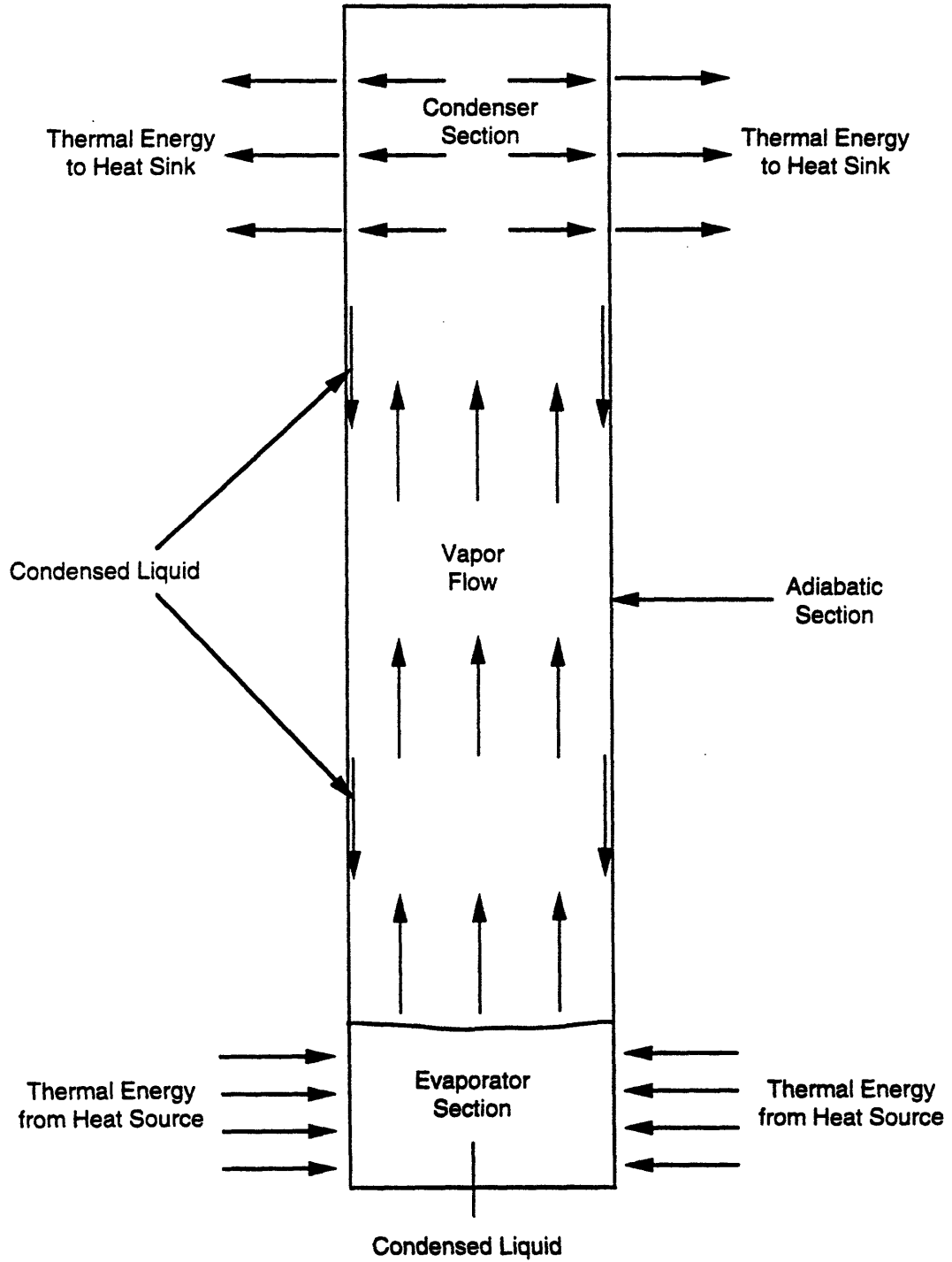


Figure 2.24. Thermal Syphon

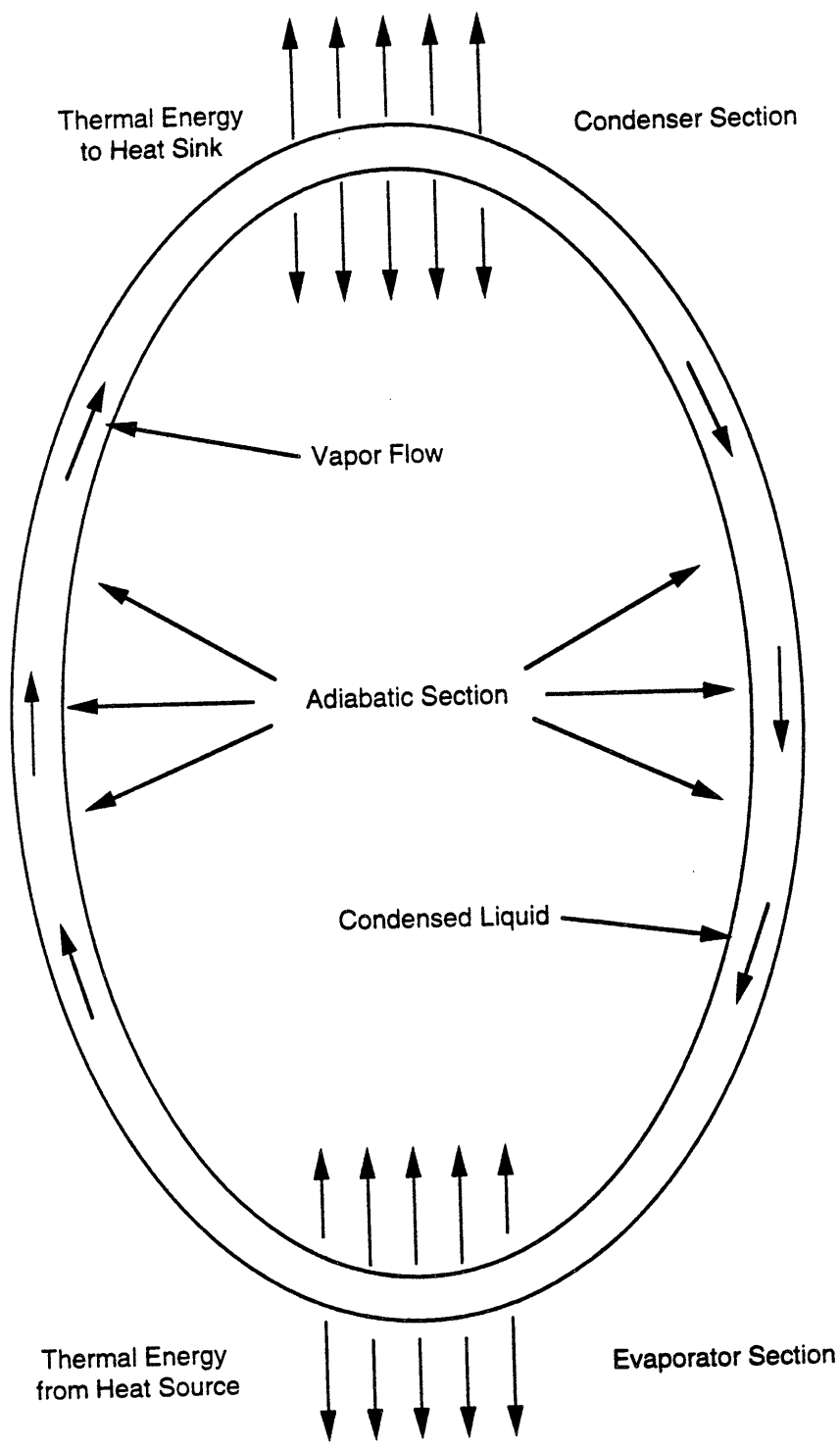


Figure 2.25. Loop Thermal Syphon

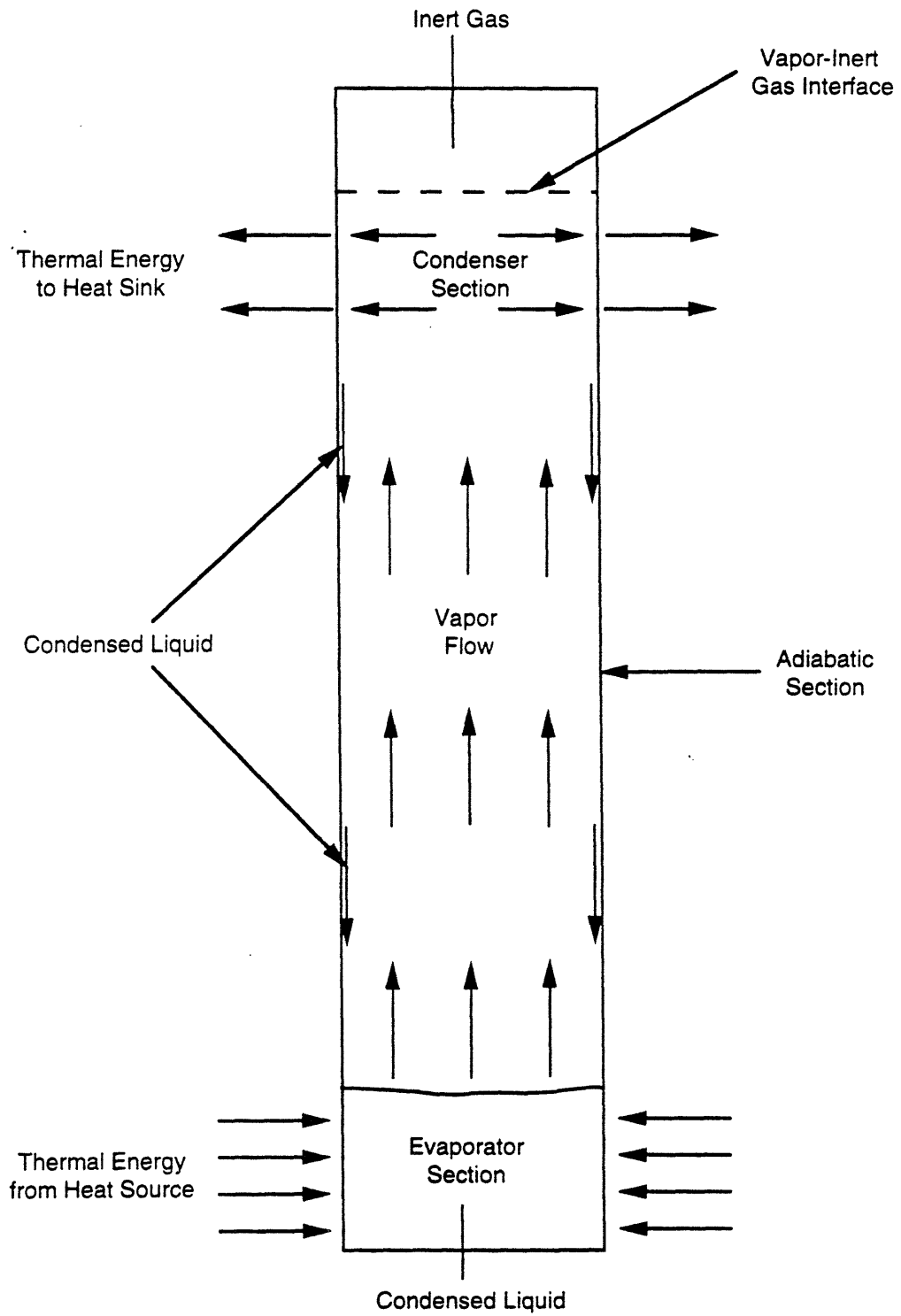


Figure 2.26. Thermal Syphon with Inert Gas

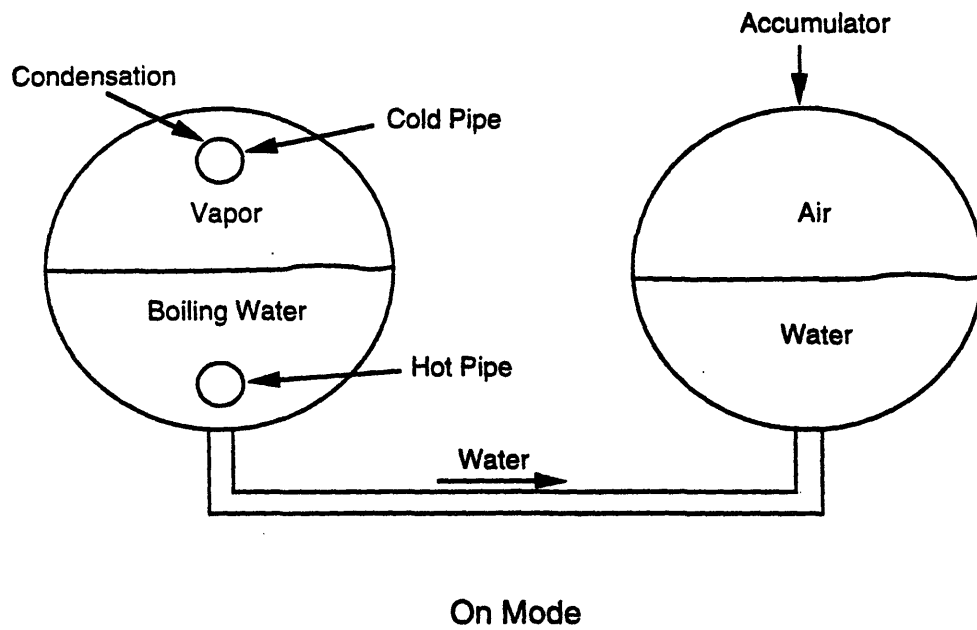
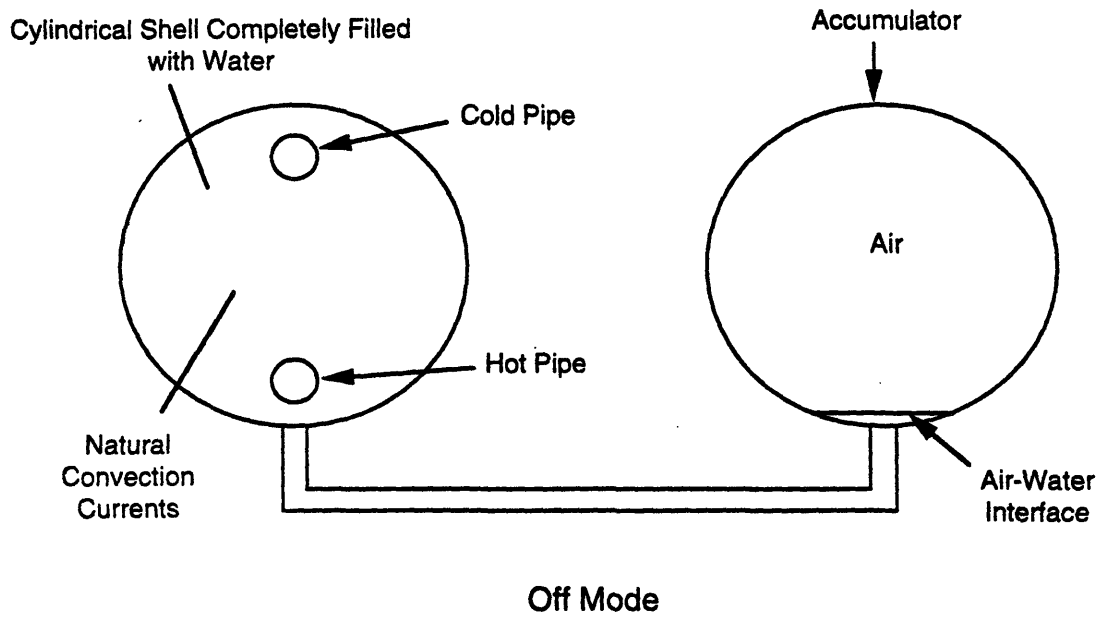


Figure 2.27. Bistable Passive Thermal Switch Without Air in the Cylindrical Shell

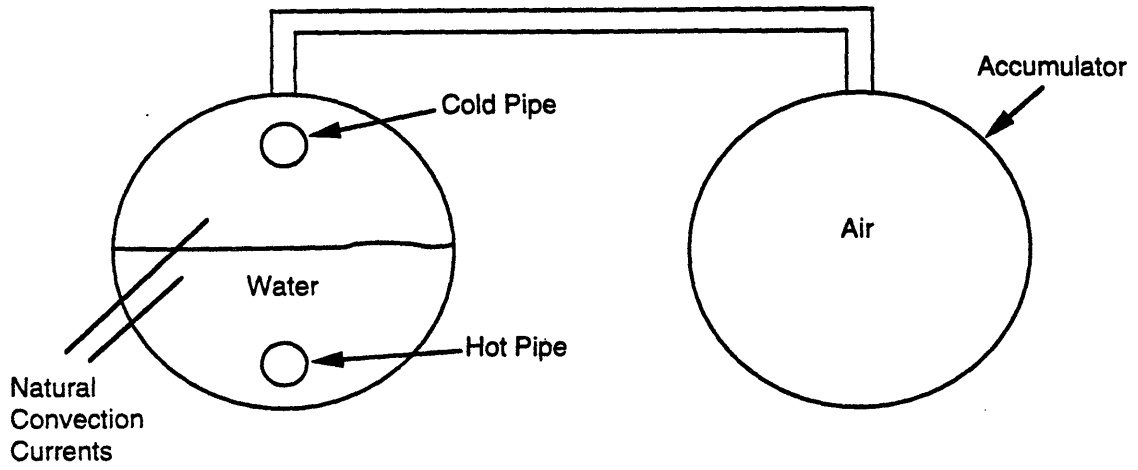
water. Thus, by controlling the shell pressure, the bistable passive thermal switch can be switched on or off. In the off mode the water in the shell is not boiling and transfers only a minimal amount of thermal energy from the hot pipe to the cold pipe via natural circulation. However, during the on mode, the water in the shell boils on the lower pipe (which, as mentioned above, is carrying fluid heated by a heat source), displaces excess water into the accumulator, and condenses steam on the upper pipe (which is carrying cold fluid leading to a heat sink). Heat transfer analysis as well as experimental data indicate two orders of magnitude difference in the heat transfer rate of the thermal switch from its on mode to its off mode.

A variation of the above thermal switch is the inclusion of air in the shell (see Figure 2.28). Specifically, the shell is only partially filled with water with the remaining volume filled with air. Thus, the cold pipe is not submerged in water. This results in a higher thermal resistance in the off mode than the previous design because of the high thermal resistance of the air space. Also, a smaller accumulator can be used. However, the presence of noncondensibles also increases thermal resistance in the on mode. Hence, which thermal switch design one should choose is determined by off-mode heat loss allowance and on-mode heat transfer requirements.

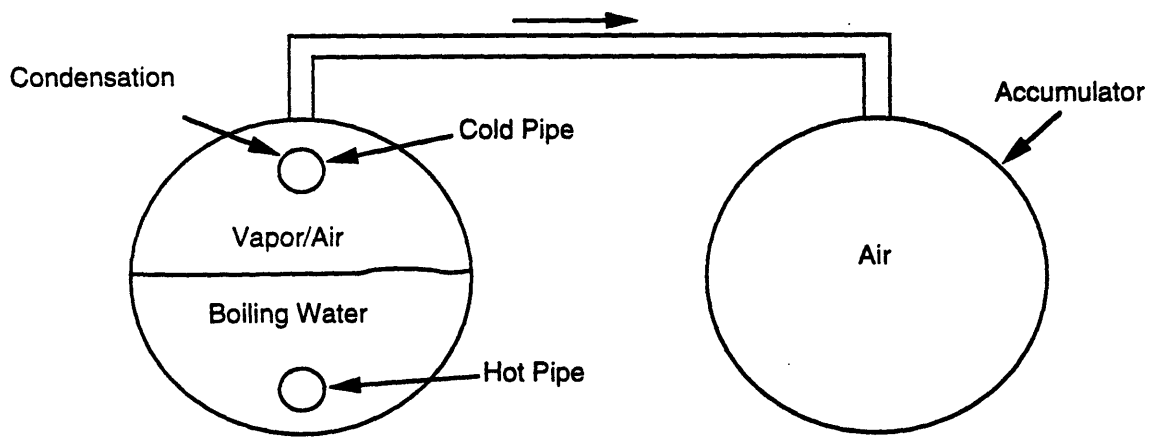
2.10 Temperature-Initiated Passive Cooling System¹¹

The last type of thermal switch discovered in the literature survey is the Temperature-Initiated Passive Cooling System (TIPACS). Shown in Figure 2.29, it was conceived and developed at Oak Ridge National Laboratory and consists of a heat-transfer system (HTS) and a temperature-control system (TCS). The following, partially taken from a paper written by the inventors of the device, C.W. Forsberg and J.C. Conklin, gives a description of the principles of operation of the device as well as its physical characteristics.

As mentioned above, TIPACS consists of two subsystems: a heat-transfer system (HTS) and a temperature-control system (TCS). The HTS is a single-phase, sealed, natural-circulation system that uses a heat-transfer fluid operating just above its vapor-liquid critical point. (The vapor-liquid critical point is the state beyond which the difference between the vapor phase and the



Off Mode



On Mode

Figure 2.28. Bistable Passive Thermal Switch With Air in the Cylindrical Shell

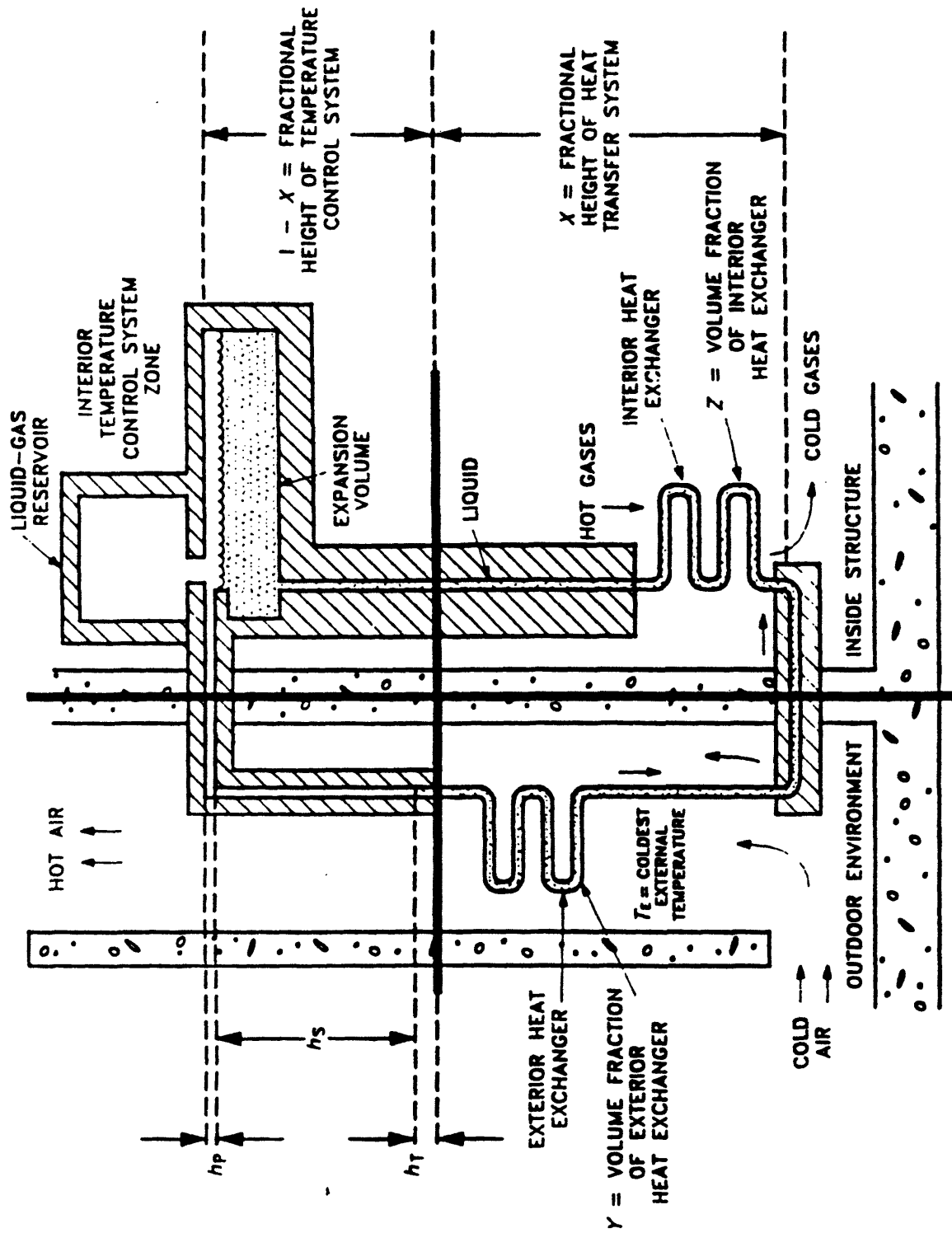


Figure 2.29. Temperature-Initiated Passive Cooling System

liquid phase no longer exists and only a supercritical-phase exists.) Thermal energy generated by the heat source is cooled by the internal TIPACS heat exchanger. The warm, lower-density supercritical fluid inside the internal heat exchanger flows upward to an air-cooled external heat exchanger. The supercritical fluid is cooled as its heat is transferred to the environment through the external heat exchanger, and the cooler, higher-density fluid flows downward back to the internal heat exchanger.

The TCS is the insulated piping and apparatus above the heat exchangers. It is a passive device that blocks the flow of fluid if the heat source temperature drops below the vapor-liquid critical point, and allows the flow of fluid if the heat source temperature is above the critical temperature of the working fluid and above the heat sink temperature. It accomplishes this via its piping geometry. Specifically, below the critical-point temperature the fluid in the system is partly liquid and partly gas, with gas-liquid interfaces in the insulated piping above the heat exchangers (i.e., in the TCS). Thus, it is this gas zone in the TCS at the top of TIPACS that prevents the liquid from flowing around the natural-circulation heat transfer loop. However, as the temperature approaches the critical point, (1) the liquid expands to fill the vapor space, (2) the two-phase system then converts to a single-phase supercritical system, (3) the vapor lock is eliminated, and (4), if the heat source temperature is above the heat sink temperature, the single-phase HTS starts up. The HTS will not start up if the heat sink temperature exceeds the heat source temperature because the external heat exchanger is at a higher elevation than the internal heat exchanger. (In this situation, hot, low-density fluid fills the TCS, while colder, higher-density fluid settles to the bottom of the HTS, creating a dynamically stable fluid configuration. Hence, no fluid circulation occurs.)

Note that HTS performance is maximized when (a) the fluid pressure is just above the fluid's critical pressure and (b) the operating temperature range from hot to cold is just above the fluid's critical temperature. This phenomenon is a direct result of the thermodynamic and transport properties of fluids near their critical points. (Four physical properties primarily determine the performance of a natural-circulation HTS: thermal expansion of the fluid with

temperature over its operating ranges, dynamic viscosity, specific heat capacity, and thermal conductivity. In each case, the best fluid properties of any fluid for heat transfer occur near the critical point. Viscosity is at a minimum. The thermal expansion coefficient, specific-heat capacity, and thermal conductivity are near their maximums. This implies very high performance near the critical point.) The TCS requires operation in this region to ensure the initiation of the TIPACS at a preset temperature, but, coincidentally, it implies excellent HTS performance.

Different startup/shutdown temperatures can be selected by choosing fluids with different vapor-liquid critical points. Because all fluids have critical point temperatures unless they thermally decompose before the critical point is reached, there is a wide choice of options—from helium at -267.96°C to mercury at 900°C .

The TCS imposes some design constraints. The TCS operation is dependent upon the expansion of the working fluid until a natural circulation HTS is created. The working fluid is both the temperature sensor and control mechanism. If internal temperatures are to control TIPACS, most of the fluid volume must be in the inside zones of the TIPACS. If the normal design of the HTS does not result in most of the liquid residing in the interior zone, more storage volume for the liquid must be added to this zone.

The TCS may contain an expansion reservoir. The expansion reservoir handles the expansion liquid from the exterior heat exchanger from the coldest design conditions to a few degrees below the critical temperature without activating TIPACS. This expansion volume is small because most of the thermal expansion of the liquid that occurs is within a few degrees of the critical point.

There is a minimum height of the interior TCS based on the design of the HTS. In a standby mode, the liquid on the inside will be hotter than the liquid on the outside and, hence, have a lower fluid density. To maintain a static balance between the interior (hot) liquid and exterior (cold) liquid, the two liquid heights must vary by height h_s (see Figure 2.29). This implies that the minimum height of the TCS is the sum of the height required for the hot-cold transition zone (h_T) in the outside TCS, and some piping height (h_p) and the height h_s .

The height of the TCS is dependent upon the placement and geometry of the expansion volume. The TCS height is minimized if the expansion volume starts directly above the minimum height and is a wide, shallow vessel. As a wide, shallow vessel, the height of fluid in the inside TCS volume does not change significantly with expansion or contraction of the liquid. In effect, the height of liquid in the inside TCS is fixed, while the height of liquid in the outside TCS varies.

The TCS may contain a gas-liquid expansion volume above the expansion reservoir. This allows the option of controlled startup of TIPACS from liquid expansion before the critical point is reached. Because of fluid properties and other phenomena, heat-transfer rates are limited compared to operation above the critical point.

Thus the Temperature-Initiated Passive Cooling System (TIPACS) is a passive cooling system that transfers heat from a hot, insulated system to a cooler external environment. It is comprised of two subsystems: a heat-transfer system and a temperature-control system. Possible applications include cooling (1) building attics, (2) electrical sheds, (3) chemical reactors, (4) utility-load leveling batteries, and (5) nuclear reactor containments.

2.11 Chapter Summary

In this chapter, the key passive thermal switches that have been developed over the last several decades are described and categorized as to heat transfer type. The existing passive thermal switches include High-Temperature Gas-Gap Thermal Switch, Electrolytic Thermal Switch, Shape-Memory Thermal Switch, Ceramic-Foam-with-Impregnated-Metal Thermal Switch, Axial Heat Pipe, Radial Heat Pipe, Electrohydrodynamic Heat Pipe, Magnetohydrodynamic Heat Pipe, Osmotic Heat Pipe, Thermal Syphon, Bistable Passive Thermal Switch, and the Temperature-Initiated Passive Cooling System. They are categorized as to type of thermal switch in Figure 2.30, and summarized in Table 2.1.

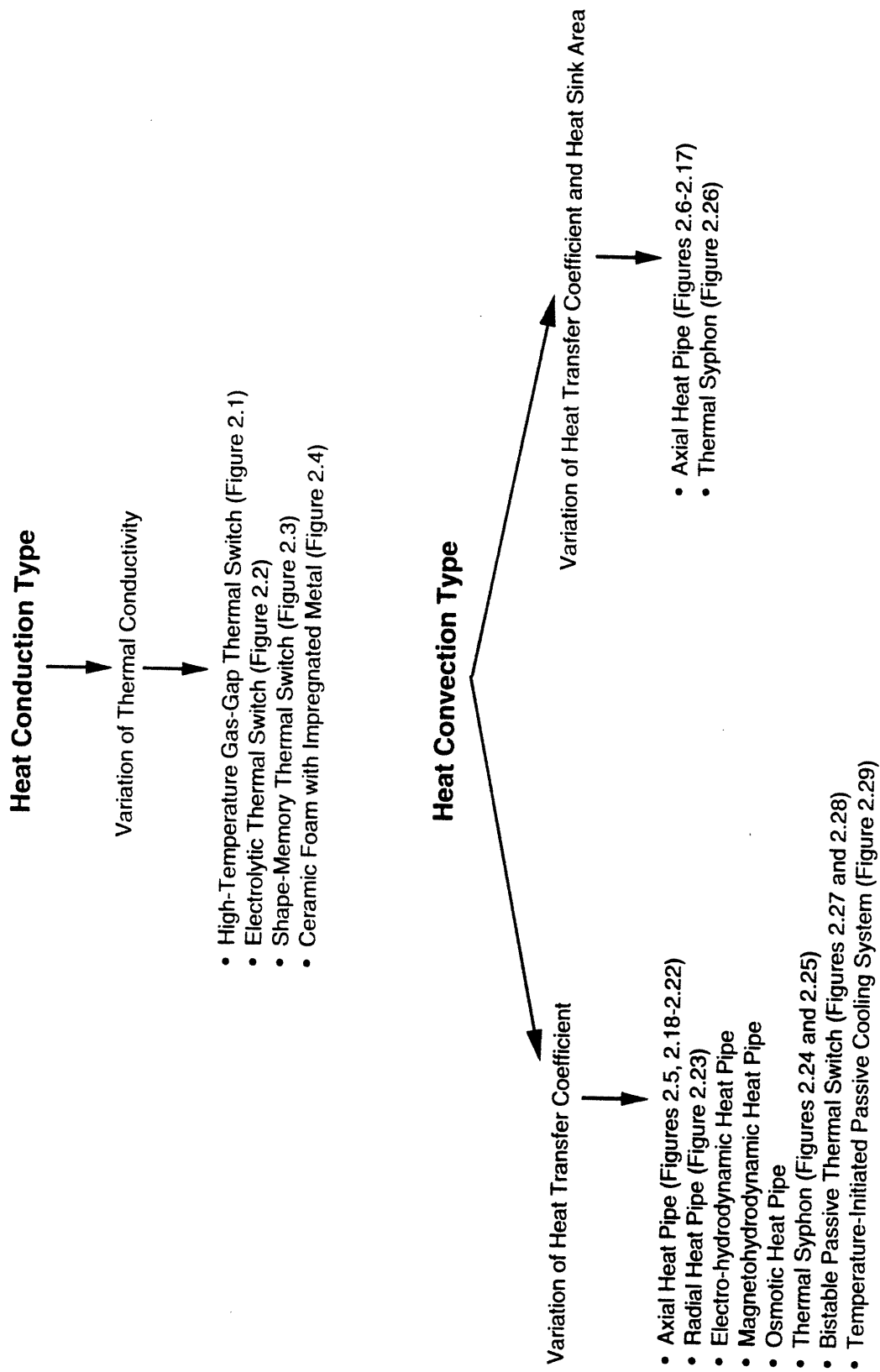


Figure 2.30. Categorization of Thermal Switches

Table 2.1

Thermal Switch	General Comments
High-Temperature Gas-Gap Thermal Switch	<p>This thermal switch involves filling the gap between the heat source and heat sink with a low-absorptivity and low emissivity metal foil, and woven quartz fibers between the layers of foil. With no gas present, the thermal switch is off. The thermal switch is turned on by injecting a gas such as helium, hydrogen, nitrogen, or argon. Temperature operating range is 100°C to 1500°C.</p>
Electrolytic Thermal Switch	<p>Device is composed of an inner electrically conductive layer of low thermal conductivity sandwiched between two metal foil electrodes of high thermal conductivity. The device is turned on by applying an electric potential across the electrodes, and turned off by removing this electric potential. Presently the switching ratio is 1.21.</p>
Shape-Memory Thermal Switch	<p>This device alters its shape with temperature. Thus, as its temperature increases it can be made to physically contact a heat sink, and as its temperature decreases the contact will be broken. The three shape-memory alloys are NiTi (Nickel and Titanium), Cu-Zn-Al (Copper, Zinc, and Aluminum), and Cu-Al-Ni (Copper, Aluminum, and Nickel).</p>
Ceramic-Foam-with-Impregnated-Metal Thermal Switch	<p>This thermal switch is comprised of ceramic foam uniformly impregnated with a metal. This thermal switch is a thermal conductor in the off-mode and thermal insulator in the on-mode. It remains a thermal conductor until the melting point of the metal impregnates is reached.</p>
Axial Heat Pipe	<p>This device is comprised of an enclosed container, usually cylindrical in shape, which contains a wick and a working fluid. The thermal energy is absorbed at one end of the heat pipe (the evaporator section) and released at the other end (the condenser section). Different working fluids with different boiling points, noncondensable gases, liquid inventory control, liquid flow control, vapor flow control, and wick modification offer a variety of ways to control when the heat pipe is in the on-mode.</p>

Radial Heat Pipe	<p>Like the axial heat pipe, it is comprised of a container, a wick, and a working fluid. However, unlike the axial heat pipe, the container is annular in shape, the direction of heat transfer is radial, and both the evaporator section and the condenser section run the entire length of the heat pipe. The evaporator section is usually concentric to the condenser section, although the converse can occur as well.</p>
Thermal Syphon	<p>The thermal syphon is basically a heat pipe without a wick. Condensate is returned to the evaporator section via the force of gravity. (Hence, the evaporator section must be at a lower elevation than the condenser section.) The shape of the thermal syphon can be either that of an axial heat pipe or a loop. Thermal syphons can be controlled via the working fluid used or through the usage of a noncondensable gas.</p>
Electrohydrodynamic Heat Pipe, Magnetohydrodynamic Heat Pipe, and the Osmotic Heat Pipe	<p>These devices are similar to the thermal syphon. The difference arises in their method of condensate return. The electrohydrodynamic heat pipe uses electrostatic volume forces to return the condensate to the evaporator section; the magnetohydrodynamic heat pipe uses magnetic volume forces, and the osmotic heat pipe uses osmotic forces for condensate return.</p>
Bistable Passive Thermal Switch	<p>This thermal switch is comprised of a metallic shell with two pipes running axially through it and linked to an accumulator. The surfaces of these two pipes are the heat transferring surfaces of the thermal switch. Hot fluid due to cooling of the heat source runs through the bottom pipe and cold fluid which circulates through the heat exchanger runs through the top pipe. The space between the two surfaces is either completely filled with pressurized water or with pressurized water and air. The pressure is adjusted so that during the off-mode of the thermal switch no boiling of the water occurs. In the on-mode, the pressure is reduced so that two-phase heat transfer can take place between the hot pipe and the cold pipe. The accumulators accommodate the displaced water or water and air during the on-mode of the thermal switch.</p>

Temperature-Initiated
Passive Cooling System
(TIPACS)

TIPACS is a passive cooling system that transfers heat from a hot internal system to a cooler external environment. It is a device that consists of two subsystems: a heat-transfer system (HTS) and a temperature-control system (TCS). The HTS is a single-phase, sealed, natural-circulation system comprised of tubing, an internal heat exchanger, and an external heat exchanger. It uses a heat-transfer fluid operating just above its vapor-liquid critical point to transfer thermal energy from the internal system to the environment. The TCS is a passive device that blocks the flow of fluid if the interior temperature drops below the vapor-liquid critical point, or if the heat sink temperature exceeds the heat source temperature. The TCS is comprised of the insulating piping and apparatus above the heat exchangers of the HTS. Different startup (and thus different shutdown) temperatures can be selected by choosing fluids with different vapor-liquid critical points.

References for Chapter Two

- [1] NASA Tech Brief; High Temperature Gas-Gap Thermal Switch; NPO-17163/TN (Refer to this number when contacting the Director of Technology Transfer Division at 301-621-0100 Ext. 241 for additional information on this thermal switch.); Feb 1989.
- [2] NASA Tech Brief; Electrolytic Thermal Switch; MFS-26074/TN (Refer to this number when contacting the Director of Technology Transfer Division at 301-621-0100 Ext. 241 for additional information on this thermal switch.); August 1989.
- [3] Duerig, T. W., Albrecht, J., and Gessinger, G. H.; A Shape-Memory Alloy for High-Temperature Applications; Journal of Metals; December 1982.
- [4] Bustard, T. S., Princiotta, F. T., and Barr, H. N.; Re-entry Protection For Radioisotope Heat Sources; Nuclear Applications & Technology; Vol. 9, October 1970
- [5] Dunn, P. D. and Reay, D. A.; Heat Pipes; Oxford, Pergamon Press, 1976.
- [6] Gregorie, K. E. and Pfefferlen, H. C.; Thermal Switch Heat Pipe; United States Patent 3,854,524; Awarded December 17, 1974.
- [7] NASA Tech Brief; High Conductance Vapor Thermal Switch; 68-10519; May 1, 1967.
- [8] Yamamoto, J.; Performance of Gas-Filled Thermal Switches; Osaka University; Suita, Osaka, Japan; 1980.
- [9] Lock, G.S.H.; Mechanical Engineering Department of the University of Alberta; Alberta, Canada.
- [10] Anand, G. and Christensen, R. N.; Bistable Passive Heat Transfer System for Emergency Core Cooling System; Joint Congress of The European Nuclear Society/The American Nuclear Society; Lyon, France September 23-28, 1990.
- 11) Forsberg, C. W. and Conklin, J.C.; Temperature-Initiated Passive Cooling System; Twenty-Ninth Intersociety Energy Conversion Engineering Conference; Monterey, California August 7-12, 1994.

Chapter Three

Conceived Passive Thermal Switches

3.1 Introduction

As mentioned in the introduction, the need for temperature control permeates many different technological areas. Manufacturing processes, energy production, operation of various kinds of mechanical devices, all involve the need for temperature control. The thermal switches discussed in Chapter Two are some of the devices that are utilized in this capacity. Heat pipes are mechanically attached to furnace surfaces, thermal syphons are interfaced with mechanical engines, shape-memory thermal switches are soldered to electronic equipment, all to remove or dissipate excessive thermal energy and, hence, prevent overheating. However, these existing passive control devices cannot be applied to all temperature control situations. In many instances, active temperature control mechanisms must be used to prevent overheating. These active systems do achieve the temperature-control objectives, but they have a higher probability of failure than passive temperature control devices. Consequently, with this in mind, new passive temperature control devices were conceived to supplement the existing ones and to provide alternative temperature control methods for situations where active temperature control mechanisms are presently used. As mentioned in Chapter One, they are first categorized and described narratively in table format, and then shown schematically.

3.2 Categorization and Description of Thermal Switches

The tables on the following pages divide thermal switch concepts into heat-conduction type, heat-convection type, and thermal-radiation type. Within each of these three major

categories are several subcategories which indicate the parameter being altered to control the switching action of the thermal switch.

Table 3.1 categorizes and discusses the heat-conduction type thermal switches. The two major subcategories are variation of thermal conductivity and variation of cross-sectional area. The variation-of-thermal conductivity concepts involve increasing the thermal conductivity of the thermal switch to turn it on, and decreasing the thermal conductivity to turn it off. The thermal switches that fall into this subcategory are the particle-bed thermal switch, the change-of-phase-structure-bar thermal switch, the dissociation thermal switch, and the phase-change thermal switch. The variation-of-cross-sectional area subcategory involves a thermal switch concept in which a bar, which is physically connected to the heat source and the heat sink, increases in cross-sectional area in the on-mode to increase the heat transfer rate between the heat source and heat sink, and decreases in cross-sectional area in the off-mode. This thermal switch is designated the variable-cross-section thermal switch.

Table 3.2 categorizes and discusses the heat-convection type thermal switches. The subcategories for these of thermal switches are variation-of-heat-transfer-coefficient and variation-of-surface-area-of-component-surfaces. The concepts listed under the first subcategory involve increasing the heat transfer coefficient of the thermal switch when the heat source becomes abnormally hot (i.e., turning the thermal switch on when the heat source overheats), and decreasing the heat transfer coefficient of the thermal switch (i.e., turning the thermal switch off) as the heat source's temperature decreases back to its normal value. The thermal switches conceived in this subcategory are the chamber thermal switch, the chemical thermal switch, the wick thermal switch, the evaporation-condensation thermal switch, and the liquid-vapor thermal switch. The second subcategory contains thermal switch concepts which involve increasing the surface area of the heat source and heat sink during the on-mode of the thermal switch, and conversely, decreasing the surface area of the heat source and heat sink during the off-mode of the thermal switch. This change in surface area is accomplished either by grain growth on the

heat source and heat sink surfaces, or by the expansion of the grooved wall attached to the heat source and heat sink surfaces.

The last table, Table 3.3, categorizes and describes thermal-radiation type thermal switches. The subcategories for these thermal switches are variation-of-surface-emissivity-of-heat-source-and-surface-absorptivity-of-heat-sink, variation-of-surface-area-of-heat-source-and-heat-sink, and variation-of-area-configuration-factor-product-of-heat-source-and-heat-sink. For the first subcategory, the thermal switches turn on by increasing the surface emissivity of the heat source and the surface absorptivity of the heat sink, and turn off by decreasing these two parameters. These changes of surface emissivity and surface absorptivity are brought about by a surface composition change of the heat source and heat sink. This surface composition change is brought about either by temperature change of the surfaces of the heat source and heat sink, or by release of a chemical into the void between the heat source surface and the heat sink surface which reacts with the surfaces (changing their surface composition and, hence, their spectral characteristics). In the next subcategory, variation-of-surface-area-of-heat-source-and-heat-sink, two thermal switch concepts are discussed. These concepts, grain growth on the heat source and heat sink surfaces and expansion of a grooved wall on the heat source and sink surfaces, are the same concepts discussed in the heat-convection types of thermal switch category. This is due to the fact that surface area of the heat source and heat sink is a performance parameter for both heat-convection types of thermal switches and thermal-radiation types of thermal switches. The last subcategory, variation-of-area-configuration-factor-product-of-heat-source-and-heat-sink, contains three thermal switch concepts. One involves using a gas in the void between the heat source and heat sink whose transmissivity increases with temperature. This allows a greater fraction of the thermal energy from the heat source to be intercepted by the heat sink as the temperature of the heat source (and, hence, gas) increases, resulting in a larger configuration factor and, hence, in a larger area-configuration-factor product. Another concept involves using two screens which lie on top of one another and are located at the heat source surface. The two screens have different coefficients of thermal expansion and different emissivities. The top

screen has a much lower emissivity than the bottom screen. Under normal temperature conditions, the top screen blocks direct viewing of the bottom screen by the heat sink. However, as the heat source overheats, the screens become hotter and expand differently, resulting in the higher emissivity bottom screen having direct view of the heat sink surface. This concept increases both the heat transfer area and the configuration factor between the heat source and heat sink, thus increasing the area-configuration-factor product. The last thermal switch concept discussed in this subcategory involves placing fins on the heat source surface and the heat sink surface. The fins from the heat source are interlocked with the fins from the heat sink. Like the previous concept, a larger area-configuration-factor product results from an increase in the heat transfer area and the configuration factor between the heat source and heat sink.

Table 3.1

Heat Conduction Types of Thermal Switches

Enhancement of Thermal Conductivity

Particle Bed Thermal Switch (Figure 3.1)

A superior thermal conducting pathway is created by adding a conducting material to a normally insulating configuration. Under normal operating conditions, only a bed of particles is present which has a low thermal conductance between the hot component and the cold component. When the temperature becomes abnormally high, a liquid or gas flows in via the melting of a rupture disk and, with the solid bed particles, creates a pathway with a larger thermal conductance. A negative aspect of this kind of thermal switch is that the liquid or gas must be mechanically pumped out once conditions have returned to normal. However, this is a minor drawback. Various parameters such as type of solid particles, size of particles, packing density of particles, surface roughness of particles, shape of particles, and type of gas or liquid need to be investigated.

Dissociation Thermal Switch (Figure 3.2)

A solid, liquid, or gas, placed in the cavity between the heat source and heat sink, dissociates as the temperature increases, yielding a gas (or several gases) which has better conducting properties than the original component and, hence, conducts away the excess heat energy. As the temperature decreases, the dissociated components recombine, forming the original solid, liquid, or gas. Different solids, liquids, and gases need to be investigated for heat transfer effectiveness, material compatibility (with the hot and cold components), and thermal cycling effects. Also, proper chemical quantities need to be determined.

Table 3.1 (cont)

Heat Conduction Types of Thermal Switches

Enhancement of Thermal Conductivity

Change of Solid-Phase Structure Bar (Figure 3.3)

A solid bar, connected to the hot component and cold component, undergoes a change in solid-phase structure as its temperature increases which, in turn, will increase its thermal conductivity. Conversely, as the temperature decreases the bar reverts back to its original solid-phase structure. The task here is to find a material which at low temperatures has a high thermal resistance, but whose thermal conducting properties improve at high temperature (via a change of phase structure).

Phase Change Thermal Switch (Figure 3.4)

A low thermal conductivity solid situated in the cavity between the components undergoes a phase change into either a liquid or gas which will provide a superior (compared to the solid) conducting pathway between the two components. As the temperature decreases, the liquid or gas will solidify into a solid once again. The type of solid to use needs to be determined and thermal cycling effects need to be investigated.

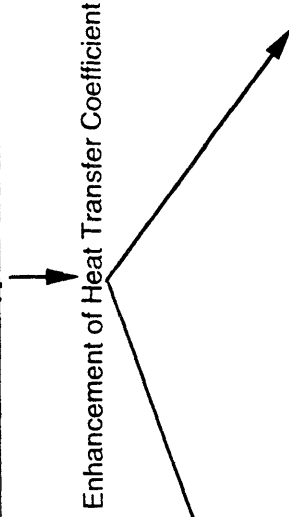
Increase of Cross-sectional Area

Variable Cross-sectional Area Bar (Figure 3.5)

A bar connected to the heat source and the heat sink increases its cross-sectional area when the heat source overheats, providing a much larger conducting pathway from the heat source to the heat sink. The increase in cross-sectional area would be brought about by gas or liquid molecules, which are released into the void when the heat source overheats, accumulating on the bar. The type of material to use for the bar and the gas or liquid needed to cause the increase in cross-sectional area of the bar need to be determined.

Table 3.2

Heat Convection Types of Thermal Switches



Evaporation-Condensation Thermal Switch (Figure 3.6)

This thermal switch has liquid present in the volume between the heat source (i.e., hot component) and the heat sink (i.e., cold component). The liquid is in physical contact with the heat source and heat sink (see Figure 3.6). As the temperature of the hot component increases, such as would occur in an accident situation, the liquid evaporates, creating a radial vapor pressure gradient from the heat source to the heat sink. This radial pressure gradient drives the vapor to the heat sink. At the heat sink, the vapor condenses, releasing thermal energy and converting back to liquid. The liquid then runs down the wall of the heat sink and returns to the pool of liquid, starting the process over again. The liquid should have a boiling point such that:

$$T_{\text{normal}} < T_{\text{boiling point of liquid}} < T_{\text{maximum allowed}}$$

heat source. In addition, fins can be attached to the heat sink (as shown in Figure 3.6) to aid the heat transfer process. Also, the liquid can be contained in tubes press-fit between the heat source and heat sink (see Figure 3.10B). Parameters such as type of liquid and liquid height need to be determined for each application.

Liquid-Vapor Thermal Switch (Figure 3.7)

A liquid is present and completely fills the volume between the hot component and the cold component. In addition, it has a low thermal conductivity and a boiling point greater than the expected normal temperature of the hot component, and less than the allowed maximum temperature of the hot component under accident conditions. This requires a liquid whose boiling point is such that:

$$T_{\text{normal}} < T_{\text{boiling point of liquid}} < T_{\text{maximum allowed}}$$

Under accident conditions, vapor bubbles form on the surface of the hot component and grow with time, ultimately touching the surface of the heat sink, releasing thermal energy, and collapsing (without ever detaching from the surface of the heat source). Of course, application of this thermal switch requires that the heat source and heat sink be in close proximity to one another. Parameters such as type of liquid, surface texture of walls, and pressure in cavity, all need to be determined.

Table 3.2 (cont)

Heat Convection Types of Thermal Switches

Enhancement of Heat Transfer Coefficient

Chamber Thermal Switch (Figure 3.8)

The gap between the hot component and the cold component is subdivided into small chambers. Fluid is present in each chamber. Running down the center of each chamber (lengthwise) is a material which divides the chamber into two cavities. The material used for dividing the chamber has the physical characteristic of shrinking when its temperature goes above a certain point, and re-expanding when its temperature goes below this point. Hence, when abnormally high temperatures are present, it will shrink, allowing convection currents to transfer thermal energy from the heat source to the heat sink, thus enhancing the heat transfer coefficient of the gap. When the temperature reaches normal limits again, it will re-expand, terminating the convection currents and, hence, minimizing the heat transfer coefficient of the gap. Type of fluid, type of material, chamber dimensions, and method of construction all need to be determined.

Wick Thermal Switch (Figure 3.9)

A wick material that provides capillary movement of a fluid is placed in the gap between the components such that the capillary movement of the fluid is from the cold heat sink to the hot heat source. A liquid, whose boiling point temperature is such that:

$$(T_{\text{normal}})_{\text{heat source}} < T_{\text{boiling point of liquid}} < (T_{\text{maximum allowed}})_{\text{heat source}}$$

is placed in the gap as well. Thus, under accident conditions, the liquid will evaporate off the hot component, condense on the cold component, and, via the wick, return to the hot component. Wick material, wick packing density, liquid type, and liquid quantity, all need to be investigated to produce a viable thermal switch.

Table 3.2 (cont)

Heat Convection Types of Thermal Switches

Enhancement of Heat Transfer Coefficient

Chemical Thermal Switch (Figure 3.10A and 3.10B)

Other ways of enhancing the heat transfer coefficient of the gap between the hot component and the cold component involve the use of a gas which will appear in the gap by dissociation of either a solid, a liquid, or a gas. The gas resulting would, in an accident situation, convert the thermal energy from the hot heat source to the cold heat sink, and then recombine, as the temperature decreased, with the other dissociation products to form the original chemical. The original chemical must have a dissociation temperature greater than the normal expected temperature of the heat source, and less than the allowed maximum temperature of the heat source under accident conditions. In other words, $(T_{normal})_{heat\ source} < (T_{dissociation})_{chemical} < (T_{maximum\ allowed})_{heat\ source}$. Also, questions concerning material compatibility, effect of thermal cycling, quantity of chemical required, and heat transfer capability of the dissociated gas all must be answered to yield a working system.

Another approach is to have the gap between the hot component and the cold component occupied by tubes which are press-fit between the two components, and which contain a low thermal conductivity solid chemical that would dissociate when the temperature of the hot component exceeded an acceptable value. The gas formed by the dissociation process would then convect, within each tube, heat energy from the hot component to the cold component. Once the temperature of the hot component was at an acceptable value again, the gas would recombine with the solid product (formed during the dissociation process) to reform the original chemical. Type of chemical, tube material, tube dimensions, tube spacing, number of tubes, and degree of press-fitting all need to be determined.

Also, one can have a nondissociating gas or liquid that enters the gap between the components via the melting of a rupture disk during an accident, and converts the excess heat energy from the hot component to the cold component. However, for this scenario, the liquid or gas would then have to be mechanically pumped out of the gap once normal operation was restored.

Table 3.2 (cont)

Heat Convection Types of Thermal Switches

Increase of Surface Area of Hot and Cold Component Surfaces

Grain Growth on Hot and Cold Component Surfaces
[Figure 3.11 (Convection)]

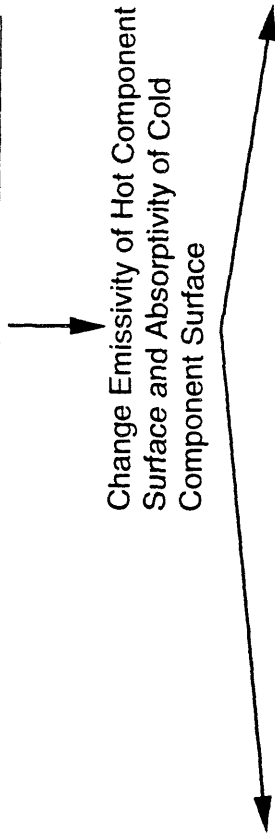
Material is placed on the hot and cold component surfaces that will grow in surface area as the temperature of the hot component increases beyond an acceptable value. This material will shrink back to its original surface area once normal temperatures are re-established. The exact kind of material and method of bonding to the hot and cold component surfaces need to be determined. Note that the material must have a very high thermal conductivity to avoid insulating the heat source and heat sink. Also, for a heat source concentric to a heat sink (as shown in Figure 3.11), grain growth should occur only on the heat source, since grain growth on the heat sink will actually reduce its surface area.

Grooved Wall with a Large Coefficient of Expansion Attached to the Hot and Cold Component Surfaces
[Figure 3.12 (Convection)]

A wall is constructed of a material that has a large coefficient of expansion. Grooves are present that will expose themselves only when the wall is in the expanded state. This wall is attached to both the hot and cold component surfaces. Thus, under accident conditions, the walls will expand, exposing their grooves and, hence, increasing their surface area. In addition, one can place flow trippers in the grooves which pop out into the flow when the grooves expose themselves. This will greatly increase the heat transfer coefficient. Type of material, construction process, and bonding method (to component surfaces) all need to be investigated. Also, as with the grain-growth concept, the grooved wall must be of a very high thermal conductivity to avoid insulating the heat source and heat sink, and should only be attached to the heat source when the heat source is concentric to the heat sink.

Table 3.3

Thermal Radiation Types of Thermal Switches



Change Emissivity of Hot Component Surface and Absorptivity of Cold Component Surface

Composition Change by Temperature (Figure 3.13)

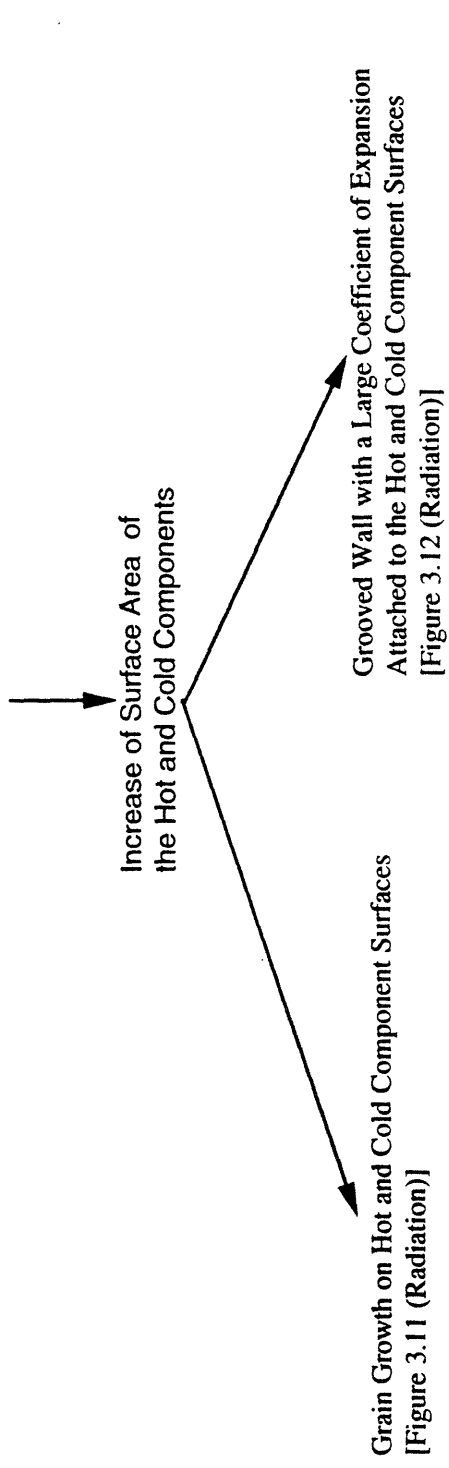
Material attached or bonded to the hot and cold component surfaces undergoes a composition change as the temperature increases which, in turn, changes its surface spectral characteristics. Specifically, the hot component surface would have bonded to it material whose surface emissivity would increase once its temperature exceeded a certain value. Similarly, the cold component surface would have material bonded to it whose surface absorptivity would increase as its temperature rose above normal. Once the temperature returned to normal, the surfaces would return to their original surface spectral characteristics. For this mechanism, such questions as wavelength and directional dependency of emissivity and absorptivity need to be answered. In addition, the effects of surface roughness, contamination, oxide coating, grain structure, particle bombardment (for nuclear applications), and radiation bombardment (for nuclear applications) all need to be investigated.

Composition Change by Chemical Reaction (Figure 3.14)

Material attached or bonded to the hot and cold component surfaces undergoes a composition change as it reacts with a gas released into the cavity between the two components. This composition change alters the surface spectral characteristics of the two surfaces, increasing the emissivity of the hot component surface (i.e., heat source surface) and increasing the absorptivity of the cold component surface (i.e., heat sink surface). The gas enters the cavity via a burst disk that has melted. A drawback to this system, however, is that another chemical must be flushed through once normal operating conditions have been re-established to return the surfaces to their original surface spectral characteristics. As in the other thermal switch concept, the effects of surface roughness, contamination, oxide coating, grain structure, particle bombardment (for nuclear applications), and radiation bombardment (for nuclear applications) all need to be investigated, as well as kinds of gases required.

Table 3.3 (cont)

Thermal Radiation Types of Thermal Switches



Grain Growth on Hot and Cold Component Surfaces
[Figure 3.11 (Radiation)]

Material is placed on the hot and cold component surfaces that will grow in surface area as the temperature increases beyond an acceptable level. This material will shrink back to its original surface area once the temperature returns to normal. The exact kind of material and method of bonding to the hot and cold component surfaces need to be determined. Note that the material must have a very high thermal conductivity to avoid insulating the heat source and heat sink. Also, for a heat source concentric to a heat sink (as shown in Figure 3.11), grain growth should occur only on the heat source, since grain growth on the heat sink will actually reduce its surface area.

Grooved Wall with a Large Coefficient of Expansion Attached to the Hot and Cold Component Surfaces
[Figure 3.12 (Radiation)]

A wall is constructed comprised of a material that has a large coefficient of expansion. Grooves are present that will expose themselves only when the wall is in the expanded state. This wall will be attached to both the hot and cold component surfaces. Thus, under high temperature conditions, the walls will expand exposing their grooves and, hence, increasing their surface area. In addition, one can place surface-area-enhancing protrusions in the grooves which pop out and blossom open when the grooves expose themselves. This will greatly increase the heat transfer area between the heat source and heat sink surfaces. However, type of material, construction process, and bonding method (to component surfaces) all need to be investigated. Also, as with the grain-growth concept, the grooved wall must be of a very high thermal conductivity to avoid insulating the heat source and heat sink, and should only be attached to the heat source when the heat source is concentric to the heat sink.

Table 3.3 (cont)

Thermal Radiation Types of Thermal Switches

Increase Area-Configuration Factor Product of Hot and Cold Component Surfaces	
<p>Low Thermally Conducting Liquid or Gas between the Components whose Transmissivity Increases with Temperature (Figure 3.15)</p> <p>This type of thermal switch has a gas or liquid occupying the cavity between the components that would have a low thermal conductivity and a low spectral transmissivity at normal operating conditions. However, during an accident or abnormal conditions, the gas or liquid would become more thermally conducting and more transmissive. Thus, the heat transfer rate between the two component surfaces would drastically increase. Once normal conditions returned, the liquid or gas would once again have a low thermal conductivity and spectral transmissivity. Experimentation would need to be done to find or develop a liquid or gas with these properties.</p> <p>Finned Components (Figure 3.17)</p> <p>The key concept here is to construct hot and cold components that have fins protruding from their surfaces. In this case the area-configuration factor is the same both in the normal and accident situation. Hence, this will mean an increase in heat loss over the unfinned situation during normal operation of the hot component, but will also mean a significantly proportional higher heat loss in the accident situation because of the higher temperatures. Thus, if high heat transfer rates are of paramount importance in an accident situation, this might be an acceptable concept. Fin shape, frequency, dimensions, and orientation all need to be determined.</p>	<p>Double-Mesh Screen Covering the Hot Component Surface (Figure 3.16)</p> <p>Two screens would be constructed that would lay over one another and be located at the hot component surface. The screen on top (i.e., the one closest to the cold component) would have a low spectral emissivity (as would the heat source surface) and block direct viewing between the underneath screen and the cold component. The screen underneath would have a larger coefficient of thermal expansion than the covering screen, and have a high spectral emissivity. During accident or abnormal conditions, the higher temperatures would cause the underneath screen to expand more than the cover screen, allowing direct heat transfer between the high emissivity screen and the cold component. Material selection and attachment methods (between the screens and hot component surface) need to be investigated and determined.</p>

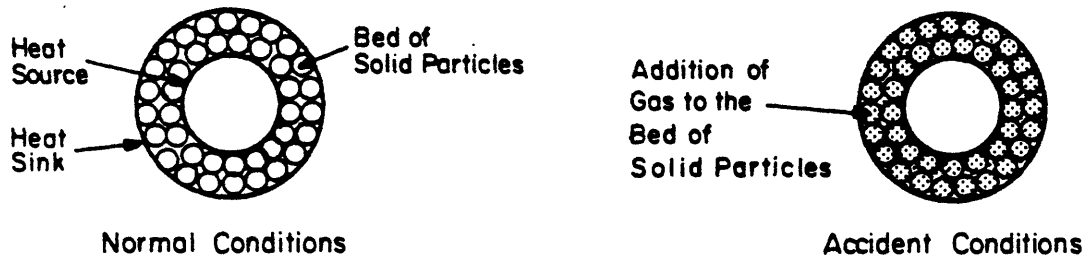


Figure 3.1. Particle Bed Thermal Switch

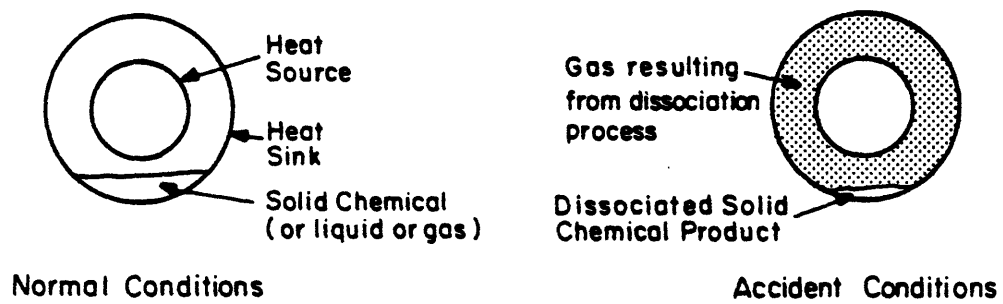


Figure 3.2. Dissociation Thermal Switch

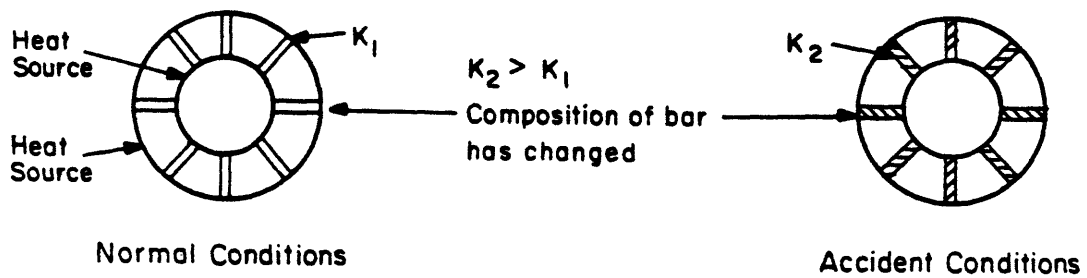


Figure 3.3. Change of Solid-Phase Structure Bar

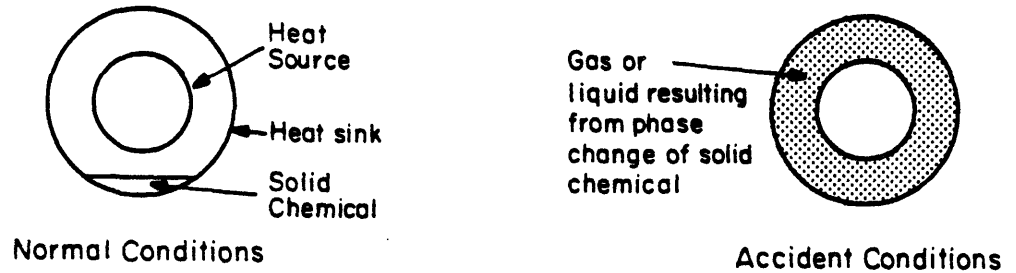


Figure 3.4. Phase Change Thermal Switch

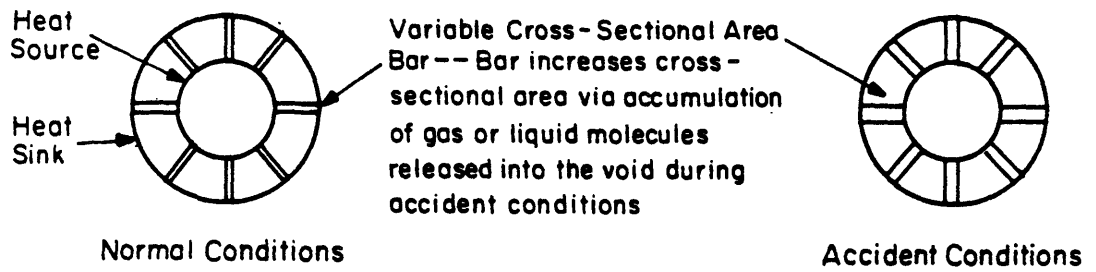


Figure 3.5. Variable Cross-Sectional Area Bar

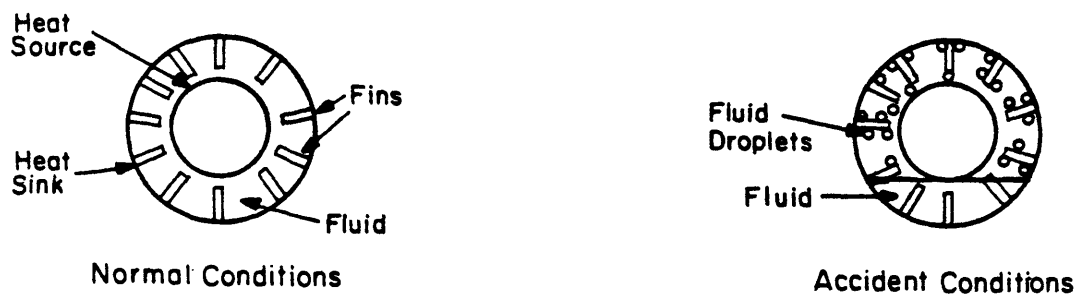


Figure 3.6. Evaporation-Condensation Thermal Switch (with Fins)

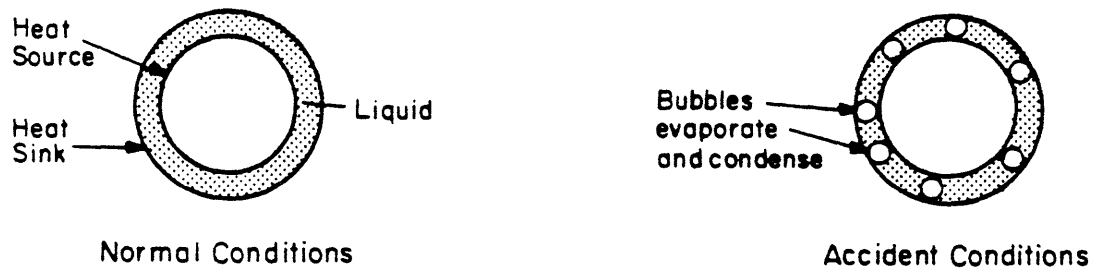


Figure 3.7. Liquid-Vapor Thermal Switch

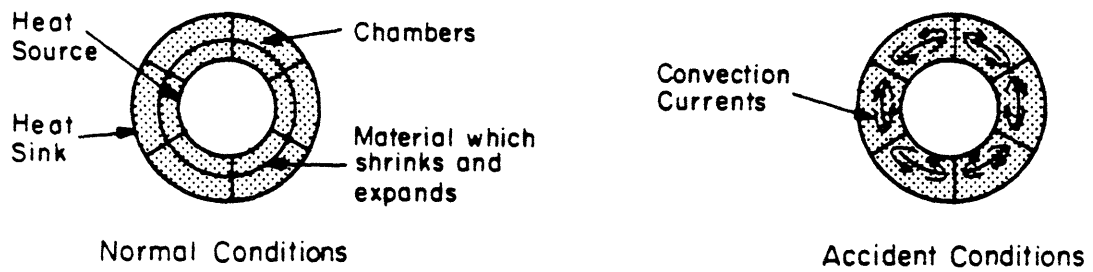


Figure 3.8. Chamber Thermal Switch

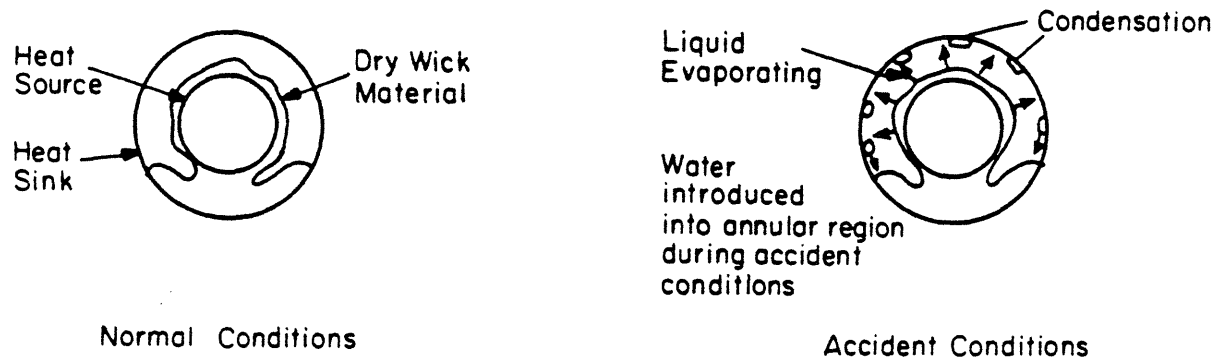


Figure 3.9. Wick Thermal Switch

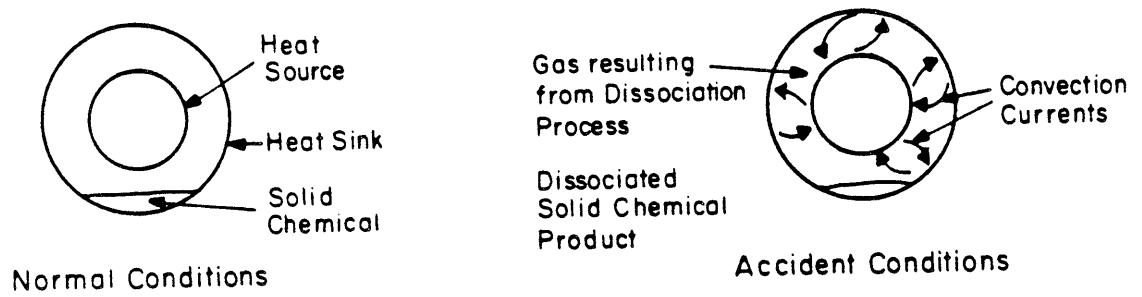


Figure 3.10A Chemical Thermal Switch
(See also Figure 3.2)

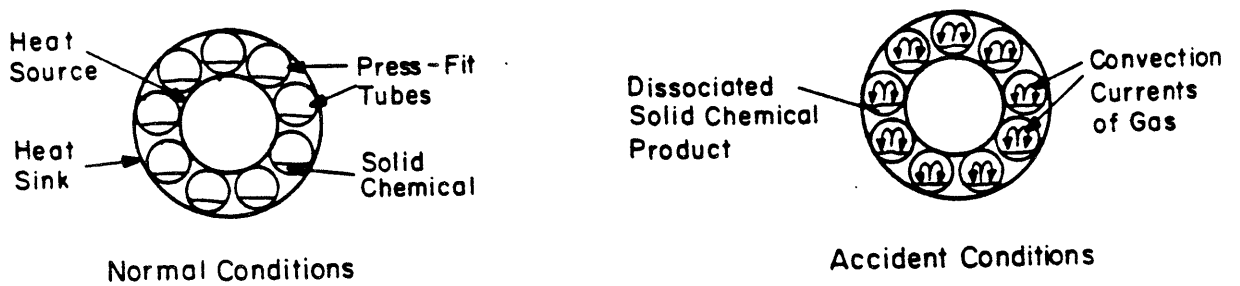
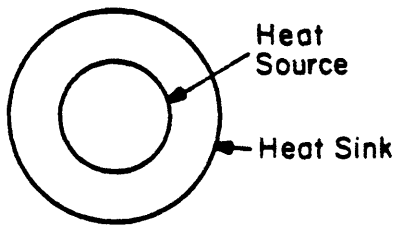
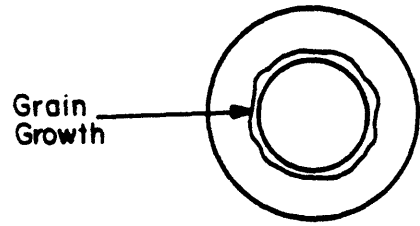


Figure 3.10B. Chemical Thermal Switch

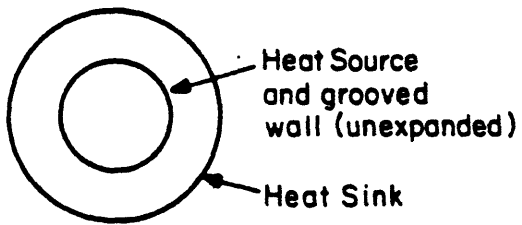


Normal Conditions

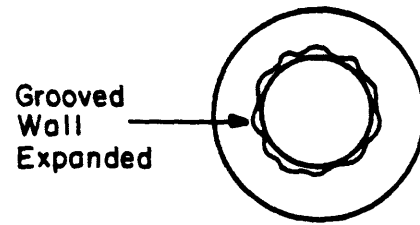


Accident Conditions

Figure 3.11 (Convection) and Figure 3.11 (Radiation).
Grain Growth on Hot Component Surface



Normal Conditions



Accident Conditions

Figure 3.12 (Convection) and Figure 3.12 (Radiation)
Attachment of Grooved Wall to the Heat Source

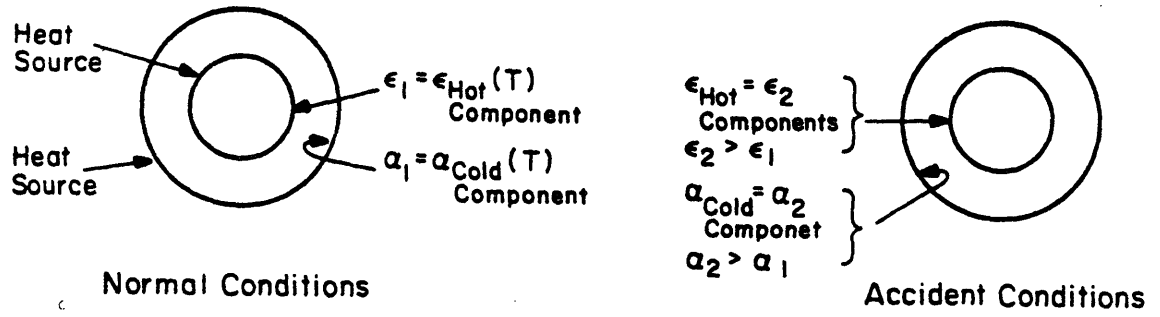


Figure 3.13. Surface Spectral Characteristics.
Change due to Surface Composition Change via Temperature

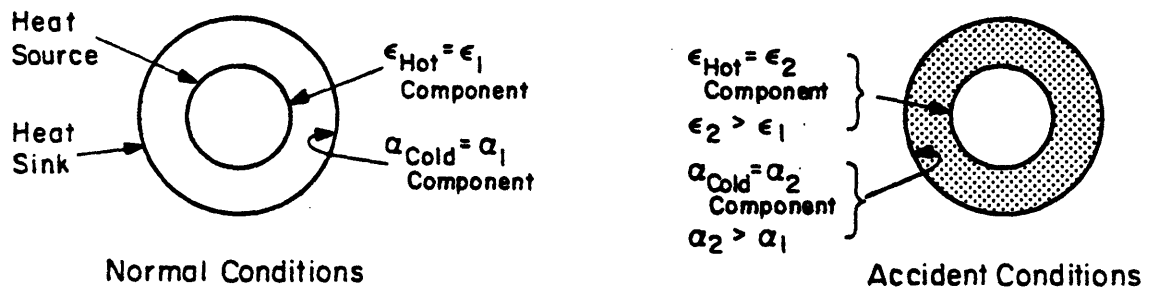


Figure 3.14. Surface Spectral Characteristics
Change due to Surface Composition Change via a Chemical Reaction

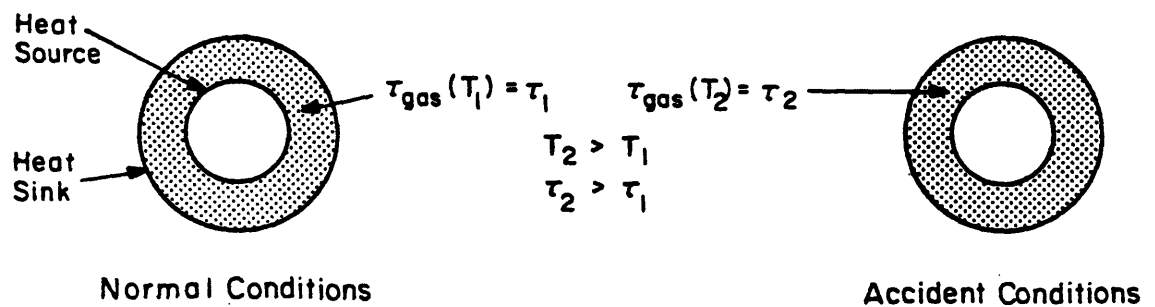


Figure 3.15. Low Thermally Conducting Liquid or Gas Between the Components Whose Transmissivity (τ) Increases with Temperature

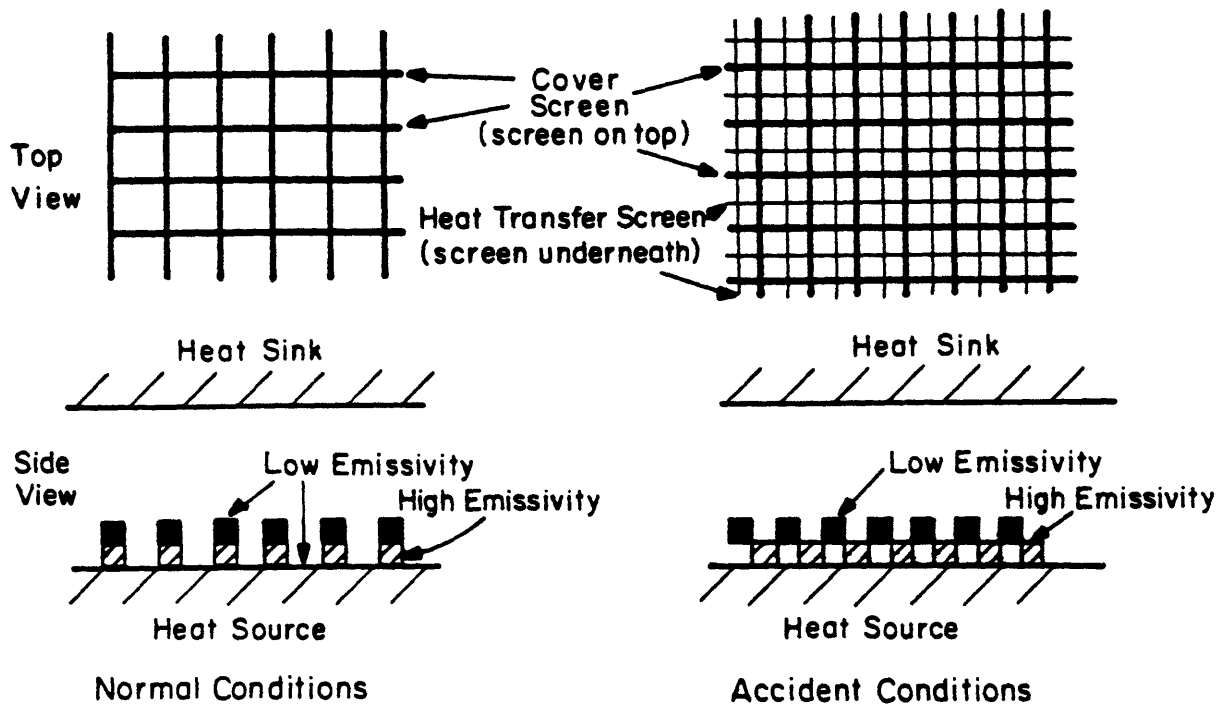


Figure 3.16. Double-Mesh Screen Covering the Hot Component Surface

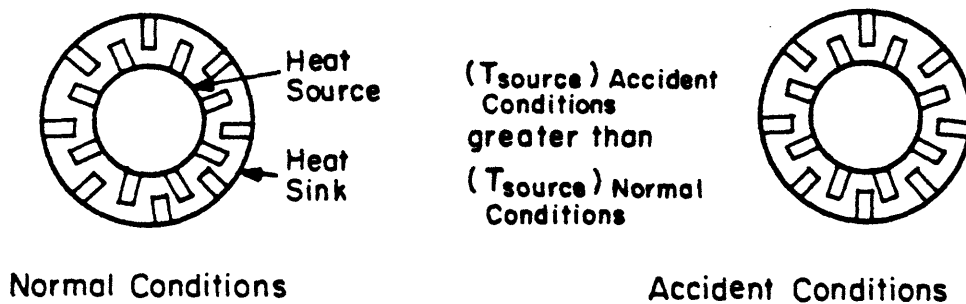


Figure 3.17. Finned Components

3.3 Chapter Summary

The thermal switches discussed in this chapter are the concepts conceived under the auspices of this project, many of which were not identified in the search of prior published literature. They were categorized as to their mode of operation. The three major categories were heat-conduction types of thermal switches, heat-convection types of thermal switches, and thermal-radiation types of thermal switches. These thermal switch concepts were further categorized as to the parameter being altered to provide the switching action of the thermal switch. For the heat-conduction types of thermal switches, the subcategories were variation-of-thermal-conductivity and variation-of-cross-sectional-area; for the heat-convection types of thermal switches, the subcategories were variation-of-heat-transfer-coefficient and variation-of-surface-area-of-heat-source-and-heat-sink; and for the thermal-radiation types of thermal switches, the subcategories were variation-of-surface-emissivity-of-heat-source-and-surface-absorptivity-of-heat-sink, variation-of-surface-area-of-heat-source-and-heat-sink, and variation-of-area-configuration-factor-product-of-heat-source-and-heat-sink. Tables 3.1, 3.2, and 3.3 describe and categorize the thermal switches conceived. Note that in many instances the functioning of the switch relies on properties or phenomena which may not be achievable to the extent desired when one attempts practical implementation. However, all versions are documented here for the sake of completeness. Based upon the engineering judgement of the project research team, the following devices appear to be the most promising: dissociation thermal switch, particle bed thermal switch, wick thermal switch, and the evaporation-condensation thermal switch. These were selecting for testing as described in Chapters 4 and 5.

Chapter Four

Dissociation and Recombination Experiments

4.1 Introduction

As mentioned in the summary of Chapter 3, experimental investigation was focused on the four thermal switches which were, prior to testing, judged to be the most technologically and economically feasible. Reiterating, they are:

1. Dissociation thermal switch
2. Particle bed thermal switch
3. Wick thermal switch
4. Evaporation-condensation thermal switch

These four types of thermal switches were tested for feasibility via three experimental configurations. Two of the three experimental configurations as well as the experiments performed using these setups are discussed in this chapter, and the third experimental configuration (and corresponding experiments performed) are discussed in Chapter 5. The experimental configurations and experiments discussed in this chapter were involved in investigating the chemical kinetics of dissociation and recombination of chemicals that might be used for the dissociation and particle bed thermal switches, with the purpose of obtaining an algorithm for successful dissociation and recombination of the chemicals selected for this application. (Dissociation is the decomposition of a chemical into its molecular constituents via addition of thermal energy, and recombination is the reassembly of these constituents into the original chemical.)

The first part of the chapter describes a dissociation/recombination experimental setup and the first two experiments performed using this experimental configuration. These first two experiments performed scoped out the dissociation and recombination kinetics of magnesium

carbonate and lead carbonate under the pressure and temperature conditions that they would be exposed to in thermal switch application. It was found that the dissociation kinetics of both chemicals tested (magnesium carbonate and lead carbonate) was acceptable for thermal switch application, but the recombination kinetics were very poor. Consequently, research effort was then focussed on finding a way to accelerate recombination of the dissociation products of the chemicals. This is discussed in the second part of the chapter. Successful results were obtained. Lastly, in the third part of the chapter, a summary of the experimental work and results is given. (Note that all the raw and reduced data for the experiments discussed in this chapter can be found in Appendix A. In addition, all the parts of the experimental setups discussed in this chapter are listed in Appendix B, which also give the part number and vendor from which they can be acquired.)

4.2 Preliminary Experiments

As mentioned above, the first two experiments performed acquired data on the chemical kinetics of dissociation and recombination of magnesium carbonate and lead carbonate under the conditions expected for usage in a thermal switch. The dissociation/recombination experimental setup constructed to acquire the data is shown in Figure 4.1. The test cavity shown was comprised of mild steel. It was constructed from a piece of mild steel piping with rectangular flanges welded to each end of the piping. The dimensions of this piece of piping were 3.635 inches O.D., 3.135 inches I.D., and 4.135 inches long. The latter two dimensions yielded an internal volume of 31.9 cubic inches. The flanges welded to the section of piping had dimensions of 4 inches by 3.5 inches by 0.375 inches. The flanges were welded such that the four-inch sides were horizontal. The back flange (i.e., the flange closest to the back of the oven) had a 1/8th-inch hole drilled halfway up the vertical face and one-inch horizontally off center. On the inside vertical surface of this back flange (i.e., the surface forming part of the inside surface of the cavity) a two-inch long piece of tubing was welded over the 1/8-inch hole. The end of the tubing protruding into the cavity was welded shut. A thermocouple was snugly

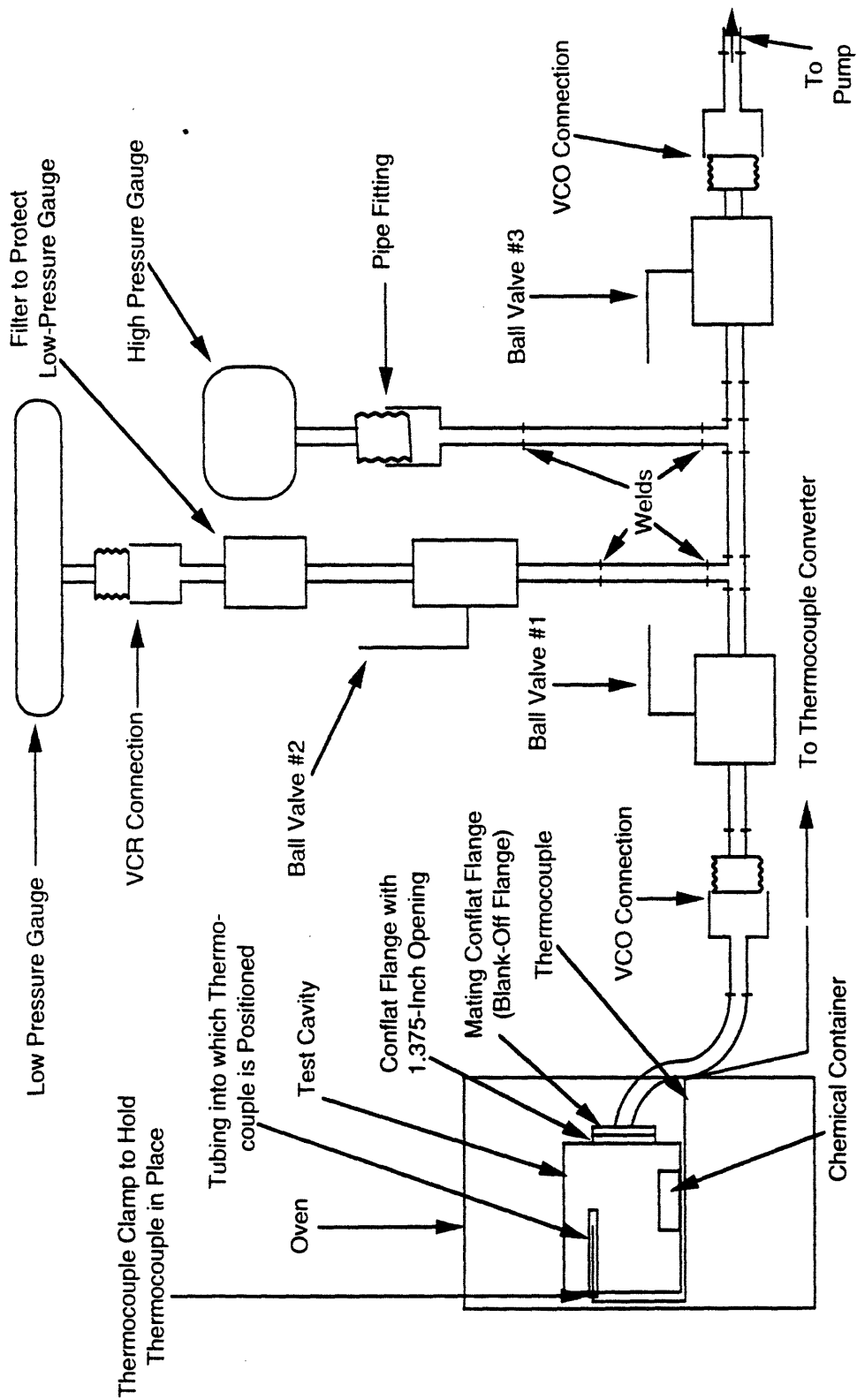


Figure 4.1 Dissociation/Recombination Experimental Setup

inserted into this tubing through the 1/8th-inch hole in the back flange (and held concentric by frictional forces) to provide temperature data for the interior of the cavity.

The front flange had a two inch hole drilled into it and a Varian conflat stainless steel flange welded over the hole. The conflat flange had a 1.375-inch opening. The mating flange to this conflat flange was a blank-off flange; a copper gasket was inserted between the two flanges. The entrance port in the test cavity was sealed using Varian conflat flanges because this was the only seal commercially available which could provide a vacuum seal at temperatures in excess of 500°C. The two flanges were torqued together using bolts comprised of A286 stainless steel. Physically, the bolts had a 12-point head, 28 threads per inch, were one inch long, and were one-quarter inch in diameter. They can be utilized in environments whose maximum temperature is 1200°F. Felpro, a product from Varian that prevents galling up to a temperature of 2400°F, was used to prevent galling between the bolts and the flanges. The mating conflat flange (i.e., the blank-off flange) had a 0.26-inch hole drilled through its center point. One-quarter inch tubing pushed in from the outside and made flush with the inside surface of this mating flange was welded into the 0.26-inch hole from the inside surface of the flange. As shown in Figure 4.1, this tubing led out of the oven to a VCO connection, which allowed, by the dismantling and assembly of the connection, for the introduction and removal of the test cavity from the oven. Beyond this VCO connection were other VCO connections, ball valves, pressure gauges, an oil filter and a vacuum pump. The ball valves were used to protect the low-pressure gauge from exposure to high pressure and to limit volume outside the oven during data acquisition to minimize error. The pressure gauges were used to provide test cavity pressure data. The high pressure gauge was a diaphragm gauge where the gauge readout was calibrated against diaphragm deflection. The low pressure gauge was a convectron gauge where pressure was determined by the thermal conductivity of the gas present (the less gas present the lower the thermal conductivity and, hence, the lower the pressure). The high pressure gauge could provide low pressure data as well but not quite as accurately as the low pressure gauge. The vacuum pump was a conventional piston vacuum pump lubricated by oil. It was capable of providing vacuums of about 15 μm of

Hg. The oil filter was a stainless steel cylinder with a stainless steel mesh inside. It was affixed atop the vacuum pump to prevent oil from diffusing into the experimental setup when low pressure existed in the tubing leading to the vacuum pump.

The chemicals that were investigated for their dissociation and recombination kinetics were magnesium carbonate (MgCO_3) and lead carbonate (PbCO_3). These chemicals were chosen because they have dissociation temperatures which would be considered borderline critical temperatures in power-producing systems. (The dissociation temperature of a chemical is defined as the temperature at which an equilibrium pressure of 1 atm would result from dissociation of the chemical. Note that a gas pressure of approximately one atmosphere is required to achieve near maximum heat transferring capability for both the dissociation thermal switch and the particle bed thermal switch.) Magnesium carbonate and lead carbonate have dissociation temperatures of 396°C and 268°C , respectively. In addition to these chemicals having the appropriate dissociation temperature, none of these chemicals or their dissociation products react with chemicals commonly found in the parts of representative thermal-power systems. Magnesium carbonate dissociates into magnesium oxide and carbon dioxide ($\text{MgCO}_3 \rightarrow \text{MgO} + \text{CO}_2$), and lead carbonate dissociates into lead oxide and carbon dioxide ($\text{PbCO}_3 \rightarrow \text{PbO} + \text{CO}_2$).

The kinetics of dissociation and recombination of the above two chemicals were investigated by experimentally determining the pressure in the test cavity as a function of temperature and time. The exact experimental procedure utilized and the results obtained are as follows.

First, a small square container was made, measuring 1.50 inches by 1.50 inches by 0.25 inches, from a sheet of stainless steel 321, to hold the chemical for which data was to be acquired. This allows easy placement and removal of the chemical from the test cavity, as well as providing a physical barrier between the test cavity wall and the chemical to prevent possible contamination of future experiments. This chemical container was then filled with the chemical of interest and sealed in the test cavity. The amount of chemical placed in the container was

twice the amount calculated to provide one atmosphere of pressure in the test cavity volume at the test chemical's dissociation temperature. (The calculations required to determine the chemical mass needed to provide one atmosphere of pressure are shown and explained in Appendix C.) Twice the amount was used to help compensate for the loss of carbon dioxide during the next step, the bake-out phase. To remove atmospheric contaminants adsorbed by the walls of the chemical container and the test cavity from exposure to the atmosphere, the test cavity was then pumped down using the vacuum pump for one hour while at room temperature, and for one hour while at 200°C, with the pumping down process continuing while the test cavity was being heated from room temperature to 200°C. (The success of this baking-out phase was checked in the next step of this experimental procedure, where outgassing pressure [i.e., background pressure] data versus temperature was obtained.) After this baking out phase the pumping section was then sealed off from the test section via ball-valve #3, and the temperature of the test cavity (and hence the chemical) was raised in 50°C increments until the cavity pressure was equal to or greater than one atmosphere, and correspondingly decreased in 50°C decrements until a temperature of 200°C was attained, or until the copper gasket between the two Varian conflat flanges failed. Approximately thirty-five minutes were required to change the temperature of the test cavity by 50°C, and, at each 50°C increment or decrement, the temperature of the test cavity was held constant for ten minutes to allow for temperature equilibration of the physical components of the setup in the oven, with the pressure being recorded at the end of this ten minute period. For the magnesium carbonate, the maximum temperature required to attain a cavity pressure equal to or greater than one atmosphere was 500°C, and for the lead carbonate it was 400°C. The minimum temperature attained for the magnesium carbonate experiment during the recombination phase (i.e., during the cool-down phase from the maximum temperature) was 300°C, due to copper gasket failure. For the lead carbonate it was 200°C, with no copper gasket failure. Thus, at the end of this first experimental step, total cavity pressure data versus temperature was obtained.

The second experimental step was, as mentioned above, the determination of the outgassing pressure contribution to the total cavity pressure. To this end, the above experimental procedure was repeated with no chemical present in the chemical container. The same temperature-time profile was followed as that above for each chemical. Thus, at the end of this second experimental step, the outgassing pressure data versus temperature was obtained.

The results of the above two experimental steps for magnesium carbonate and lead carbonate are shown in Figures 4.2 and 4.3, respectively. First, note that the outgassing pressure contribution to the data was negligible. Indeed, the maximum outgassing pressure was -14.603 psig (-14.700 psig is a perfect vacuum). Hence, this indicates that the baking-out procedure employed was sufficient in removing atmospheric contaminants from the walls of the chemical container and test cavity. Second, as one can see by inspection of the plots, the dissociation aspect of both experiments was successful. Both chemicals, via the release of carbon dioxide by dissociation, were able to pressurize the test cavity to one atmosphere. (The carbon dioxide from the lead carbonate created atmospheric pressure in the test cavity at a lower temperature than the carbon dioxide from the magnesium carbonate because, as mentioned earlier, the lead carbonate has a lower dissociation temperature than the magnesium carbonate.) Third, the chemical kinetics governing recombination of the metal oxides (MgO and PbO) with CO₂ were much poorer than the dissociation kinetics. Indeed, the results indicate that virtually no recombination took place during the time allotted (the decrease in pressure seen in the plots is due to the decrease in temperature of the carbon dioxide). Thus, since the recombination aspect of the experiment was the only part that failed, attention was now turned to finding a method of recombining the chemical constituents to recreate the original carbonate so that it could be used again.

4.3 Recombination Experiments

The recombination experiments involved using two different experimental setups (with one of the experimental setups being the dissociation/recombination experimental setup.) Two

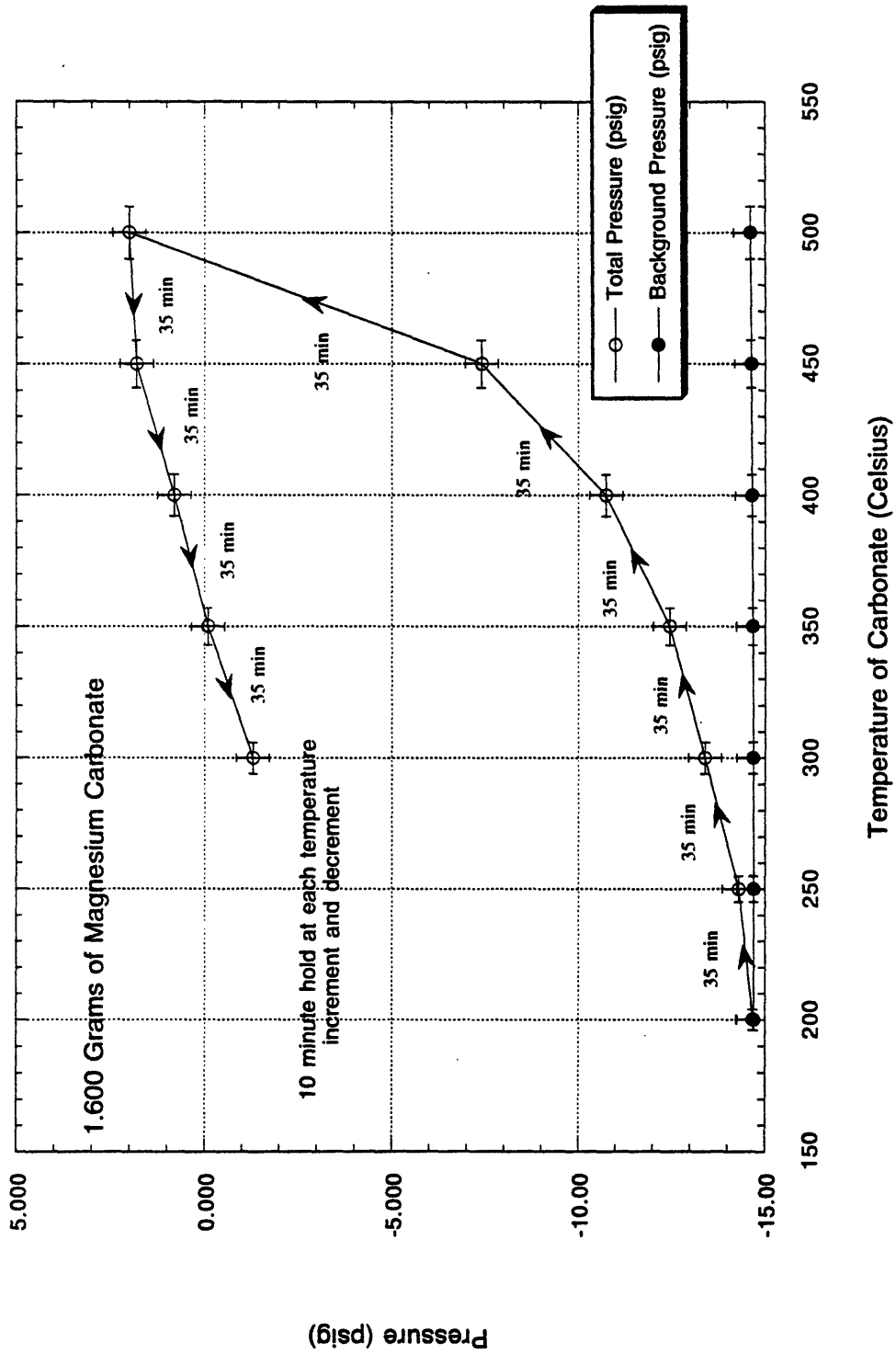


Figure 4.2. Dissociation/Recombination Experimental Results for Magnesium Carbonate

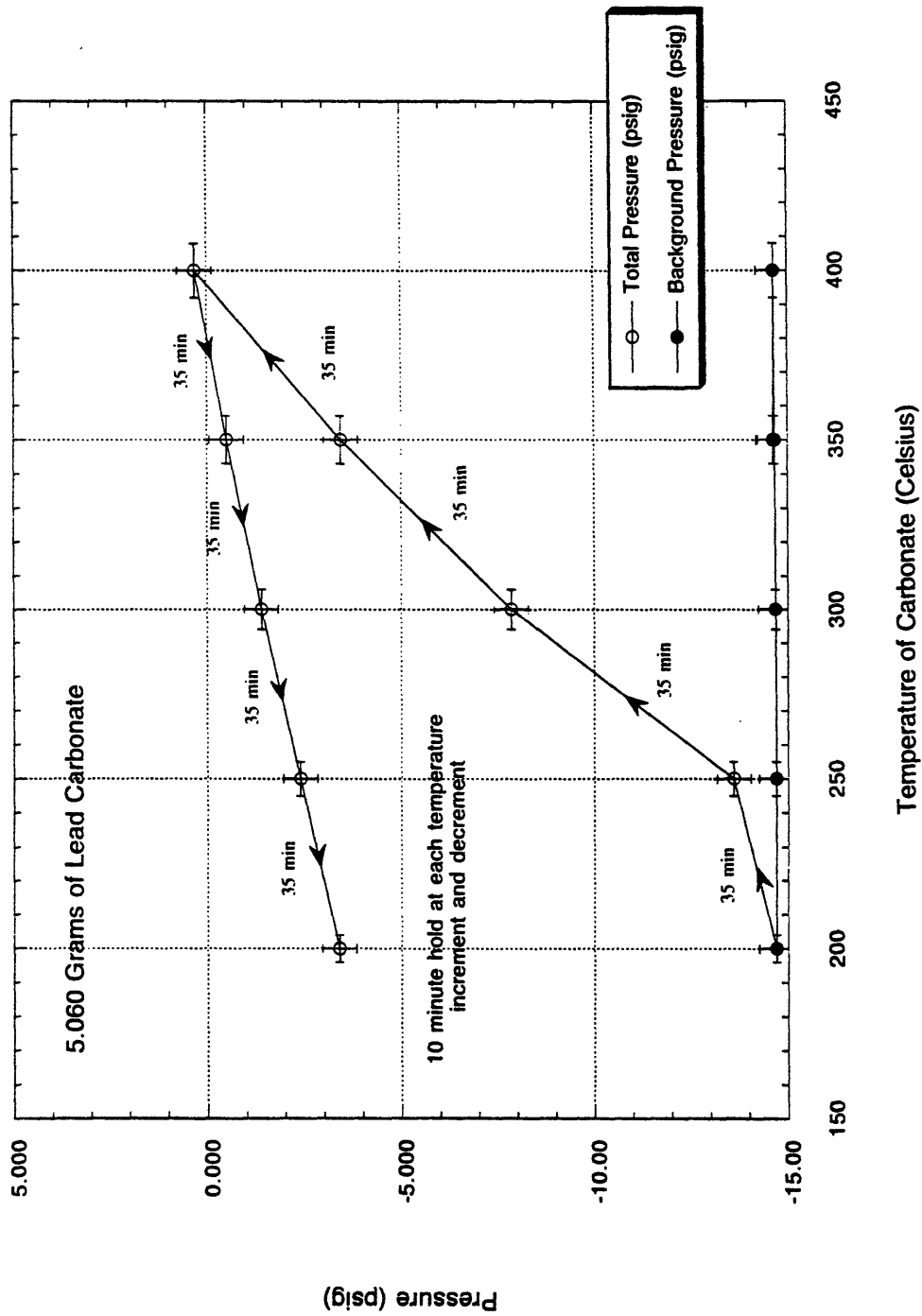


Figure 4.3. Dissociation/Recombination Experimental Results for Lead Carbonate

different experimental setups were required due to the different concepts investigated in search of a method to recombine carbon dioxide with the metal oxide. The experiments performed and the results obtained are as follows.

The first recombination experiment performed involved placing 1.600 grams of magnesium carbonate in the test cavity again and repeating the dissociation/recombination experiment. However, contrary to the previous experiment involving magnesium carbonate, the chemical was divided into two equal amounts of 0.800 grams and placed in two separate containers in the test cavity. The purpose of placing the chemical into two containers rather than one was to increase its surface area. It was hypothesized that perhaps the recombination process was being limited by the diffusion process of CO₂ into MgO. In addition, during the reset period, the temperature of the test cavity was held at 300°C for 19 hours to favor recombination (which need not be as rapid as dissociation in a practical thermal switch). The test results, plotted in Figure 4.4, did indicate some, albeit minimal, success. With no recombination, calculations indicated that the pressure of the CO₂ in the test cavity at the end of the test should have been -2.35 psig. Experimentally, a pressure of -2.70 psig was obtained.

Thus, with these test results in mind, a second experiment was performed. In this second experiment, extra recombination sites for the carbon dioxide were provided. Specifically, 7.990 grams of magnesium oxide were placed in the test cavity along with 1.600 grams of magnesium carbonate. The 7.990 grams of magnesium oxide were manufactured by separately baking 16.734 grams of magnesium carbonate in the test cavity at 423°C for 36 hours. During this 36-hour period, the test cavity was continually pumped clean of carbon dioxide. Once the resulting 7.990 grams of magnesium oxide had cooled (approximately eight hours later), 1.600 grams of magnesium carbonate were added to the test cavity. As in the first recombination experiment discussed in the previous paragraph, the magnesium carbonate was divided into two equal amounts of 0.800 grams and placed in two separate chemical containers. In addition, the magnesium oxide was allowed to sit in the test cavity directly (i.e., not in a chemical container), to maximize its surface area. As in all previous experiments, the temperature was increased to

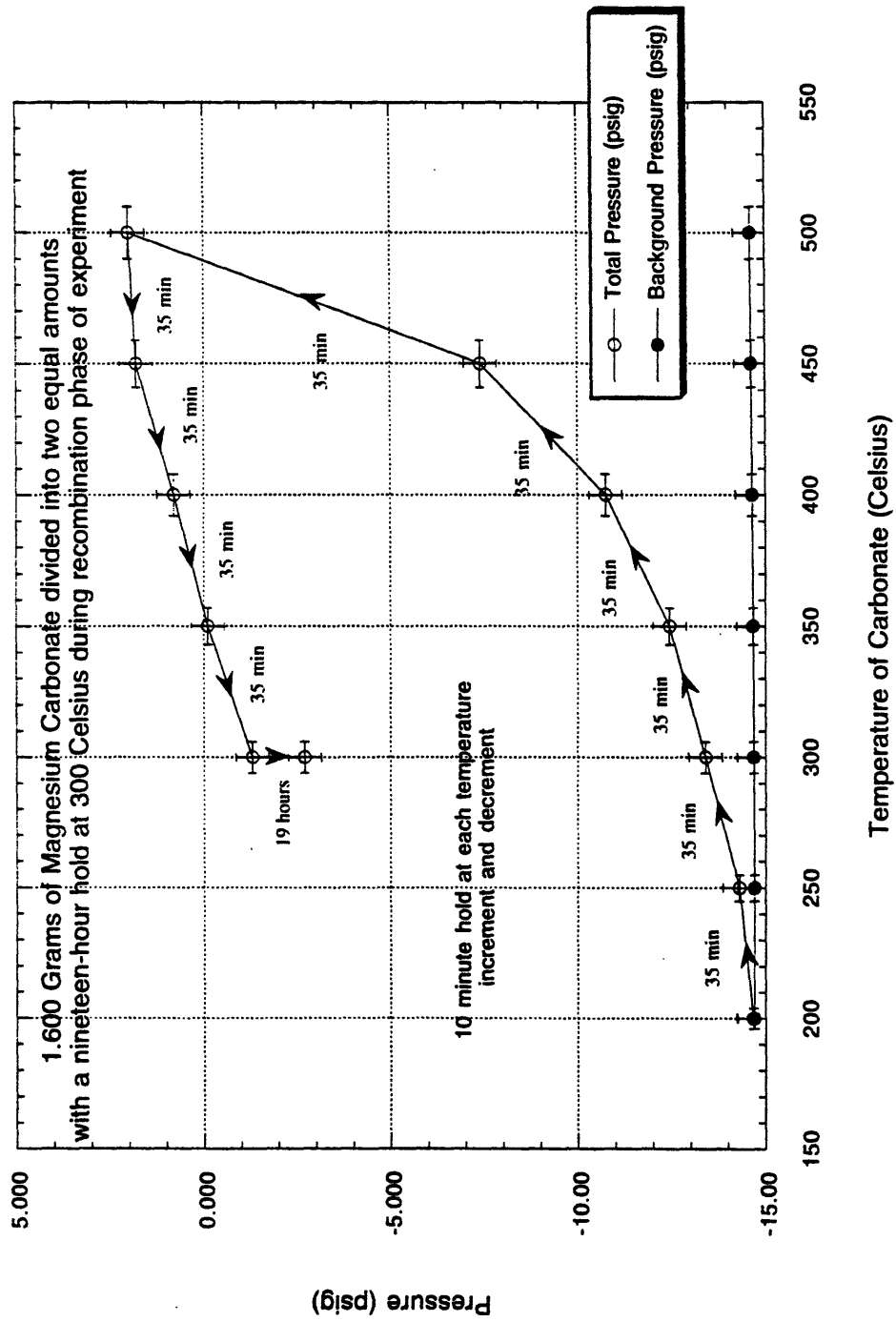


Figure 4.4 Recombination Experimental Results with Increased Surface Area of MgO and a Nineteen-Hour Hold at 300 Celsius

the maximum temperature of the experiment in 50°C increments, and decreased to 300°C in 50°C decrements, with the temperature held constant at each 50°C increment and decrement for 10 minutes. The pressure was recorded at the end of each ten minute hold. Once 300°C was reached, the test cavity was held at this temperature for 19 hours. The results, plotted in Figure 4.5, indicate that the extra recombination sites for the carbon dioxide did aid the recombination process. With no recombination, the final pressure should have been approximately -2.35 psig. Experimentally, however, a final pressure of -7.00 psig was obtained.

Thus, all the data supported the hypothesis that the recombination process was being limited by the diffusion process of the CO₂ into the MgO. Indeed when the data was presented to chemists Dr. Hamo Zur Loye of MIT, Dr. Frank Wagner of Strem Chemicals, and Kimberly Buntz of Chem Service, all drew the same conclusion as well. They believed the carbon dioxide was diffusion limited because of a carbonate layer formed on the surface of the metal oxide (MgO) by the carbon dioxide molecules combining with the metal oxide molecules. Apparently, the carbonate layer prevented or greatly inhibited the carbon dioxide gas from penetrating the surface of the metal oxide piles. To remedy the problem, all three suggested adding water during the recombination process. It was their opinion that with water present, the carbon dioxide gas would dissolve into the water to form liquid carbonic acid (H₂CO₃), which would then, due to liquid capillary action, be able to penetrate into the interior of the pile of metal oxide present. The interior MgO molecules would then extract carbon dioxide from the liquid carbonic acid, yielding magnesium carbonate and water.

However, before this concept was investigated, which would require a new experimental setup, it was desired to investigate one other idea, which required only a slight modification of the existing dissociation/recombination experimental setup. The modification involved removal of the low-pressure gauge from the setup, and in its place, the attachment of a carbon dioxide line from a CO₂ canister. (The resulting experimental setup is shown in Figure 4.6.) The idea was to pressurize the system with CO₂ during the recombination process to aid the penetration of CO₂ into the metal oxide piles. The experiment performed was as follows.

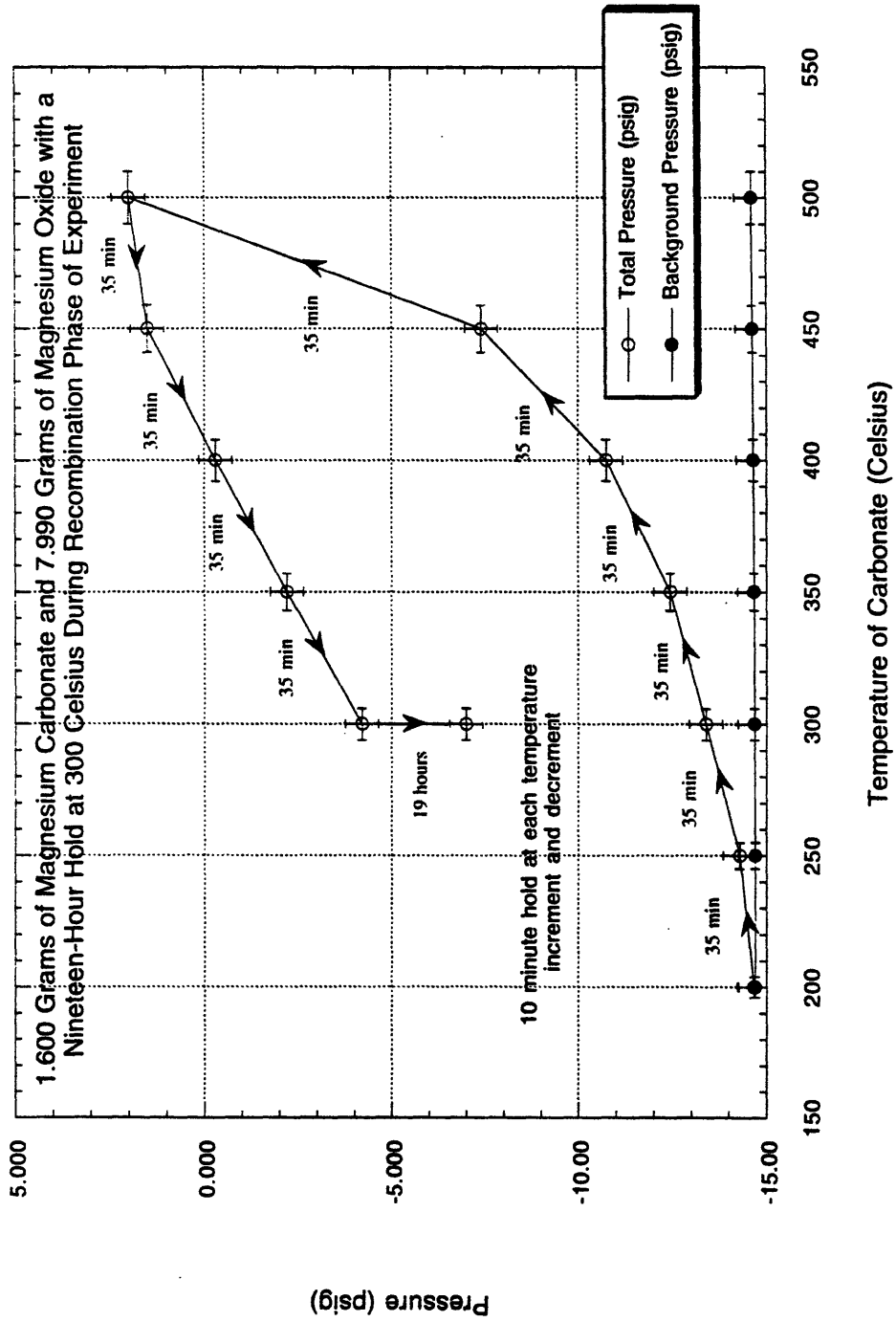


Figure 4.5 Recombination Experimental Results with Increased Recombination Sites and a Nineteen-Hour Hold at 300 Celsius

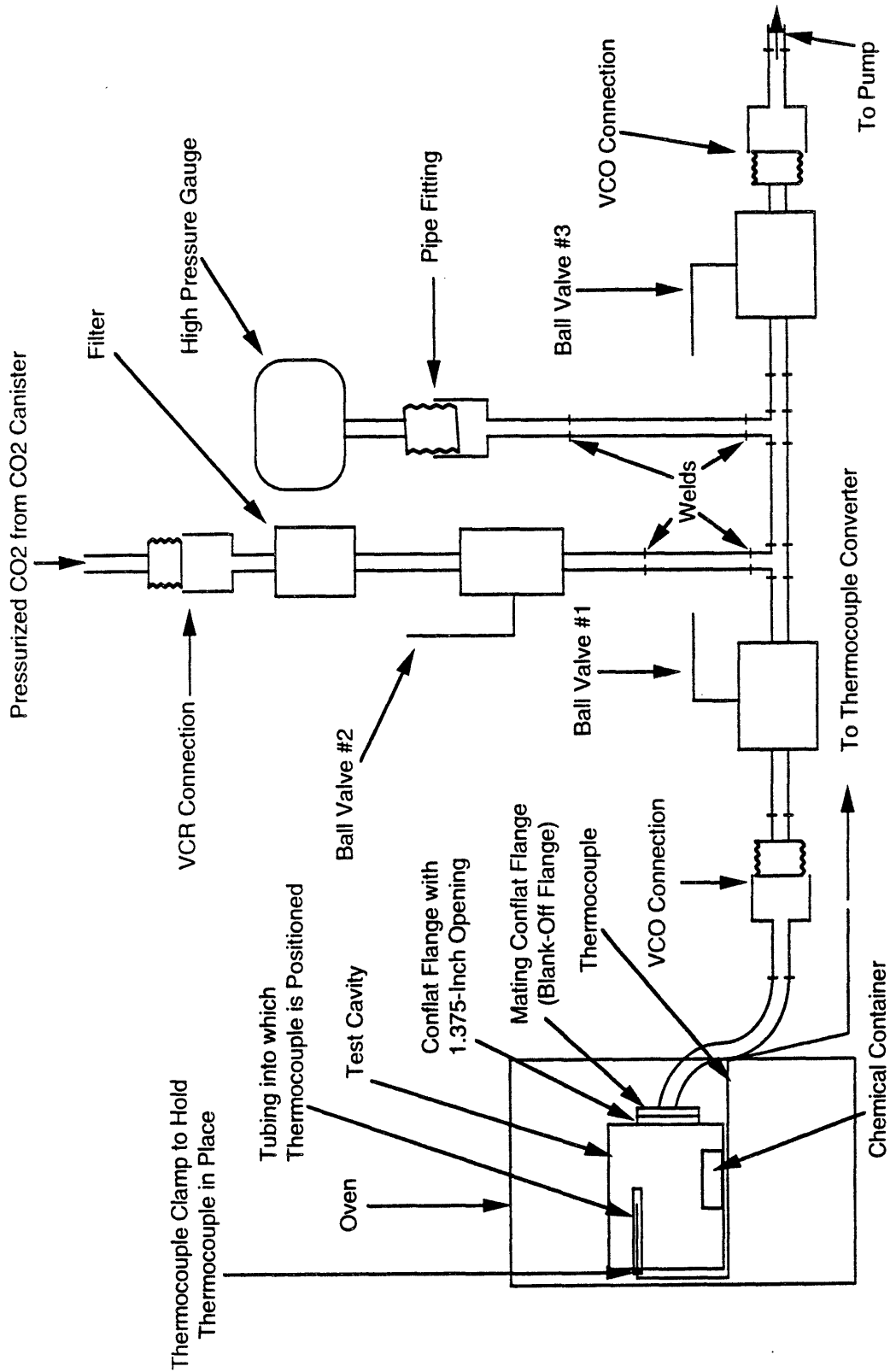


Figure 4.6 Recombination-Pressurization Experimental Setup

First, 2.02 grams of magnesium carbonate were placed in an open quartz container, which was then inserted into the furnace and baked for 10 hours at 510°C. For 2.02 grams of MgCO₃, calculations showed that 0.97 grams of MgO should remain after the carbon dioxide had been baked off. At the end of the 10 hour bake-out period, this was precisely the mass of the chemical remaining in the quartz container. Hence, all of the CO₂ had dissociated from the MgO and diffused away. Next, these 0.97 grams of MgO were placed in the two separate chemical containers (instead of one) to increase the surface area of the MgO exposed to the carbon dioxide gas. These chemical containers were then placed in the test cavity, which was then placed in the furnace. Following this, the test cavity was attached to the external tubing of the experimental setup (yielding the experimental setup shown in Figure 4.6). The test cavity was then baked-out and pumped down for 18 hours to eliminate most of the contaminant gases. The bake-out temperature was 300°C. Next, after completion of the bake-out phase of the experiment, with the test cavity still at 300°C, the system was purged of any remaining gas molecules by filling the system with CO₂ to a pressure of 3.0 psig, and then pumping the carbon dioxide gas out with the vacuum pump. This process of filling the system with carbon dioxide and pumping it out was repeated three times. After the third time, the vacuum pump and CO₂ source were sealed off from the system (i.e., test cavity, pressure gauge, and accompanying tubing) via ball valves #2 and #3, and the system monitored for leaks. The pressure read a constant -14.7 psig for twenty minutes. Thus it was concluded that no leaks were present. Hence, with the MgO in place at a temperature of 300°C, and a good vacuum established in the system, the experiment could now be performed.

The test cavity was pressurized with CO₂ gas to 2.7 psig while at 300°C, and held at these conditions for 24 hours. At the end of this 24-hour period, the power to the oven was terminated and the test cavity allowed to cool for 24 hours. During this cool-down phase of the experiments, the pressure due to the carbon dioxide gas was maintained at 2.7 psig. (Note that the copper gasket of the conflat flange did not fail at 300°C as in other experiments because for this experiment the maximum temperature was 300°C.) Next, 48 hours after the start of the

experiment, the chemical was removed from the test cavity and weighed. The scale indicated that virtually no recombination had taken place. (Sources of error such as spillage of the chemical in the test cavity and miscalibration of the pressure gauge and mass scale were checked for and eliminated.) Thus it was concluded that the pressure at which the recombination experiment was performed was too low, allowing for only superficial penetration of the CO_2 into the two MgO piles. Thus, since it appeared that very high pressures would be needed to obtain any worthwhile amount of recombination (which would be unacceptable in many applications), attention was turned to the concept suggested by the three chemists of using water to aid the recombination process. (Note that if more MgO had been used yielding more recombination sites, more recombination would have taken place. However, it was desired to find a recombination algorithm that could yield the desired amount of magnesium carbonate for minimal extra amounts of metal oxide present.)

To this end, an experiment was constructed in which carbon dioxide saturated with water flowed over the magnesium oxide. As mentioned earlier, it was the consensus of the three chemists consulted that, with water present, the CO_2 gas would dissolve into the water to form liquid carbonic acid (H_2CO_3), which would then, due to liquid capillary action, be able to penetrate throughout the piles of metal oxide present, allowing the carbon dioxide to recombine with the metal oxide molecules. The experiment setup built to investigate this concept is shown in Figure 4.7. It consisted of a CO_2 canister, a 500 ml filtering flask, a 100×50 mm crystal dish, and an oven. The CO_2 canister was the source of the carbon dioxide. Under pressure, the CO_2 flowed from the canister into the filtering flask, where it became saturated with water vapor. The CO_2 flowed into the water via a 3 mm glass tube. Small diameter tubing was chosen to enhance the mixing of the carbon dioxide gas with water. Following this, the wet gas flowed out of the flask and into the crystal dish situated in the oven, which contained the magnesium oxide. The crystal dish was covered by a rubber stopper capable of withstanding temperatures in excess of 150°C . The rubber stopper sealed the crystal dish only by a press fit. This way, if the gas pressure became too great, it would pop off. The rubber stopper had two holes drilled into it,

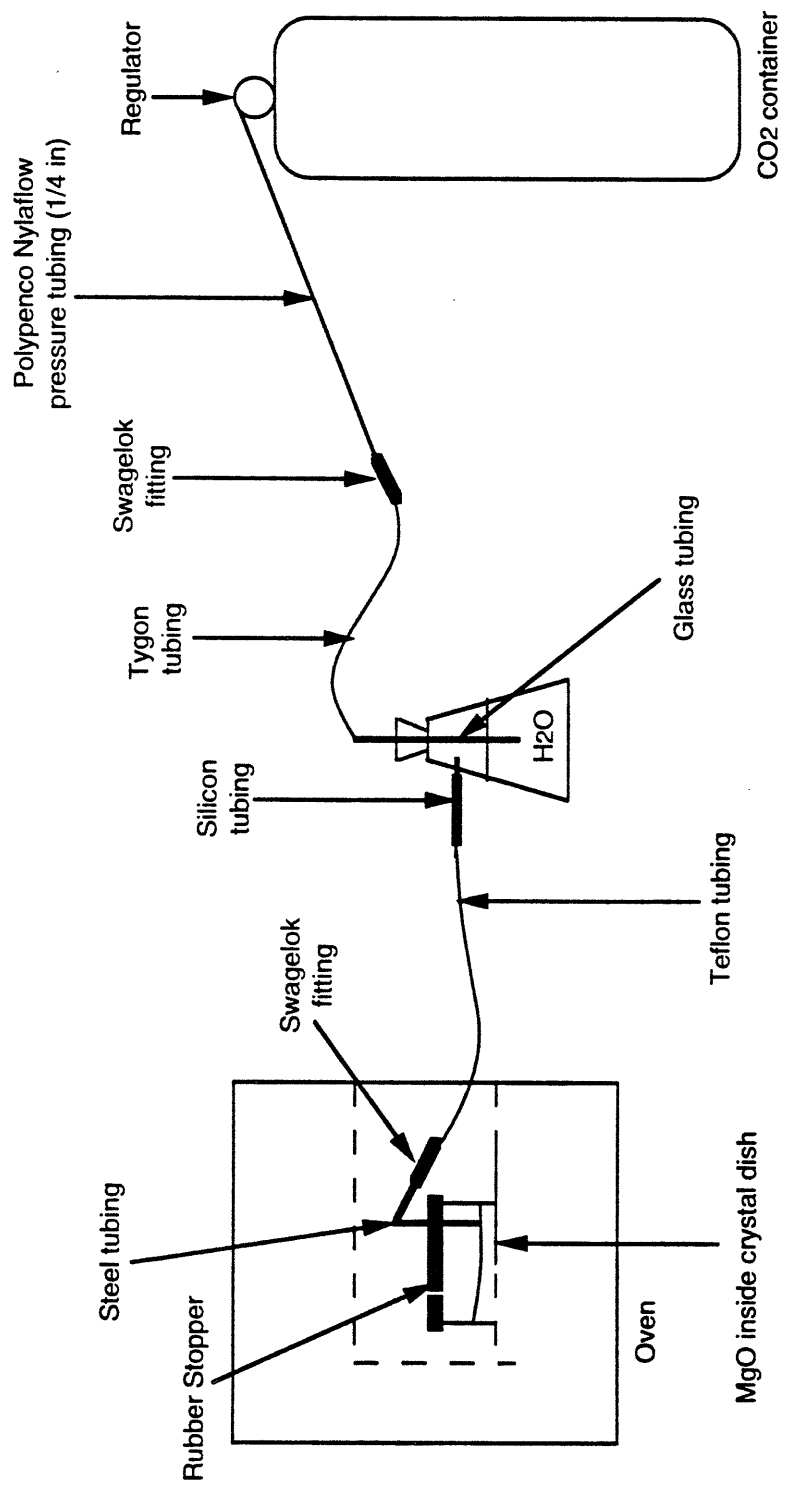


Figure 4.7 Apparatus for Combining Moist CO₂ with MgO

diametrically opposed, four inches apart. One of the holes had stainless steel tubing protruding through it, through which the water saturated carbon dioxide entered. The other hole in the stopper allowed for the exit of this gas. Stainless steel tubing was used since it would not be crushed shut by the undersized hole in the rubber stopper (an undersized hole was used to allow good sealing between the tubing and the stopper), and because it will not kink from the tubing contortions necessary to get the water saturated carbon dioxide into the crystal dish. As shown in Figure 4.7, this one-quarter inch stainless steel tubing was linked, via a one-quarter inch union swagelok, to teflon tubing, which then interfaced with silicone tubing. Flexible teflon tubing was used in the oven area because it can be exposed to temperatures of up to 260°C without decomposing or melting, and because its flexibility allows it to easily follow the convoluted path necessary to leave the oven. Silicone tubing was used to mate with the teflon tubing because it was the only tubing readily available that had an internal diameter and an elasticity that allowed both tubings to separate from one another if the pressure became too great.

This experiment was performed three times. The first time it was performed, the MgO was at 100°C. The amount of MgO present at the start of the experiment was 1.34 grams. The mass of the chemical present at the end of the experiment was 1.57 grams. Thus, 0.23 grams of carbon dioxide and/or water had combined with the MgO. For complete $\text{CO}_2 + \text{MgO}$ recombination (i.e., all the MgO being converted to MgCO_3), the final mass would have been 2.80 grams. Hence, at most, only 15.75 percent of the MgO had been converted to MgCO_3 . (To determine precisely how much CO_2 had recombined with the magnesium oxide, it would have been necessary to bake the sample in the oven at 325°C for approximately four hours. This would have decomposed any magnesium hydroxide and hydrates that might have formed during the experiment. This baking of the sample was not done because it was obvious that not enough carbon dioxide had recombined with the magnesium oxide at 100°C.)

The second time the experiment was performed the MgO was at room temperature, with 1.98 grams of MgO present. The experiment was performed at this lower temperature to allow for more water (and hence more carbonic acid) to be present in the crystal dish during the

experiment. (It was hypothesized that too much condensed water had evaporated in the previous experiment, thereby compromising the recombination process.) At this lower temperature, a great deal of water condensation took place in the crystal dish. After the experiment was completed the chemical was baked at 325°C for four hours to decompose any magnesium hydroxide and hydrates that might have formed, thus evaporating any absorbed water. The final mass of the chemical was found to be 3.03 grams. Thus, 51.4% of the MgO was converted to MgCO₃. Apparently, as anticipated, the lower temperature did aid the recombination process.

The third time the experiment was performed it was again performed at room temperature. However, contrary to the previous experiment, the water level in the crystal dish resulting from condensation was attentively monitored. When the water level became too high in the experiment (i.e., greater than 0.125 inches above the surface of the magnesium oxide), dry carbon dioxide was pumped into the crystal dish instead of moist carbon dioxide. Hence, this ensured that a high concentration of CO₂ dissolved in the water was maintained throughout the experiment. As in the previous experiment, after the twenty four hour recombination period had elapsed, the dish containing the chemical was placed in an oven and baked at 325°C for four hours to boil off any water remaining in the dish as well as decompose any hydrates and magnesium hydroxide that might have formed during the recombination period. The mass of the chemical immediately after this four hour bake-out period was found to be 6.35 grams. The initial amount of magnesium oxide was 3.53 grams. Hence, 73.25% of the original 3.53 grams of MgO had been converted to MgCO₃. (In other words, the final mass distribution of the chemical was 5.41 grams of magnesium carbonate and 0.94 grams of magnesium oxide.) Next, the test cavity used to obtain the pressure-temperature plots of the chemical specimens was baked clean and checked for leaks. No leaks were found and the level of cleanliness obtained was well within acceptable experimental bounds. (With no vacuum pump engaged, the cavity pressure was a constant -14.7 psig at 485°C during a four hour monitoring period.) Lastly, to verify that the reconstituted chemical would perform as desired, the 6.35 grams of mixed MgCO₃ and MgO were placed in the test cavity to obtain its pressure-temperature plot. As in the past, with the

vacuum pump engaged, contaminants adsorbed by the chemical specimen, the chemical container, and the internal walls of the test cavity due to exposure to the atmosphere were boiled off. (For this chemical specimen, because it had been underwater, a two-hour 325°C baking-out process was performed instead of the lower temperature baking-out process performed in earlier experiments. Hence, this guaranteed the decomposition of all hydrates and magnesium hydroxide in the chemical specimen that might have formed, as well as the boiling off of all atmospheric contaminants adsorbed by the chemical specimen, the chemical container, and the walls of the test cavity.) Then, with the vacuum pump disengaged, the temperature of the chemical was raised in two 25°C increments and one 50°C increment until the cavity pressure was greater than one atmosphere, and then lowered in seven 25°C decrements until the copper gasket failed. (For this experiment, the copper gasket failed at 250°C.) As in previous experiments, there was a 10-minute hold at each temperature increment and decrement, with the pressure being recorded at the end of the 10-minute period. The plot of pressure versus temperature for this chemical specimen can be found in Figure 4.8. As one can see, the pressure-temperature profile yielded by the dissociation of the reconstituted magnesium carbonate is the profile desired.

The success of this recombination method makes several thermal switch concepts possible, and warrants their further investigation. One of these thermal switches, the particle bed thermal switch, is further discussed in Chapter 5. Note that the set point of dissociation of these thermal switches can be varied by using another carbonate. For instance, calcium carbonate dissociates at 950°C, and lead carbonate dissociates at 268°C. Although the recombination process using moist CO₂ has not been checked using these other carbonates, it is highly probable that they will recombine using the wet CO₂ recombination process as well, since both chemicals also dissociate into a metal oxide and carbon dioxide gas.

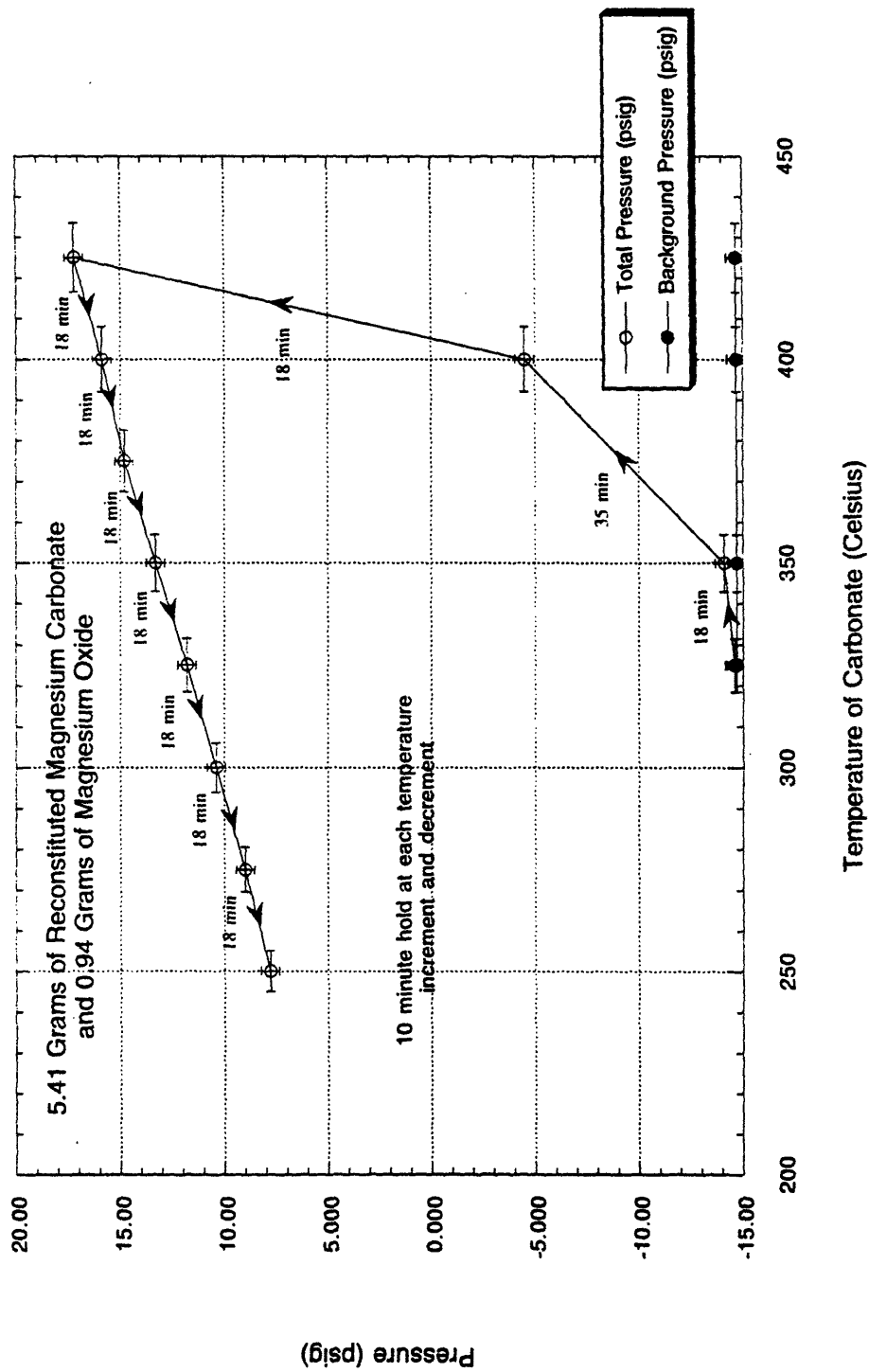


Figure 4.8 Dissociation Results Reconstituted Magnesium Carbonate

4.4 Chapter Summary

The creation of carbon dioxide gas by dissociation of a metal carbonate in a vacuum in a cavity was confirmed to occur in the temperature range of present interest. The dissociation process of the metal carbonate in a vacuum into a metal oxide and carbon dioxide gas was found to always occur, with the amount of carbon dioxide gas created (and, hence, pressure attained) determined by the temperature of the carbonate. (This assumes, of course, that enough carbonate is present to provide the chemical kinematic equilibrium amount of carbon dioxide gas. If a sufficient amount of carbonate is not present, then all the carbonate dissociates and the final pressure is directly proportional to the temperature of the carbon dioxide gas.) In addition, it was found that pressurization of the cavity as a function of temperature could be altered by changing the carbonate being used. A carbonate with a lower dissociation temperature pressurized the cavity to one atmosphere at a lower temperature. (It should be noted that it must still be shown that release of the carbon dioxide gas occurs over a sufficiently short period of time to initiate the protective temperature control action required of thermal switches. This could not be done using the dissociation/recombination experimental setup because of the long thermal time constant of the ovens available.)

Concerning recombination, several different concepts were investigated to achieve reassembly of magnesium oxide and carbon dioxide gas resulting from the dissociation of magnesium carbonate. The concepts investigated were:

1. Increasing the number of recombination sites available to the carbon dioxide gas by increasing the surface area of the magnesium oxide, and maintaining a nineteen-hour hold at 300°C.
2. Increasing the number of recombination sites by addition of extra magnesium oxide to the experiment, and maintaining a nineteen-hour hold at 300°C.
3. Increasing the pressure of the carbon dioxide gas for 48 hours.
4. Flowing moist carbon dioxide gas over the magnesium oxide for 24 hours.

The first concept resulted in a minimal amount of recombination taking place, and the third concept did not result in any measurable reassembly of magnesium oxide and carbon dioxide gas. However, the second and fourth concepts did yield significant recombination of the dissociation products MgO and CO₂, with the last concept providing enough reconstituted magnesium carbonate that it could be used to pressurize the test cavity to over one atmosphere via dissociation.

Chapter Five

The Heat Transfer Coefficient Experiment

5.1 Introduction

The heat transfer coefficient experiment was built to acquire temperature and heat flux data on the thermal switches conceived so that the heat transfer coefficient of the thermal switches could be calculated. For this aspect of the research project, the particle bed thermal switch, the wick thermal switch, and the water (evaporation-condensation) thermal switch were the ones selected.

Heat flux and the corresponding temperature data were acquired for both the on-mode and the off-mode of these three thermal switches. This allowed for calculation of both on-mode heat transfer coefficients and off-mode heat transfer coefficients. In addition, for each thermal switch, the thermal switching ratio, defined as the on-mode heat transfer coefficient divided by the off-mode heat transfer coefficient, was calculated. The experimental apparatus built is discussed in Section 5.2, the experimental procedure utilized and the raw data reduction algorithm employed are discussed in Section 5.3, and a description of the thermal switches and the reduced results obtained are discussed in Section 5.4. The last section, Section 5.5, gives a chapter summary.

5.2 Experimental Setup

The key aspects of the heat transfer coefficient experiment are shown in Figure 5.1. A heater, 48 inches long with an active heater length of 18 inches and a diameter of 0.996 inches, was positioned concentrically inside a 27-inch long horizontal stainless steel pipe. The stainless steel pipe and heater were located underwater in a stainless steel barrel during experimentation. The stainless steel pipe had an inside diameter of 2.00 inches and an outside diameter of 2.25 inches.

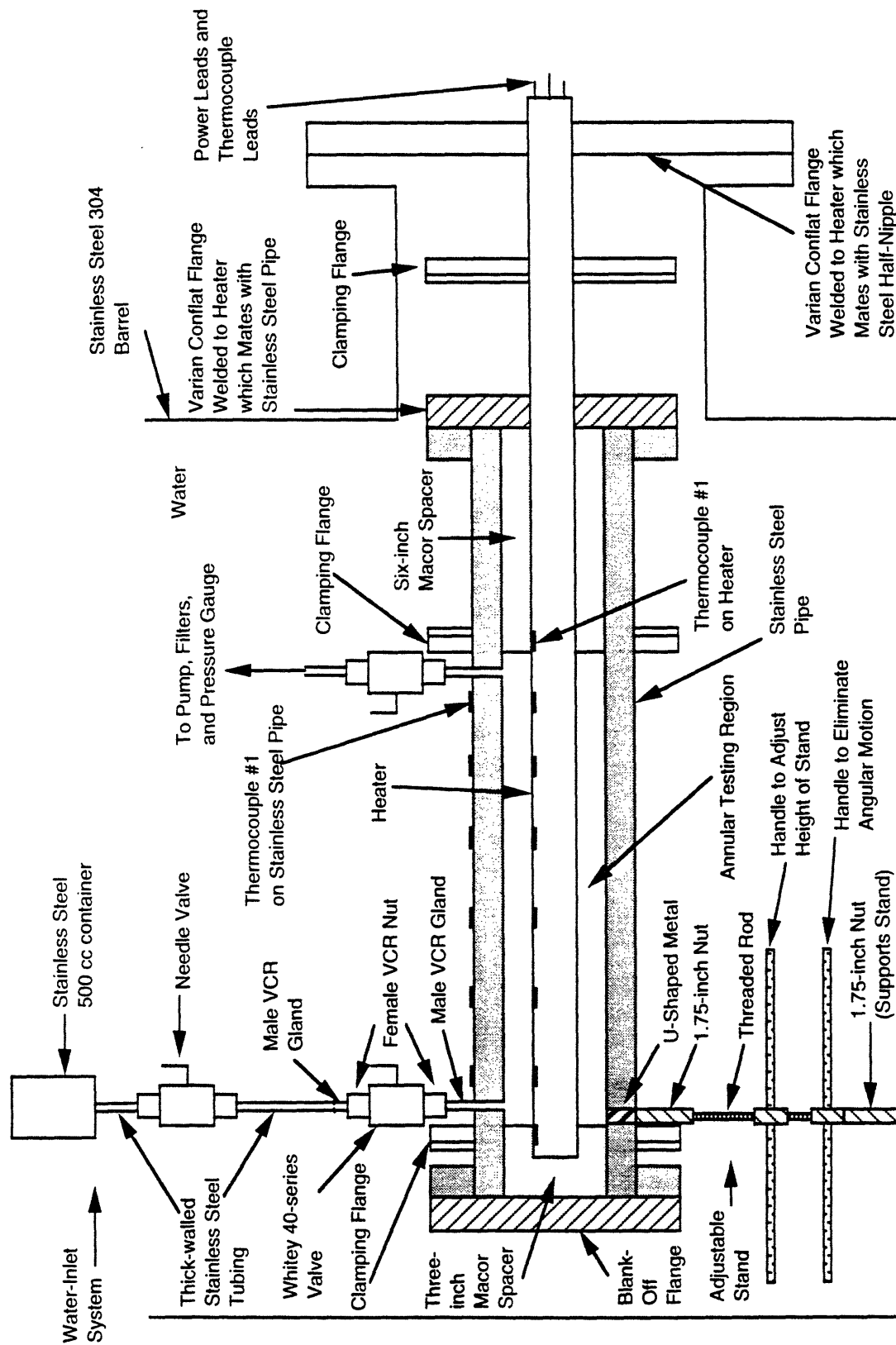
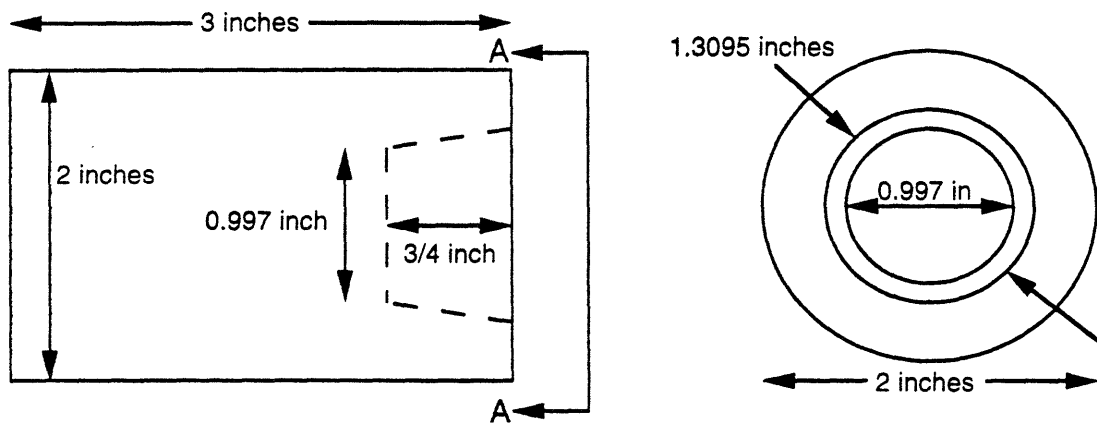
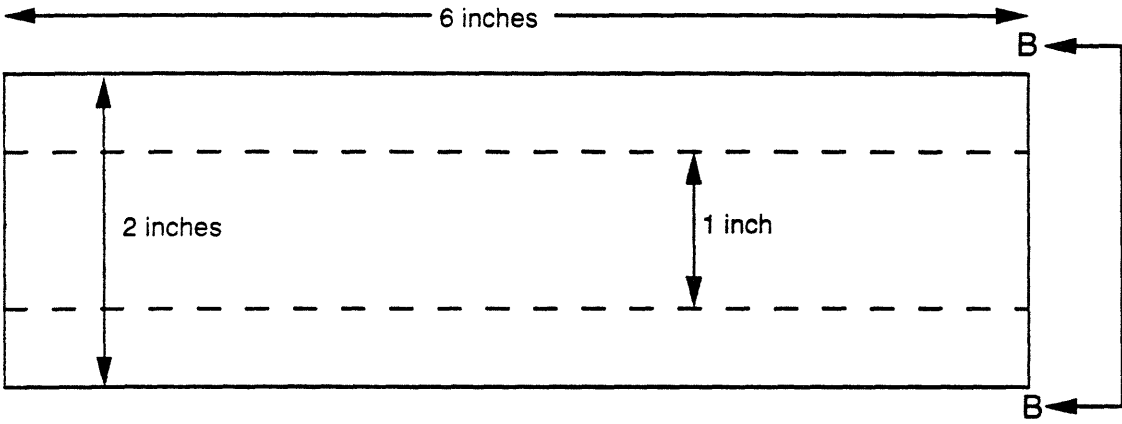


Figure 5.1 Partial Experimental Setup of Heat Transfer Coefficient Experiment

The heater, cylindrical in shape, had two unheated segments and one heated segment. The two unheated lengths were 0.75 and 29.25 inches long, and were positioned at each end of the 48-inch long heater, with the 18-inch heated length between them. The end of the heater with the 0.75-inch unheated length was welded shut, while the other end with the 29.25-inch unheated length was closed off with packed magnesium oxide, and had thermocouple and power leads emanating from it. The sheath of the heater was comprised of stainless steel 304. A Varian conflat flange was welded on the 29.25-inch unheated length at a position of 6.00 inches from the 18 inch active heating length, with the sealing surface of the conflat flange facing the active heating length. The 27-inch stainless steel pipe also had conflat flanges welded to it, one at each end with the mating surface facing outward. Thus, when the heater was slid into the stainless steel pipe, the 0.75-inch unheated length, the 18-inch heated length, and 6 inches of the 29.25-inch unheated length were completely enclosed by the stainless steel pipe. The end of the pipe where the sealed off heater end was situated (i.e., where the 0.75-inch unheated length was located) was vacuum-sealed by the mating of the conflat flange of the stainless steel pipe at this end with a blank-off flange. At the other end, the Varian conflat flange welded to the 29.25-inch unheated length of the heater was mated with the other conflat flange of the stainless steel pipe to provide a vacuum seal at this end as well. Two cylindrical ceramic spacers (shown in Figure 5.2) comprised of Macor, a machinable ceramic from Corning, were positioned over each of the unheated lengths enclosed by the stainless steel pipe to provide support for the heater to keep it concentric during the experiment, and to act as thermal insulators to reduce end losses due to radiative heat transfer from the 18-inch active heater length to the flanges of the stainless steel pipe. The ceramic spacer insulating the end of the enclosed 0.75-inch unheated length was three inches long, had a two inch O.D., and had a 0.75-inch deep tapered hole drilled into one of its vertical faces into which the heater mated. The tapered hole was 0.997 inches in diameter at its base and 1.3095 inches in diameter at the top (i.e., at the vertical face of the Macor spacer). The hole was tapered to allow for easy mating of the ceramic spacer and the heater during assembly of the experimental setup. Lateral movement of the three-inch long Macor spacer was prevented by the heater and the blank-off flange attached at that



View AA



View BB

Figure 5.2 Macor Spacers

end. At the other end, the Macor spacer was six inches long with a 2 inch O.D. and a 0.997-inch thru-hole drilled through it. Frictional forces at the Macor-heater surface and the Macor-stainless-steel-pipe surface held it in place.

Thus, the resulting 18-inch long annular region between the active heater length and the inside surface of the stainless steel pipe was where the thermal switches were tested. It provided a working volume of 696.85 cubic centimeters. Various systems were tied into this test region (one of which is shown in Figure 5.1, the water inlet system) to allow for the altering of such parameters as pressure, gas composition, and water content. These systems are discussed later in this section.

In addition to using ceramic spacers to reduce thermal energy end losses from this 18-inch long test section, thermal energy end losses were also reduced by utilizing three clamping flanges comprised of stainless steel and teflon, and three insulating sleeves comprised of silicone with an aluminum foil coating. The three clamping flanges provided a clamping and sealing surface for two of the insulating sleeves. (The third insulating sleeve clamped directly to the remaining section of the 29.25-inch unheated length which was not insulated by the other two sleeves. This arrangement allowed for easy assembly and disassembly of the experiment while at the same time helping to keep end losses to a minimum.) The three clamping flanges manufactured were composed of a 5/32-inch thick stainless steel 304 ring and a 27/32-inch thick teflon ring. Two of the three clamping flanges had an internal diameter of 2.251 inches, while the third clamping flange had an internal diameter of 1.001 inches (see Figures 5.3 to 5.6). All three clamping flanges had an external diameter of 3.375 inches. The two clamping flanges with an internal diameter of 2.251 inches were welded to the stainless steel pipe, while the one clamping flange with an internal diameter of 1.001 inches was welded to the 29.25-inch unheated section of the heater (see Figure 5.7 for their exact location). The surface of the clamping flanges welded to the pipe and heater was the stainless steel ring internal diameter surface. The teflon ring was used to insulate against heat loss from the stainless steel ring (since its thermal conductivity and, hence, heat transfer to water are much less than that of stainless steel), as well as provide the clamping surface for the insulating

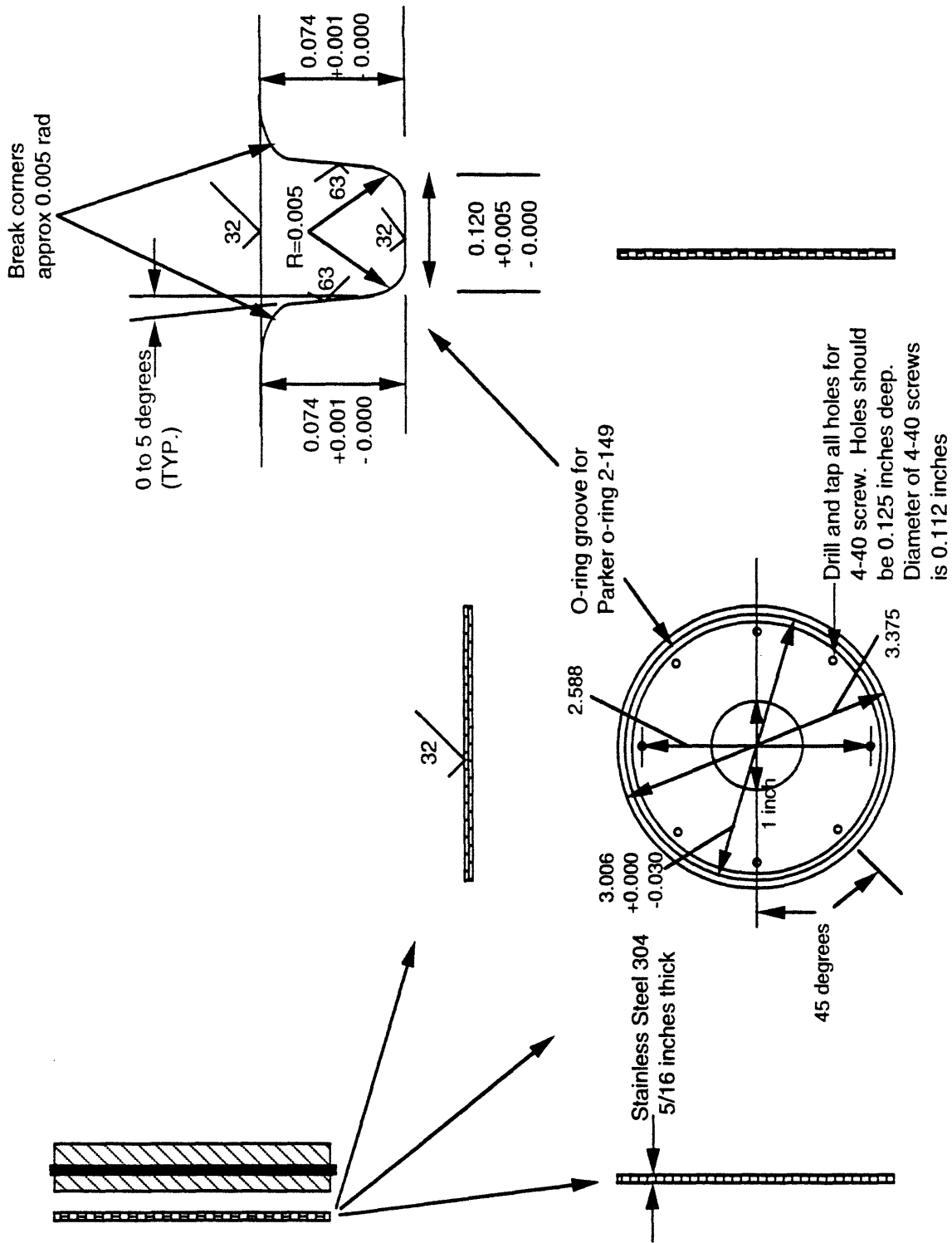


Figure 5.3. Stainless Steel Ring for Heater Flange

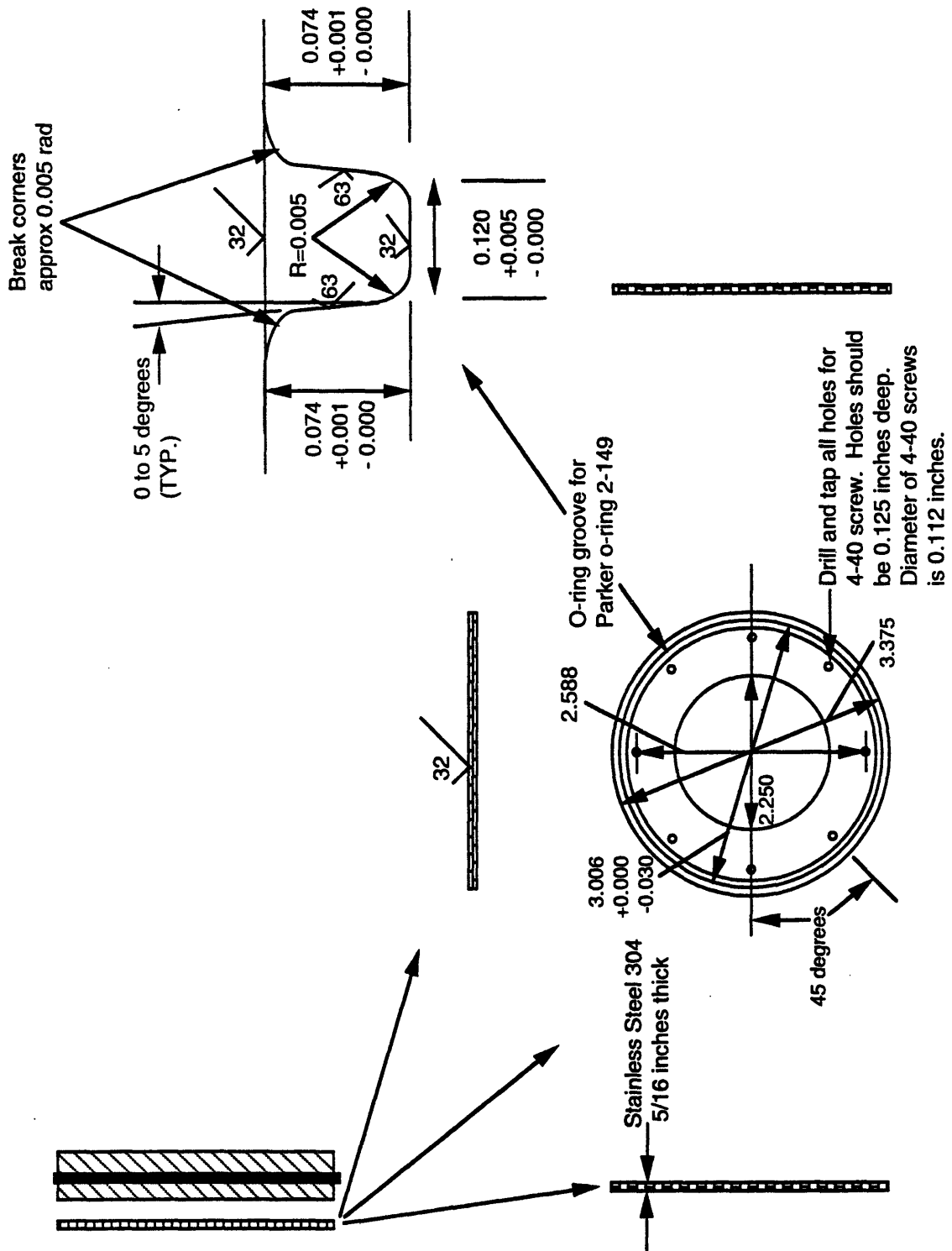


Figure 5.4. Stainless Steel Ring for Stainless Steel Pipe Flanges

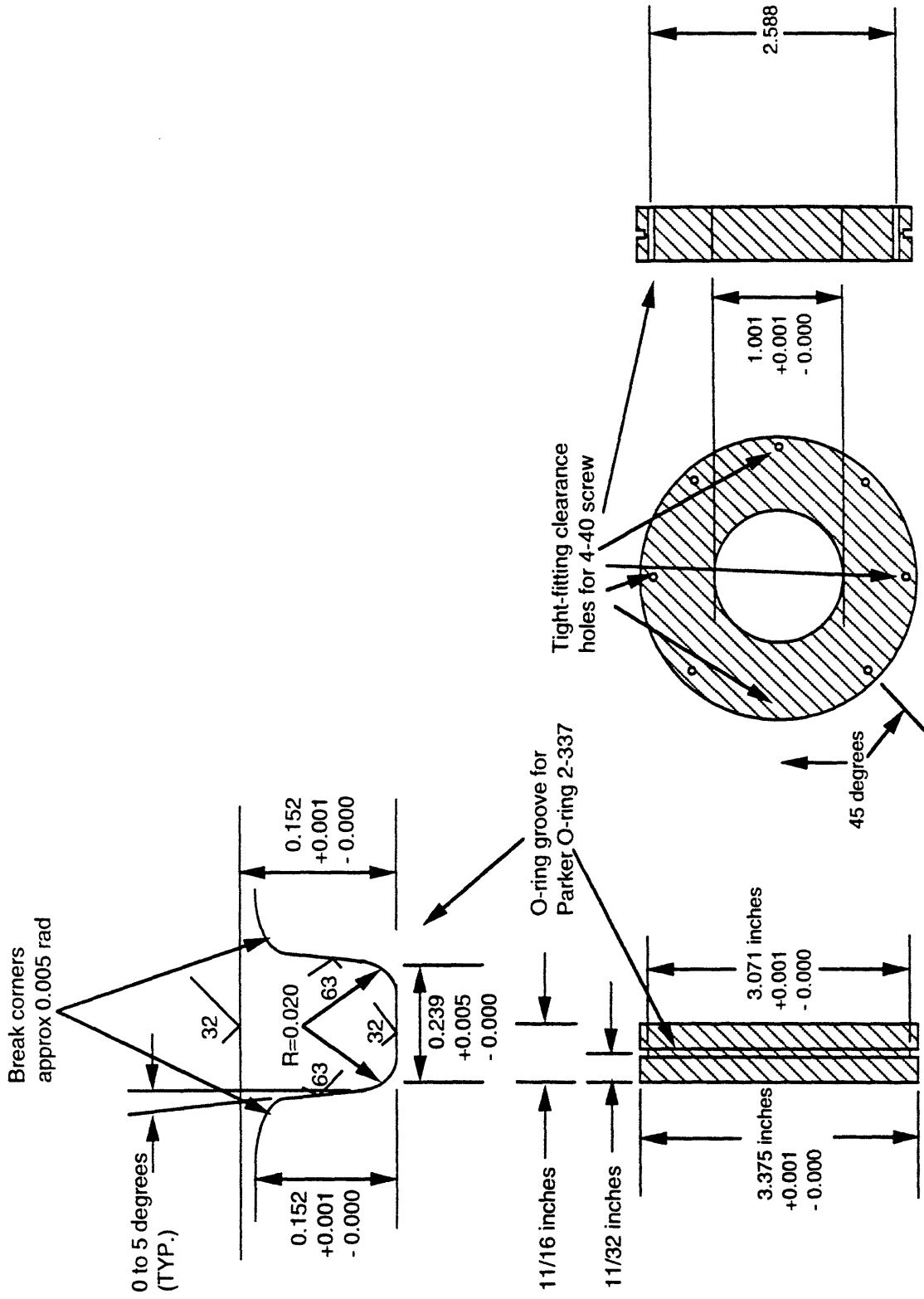


Figure 5.5. Teflon Ring for Heater Flange

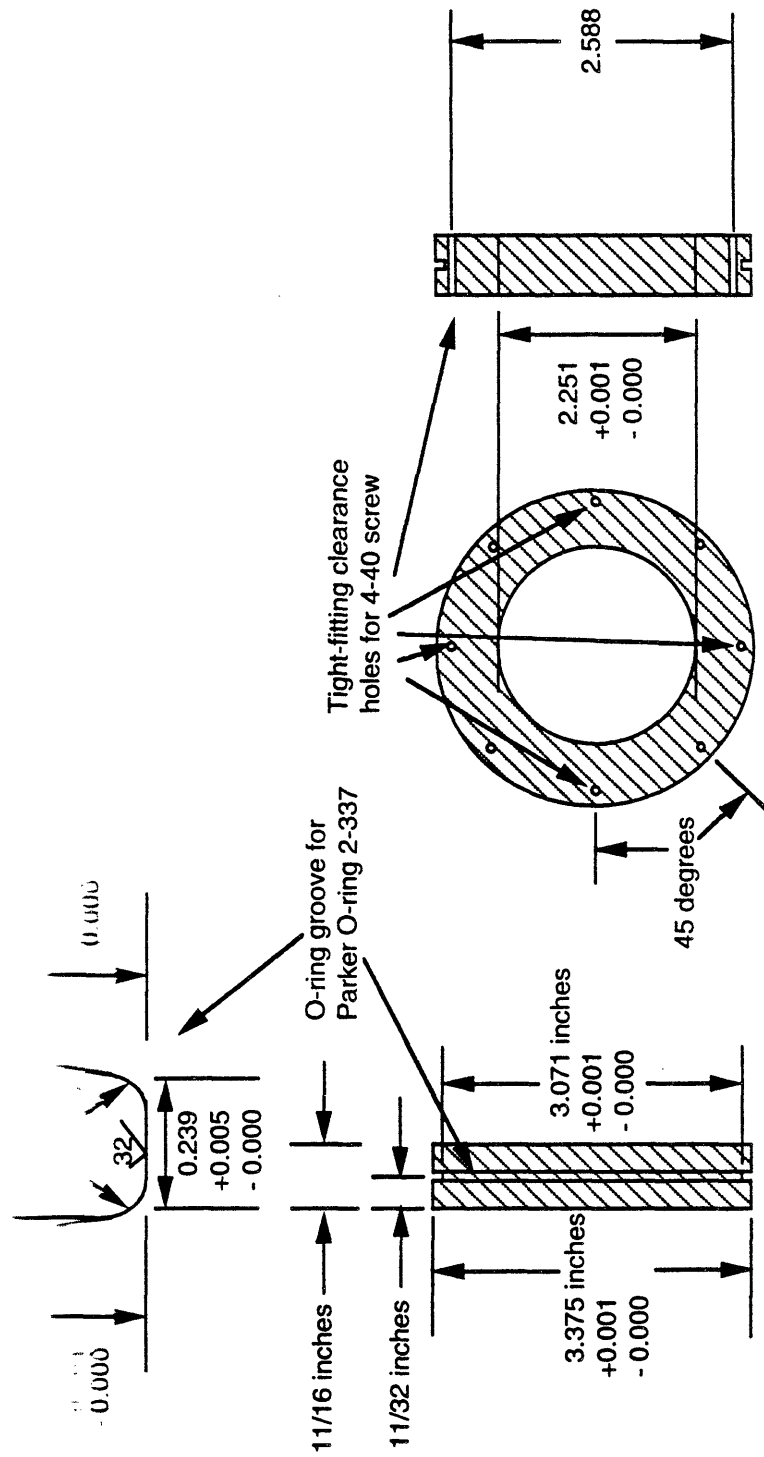


Figure 5.6. Teflon Ring for Stainless Steel Pipe Flanges

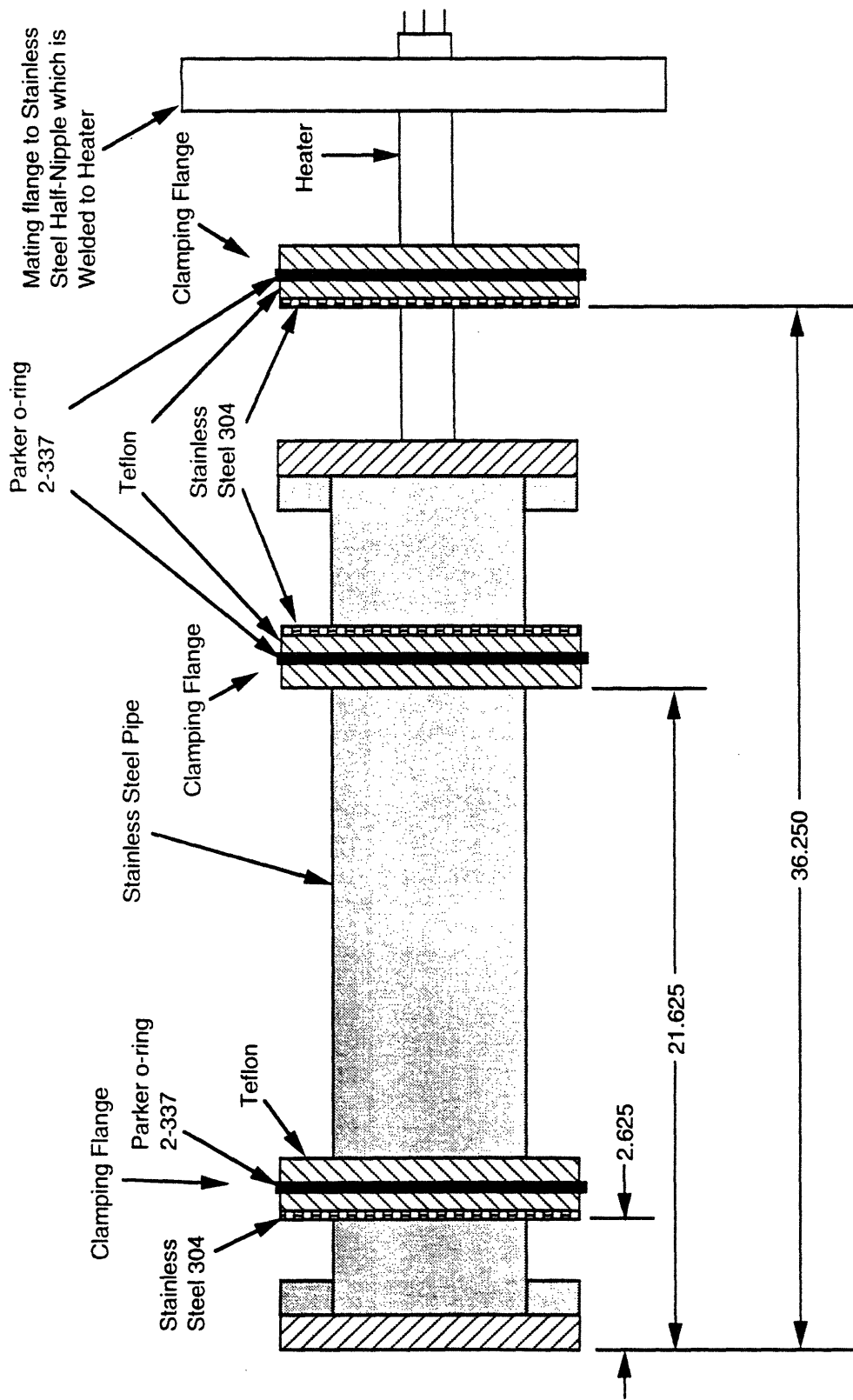


Figure 5.7. Location of Clamping Flanges (inches)

sleeves. The insulating sleeve clamping surface on the teflon ring was the 3.375-inch diameter curved surface of the teflon ring where the one-quarter-inch thick O-ring was located. The teflon ring was held to the stainless steel ring by eight 4-40 screws positioned every 45 degrees at a radius of 1.4045 inches. The screws entered through the teflon and screwed into the stainless steel ring. The 4-40 screw holes in the stainless steel were blind threaded holes 0.125 inches deep. (From a thermal insulating point of view, it would have been better to have the screws enter through the stainless steel ring and thread into the teflon. This way, the metal screws, which conduct thermal energy better than the teflon, would not have been exposed to the water in the stainless steel barrel. However, in the design stage of these flanges, it was discovered that the teflon screw threads would not support the shear stresses required. In any case, since the 4-40 screws had such a small cross sectional area, the insulating compromise was not too great.) There were two O-rings present to seal against water leakage; one at the stainless steel ring-teflon ring interface, and one, as mentioned above, on the 3.375-inch diameter curved surface of the teflon ring. The O-ring at the stainless steel ring-teflon ring interface was located at a radius of 1.537 inches. This O-ring kept any water leaking through the 4-40 clearance holes in the teflon confined to the water side of the flange. The O-ring on the insulating sleeve clamping surface prevented water leakage between the teflon ring and insulating sleeves. Hose clamps were used to secure the insulating sleeves to the teflon rings. Hose clamps were also used to secure the remaining insulating sleeve directly to the section of the 29.25-inch long unheated section of the heater which was not insulated by the other two sleeves. Thus, the insulating sleeves enveloped the areas of the stainless steel pipe which were not radially opposite the heated section of the heater, and the unheated section of the heater outside the stainless steel pipe. The stainless steel-teflon flanges were oriented such that the uncovered stainless steel ring surface (i.e., the surface not interfaced with the teflon) faced inward towards the insulated region so as not to be exposed to the water in the barrel. Hence, this insulating design kept axial heat energy losses to a minimum, since the only surfaces (besides the small heads of the 4-40 screws) in direct contact with the open water of the barrel were the insulating sleeves and the teflon of the clamping flanges, all of which had poor

heat transfer capability. Figure 5.8 shows the complete insulation system design with the insulating sleeves present. Note that for disassembly of the experimental setup to change the thermal switch, insulating sleeve #1 (refer to Figure 5.8) was slid directly off the end of the experimental setup, while insulating sleeve #2 was slid over insulating sleeve #3, which remained stationary. This readily exposed the two conflat flanges of the stainless steel pipe, allowing for easy disassembly of the setup.

The temperature measuring system utilized in the experiment was comprised of fourteen thermocouples and a Hewlett-Packard data acquisition unit. Of the fourteen thermocouples used, eight were situated on the heater, directly below its surface, and six were situated on the outside surface of the stainless steel pipe radially opposite the six central heater thermocouples, and radially located at the midpoint of the wall of the stainless steel pipe. The fourteen thermocouples' axial location relative to the sealing surface of the conflat flange (which was welded to the 29.25-inch unheated length of the heater and which mated with the stainless steel pipe) is shown in Figure 5.9.

The fourteen thermocouples used were K-type (Chromel-Alumel), ungrounded thermocouples with 30 gauge wire. Chromel-Alumel thermocouples with 30 gauge wire were used because this type of thermocouple has good temperature sensitivity for the temperatures the heater and stainless steel pipe attained during the experiment. Ungrounded thermocouples (instead of grounded thermocouples) were used to avoid any skewing of the data by possible ground loop currents that might have been present. There was a slight increase in the response time of the temperature reading, but this had no consequence for this experiment since data were acquired at steady state conditions.

The eight heater thermocouples were supplied and implanted by Watlow, the heater manufacturer. The six thermocouples located on the outside surface of the stainless steel pipe were purchased from Omega Engineering and attached at MIT. The eight heater thermocouples were bare wire thermocouples surrounded by MgO and protected from damage or breakage by their subsurface location. The six stainless steel pipe thermocouples were more exposed, and, hence, were encased in a stainless steel 304 sheath for protection. The thermocouple junction and

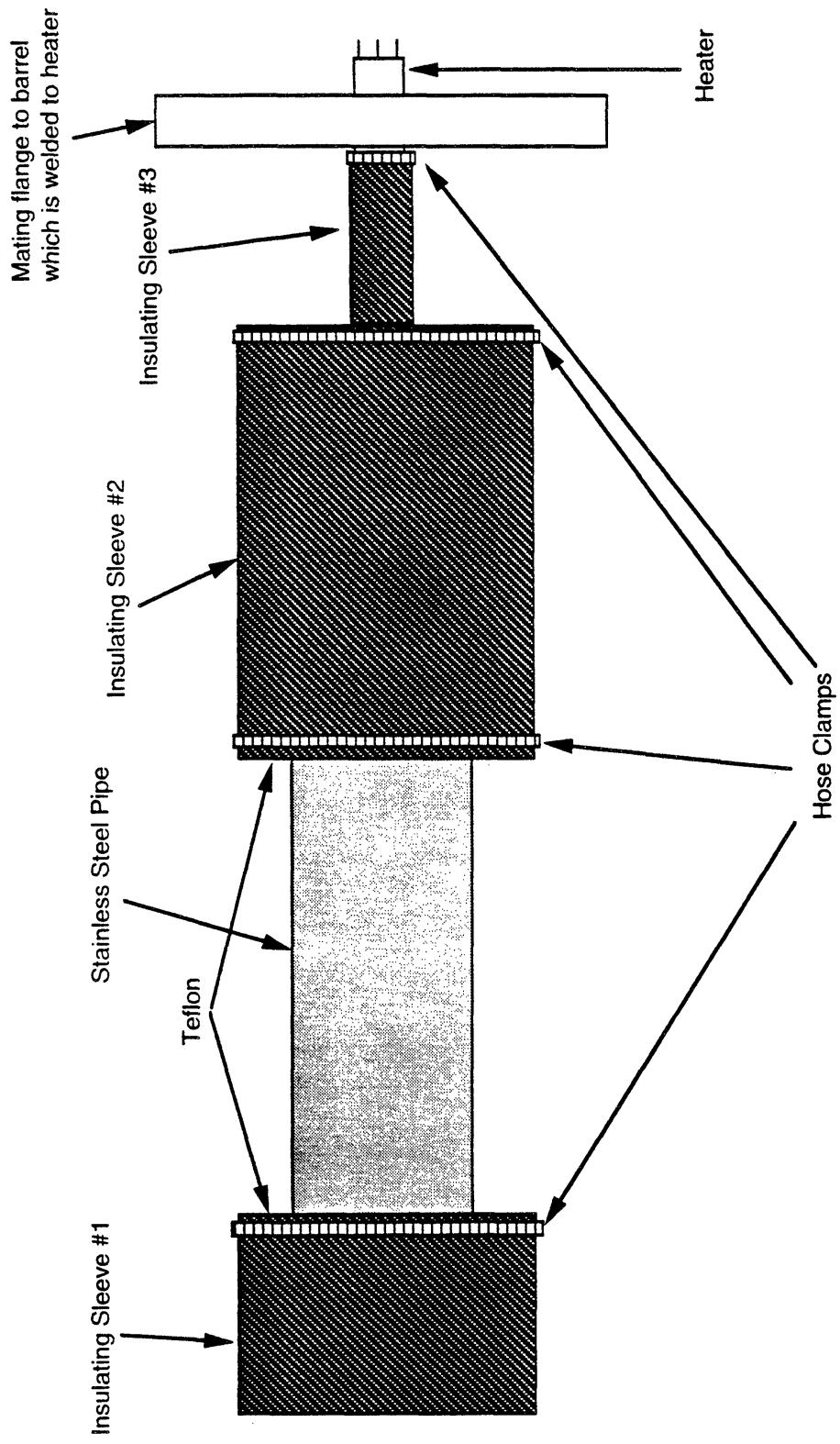


Figure 5.8. Complete Insulation System Design

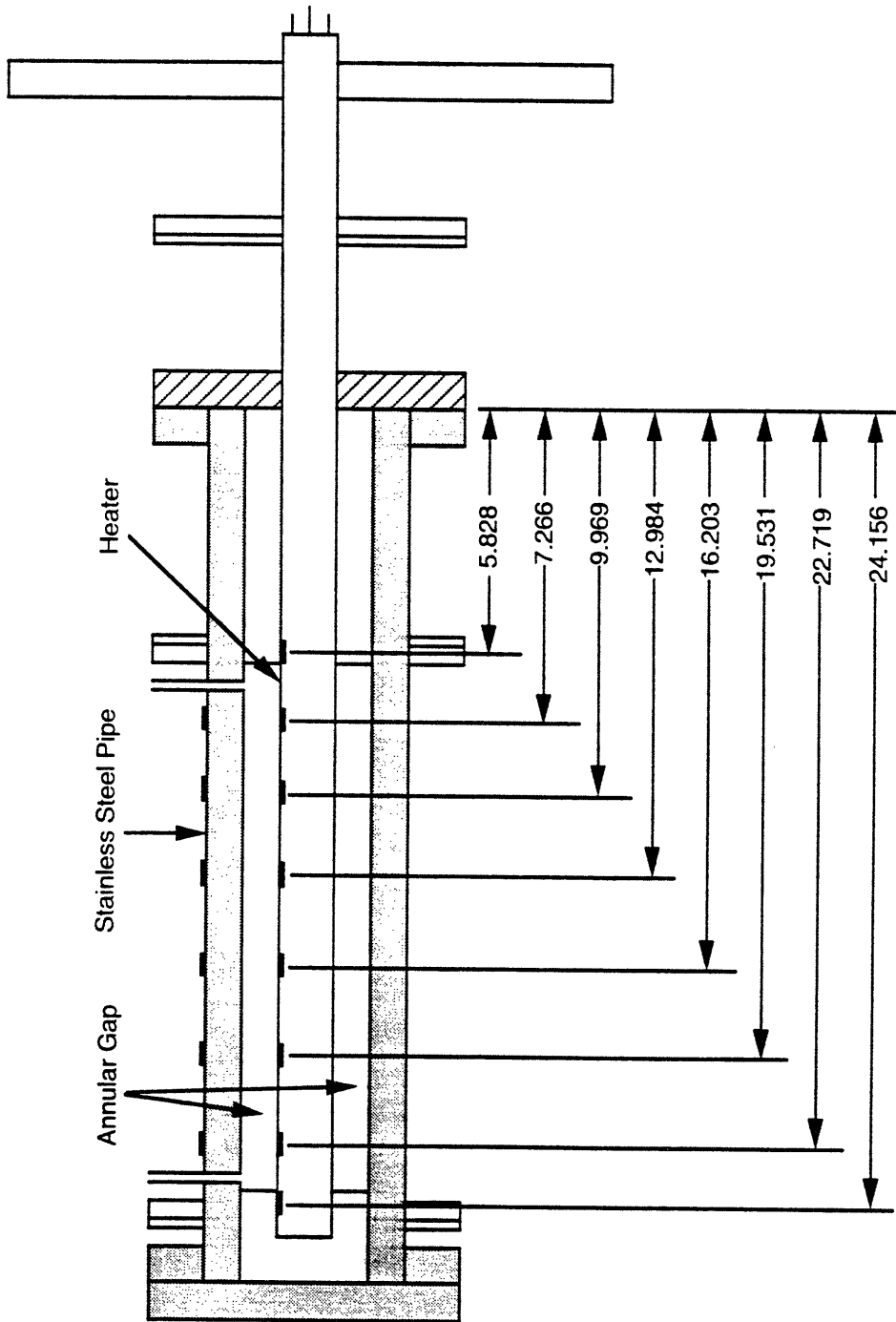


Figure 5.9. Thermocouple Locations (inches)

accompanying wires for these six stainless steel pipe thermocouples were electrically insulated from the stainless steel sheath by MgO. The thermocouple diameter including the sheath was 1/16 of an inch. The only disadvantage in using sheathed thermocouples is that an axial length of at least 10 diameters of the thermocouple from the thermocouple junction must be maintained at the same temperature as the thermocouple junction to avoid excessive thermal energy loss by axial heat conduction through the stainless steel sheath, away from the position of the thermocouple junction. If an axial length of at least 10 diameters from the thermocouple junction is not at the same temperature as the thermocouple junction, the temperature reading of the thermocouple will be well below the actual temperature of that point.

Thus to validly measure the temperature of the wall of the stainless steel pipe at its radial midpoint at the six axial locations specified earlier, the following mechanical adhesion process was followed. First, six grooves 1/16th of an inch in width and 3/32nd of an inch deep were cut into the stainless steel pipe at the six axial locations of the central six thermocouples of the heater. The grooves were made by mounting the pipe on a lathe and using a cutting tool. Second, six butt welds were placed and polished in the grooves at the same angular locations of the six central thermocouples of the heater. (In other words the butt welds were radially opposite the six central heater thermocouples.) Third, 3/32nd of an inch holes were drilled into 6 hose clamps into which the thermocouples slid. The hose clamps were used as mechanical fasteners of the thermocouples to the stainless steel pipe. Fourth, the first five inches (80 diameters of the sheath) of the thermocouple measured from the tip of the thermocouple where the thermocouple junction is located were bent in a radius of curvature of 1.06 inches (the radial distance from the axial centerline of the stainless steel pipe to the axial centerline of the thermocouple's position in its groove). Fifth, the six thermocouples were placed in the grooves and butted up against the welds. This resulted in six thermocouple junctions being radially opposite the six central heater thermocouples. In addition, the five-inch arc made in step four resulted in the thermocouples being wrapped around the stainless steel pipe for three quarters of a turn, and then vertically and tangentially leaving the stainless steel pipe. Hence, with the thermocouples now properly

positioned, they were then mechanically clamped to the stainless steel pipe using the hose clamps. (Note that the holes drilled in the hose clamps were positioned such that, when the thermocouples were clamped into place, the solid area of the hose clamps [i.e., the area with no thread] covered the first 40 diameters of the thermocouple, shielding the top side of the thermocouple.)

The six thermocouples attached to the stainless steel pipe were made 30 inches long. This was to ensure that after they were attached to the pipe, the mechanical banana clip located at the end of the thermocouple and used to link the thermocouple to instrumentation, was positioned above the waterline in the stainless steel barrel. Hence, the water in the stainless steel barrel used as a heat sink could not short circuit the thermocouple voltage signal.

The eight heater thermocouples and the six thermocouples attached to the stainless steel pipe, along with one other thermocouple used to measure the temperature of the water in the stainless steel barrel, were all linked to an HP3852A data acquisition unit. This electronic unit converted the thermocouple voltages to temperature readings and displayed the readings on its front panel. The data acquisition unit was calibrated by Hewlett-Packard prior to data acquisition.

The heater, stainless steel pipe, accompanying thermocouples, and insulating sleeves, entered the stainless steel barrel via a port in the side of the barrel. The port was created by drilling a hole in the stainless steel barrel, and welding a stainless steel half-nipple into the hole. (A half-nipple is a pipe with a conflat flange welded to one end of the pipe.) The end of the stainless steel half-nipple without the conflat flange was the end welded to the stainless steel barrel. It was welded flush with the inside surface of the wall of the barrel. The stainless steel half-nipple was three feet long with a 6.5-inch O.D. and a 6.0-inch I.D. The centerline of the half-nipple was 18.25 inches below the top of the stainless steel barrel. The conflat flange on the stainless steel half-nipple was 8 inches in diameter. An 8-inch conflat flange was welded to the end of the 29.25-inch unheated length of the heater (from which emanated the wires of the heater thermocouples and the power leads of the heater) to mate with the 8-inch conflat flange on the stainless steel half-nipple. The mating of the two 8-inch conflat flanges provided a water tight seal at the entrance port of the stainless steel barrel for the heater and the stainless steel pipe. In addition this support, in

conjunction with an adjustable-height support stand at the other end of the heater-stainless-steel-pipe setup, held the heater and stainless steel pipe in a horizontal position. (Without the support stand the heater and pipe were found to have an unacceptable deflection when mounted in the barrel.) The adjustable stand at the other end of the heater was comprised of 3/8-16 threaded stainless steel rod, two 1.75-inch long stainless steel nuts, two 0.75-inch long stainless steel nuts with stainless steel rods welded to them for turning handles, and a one-quarter inch thick piece of stainless steel bar (approximately 4 inches long and 0.5 inches wide) bent into a U-shape with a radius of curvature equivalent to the outside radius of the stainless steel pipe (see Figure 5.1). As shown in the figure, this U-shaped piece of metal cradled the stainless steel pipe between the clamping flange for the insulating sleeve at this end and the VCR gland-nut combination welded at this location. (This VCR gland-nut combination welded at this end mated with either the water-inlet system or the CO₂ pressurization system used to alter test conditions in the 18-inch annular test region. The water-inlet system and the CO₂ pressurization system are discussed later in this section.) At the lowest point of this U-shaped piece of metal was welded, along its axial axis, one of the 1.75-inch long nuts. This nut was drilled out to allow free rotational movement of the rod. Vertically below this nut was welded the other 1.75-inch nut to the base of the barrel. The stainless steel rod was threaded into this nut welded to the base of the barrel to provide support for the stand. The end of the rod was positioned approximately halfway through this nut when the heater and stainless steel pipe were precisely horizontal. This allowed both an upward and downward 0.875-inch vertical adjustment about this horizontal point. (Angular orientation of the thermal switch with respect to the horizontal is a parameter that might be investigated in the future. In addition, this vertical degree of freedom of the support stand allowed it to be moved out of the way during introduction and removal of the heater and pipe from the stainless steel barrel.) One of the 0.75-inch nuts was positioned directly above this 1.75-inch nut welded to the base of the barrel. The purpose of this 0.75-inch nut was to eliminate any angular play in the adjustable stand (since the threads of the nut welded to the base of the barrel were slightly larger than the threads of the stainless steel rod). This was accomplished by tightening this 0.75-inch nut against the 1.75-inch

nut supporting the threaded stainless steel rod. One-quarter inch stainless steel plain rod approximately three inches long was welded to diametrically opposing sides of this 0.75-inch nut to allow tightening of this nut against the 1.75-inch nut without the need of a wrench. (The stainless steel plain rods were welded to the 0.75-inch long nut such that their axial axis was perpendicular to the axial axis of the nut.) Turning of the threaded rod was accomplished using the other 0.75-inch nut which was screwed onto the threaded rod and welded to it approximately halfway between the two 1.75-inch nuts. As with the other 0.75-inch nut, one-quarter inch stainless steel plain rod approximately three inches long was welded to the sides of the nut to aid in turning the nut (and, hence, adjustment of the support stand).

As mentioned previously, the water in the stainless steel barrel was the heat sink of the experiment. Water was introduced into the barrel by tygon tubing attached to a water faucet. During testing, this water was mixed by blowing compressed air through perforated tubing located at the bottom of the barrel. This prevented thermal stratification of the water and, hence, provided for a more consistent heat sink boundary condition from test to test. The tubing spanned the diameter of the barrel and was 0.375 inches in diameter with 0.25-inch holes drilled into both sides of it. The holes were spaced 0.50 inches apart. At the end of the testing, when a new thermal switch had to be inserted into the annular test section, the water in the barrel was pumped out using a water pump mounted off-center at the top of the barrel. The pump was comprised of an electric motor and a 30-inch long shaft which was one inch in diameter. The motor sat at the top of the pump with the shaft extending out the bottom of the motor and into the water to the base of the barrel. The shaft of the pump was press-fit into a 2 X 4 inch block of wood 2 feet long. The wood was positioned at the top of the shaft directly below the electric motor. The pump was mated with the barrel by bolting the block of wood to a stainless steel plate 4 inches wide welded to the top of the barrel. A block of wood was used to interface the pump to the barrel to absorb some of the acoustic energy travelling from the pump to the barrel.

The control panel and circuit that were used to power the heater are shown in Figures 5.10 and 5.11, respectively. The control panel consisted of a variac (model type W20M), and ammeter

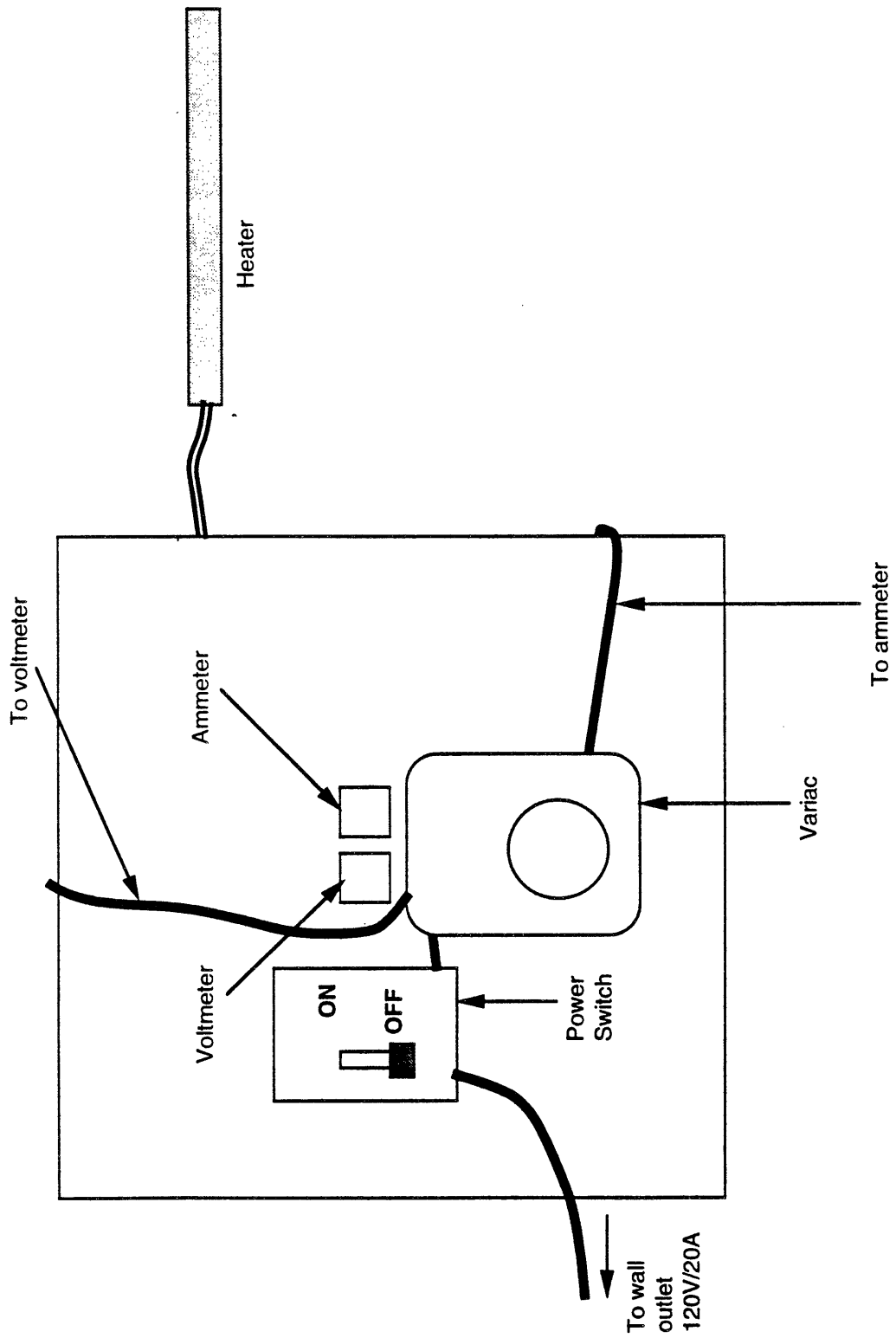


Figure 5.10. Heater Control Panel

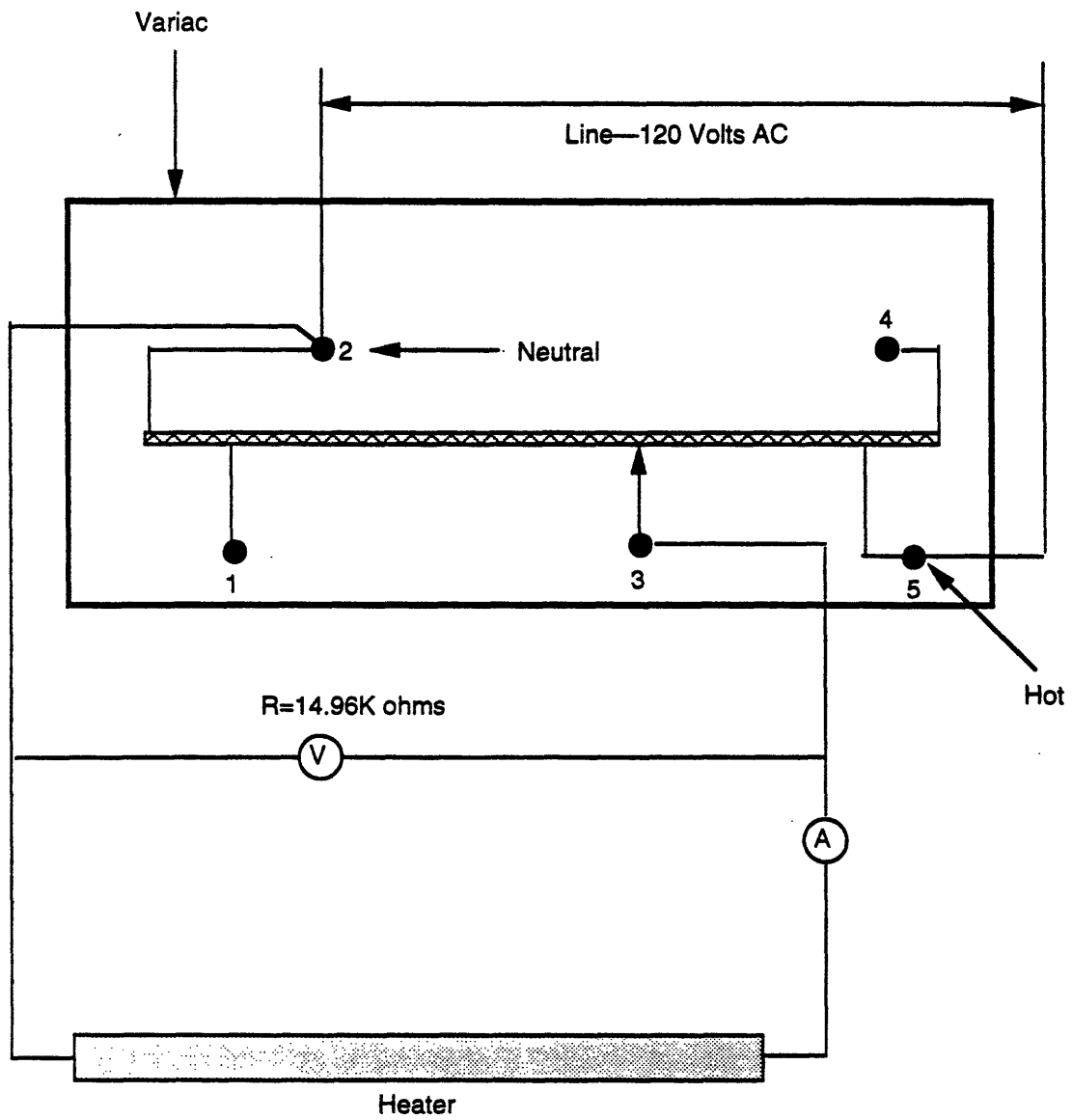


Figure 5.11. Circuit to Power Heater

(Yokogawa, 0–20 amps), a voltmeter (Yokogawa 0–150 volts), and a switch fuse box (240 volts maximum, 30 amps maximum). The ammeter showed the current present in the heater, while the voltmeter gave the electric potential across the heater's terminals. Their product (current multiplied by voltage) yielded the power input to the heater. The variac controlled the electrical power input to the heater. The variac was wired (see Figure 5.11) to provide an output voltage that was 17% greater than the input line voltage, with a maximum allowable output current of 20 amps. For the line voltage that was present in the building, this meant a maximum output voltage of 135.6 volts. For the heater that was used in this experiment, which had a heater coil resistance of approximately 9.36 ohms, this meant a heater current of 14.49 amps. Thus, this circuit could supply a maximum 1964.5 watts of heater power, which corresponded to a surface heat flux of 53.85 kW/m². It also yielded a maximum heater surface temperature that was well in excess of what was required for all of the experiments performed. (Note that other means of controlling heater power input such as QPAC's, VPAC's, and temperature controller devices manufactured by Watlow, were investigated as well, but these systems did not offer the same ease and accuracy for supplying and measuring heater power input as did the variac system outlined above. Consequently the variac system with the accompanying meters was chosen.)

For the experiments planned, a vacuum pumping system, water inlet system, and CO₂ pressurization system were required to be interfaced with the 18-inch annular test section. The key components of the vacuum pumping system were the vacuum pump, the pressure/vacuum gauge, the water filter, and the foreline trap. The function of the vacuum pump was to pump down the annular region, thus creating a vacuum where the thermal switch was being tested. The purpose of the pressure/vacuum gauge was to indicate the pressure in the annular region. The function of the water filter was to collect any moisture before it reached the vacuum pump (thus protecting the pump and extending its longevity), and the function of the foreline trap was to prevent oil vapors from the vacuum pump from diffusing into the system when low pressure existed in the tubing leading to the vacuum pump. The specific arrangement and linking setup of these components is shown in Figure 5.12 and explained below.

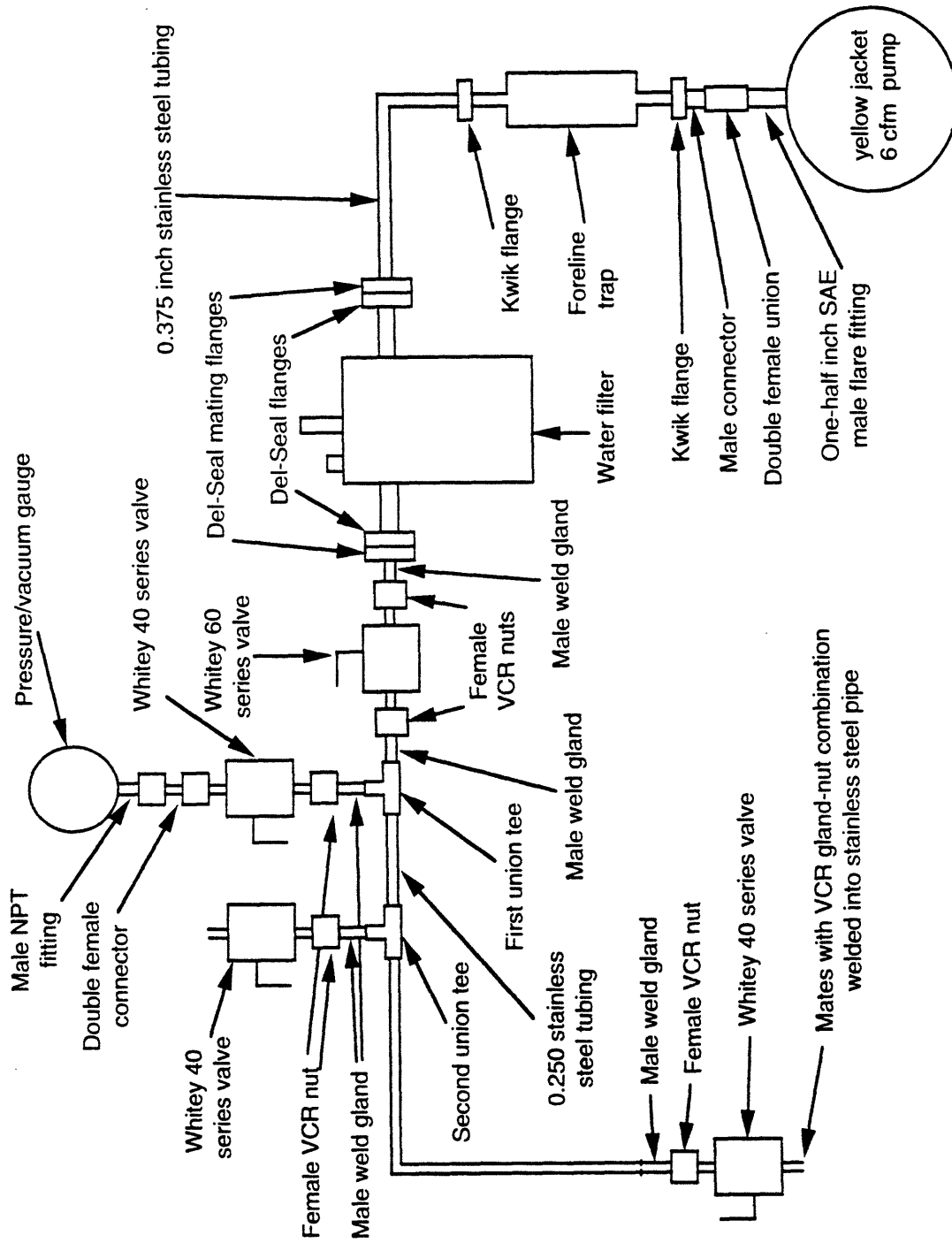


Figure 5.12. Vacuum Pumping System

The system pumping was provided by a six cubic-feet-per-minute, two-stage, rotary vane pump. The intake port on the pump was a one-half inch SAE male flare fitting. Connected to this intake port was a double female union. On the other side of this female union was a male connector which converted from a one-half inch SAE male flare fitting to a one-half inch male NPT fitting. This male NPT fitting mated with a kwik flange which had a one-half inch female NPT fitting. The foreline trap containing the stainless steel sieve element mated with this kwik flange. At the top of the foreline trap was another kwik flange. This kwik flange had a 0.375-inch hole at its center into which 0.375-inch tubing was inserted and welded. This stainless steel tubing led to the water filter. The water filter had two 2.75-inch diameter Del-Seal flanges which were diametrically opposite to one another across the water filter. The water filter was oriented such that one of the flanges faced the pump and the other faced the pressure/vacuum gauge. The 0.375-inch tubing leading from the foreline trap was welded to a Del-Seal mating flange which was bolted to the Del-Seal flange of the water filter facing the pump. Mated to the other Del-Seal flange of the water filter (facing the pressure/vacuum gauge) was another Del-Seal mating flange. This mating flange was welded to one-quarter-inch tubing which was welded to a two-port Whitey 60 series valve. This valve provided isolation of the test section and the pressure/vacuum gauge from the vacuum pump and filters during testing. At the other port of the Whitey 60 series valve was welded another piece of tubing which was welded to a union tee. The vertical leg of this union tee was welded to a male gland fitted with a female VCR nut. This gland and nut mated to a two-port Whitey 40 series valve, which had a double female connector attached to its other port. The double female connector was comprised of a gland and VCR nut combination, and a one-quarter inch female NPT fitting. The gland-nut combination mated with the Whitey 40 series valve, and the female NPT fitting mated with the male one-quarter inch NPT fitting on the pressure/vacuum gauge. The horizontal leg of the union tee was welded to one-quarter inch stainless steel tubing leading to the horizontal leg of a second union tee. The perpendicular leg of this second union tee was welded to a male weld gland, to which was attached a female VCR nut. This male gland and female VCR nut mated with a two-port Whitey 40 series valve, which provided venting for the

system back to atmospheric pressure when desired. The other horizontal leg of this second union tee was welded to one-quarter inch stainless steel tubing, which led to the heater and stainless steel pipe positioned in the stainless steel barrel. At the heater and stainless steel pipe the tubing was welded to a male-gland-female-nut combination, which mated to another two-port Whitey 40 series valve. This valve, which isolated the test section from all other aspects of the pumping system, was attached to a VCR gland-nut combination which was welded into a thru-hole in the stainless steel pipe leading into the test section.

The water inlet system allowed for the introduction of measured amounts of water into the annular region between the heater and stainless steel pipe. It was comprised of a needle valve, a two-port Whitey 40 series valve, a graduated 500 cubic centimeter stainless steel container, a one-quarter inch VCR female-nut-male-gland combination, and 3/8 inch thick-walled stainless steel tubing. It was constructed as follows (see Figure 5.1). The graduated stainless steel cylinder, with a 3/8-inch hole drilled into its base, had the thick-walled stainless steel tubing welded into this hole. The tubing was flush with the inside surface of the cylinder. Three inches below the base of the cylinder the tubing was welded to a needle valve. The needle valve was used to allow precise control of the introduction of water into the system. It was located at this position to allow, while water was being introduced into the test section, direct viewing of the graduated markings etched into the inside wall of the stainless steel cylinder so the proper amount of water would be introduced. Approximately fifteen inches below this needle valve the stainless steel tubing was welded to a male VCR gland. This male VCR gland had a female VCR nut associated with it and together they interfaced with a two-port Whitey 40-series valve. The other side of this valve mated with a VCR gland-nut combination which was welded into a thru-hole in the stainless steel pipe leading into the test section. (Note that this connection occurred at the end opposite where the vacuum pumping system was connected). This Whitey 40-series valve at the bottom of this setup was required to isolate the test section volume from the extra volume provided by the tubing.

The filling and pressurization of the annular region with CO₂ gas was accomplished using a CO₂ canister, a CO₂ regulator, one-quarter inch nylon tubing, and a two-port Whitey 40 series

valve. The CO₂ regulator was directly attached to the CO₂ canister. The nylon tubing connected the CO₂ regulator to the Whitey 40 series valve. The nylon tubing mated with the Whitey 40 series valve via a swagelok, a swagelok-male VCR fitting, and a double female union (see Figure 5.13). The valve mated with the same male VCR gland and female VCR nut used by the water-inlet system of the stainless steel pipe. (Hence, the water-inlet system was not present in the experimental setup when the CO₂ pressurization system was being used.) As in the water-inlet system, the Whitey 40 series valve was used to isolate the annular volume where the thermal switches were being tested from the extra volume provided by the tubing leading into the annular volume. The CO₂ regulator was used to control the CO₂ pressure in the annular region.

Thus, the above described experimental setup provided the raw data required to determine the on-mode and off-mode heat transfer coefficients for the thermal switches being tested. (A list of the parts of the experimental setup and the vendor from which they can be obtained is given in Appendix B.) The raw data required was the electrical power input to the heater and the corresponding temperatures at the location of the thermocouples. Once the raw data was acquired, an algorithm was employed (which was in computer code form) to convert the raw data to on-mode and off-mode heat transfer coefficients of the thermal switches. The exact experimental procedure followed to acquire the raw data, and the algorithm utilized to reduce the data is discussed below.

Section 5.3 Experimental Procedure and Raw Data Reduction Algorithm

For both the on-mode and off-mode of the thermal switches, the initial heater power input was approximately 57 watts. Heater power input was kept at this initial value until quasi-steady state was reached by the system. (Note that, at times, the variac had to be adjusted to maintain a constant heater power input because the resistance of the electric coils of the heater changed with temperature.) For these experiments, quasi-steady state was considered to have been attained when there was less than a 1°C change in the readings of the thermocouples over a thirty minute period. At this point, the heater power input and all the thermocouple readings were recorded.

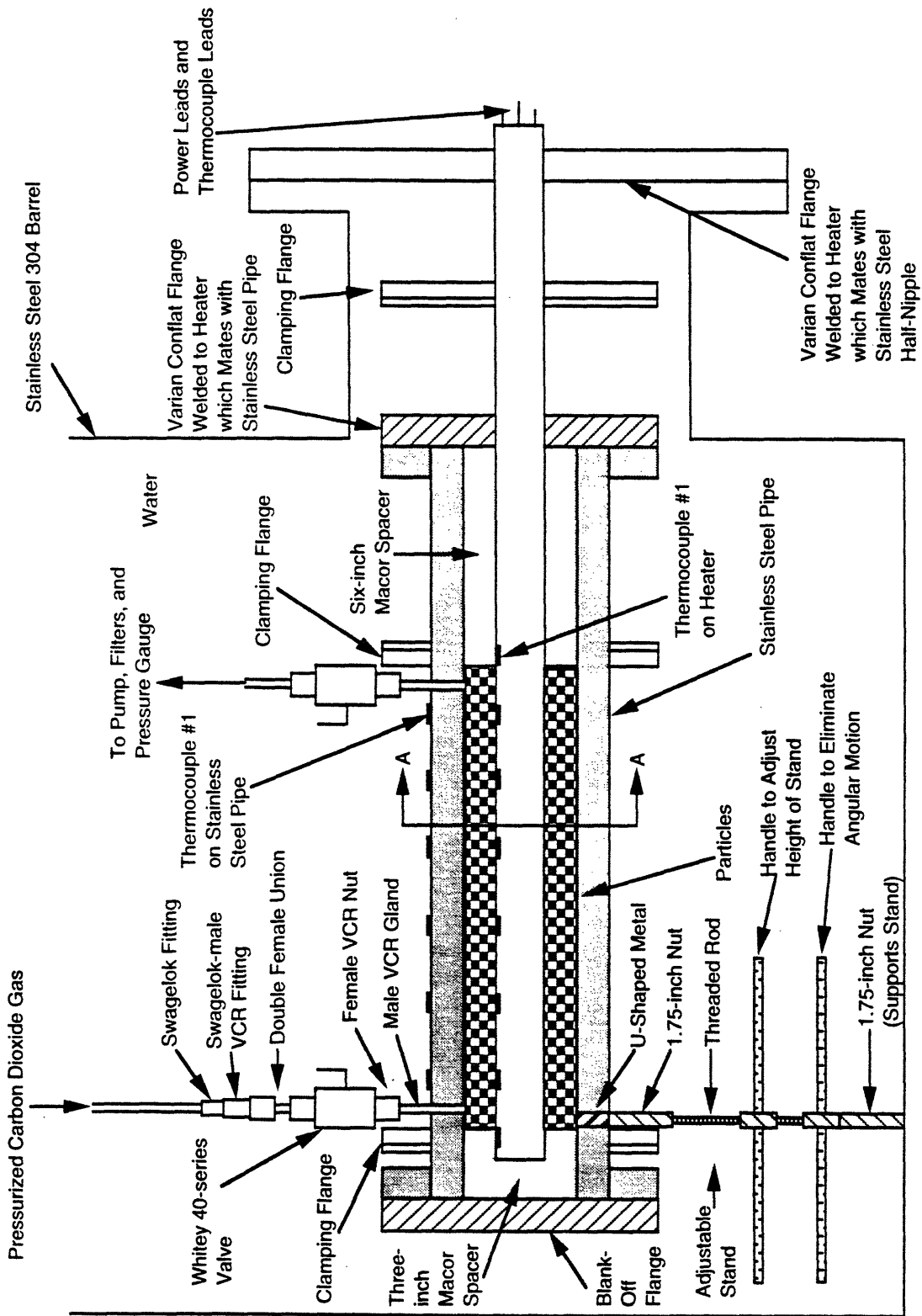


Figure 5.13. Particle Bed Thermal Switch

Next, the electrical power input to the heater was increased to approximately 105 watts by altering the variac setting. Again, this heater power value was kept constant, and at quasi-steady state, the raw data was recorded. This process was repeated with larger and larger heater input powers until the maximum heater input power was reached, or until the temperature readings of the heater thermocouples were approximately 500°C. (Although the heater maximum operating temperature is approximately 800°C, the 500°C termination point was used to extend the heater's longevity so that more experiments could be performed in the future.) Once raw data acquisition was completed for all three thermal switches in both the on-mode and off-mode, the following algorithm was employed to obtain the heat transfer coefficients of the thermal switches for each mode of operation as a function of temperature difference between the heater surface and the inside stainless steel pipe surface, and as a function of heater surface flux.

The temperature data from the eight heater thermocouples were used to derive seven cubic polynomials (i.e., one cubic polynomial for each successive pair of thermocouples). The cubic polynomials had the following characteristics:

$$1. \quad T_1(x_1) = t_1 \quad (5.1)$$

$$T_j(x_{j+1}) = T_{j+1}(x_{j+1}) = t_{j+1} \quad j = 1, 2, \dots, 6 \quad (5.2)$$

$$(x_8) = t_8 \quad (5.3)$$

where: T_j = cubic polynomial for temperature distribution between
thermocouple j and thermocouple $j+1$

x_j = axial location of thermocouple j

t_j = temperature reading of thermocouple j

$$2. \quad d[T_j(x_{j+1})]/dx = d[T_{j+1}(x_{j+1})]/dx \quad j = 1, 2, \dots, 6 \quad (5.4)$$

$$3. \quad d^2[T_j(x_{j+1})]/dx^2 = d^2[T_{j+1}(x_{j+1})]/dx^2 \quad j = 1, 2, \dots, 6 \quad (5.5)$$

$$4. \quad d^2[T_1(x_1)]/dx^2 = d^2[T_7(x_8)]/dx^2 = 0 \quad (5.6)$$

These seven cubic polynomials provided a very accurate analytical description of heater surface temperature as a function of axial location between thermocouple #1 and thermocouple #8.

Next, knowing that tightly packed MgO was present in the internal part of the heater from the center to the radial location $r = 0.338$ inches, and stainless steel 304 was present from $r = 0.338$ inches to $r = 0.498$ inches (the outside radius of the heater), the composite thermal-conductivity-cross-sectional-area product of the heater was calculated:

$$\begin{aligned} A_{cs} \text{ of MgO} &= \pi[(0.338 \text{ in})^2 - (0.000 \text{ in})^2] & (5.7) \\ &= 0.3589 \text{ in}^2 \\ &= 2.317 \times 10^{-4} \text{ m}^2 \end{aligned}$$

$$\begin{aligned} A_{cs} \text{ of SS 304} &= \pi[(0.498 \text{ in})^2 - (0.338 \text{ in})^2] & (5.8) \\ &= 0.4202 \text{ in}^2 \\ &= 2.712 \times 10^{-4} \text{ m}^2 \end{aligned}$$

$$K \text{ of MgO} = 14.4 \text{ (Btu-in)/(hr ft}^2 \text{ }^\circ\text{F)} = 2.076 \text{ W/(m}^\circ\text{C)} \quad (5.9)$$

$$K \text{ of SS 304} = 105.6 \text{ (Btu-in)/(hr ft}^2 \text{ }^\circ\text{F)} = 15.228 \text{ W/(m}^\circ\text{C)} \quad (5.10)$$

$$\begin{aligned} (KA_{cs})_{\text{heater}} &= (KA_{cs})_{\text{MgO}} + (KA_{cs})_{\text{SS 304}} & (5.11) \\ &= [(2.076 \text{ W/(m}^\circ\text{C)})(2.317 \times 10^{-4} \text{ m}^2) \\ &\quad + (15.228 \text{ W/(m}^\circ\text{C)})(2.712 \times 10^{-4} \text{ m}^2) \\ &= 4.611 \times 10^{-3} \text{ (W m)/}^\circ\text{C} \end{aligned}$$

where: A_{cs} = cross-sectional area (m^2)
 K = thermal conductivity $\text{W/(m}^\circ\text{C)}$
 $(KA_{cs})_{\text{heater}}$ = thermal-conductivity-cross-sectional-area product
of the heater ($\text{W m)/}^\circ\text{C}$

As mentioned previously, the active heater length was 18 inches long. For data reduction this 18-inch active heater length was segmented into 511 cylinders of uniform length (i.e., each cylinder was $18/511$ inches long). Hence, knowing the input power of the heater from the ammeter and voltmeter of the electrical circuit powering the heater, as well as the fact that the heater was constructed to provide a uniform radial heat source flux from its heating coils along the 18-inch active heater length, and utilizing the two pieces of information of the temperature of the heater as a function of axial location and the thermal-conductivity-cross-sectional-area product of

the heater, the net radial heat transfer rate from each heater cylinder to the stainless steel pipe was calculated:

$$q_r = q_{in} - q_{out} \quad (5.12)$$

$$= q_h/511 - [(KA_{CS})_{heater} (dT/dx|_L - dT/dx|_R)] \quad (5.13)$$

$$= (IV)/511 - [(4.611 \times 10^{-3} \text{ (W m)/}^\circ\text{C})(dT/dx|_L - dT/dx|_R)] \quad (5.14)$$

where:

q_r = radial heat transfer rate from the cylindrical heater element (watts)

q_{in} = radial heat transfer rate into the cylindrical heater element from the heating coils(watts)

q_{out} = axial heat transfer rate out of the cylindrical heater element (watts)

q_h = power output of entire heater from heating coils (watts)

$(KA_{CS})_{heater}$ = thermal-conductivity-cross-sectional-area product
of the heater (W m)/ $^\circ\text{C}$

I = current input to heater (amps)

V = voltage drop across heater terminals (volts)

$dT/dx|_L$ = axial temperature gradient at left boundary of
cylindrical heater element ($^\circ\text{C/m}$)

$dT/dx|_R$ = axial temperature gradient at right boundary of
cylindrical heater element ($^\circ\text{C/m}$)

Next, knowledge of the net radial heat flux from each heater cylinder radially opposite the six thermocouples attached to the stainless steel pipe, and knowledge of the temperature readings of each of these six thermocouples allowed, via the analytical equation given below, the calculation of the temperature of the inside surface of the stainless steel pipe at the same axial locations as the external thermocouples. The equation utilized is:

$$T_i(x) = [(q_r/l)(\ln(r_o/r_i))/(2\pi K_{SS\ 304})] + T_o(x) \quad (5.15)$$

where: $T_i(x)$ = temperature of the inside wall of the stainless steel pipe at axial location x
where the thermocouple is located ($^\circ\text{C}$)

q_r = radial heat transfer rate of the cylindrical heater element (watts)

- l = length of the cylindrical heater element = 18/511 inches = 8.95×10^{-4} m
- r_o = radial location of thermocouple on stainless steel pipe = 1.065 inches = 2.71×10^{-2} m
- r_i = inside radius of the stainless steel pipe = 1.000 inches = 2.54×10^{-2} m
- K_{SS304} = thermal conductivity of stainless steel pipe = 15.228 W/(m°C)
- $T_o(x)$ = temperature of the outside wall of the stainless steel pipe at axial location x and radial location r_o (°C)

Hence, with the temperature known at six axial locations on the inside stainless steel pipe surface, five cubic polynomials were derived (one cubic polynomial for each successive pair of thermocouples) which gave the temperature of the inside surface of the stainless steel pipe as a function of axial location. This approach is the same approach that was used to model the axial temperature distribution of the heater surface. Thus, with the axial temperature distribution modelled for both the heater surface and inside stainless steel pipe surface, the average temperature of each of the elements comprising each surface could now be determined. The equation that was utilized to do this is:

$$T_n = \left(\int_{x_n - \frac{l}{2}}^{x_n + \frac{l}{2}} T(x) dx \right) / l \quad (5.16)$$

- where:
- T_n = average temperature of cylindrical element n of the heater surface or annular element n of the inside stainless steel pipe surface (°C)
 - $T(x)$ = temperature distribution as a function of axial position x for heater surface or inside stainless steel pipe surface (°C)
 - x_n = center axial position of cylindrical element n of the heater surface or annular element n of the inside stainless steel pipe surface
 - l = length of element n = 18/511 inches = 8.95×10^{-4} m

Knowledge of the average temperature of each element on both the heater surface and inside stainless steel pipe surface, as well as the radial thermal power output of each 18/511-inch long cylindrical heater element, then allowed calculation of the heat transfer coefficient of the annular elements comprising the thermal switch. The equation used to do this is:

$$U_n = [(q_r)_n / (\pi D_h l)] / [(T_n)_{heater} + (T_n)_{pipe}] \quad (5.17)$$

where:

- U_n = heat transfer coefficient of annular element n of the thermal switch
(watts/m²/°C)
- $(q_r)_n$ = radial heat transfer rate through annular element n of the thermal switch
(watts)
= radial power output of cylindrical heater element n (watts)
- D_h = outside diameter of heater = 0.996 inches = 2.53 X 10⁻² m
- l = length of cylindrical heater element n = 18/511 inches = 8.95 X 10⁻⁴ m
- $(T_n)_{heater}$ = average surface temperature of cylindrical heater element n (°C)
- $(T_n)_{pipe}$ = average inside surface temperature of annular element n of
the stainless steel pipe (°C)

The computer code written which incorporated this data reduction algorithm (documented in Appendix D) has as one of its inputs the left and right axial boundaries of the interval over which the mean heat transfer coefficient was to be calculated. For this project, the left axial boundary was chosen to be at thermocouple #3 and the right axial boundary was chosen to be at thermocouple #6. This choice of axial boundaries further reduced any end effects. Thus, the overall mean heat transfer coefficient of the thermal switch was the arithmetic average of the heat transfer coefficient of the annular elements comprising the thermal switch over this interval.

After completion of this raw data reduction algorithm for all three thermal switches in both the on-mode and off-mode under various test conditions (i.e., air present, vacuum present, etc.) for all the heater power settings investigated, the next step performed was the calculation of the average temperature difference between the heater surface and the inside stainless steel pipe surface

for the axial interval over which the heat transfer coefficient of the thermal switch was calculated. As just stated, for this project, this axial interval extended from thermocouple #3 to thermocouple #6. This average temperature difference between the heater surface and inside stainless steel pipe surface was obtained by dividing the average radial heat flux at the surface of the heater over this interval by the average heat transfer coefficient of the thermal switch over this interval. Once this step was completed, plots were then made of the on-mode heat transfer coefficient and the off-mode heat transfer coefficient versus average temperature difference between the heater surface and the inside stainless steel pipe surface. On these plots, each data point was marked to indicate a different heater surface flux because some of the thermal switches maintained a constant or near constant temperature difference between the heater surface and inside stainless steel pipe surface for heater surface fluxes beyond a particular value. Once these plots were obtained, the ratio of on-mode heat transfer coefficient to off-mode heat transfer coefficient was calculated as a function of temperature difference between the heater surface and inside stainless steel pipe surface. Plots were also made of this information, with the heat transfer coefficient ratio along the ordinate, and the temperature difference between surfaces along the abscissa. The markings on these plots indicate specific heat transfer coefficient ratios obtained from the heat transfer coefficient plots for a particular temperature difference. The next section shows these heat transfer coefficient and heat transfer coefficient ratio plots for the different thermal switches tested. In addition, a description of each thermal switch tested and the accompanying test conditions is given, as well as a discussion of all the plots. (The raw and reduced data for the plots can be found in Appendix E.)

5.4 Description of Thermal Switches and Reduced Results

5.4.1 Particle Bed Thermal Switch

The first thermal switch that was investigated was the particle bed thermal switch. The particle bed thermal switch was assembled by filling the annular region between the heater and the stainless steel pipe with silicon carbide particles (see Figures 5.13 and 5.14). The silicon carbide

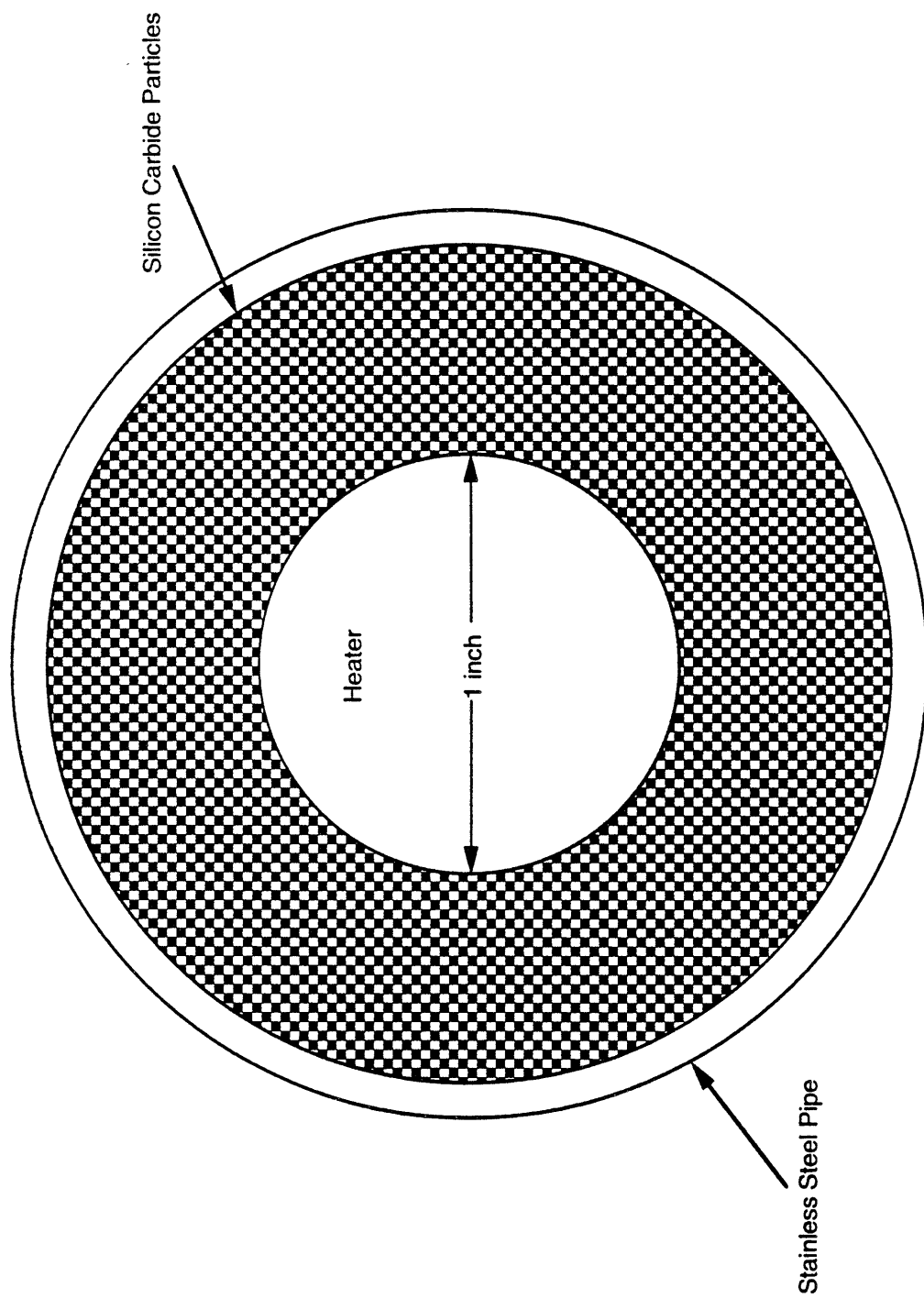


Figure 5.14. View AA of Figure 5.13--Cross-sectional View of Particle Bed

particles were introduced into the annular region via a small hole drilled into the three-inch long Macor spacer (which covered the 0.75-inch unheated length of the heater). The heater and stainless steel pipe were held vertically during the filling process to prevent voids from forming in the annular region. The diameter distribution of the silicon carbide particles ranged from 0.841 mm to 1.679 mm. (However, the particles were not of a spherical shape. Under magnification, the particles appeared to be irregular in shape, with flattened surfaces and rounded corners. They appeared to be produced by the fracture of large crystalline entities.) The particle bed void fraction was experimentally found to be 0.47. (The void fraction of the particle bed was obtained by pouring silicon carbide particles into a measuring container and then filling the container with enough water such that the water height equalled the particle bed height. The ratio of the volume of water used to the volume occupied by the particle mass is the void fraction.) The thermal conductivity of the silicon carbide was taken to be approximately $41 \text{ W/(m}^2 \text{ K)}$. During the off-mode of the particle bed thermal switch a vacuum was created in the voids of the particle bed. The vacuum obtained using the roughing pump of this experimental setup was 2.59 torr. During the on-mode of the particle bed thermal switch, the voids were filled with carbon dioxide gas to a pressure of one atmosphere. The heat transfer coefficients obtained for the particle bed thermal switch for both the on-mode and the off-mode are shown in Figure 5.15. The heat transfer coefficients are plotted against the average temperature difference (ΔT) between the heater surface and the inside stainless steel pipe surface. As one can see by inspection of the plot, the heat transfer coefficient in both the on-mode and off-mode increases monotonically with ΔT .

The ratio of the heat transfer coefficient in the on-mode to that in the off-mode is shown in Figure 5.16. It is a curve that has an absolute minimum at $\Delta T = 0 \text{ K}$, a local maximum at $\Delta T \approx 38 \text{ K}$, a local minimum at $\Delta T \approx 228 \text{ K}$, and monotonically increases thereafter. Apparently at the lower ΔT 's the presence of the carbon dioxide gas (in the on-mode of the thermal switch) enhances the heat conduction mode of heat transfer from the heat source to the heat sink more than the concurrent enhancement in the thermal radiative heat transfer mode, whereas at the higher ΔT 's, radiative heat transfer is enhanced to a greater extent. Thus, since in the off-mode of the

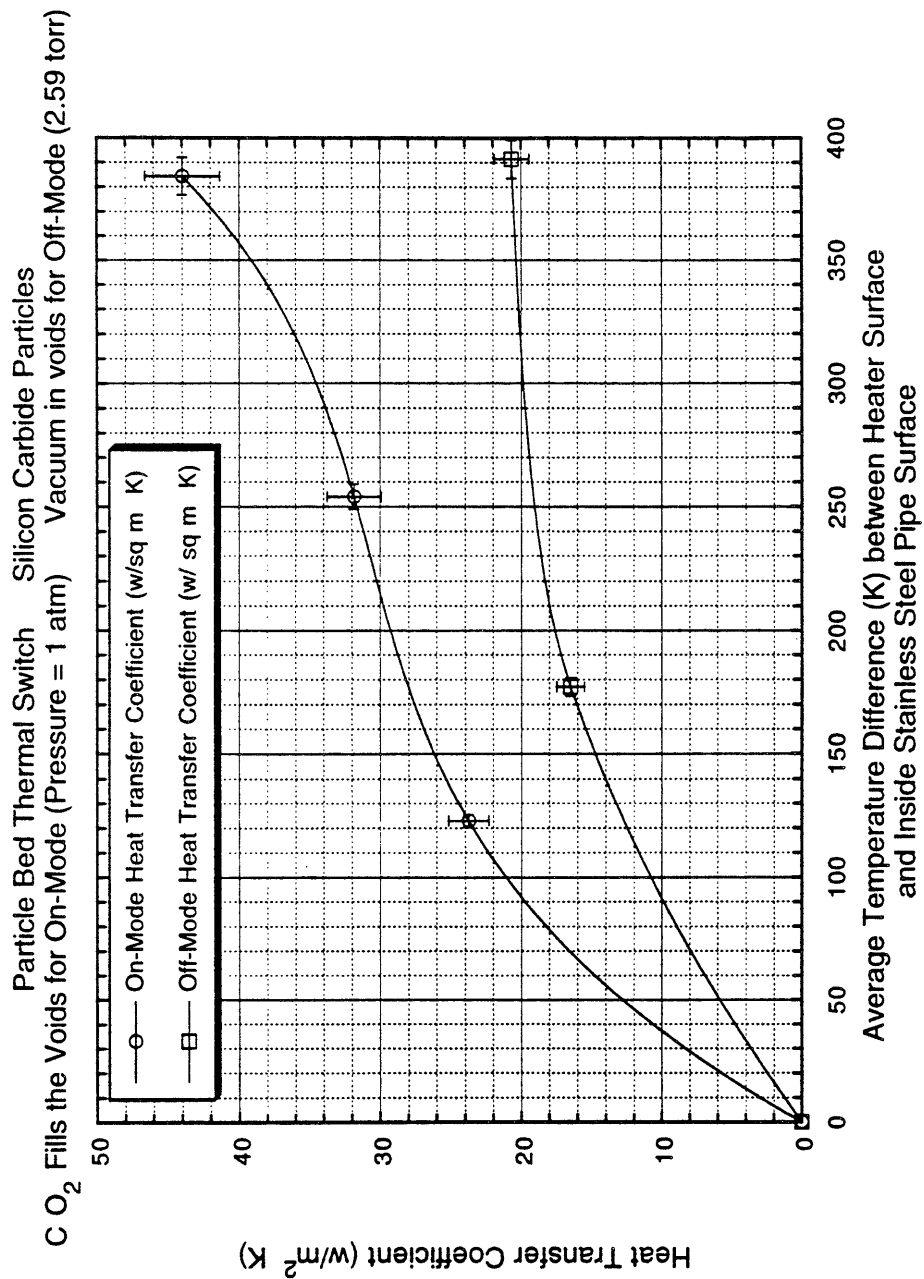


Figure 5.15. Particle Bed On-Mode and Off-Mode Heat Transfer Coefficients as a Function of Temperature Difference

Particle Bed Thermal Switch Silicon Carbide Particles
 C O₂ Fills the Voids for On-Mode (Pressure = 1 atm) Vacuum in voids for Off-Mode (2.59 torr)

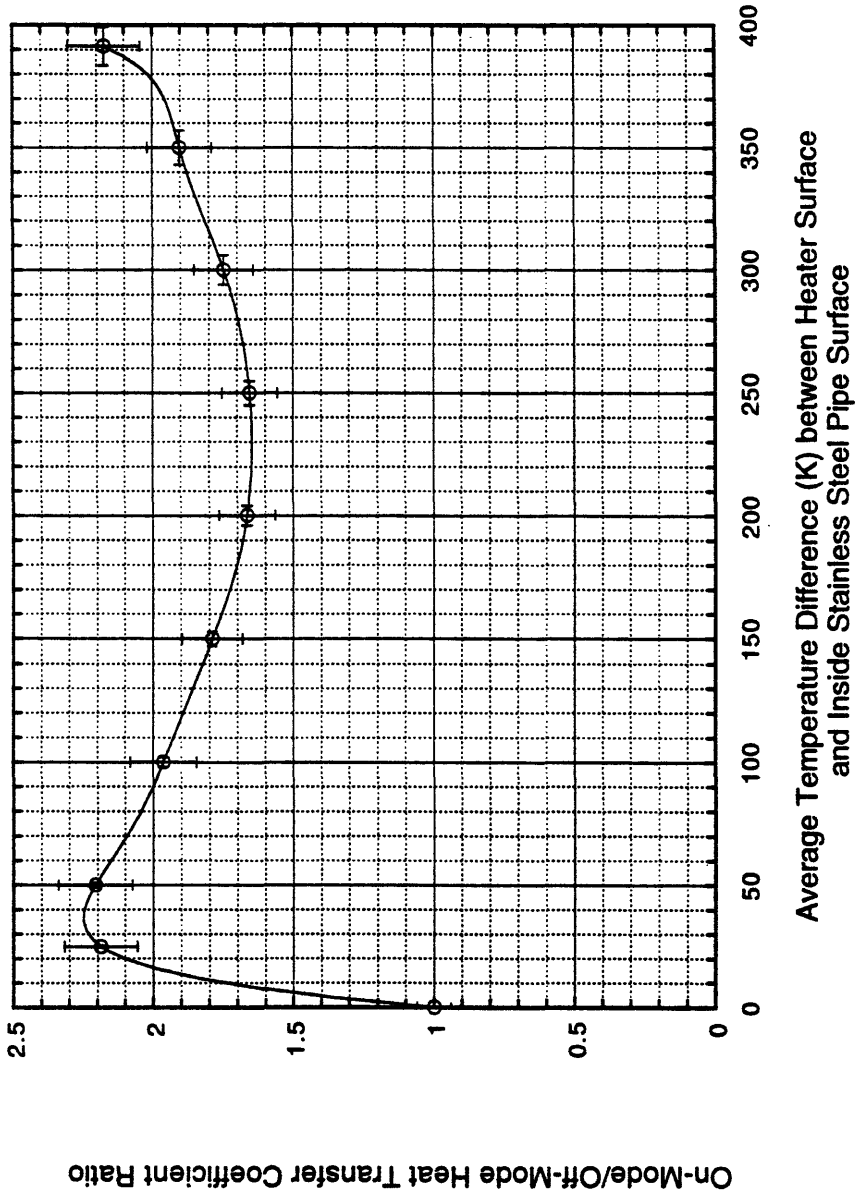


Figure 5.16. Particle Bed Thermal Switch Heat Transfer Coefficient Ratio

thermal switch the dominant mode of heat transfer from the heat source to the heat sink is thermal radiation (there is some heat conduction but this is minimal), the heat transfer coefficient ratio of on-mode to off-mode will peak at the lower ΔT 's due to the dominant heat conduction mode of heat transfer (in the on-mode of the thermal switch), decrease from this peak, reach a minimum, and begin to rise as the transition is made in the dominance of heat transfer mode in the on-mode of the thermal switch, and then monotonically increase as thermal radiation firmly establishes itself as the dominant mode of heat transfer. More testing, of course, such as using a gas with a different thermal conductivity and using bed particles with a different emissivity, would have to be performed to firmly establish the validity of this hypothesis. However, this is probably not warranted since, as shown by the heat transfer coefficient ratio plot, the switching ratio of the thermal switch is only about two for the ΔT 's of interest and the vacuum obtained in the off-mode of the thermal switch (2.59 torr). The theory of particle bed heat transfer developed by E. U. Schlunder (Proceedings of the Seventh International Heat Transfer Conference, Volume 1, pp195-211, 1982) indicates that this switching ratio can be approximately doubled by creating a vacuum (in the off-mode of the thermal switch) of approximately one micron, but even a switching ratio of four would have limited application. Also, it is very difficult to obtain a one micron vacuum in a particle bed. Thus, while the particle bed is interesting conceptually, it is highly improbable that it will find significant industrial application.

5.4.2 Wick Thermal Switch

A thermal switch that showed a better heat transfer performance was the wick thermal switch. The wick thermal switch involved wrapping the heater in a wick material which extended down to the stainless steel pipe at the lowest point of the heater cross-section (see Figures 5.17 and 5.18). During the on-mode of the thermal switch, water was introduced into the stainless steel pipe (by the water inlet system) which was pumped by the wick, via capillary action, from the stainless steel pipe to the heater. The wick, which was comprised of zirconium oxide felt having a surface density of 0.065 g/cm², with overall dimensions of 6.375 X 18.000 X 0.100 inches, was

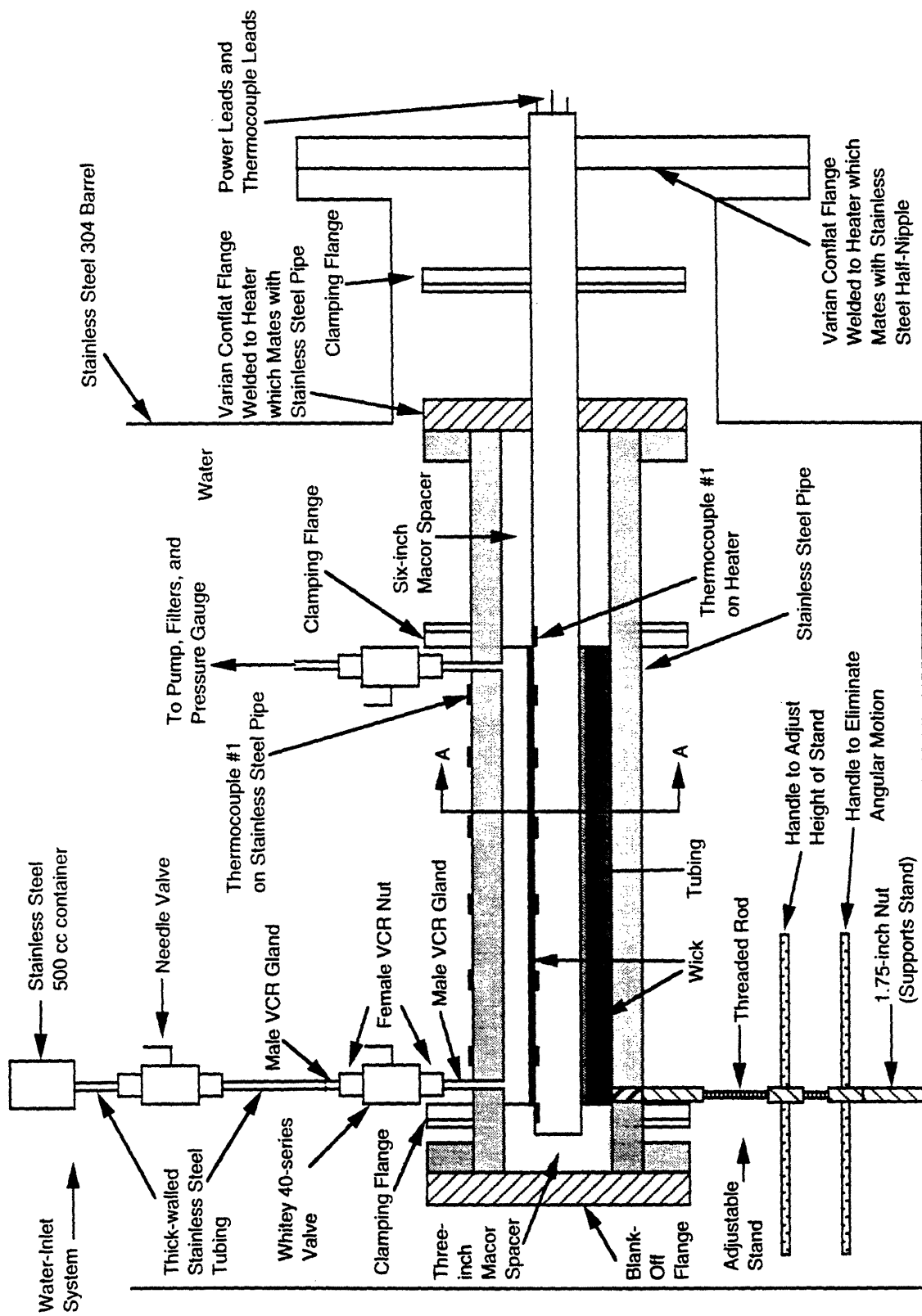


Figure 5.17 Wick Thermal Switch

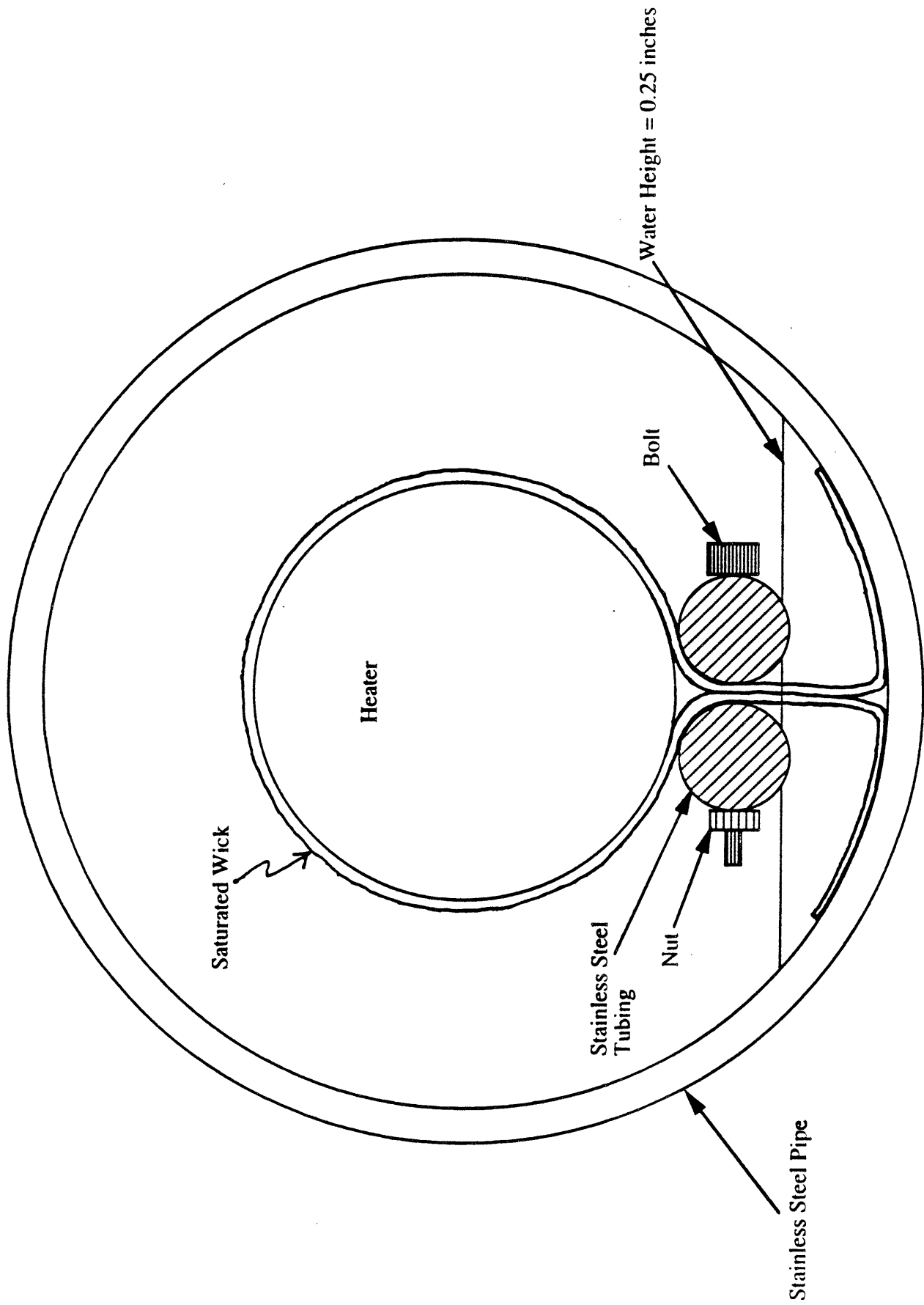


Figure 5.18. View AA of Figure 5.17—Cross-sectional View of Wick

held tight around the heater by bolting together two pieces of stainless steel 304 tubing (with the wick in between) at the bottom of the heater. The two pieces of stainless steel tubing used to clamp the wick to the heater were one-quarter inch in diameter and 18 inches long. Thru holes for 4-40 screws were drilled every half inch. Three 4-40 screws (and accompanying nuts) were used, with one placed at each end of the tubing, and one in the middle.

Two different on-mode setups and two different off-mode setups were tested. The two different on-mode setups investigated were wick-vacuum-water, and wick-air-water. For the first setup, the vacuum was at 1.65 torr, and for the second setup, the air was at a pressure of one atmosphere. The amount of water used in both setups was 184.5 grams. This amount of water allowed for full saturation of the wick (118.0 grams), plus a reservoir of water 0.25 inches high in the annular region between the stainless steel pipe and the heater. The two different off-mode setups investigated were wick-vacuum and wick-air. (Again, the vacuum was at 1.65 torr, and the air was at one atmosphere.)

The heat transfer coefficients obtained for the wick thermal switch for all four setups are plotted in Figure 5.19 against the average temperature difference between the heater surface and inside stainless steel pipe surface. The results of the two off-modes are as expected, with the wick-air setup having a slightly higher heat transfer coefficient than the wick-vacuum setup due to the extra mode of heat transfer present (heat conduction). However, the results for the on-mode setups are different than expected. Prior to testing, it was speculated that the wick-vacuum-water setup with no noncondensibles present would have a much higher heat transfer coefficient than the wick-air-water setup, since the presence of noncondensibles inhibits heat transfer in the condensation process. However, in studying Figure 5.19, one sees that the wick-vacuum-water setup is superior to the wick-air-water setup only for the first four heater surface fluxes investigated: 1.57, 2.88, 7.95, and 16.81 kw/m^2 . (Each distinct heater surface flux is denoted by a symbol on the plots.) For the last four heater surface fluxes investigated, 24.40, 33.07, 43.42, and 52.66 kw/m^2 , the wick-air-water setup has a larger heat transfer coefficient than the wick-vacuum-water setup. (The heater surface flux at which the two curves cross is approximately 19 kw/m^2 .)

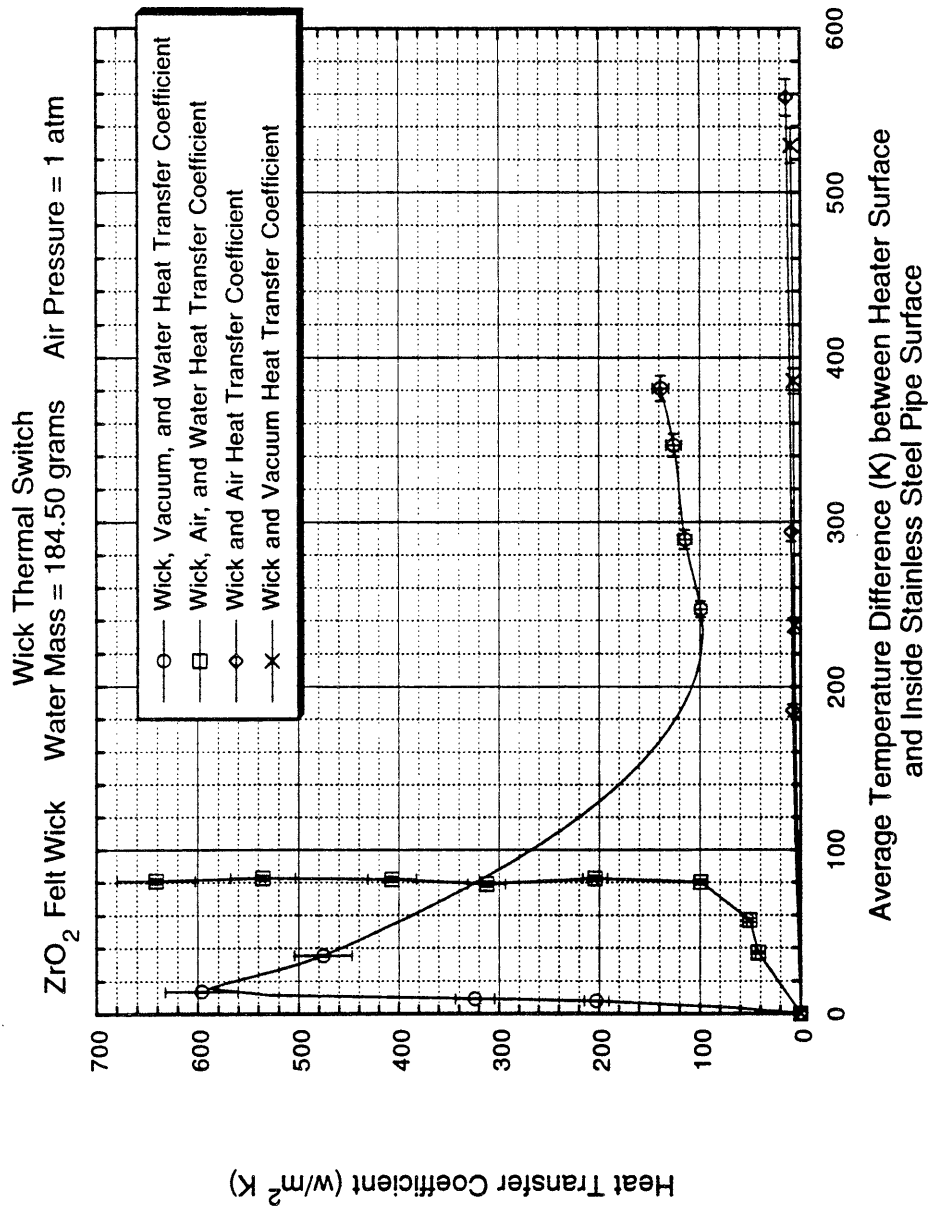


Figure 5.19. Wick Thermal Switch On-Mode and Off-Mode Heat Transfer Coefficients

Indeed, so successful was the wick-air-water setup at these higher fluxes that, as shown by Figure 5.19, the average temperature difference between the heater surface and the inside stainless steel pipe surface never exceeded 82.6 K. Apparently, for the wick-vacuum-water setup, some phenomenon, possibly wick dryout, occurred for a heater flux greater than 7.95 kw/m^2 (i.e., a heat transfer coefficient of $640 \text{ w/m}^2 \text{ K}$). This degradation in heat transfer capability for heat fluxes greater than 7.95 kw/m^2 occurred for the wick-vacuum-water setup and not the wick-air-water setup possibly because more water was in the vapor phase with a vacuum present than with air present (at one atmosphere) for a given heater surface flux. This hypothesis should be investigated further since the data indicates that solution of this problem would result in a thermal switch with very high on-mode heat transfer coefficients.

The on-mode/off-mode heat transfer coefficient ratio versus average temperature difference between the heater surface and the inside surface of the stainless steel pipe for the wick-vacuum-water setup and the wick-air-water setup is shown in Figures 5.20 and 5.21. For Figure 5.20, the off-mode is the wick-vacuum setup, and for Figure 5.21 it is the wick-air setup. Since both off-mode lines of Figure 5.19 have a very small slope, Figures 5.20 and 5.21 look similar to Figure 5.19. Figure 5.20 shows slightly higher on-mode/off-mode heat transfer coefficient ratios than Figure 5.21 because the wick-vacuum off-mode setup has only one mode of heat transfer (thermal radiation), and the wick-air off-mode setup has two (thermal radiation and conduction).

Thus, for the wick thermal switch, the wick-vacuum setup is the preferred off-mode setup since it yields lower heat transfer coefficients (albeit only slightly) than the wick-air setup. (As mentioned earlier, the vacuum required for the wick-vacuum setup is minimal, capable of being provided by a standard roughing pump, as was done in the experiment.) Concerning the on-mode of the thermal switch, for surface heat fluxes from the heat source that are less than 19 kw/m^2 , the wick-vacuum-water setup is superior in heat transferring capability to the wick-air-water setup, whereas for higher surface heat fluxes the reverse is true. Note that if wick dryout is the problem associated with the wick-vacuum-water setup for the higher heat fluxes, then addition of more water to the setup may allow use of the setup at higher heat fluxes. Also, even though the heat

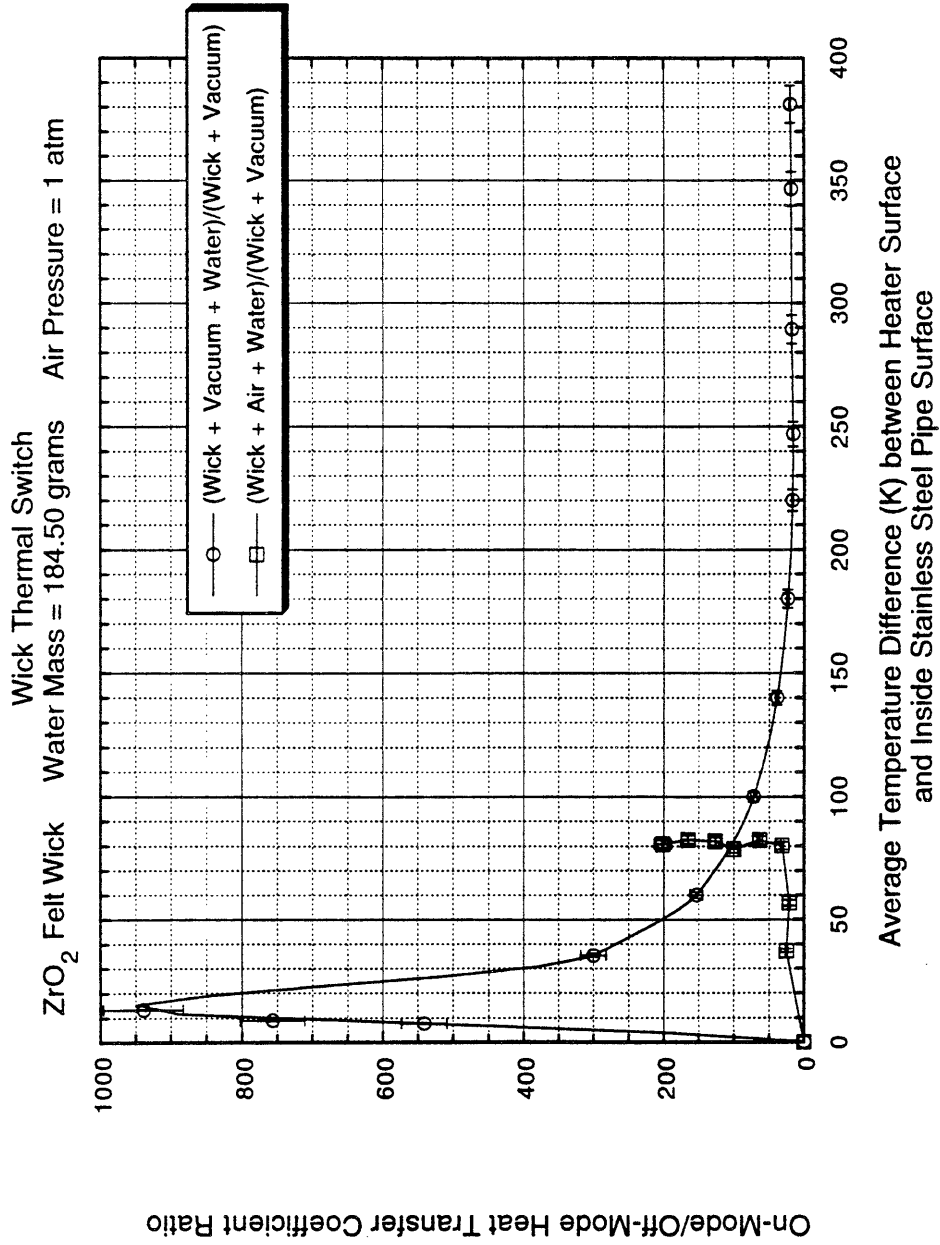


Figure 5.20. Wick Thermal Switch Heat Transfer Coefficient Ratio. Off-Mode is Wick + Vacuum

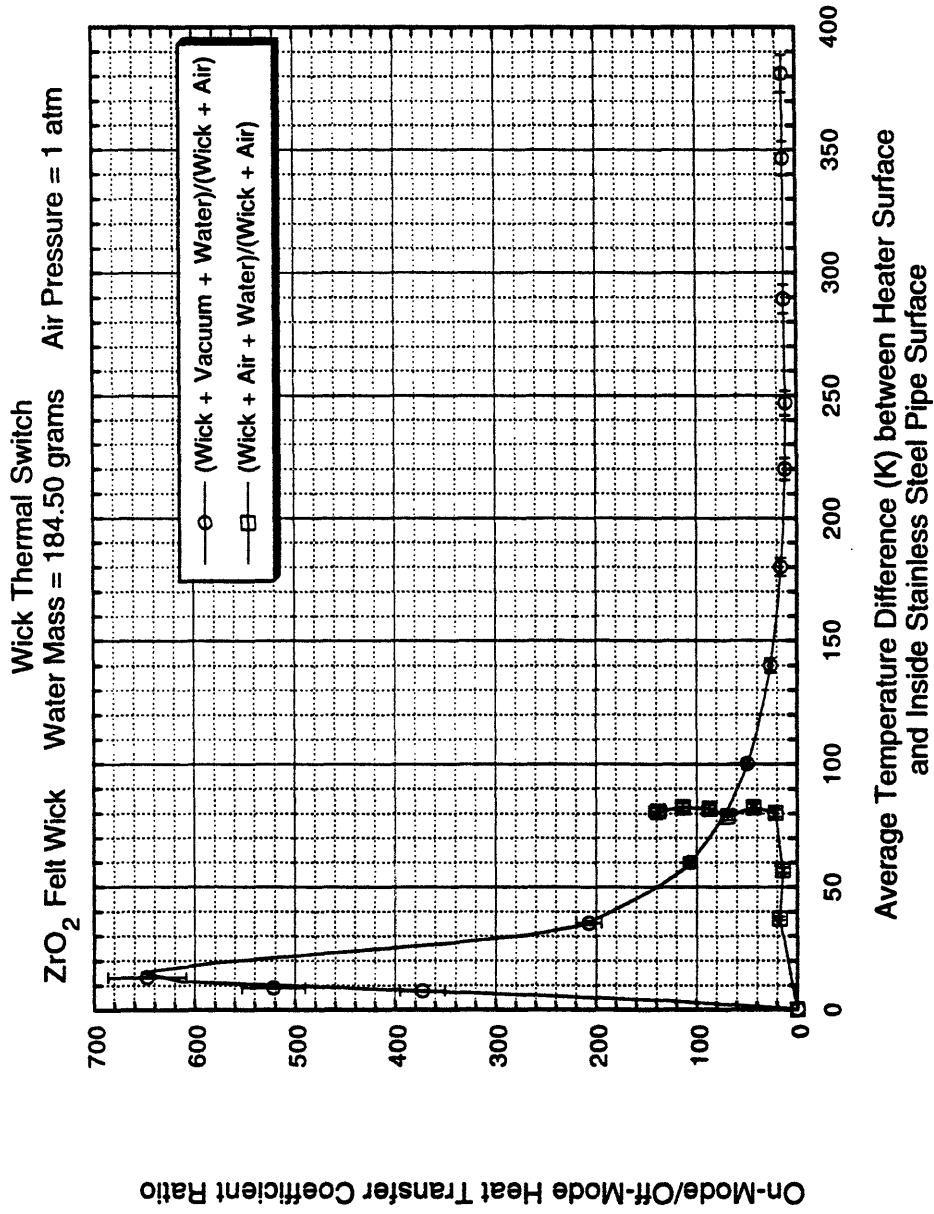


Figure 5.21. Wick Thermal Switch Heat Transfer Coefficient Ratio. Off-Mode is Wick + Air

transfer coefficients of the last four heater surface fluxes investigated are substantially less than for the first four fluxes investigated, their values are still reasonably high.

5.4.3 Water Thermal Switch

The thermal switch which indisputably showed the best overall performance was the water thermal switch. The water thermal switch involved the addition of water to the annular region between the heater and stainless steel pipe during the on-mode of the thermal switch. For this thermal switch, four different on-mode and two different off-mode setups were tested. The four different on-mode setups tested in the annular region between the heater and stainless steel pipe were (see Figures 5.22 to 5.25):

1. 311.6 grams of water and vacuum (1.65 torr)
2. 311.6 grams of water and air (at a pressure of one atmosphere)
3. 628.1 grams of water and vacuum (1.65 torr)
4. 628.1 grams of water and air (at a pressure of 1 atmosphere)

The off-mode setups tested were:

1. vacuum (1.65 torr) in the annular region
2. air at a pressure of one atmosphere in the annular region

The two different water masses used for the on-mode yielded two different water heights and, hence, two different levels of immersion of the heater. The 311.6 grams of water resulted in a water height of 0.88 inches (measured from the lowest point of the inside surface of the stainless steel pipe), and immersion of 42% of the perimeter of the 0.996-inch diameter heater situated at the center of the stainless steel pipe. Hence, 38% of the diameter of the heater was underwater (see Figure 5.23). For the 628.1 grams of water, this resulted in a water height of 1.75 inches and, hence, total immersion of the heater. Like the wick thermal switch, the water was introduced into the annular region using the water inlet system.

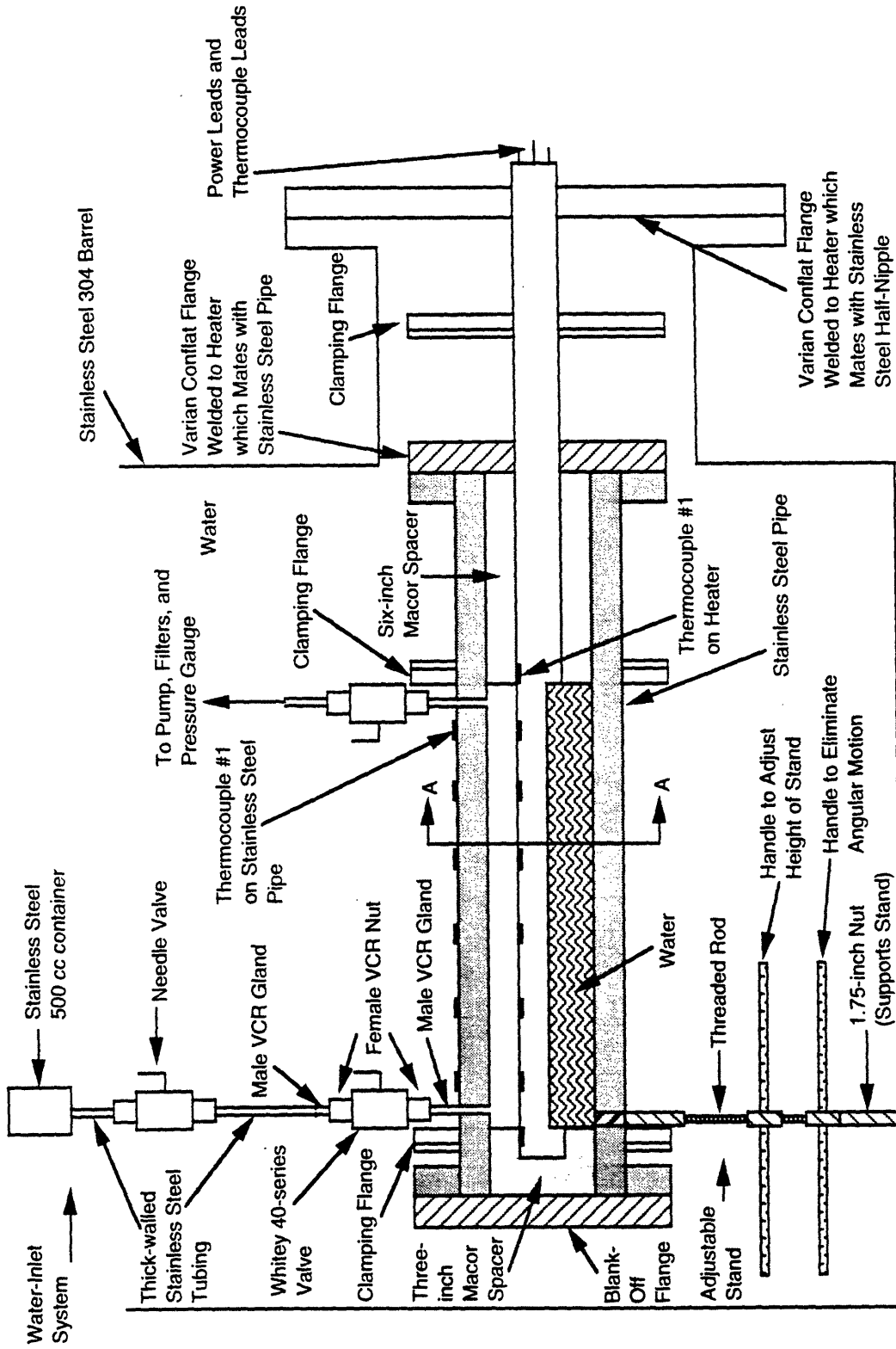


Figure 5.22. Water Thermal Switch—Water Height = 0.88 Inches

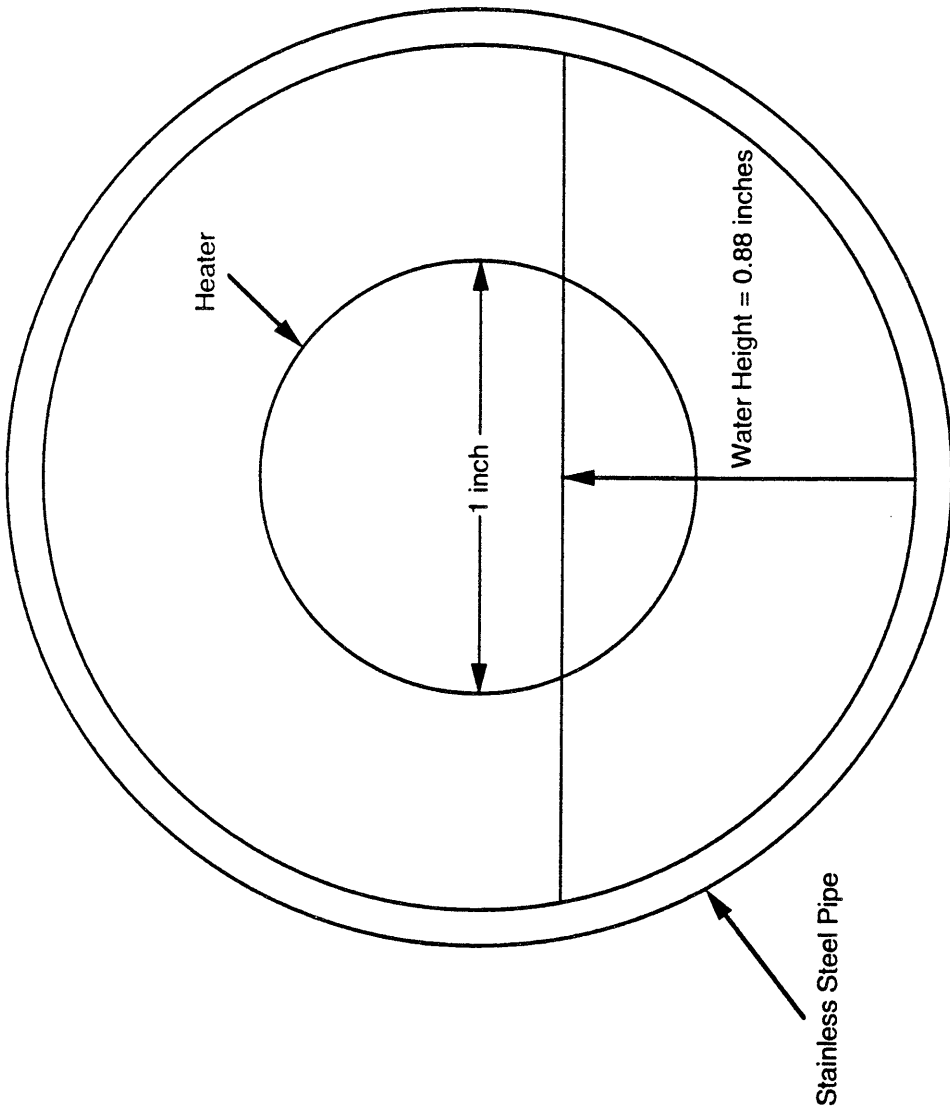


Figure 5.23. View AA of Figure 5.22--Water Thermal Switch

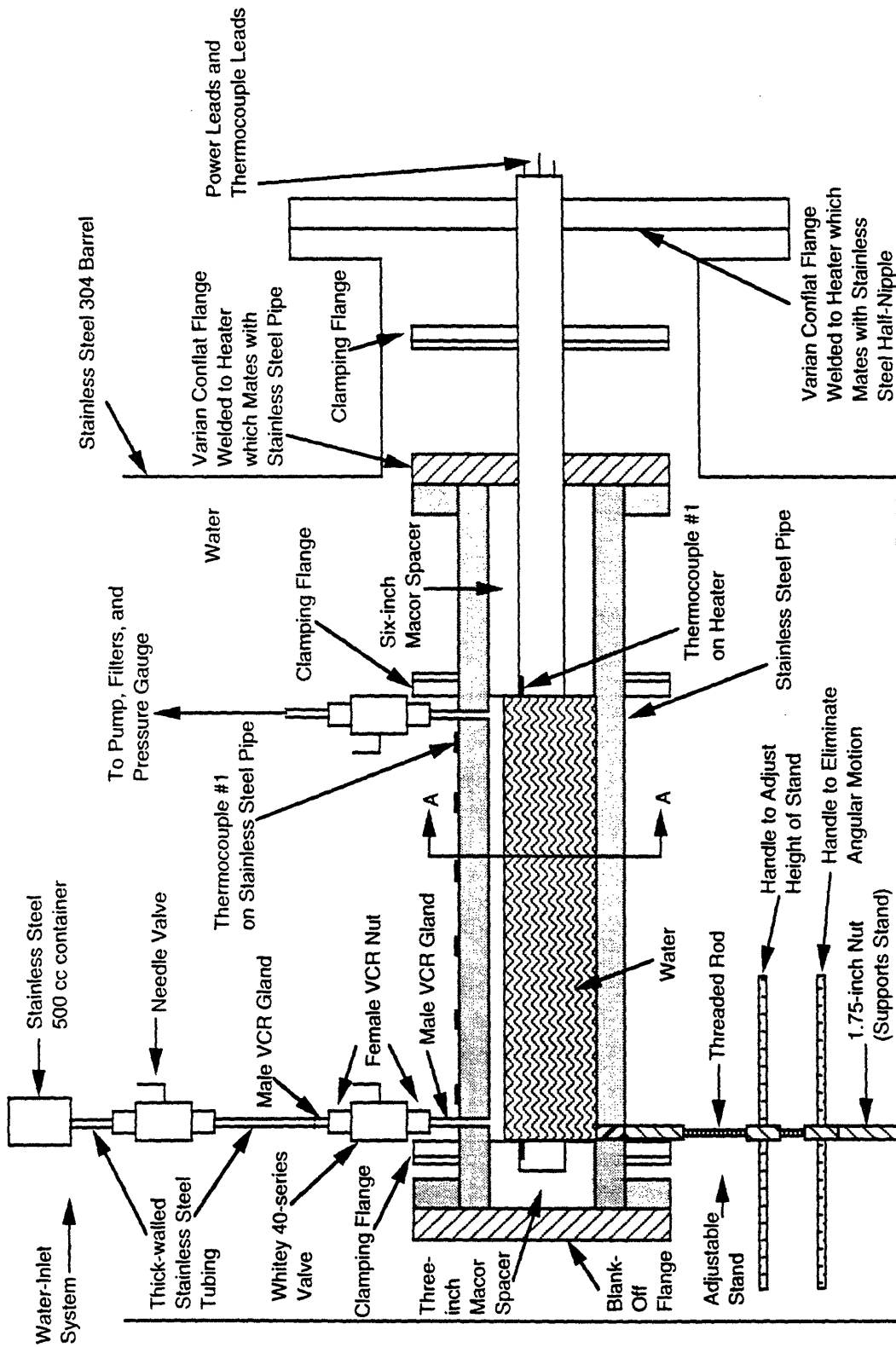


Figure 5.24 Water Thermal Switch--Water Height = 1.75 Inches

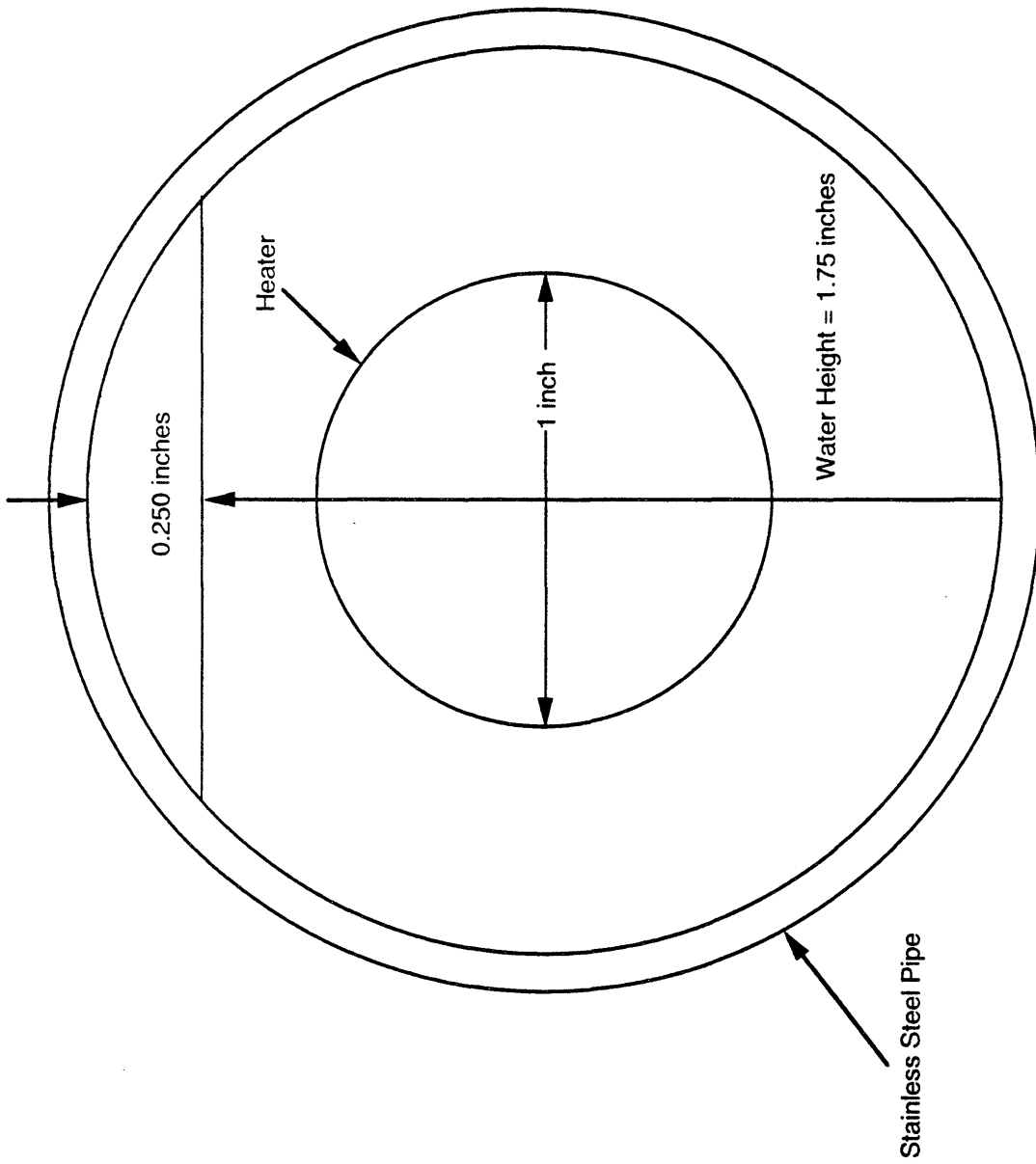


Figure 5.25. View AA of Figure 5.24—Water Thermal Switch

A plot of the heat transfer coefficients versus average temperature difference between the heater surface and the inside stainless steel pipe surface obtained for each setup is shown in Figure 5.26. Concerning the on-mode setups, for both water masses tested, the on-mode setups involving a vacuum always had higher heat transfer coefficients than the on-mode setups with air. Apparently for this thermal switch, even with a vacuum present, there was always sufficient water in contact with the heater to prevent any gross degradation of the thermal switch heat transfer coefficient. In addition, the absence of noncondensibles in the vacuum setup prevented inhibition of the condensation process. Hence, the evaporation-condensation process was always superior in heat transferring capability for the water-vacuum setups than the water-air setups. However, in studying the plots of Figure 5.26, it appears that this evaporation-condensation process for the water-vacuum setups does not become substantial until a ΔT (between the heater surface and inside stainless steel pipe surface) of approximately 40 K and 46 K is reached for the smaller water mass and the larger water mass, respectively. Prior to this point, heat conduction and/or convection through the water appears to be the main mode of heat transfer from the heat source to the heat sink. This is supported by the fact that, for each water mass tested, the heat transfer coefficient curve for the water-air setup is close to the curve for the water-vacuum setup up to the ΔT at which the evaporation-condensation process becomes dominant. It is also supported by the fact that the larger water mass (for both the water-air and water-vacuum setups) has superior heat transfer capability in comparison to the smaller water mass (for both setups) up to a ΔT of approximately 40 K, at which point both water-vacuum setups become superior in heat transferring capability, with the smaller water mass showing larger heat transfer coefficients. Apparently, once the evaporation-condensation process becomes the dominant mode of heat transfer from the heat source to the heat sink, the extra water of the 628.1 gram water-vacuum thermal switch tends to inhibit energy transport. This indicates that there is an optimum water level for the evaporation-condensation process. For the water-air setups, the 628.1 gram water-air setup is always superior in heat transferring capability to the 311.6 gram water-air setup for all ΔT 's of concern.

Water Thermal Switch

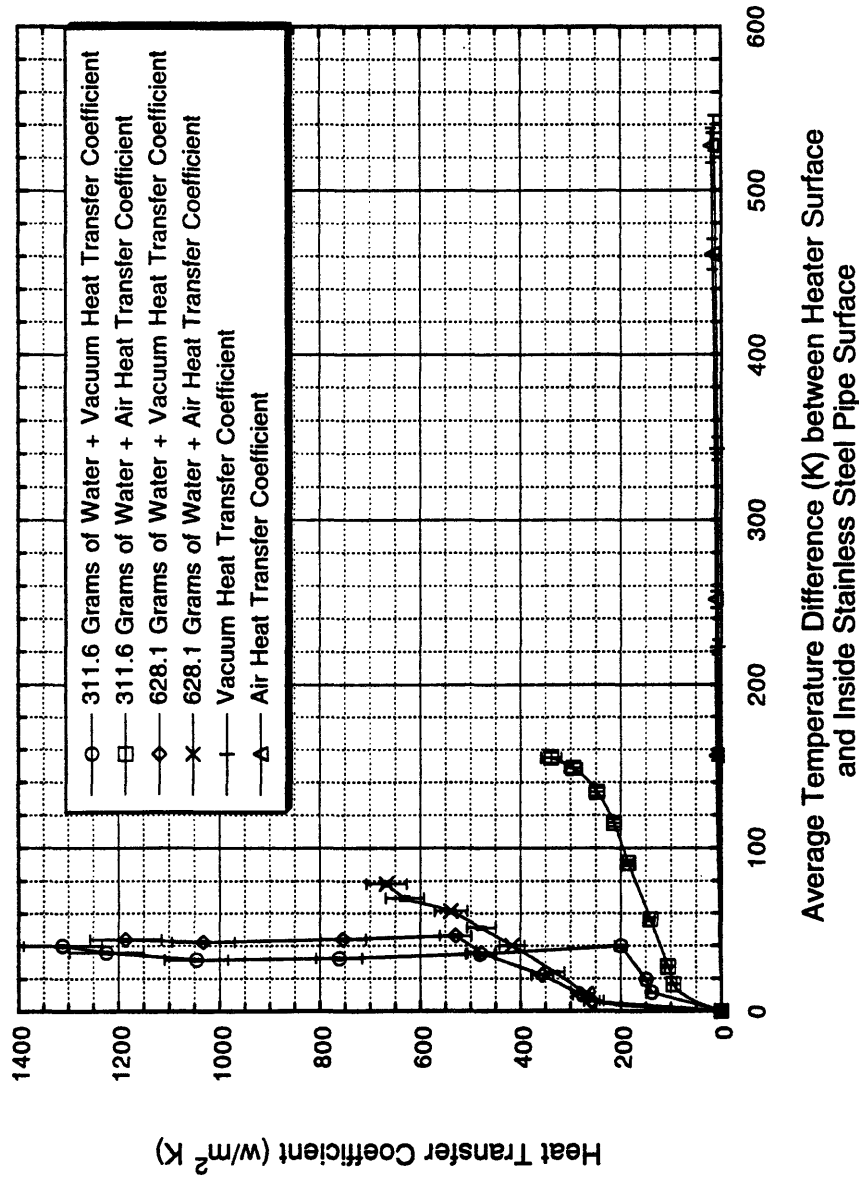


Figure 5.26. Water Thermal Switch On-Mode and Off-Mode Heat Transfer Coefficients

Concerning the off-mode, the experimental results are as expected, with the vacuum showing lower heat transfer coefficients than the air (which is at a pressure of one atmosphere). These results are expected since, as discussed for the wick thermal switch, the vacuum allows only one mode of heat transfer (thermal radiation), and the air allows additional modes of heat transfer (conduction and convection) from heat source to heat sink.

The ratio of on-mode heat transfer coefficient to off-mode heat transfer coefficient is shown in Figures 5.27 and 5.28. For Figure 5.27, the off-mode is a vacuum (1.65 torr) in the annular region between the heater and the stainless steel pipe, and for Figure 5.28 it is air at one atmosphere in the annular region. Both figures look similar to one another because the heat transfer coefficients for the air (at one atmosphere) are only slightly larger than the heat transfer coefficients for the vacuum for all ΔT 's investigated. The heat transfer coefficient ratio curves show that for all four on-mode setups, the ratio of on-mode heat transfer capability to off-mode heat transfer capability peaks at a ΔT less than 20 K, and then begins to decrease as ΔT increases. Apparently, heat transferring capability in the on-mode increases more rapidly than that in the off-mode initially (for a ΔT less than 20 K), with the reverse occurring for immediately higher ΔT 's. For the water-air setups, this trend continues for all subsequent ΔT 's, with the exception of the last few ΔT 's at which data was acquired, where there is a very minimal increase in the ratio. These latter data points, being at higher ΔT 's, correspond to high vapor generation rates, hence, agitation, which may counter the heat transfer inhibiting effect of the noncondensibles. For the water-vacuum setups, this trend of decreasing heat transfer coefficient ratio with increasing ΔT continues until the evaporation-condensation process becomes dominant. (As mentioned earlier, for the smaller water mass this occurs for a $\Delta T \approx 40$ K, and for the larger water mass it occurs for a $\Delta T \approx 46$ K.) At this point, the heat transfer coefficient ratio begins to increase with increasing heater surface flux, with the average temperature difference between the heater surface and the inside surface of the stainless steel pipe (i.e., ΔT) remaining approximately constant. For the larger water mass, the increase in the heat transfer coefficient ratio is monotonic. For the smaller water mass, the ratio peaks at the next to last surface heat flux investigated (43.93 kw/m²), and then slightly

Water Thermal Switch

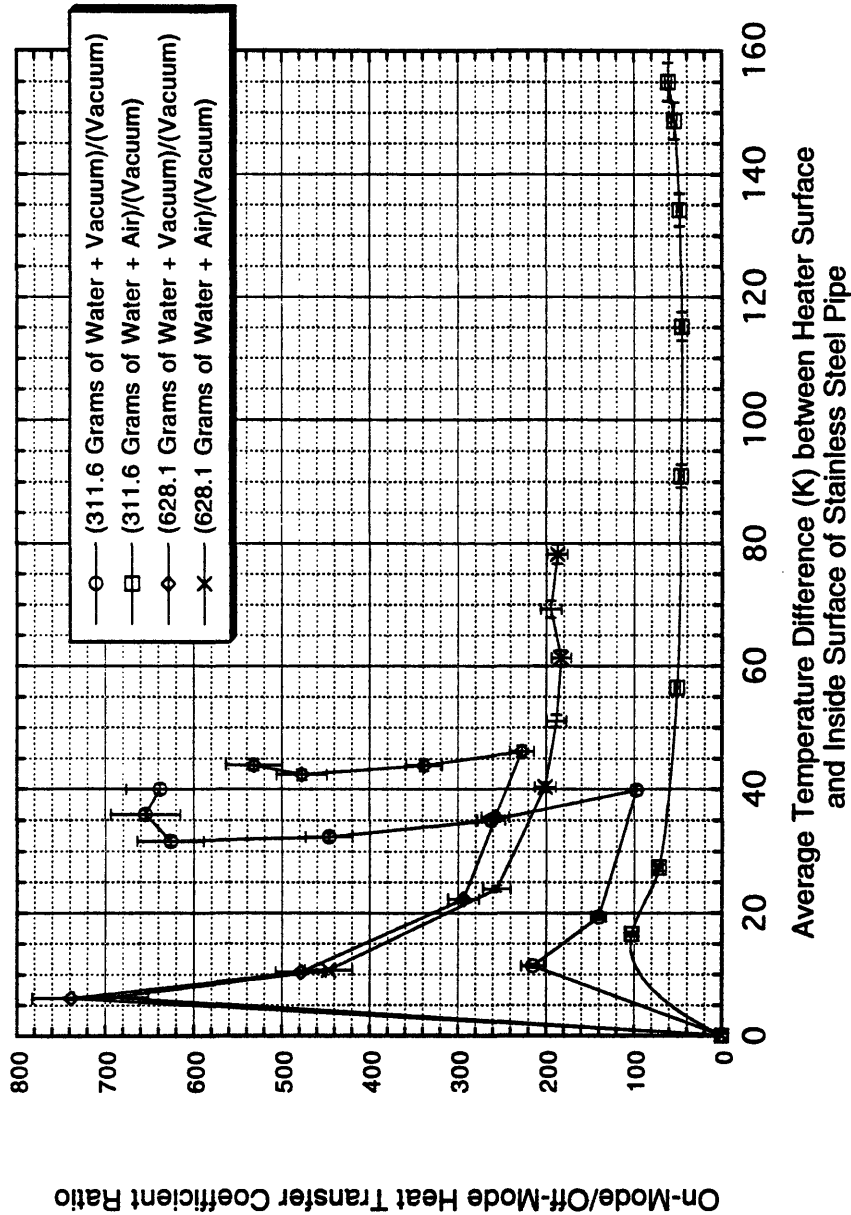


Figure 5.27. Water Thermal Switch Heat Transfer Coefficient Ratio.
Off-Mode is a Vacuum at 1.65 torr.

Water Thermal Switch

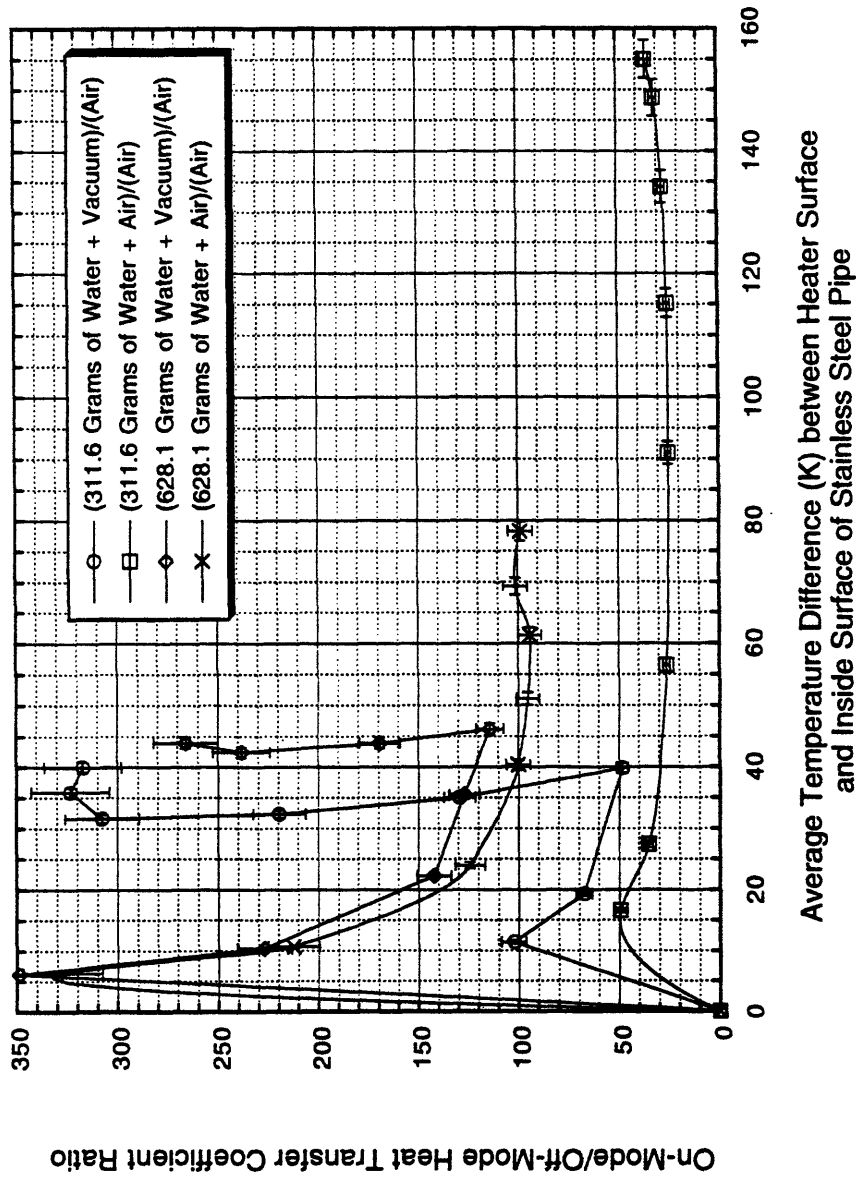


Figure 5.28. Water Thermal Switch Heat Transfer Coefficient Ratio. Off-Mode is Air at 1.0 atm.

decreases for the last heater surface flux investigated (52.46 kw/m^2). These last few data points seem to indicate that the water-vacuum thermal switch comprised of 311.6 grams of water is at or near the maximum heat transfer coefficient ratio for this experimental setup: a value somewhere around 645. (It is interesting to note that the Bistable Passive Heat Transfer System for emergency core cooling conceived by Anand and Christensen [see Chapter 2] presently has a maximum heat transfer coefficient ratio of about 100.)

5.5 Chapter Summary

On-mode and off-mode heat transfer coefficient data were acquired for three thermal switches. The experimental setup built to obtain this data involved a horizontal cylindrical heater enclosed in a larger diameter cylindrical stainless steel pipe. The stainless steel pipe was surrounded by a pool of water. The heater was the heat source and the stainless steel pipe was the immediate heat sink, with the pool of water being the ultimate heat sink. The annular void between the heater and stainless steel pipe contained the thermal switch media. The first thermal switch investigated was the particle bed thermal switch. For this thermal switch, the annular volume was filled with silicon carbide particles ranging in size from 0.8 mm to 1.25 mm. In the off-mode of the thermal switch (i.e., the thermal decoupling mode between the heat source and heat sink), the annular region was evacuated of most gas molecules by a vacuum pump (final pressure was 2.59 torr) so that, for the most part, only the bed of silicon carbide particles remained. In the on-mode, carbon dioxide gas was injected into the interstitial regions of the particle bed until a pressure of one atmosphere was obtained. The ratio of on-mode heat flux to off-mode heat flux (i.e., the switching ratio of the thermal switch) was approximately two for temperature differences (ΔT) between the heat source and heat sink ranging from 20 K to 390 K. (The temperature difference between the heat source and heat sink was varied by altering the heater surface flux.)

The next thermal switch tested was the wick thermal switch. It was comprised of zirconium oxide felt wrapped around the heater and, at the lowest point of the cross-section of the heater, extended down to the stainless steel pipe. Two different off-modes and two different on-

modes were tested. The two off-modes tested were wick and a vacuum (1.65 torr) present in the annular region, and wick and air (one atmosphere) present in the annular region. The two on-modes tested were wick-air-water in the annular volume, and wick-vacuum-water in the annular volume. For the off-mode, the wick-vacuum setup was slightly superior to the wick-air setup in thermally decoupling the heat source from the heat sink for all ΔT 's investigated (0 K to over 500 K) for this mode of operation. For the on-mode of the thermal switch, the wick-vacuum-water setup was superior to the wick-air-water setup up to a ΔT of 80 K (heater surface flux of 19 kw/m²), beyond which the converse was true. However, no matter what on-mode was utilized, the heat transferring capability of this thermal switch in the on-mode was greatly superior to the heat transferring capability of the particle bed thermal switch for all ΔT 's investigated. In addition, the wick thermal switch also had superior thermal switching ratios to those of the particle bed, with values as high as 948.

The last thermal switch investigated was the water thermal switch. For this thermal switch, two different off-mode and four different on-mode setups were tested. The two off-mode setups investigated were vacuum (1.65 torr) in the annular region, and air at a pressure of one atmosphere in the annular region. The four different on-mode setups investigated were: 311.6 grams of water and vacuum (1.65 torr), 311.6 grams of water and air (at a pressure of one atmosphere), 628.1 grams of water and vacuum, and 628.1 grams of water and air. As expected, the off-mode involving the vacuum showed superior performance to the off-mode involving air in thermally decoupling the heat source from the heat sink. Concerning the on-mode setups, for each water mass tested, the on-mode setups involving a vacuum always had higher heat transfer coefficients than the on-mode setups with air. Of the two on-mode setups involving a vacuum, the 628.1 gram water-vacuum setup had higher heat transfer coefficients than the 311.6 gram water-vacuum setup up to a ΔT of approximately 40 K, at which point the converse became true. For the water-air setups, the 628.1 gram water-air setup was always superior in heat transferring capability to the 311.6 gram water-air setup. The switching ratios obtained by the water thermal switch varied from 25 to 750, depending on what on-mode and off-mode setup was being utilized. Although

the wick thermal switch had a larger peak switching ratio value, the water thermal switch had larger values over a broader range of heater surface fluxes.

Chapter Six

Summary and Recommendations for Future Work

6.1 Introduction

For this research project, data has been acquired on the kinematics of the dissociation and recombination of magnesium carbonate and lead carbonate. In addition, a successful recombination algorithm has been developed to recombine the dissociation products of magnesium carbonate to recreate the original chemical. Lastly, heat transfer coefficient data for three different thermal switches for both on-mode and off-mode performance has been obtained. A summary of the key experimental results obtained for all experimental testing is shown in Table 6.1 on the next two pages. These results, and recommendations for future work based upon these experimental results, are discussed in the next section. In addition, Figure 6.1 (which follows Table 6.1) shows the highest switching ratios obtained for some of the thermal switches tested in the heat-transfer-coefficient experimental setup.

6.2 Recommendations for Future Work

As mentioned above and discussed extensively in Chapter Four, successful procedures were devised for dissociation and recombination of magnesium carbonate. In addition, lead carbonate was successfully dissociated. Although recombination was not attempted for the lead carbonate, it is highly probable that the scheme developed for recombination of the magnesium carbonate would have been successful in creating reconstituted lead carbonate as well, since the dissociation constituents of the lead carbonate are very similar to those of magnesium carbonate; that is, a metal oxide and carbon dioxide gas. Indeed, for virtually any metal carbonate, since its dissociation products are a metal oxide and carbon dioxide gas, this recombination algorithm will

Table 6.1
Summary of Results

Thermal Switch	Off-Mode Tested	On-Mode Tested	Heat Transfer Coefficient Ratio ($\Delta T = \text{Temperature difference}$ Kelvin between heater surface and inside surface of stainless steel pipe)	General Comments
Dissociation Thermal Switch				Successful dissociation and recombination procedures were devised for MgCO_3 . Successful dissociation attained for PbCO_3 . No recombination attempted with dissociation products of PbCO_3 .
Particle Bed Thermal Switch	Vacuum (2.59 torr) + Silicon Carbide Particles	Carbon Dioxide Gas at 1 atm + Silicon Carbide Particles	Approximately 2 for $0.00 \leq \Delta T \leq 391.40$	Low heat transfer coefficients and very low switching ratios
Wick Thermal Switch	Wick + Vacuum (1.65 torr) Wick + Air (1 atm)	Wick + Water (184.5g) + Vacuum (1.65 torr) Wick + Water (184.5g) + Air (1 atm) For both on-mode setups, the wick was fully saturated with water and the excess water height was 0.25 inches. (Hence, there was 0% submergence of the heater due to the excess water height.)	(Wick + Water + Vacuum)/ (Wick + Vacuum) $0.00 \leq \Delta T \leq 13.33$ 1.00 to 939.22 $13.33 \leq \Delta T \leq 246.93$ 939.22 to 16.17 $246.93 \leq \Delta T \leq 381.11$ 16.17 to 19.55 (Wick + Water + Vacuum)/ (Wick + Air) $0.00 \leq \Delta T \leq 13.33$ 1.00 to 647.18 $13.33 \leq \Delta T \leq 246.93$ 647.18 to 11.23 $246.93 \leq \Delta T \leq 381.11$ 11.23 to 13.79 (Wick + Water + Air)/ (Wick + Vacuum) $0.00 \leq \Delta T \leq 82.61$ 1.00 to 201.04 (Wick + Water + Air)/ (Wick + Air) $0.00 \leq \Delta T \leq 82.61$ 1.00 to 138.60	For the off-mode setups, the wick + vacuum setup always was superior to the wick + air setup in thermally decoupling the heat source from the heat sink. For the on-mode setups, the wick + water + vacuum setup had higher heat transfer coefficients than the wick + water + air setup up to a heater surface flux of 19.0 kw/m^2 ($\Delta T = 80\text{K}$), at which point the converse became true. Both off-mode and on-mode setups were superior in performance to the particle bed thermal switch at all times during testing.

Table 6.1 Continued

<p>Water Thermal Switch</p>	<p>Vacuum (1.65 torr) Air (1 atm)</p>	<p>311.6g of Water + Vacuum (1.65 torr) 311.6g of Water + Air (1 atm) 628.1g of Water + Vacuum (1.65 torr) 628.1g of Water + Air (1 atm) The 311.6 grams of water resulted in immersion of 42% of the perimeter of the heater (and, hence, 38% of its diameter). The 628.1 grams of water resulted in total immersion of the heater.</p>	<p>(311.6g of Water + Vacuum)/ (Vacuum) 0.00 ≤ ΔT ≤ 11.38 1.00 to 215.04 11.38 < ΔT ≤ 39.83 215.04 to 97.35 39.83 < ΔT ≤ 39.99 97.35 to 654.26 (311.6g of Water + Vacuum)/ (Air) 0.00 ≤ ΔT ≤ 11.38 1.00 to 102.33 11.38 < ΔT ≤ 39.83 102.33 to 48.41 39.83 < ΔT ≤ 39.99 48.41 to 323.38 (311.6g of Water + Air)/ (Vacuum) 0.00 ≤ ΔT ≤ 16.60 1.00 to 102.83 16.60 < ΔT ≤ 115.20 102.83 to 45.68 115.20 < ΔT ≤ 155.03 45.68 to 61.11 (311.6g of Water + Air)/ (Air) 0.00 ≤ ΔT ≤ 16.60 1.00 to 49.33 16.60 < ΔT ≤ 90.99 49.33 to 24.91 90.99 < ΔT ≤ 155.03 24.91 to 35.52 (628.1g of Water + Vacuum)/ (Vacuum) 0.00 ≤ ΔT ≤ 6.09 1.00 to 738.63 6.09 < ΔT ≤ 46.13 738.63 to 227.27 39.99 < ΔT ≤ 46.13 97.35 to 654.26</p>	<p>The vacuum off-mode setup was always superior to the air off-mode setup in thermally decoupling the heat source from the heat sink. For each water mass, the vacuum on-mode setup was always superior to the air on-mode setup. For each air on-mode setup, the larger water mass was always superior to the smaller water mass. For each vacuum on-mode setup, the larger water mass was superior to the smaller water mass until the evaporation/condensation process (apparently) became the dominant mode of heat transfer. The water thermal switch had the best overall performance of all thermal switches tested.</p>
-----------------------------	---	--	---	--

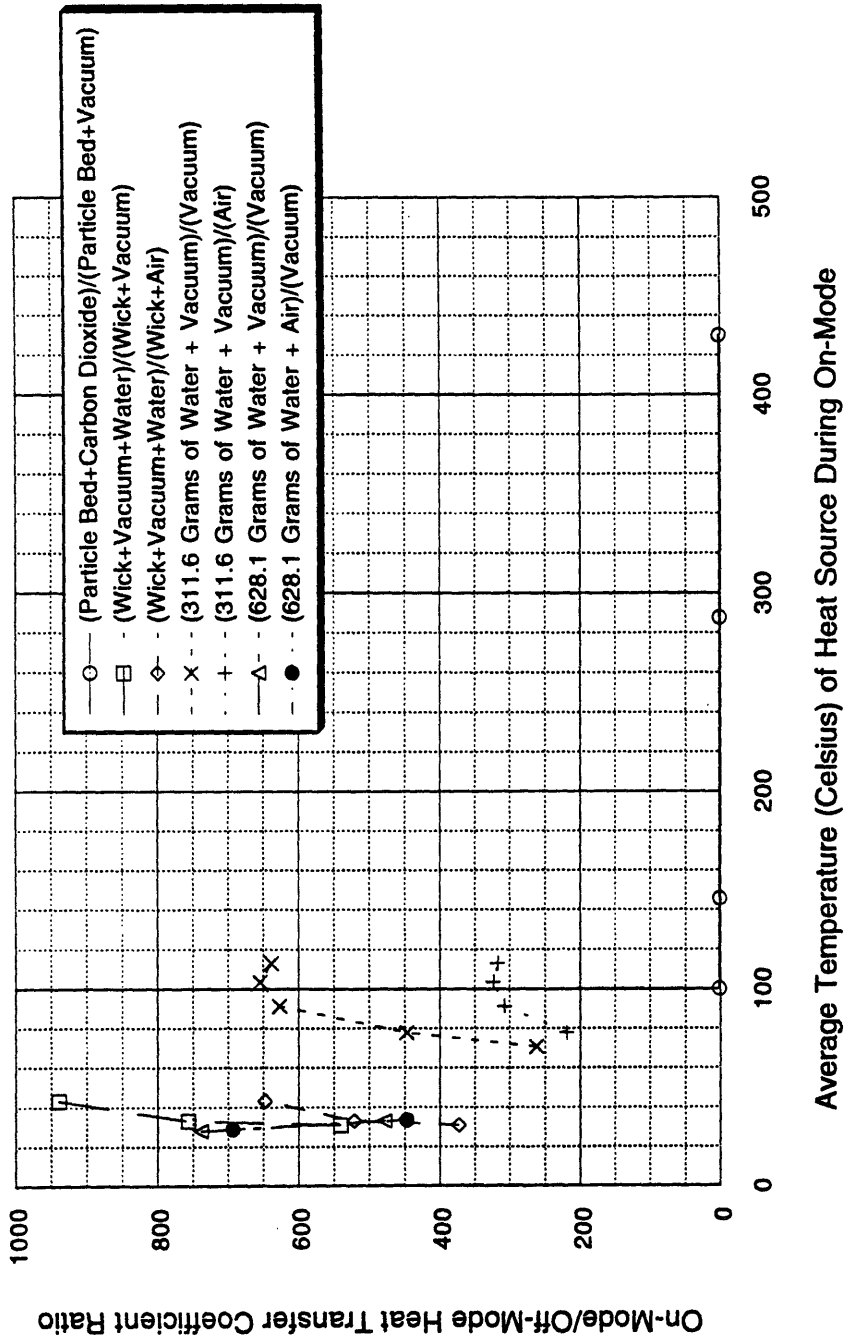


Figure 6.1. Best Performance Characteristics of Some of the Thermal Switches Investigated

probably be successful. Concerning the dissociation process of a metal carbonate, it is even more probable of being successful since the chemical parameters, Gibbs free energy and the enthalpy of formation, of all the metal carbonates indicate that the metal carbonates will always drive toward dissociation with the absorption of thermal energy. Thus, because it appears that the usage of a metal carbonate is an effective way of introducing carbon dioxide gas into a volume, and that a successful recombination algorithm has been developed to reconstitute the metal carbonate, the following is recommended. Other metal carbonates should be investigated to provide a range of dissociation temperatures, since each metal carbonate dissociates at a different temperature. Pressure versus temperature plots can be obtained using the dissociation/recombination experimental setup discussed in Chapter Four. This will provide an indication of the switching-on action each carbonate can provide. The metal carbonate recombination algorithm (use of moist CO_2) should then be tested on each metal oxide created by dissociation. Successful recombination will be indicated by pressure versus temperature plots similar to those obtained from the original chemical.

In addition to testing chemicals which yield carbon dioxide gas during dissociation, it is recommended that other chemicals be tested in the dissociation/recombination experimental setup which yield other types of gases. These other types of gases may be required for different kinds of thermal switches, or may be required for different applications of the same thermal switch due to chemical reaction concerns of the materials present. Also, other types of gases have higher thermal conductivities than carbon dioxide gas. Hence, the usage of other types of gases may yield superior heat transfer results. As with the metal carbonates, it is highly probable that the dissociation of these other chemicals will proceed as desired, with no need to develop a dissociation algorithm. However, the recombination process will probably require research and development, since chemical kinetics usually favors dissociation and not recombination.

A problem with this method of creating gas in a volume by dissociation of a solid chemical is that the gas does not begin to be created in substantial quantities until the chemical itself reaches a temperature near its dissociation temperature. Thus, if the gas is being used to thermally couple

or aid in thermally coupling a heat source and a heat sink, and the chemical is not in direct contact or close proximity to the heat source, then the heat source will become extremely hot before the temperature of the chemical is elevated to near its dissociation temperature. Hence, a method must be found to hold the chemical in contact or close proximity to the heat source. One method might be to place the chemical in metal tubing with holes drilled into it, and mechanically adhere the tubing to the heat source. The holes, of course, should be drilled on the top of the tubing to prevent the chemical from falling out of the tubing. A recommended experiment to test this concept (using the heat transfer coefficient experimental setup) is as follows. First, make several 18-inch long pieces of stainless steel tubing, one-quarter inch in diameter, and drill one-sixteenth holes in them at their apex every half-inch. Second, place the chemical in the tubing evenly distributed. The amount of chemical placed in the tubing should be that amount required to create one atmosphere of pressure in the annular volume between the heater and stainless steel pipe at the dissociation temperature of the chemical. Third, position the tubing uniformly around the circumference of the cylindrical heater and mechanically adhere the tubing to it either by hose clamps or nichrome wire. (Thus, the heat transfer path will be heater surface to tubing wall to chemical.) Lastly, acquire pressure versus temperature data using the algorithm employed for the dissociation experiments discussed in Chapter Four to see if sufficient pressure is obtained in the annular region between the heater and stainless steel pipe when the heater is slightly above the chemical's dissociation temperature. If sufficient pressure is not obtained at the desired heater surface temperature, then the thermal resistance along the heat transfer path from the heater surface to the chemical is too great, and changes must be made (such as using tubing comprised of a metal with a larger thermal conductivity) or a different approach must be used.

If a method is found that is successful in closely thermally coupling the heat source to the chemical, then it is recommended that transient experiments also be performed. These experiments would involve increasing the heater surface flux in a step change, and monitoring the rate of pressure increase in the annular volume, and the rate of surface temperature change of the heater. If the thermal switch is to find real life application, the pressure in the annular volume must

increase quickly, and it must result in stabilization of the heater temperature below a predetermined critical temperature. This type of experiment is important since it simulates the kind of emergency situation in which the thermal switch will perform.

As discussed in Chapter Five, the three thermal switches tested in the heat-transfer-coefficient experimental setup, the particle bed thermal switch, the wick thermal switch, and the water evaporation-condensation thermal switch, all functioned, albeit with varying degrees of success. The particle bed thermal switch was the least successful, allowing a temperature difference between the heat source and heat sink of approximately 400K for a heater surface flux of only 16.91 kw/m². In addition, it had a heat transfer coefficient ratio of only approximately two for average temperature differences between the heat source and heat sink ranging from 15K to approximately 400K. According to the theory developed by E. U. Schlunder, the heat transfer coefficient ratio could be increased to approximately four by pulling a one-micron vacuum in the off-mode, but even a switching ratio of four would result in a thermal switch of limited engineering application. Thus, it is recommended that no further experiments be performed on the particle bed thermal switch, since it will probably not find widespread usage.

The wick thermal switch yielded much more successful results. The wick-air-water on-mode setup had a maximum heat transfer coefficient of 641.16 w/(m² K), and heat transfer coefficient ratios up to 201.04 for a wick-vacuum off-mode, and up to 138.60 for a wick-air off-mode. In addition, the wick-air-water on-mode setup allowed a maximum temperature difference between the heat source and heat sink of only 82.61K for all surface heat fluxes investigated. Of particular interest is the fact that the data indicates that the wick-air-water setup can maintain this ΔT for significantly higher surface heat fluxes.

For heater surface fluxes less than 19.0 kw/m², the wick-vacuum-water on-mode setup yielded an even better performance than the wick-air-water setup, with peak performance occurring at a surface heat flux of 7.95 kw/m². At a heater surface flux of 7.95 kw/m², the heat transfer coefficient was 596.42 w/(m² K), and the heat transfer coefficient ratio was 939.22 for a wick-vacuum off-mode, and 647.18 for a wick-air off-mode. In addition, the ΔT was only 13.33K. (At

the same heater surface flux for the wick-air-water setup, the heat transfer coefficient was 99.14 w/(m² K), and the heat transfer coefficient ratios were 31.29 and 21.57 for a wick-vacuum off-mode and a wick-air off-mode, respectively. The temperature difference between the heater surface and inside stainless steel pipe surface was 80.17K.) For surface heat fluxes greater than 7.95 kw/m², there was a continual degradation in performance of the wick-vacuum-water thermal switch. Apparently, some physical phenomenon, possibly wick dryout, began to occur at the heater surface flux of 7.95 kw/m².

Thus, given the above results, the following is recommended. First, for the wick-air-water setup, repeat the experiment at higher surface heat fluxes. As mentioned above, no degradation in performance was noted as the surface heat flux was increased to the maximum value capable of being provided by the present electrical wall source powering the heater. Of course, to perform this experiment, a new electrical wall source will have to be used, and, for voltages above 150 volts and currents above 20 amps, a new voltmeter and ammeter will be needed. Also, the variac will have to be replaced, since its operating range is 0-140 volts, 0-20 amps.

Second, repeat the experiment for the wick-vacuum-water setup with more water present. If wick dryout is the problem due to too much water being in the vapor phase, then the addition of more water to the setup may remedy the problem by providing more liquid for wick wetting. Remedying this problem should be aggressively pursued because the data indicates that solution of this problem will yield a thermal switch with very high on-mode heat transfer coefficients and, hence, very large switching ratios. Also, other wick materials should also be investigated, and the minimum amount of water needed to provide thermal switch action should be determined.

The water thermal switch indisputedly showed the best overall performance. Both water-vacuum on-mode setups (311.6 grams of water + vacuum, and 628.1 grams of water + vacuum) had maximum on-mode heat transfer coefficients well above a 1000 w/(m² K), and maximum heat transfer coefficient ratios above 600 for the vacuum off-mode setup, and above 300 for the air off-mode setup. (Quite curiously, the smaller water mass setup had larger heat transfer coefficients and, hence, larger heat transfer coefficient ratios, than the larger water mass setup for

the higher heat fluxes investigated.) In addition both water-vacuum setups kept the temperature difference between the heater surface and inside stainless steel pipe surface below 47K for all heater surface fluxes investigated. Indeed, like the wick-air-water thermal switch, the data indicates that this average ΔT can be maintained for even higher heat fluxes, resulting in higher on-mode heat transfer coefficients and, hence, higher heat transfer coefficient ratios. The water-air setups (311.6 grams of water + air, and 628.1 grams of water + air) showed good performance as well, although not as stellar as the water-vacuum setups. The larger water mass setup had a maximum heat transfer coefficient of 667.43 w/(m² K), and, for the higher surface heat fluxes investigated, maximum heat transfer coefficient ratios of 200.88 and 101.12 for the vacuum off-mode setup and the air off-mode setup, respectively. The maximum temperature difference allowed by this on-mode setup was 78.25K, and occurred at the highest heat flux investigated, 51.85 kw/m². The smaller mass water-air setup had a maximum heat transfer coefficient of 338.41 w/(m² K), and maximum heat transfer coefficient ratios of 61.11 and 35.52 at the higher heat fluxes for the vacuum off-mode setup and the air off-mode setup, respectively. The maximum ΔT allowed was 155.03K, and, like the larger water mass setup, occurred at the maximum heat flux investigated. Both water-air setups did not show a stagnancy in the temperature difference between the heater surface and inside stainless steel pipe surface at the higher surface heat fluxes like the water-vacuum setups, but the data did show minimal increase in ΔT for an increase in the surface heat flux (at the higher surface heat fluxes investigated).

Thus, given the above results, the following is recommended. First, since all four on-mode setups were able to maintain the average temperature difference between the heater surface and inside stainless steel pipe surface at values well below what would be required in many applications of this thermal switch, and that the change in ΔT with increase in surface heat flux was either zero or very small at the higher surface heat fluxes investigated, the experiments discussed in Chapter 5 for the water thermal switch should be repeated for larger surface heat fluxes. The larger the maximum heat flux at which this thermal switch can be shown experimentally to function, the more widespread will be its potential application. (The present heater, with a new electrical source,

can provide heater surface fluxes up to 137 kw/m^2 .) Of particular interest is the performance of the two vacuum setups, since, as mentioned above, both were able to maintain very low ΔT 's for all the surface heat fluxes investigated, and both yielded no increase in ΔT for the higher heat fluxes.

The second recommendation involves finding the optimum water level for the water-vacuum setups for the higher surface heat fluxes investigated. Specifically, from the data acquired it appears that, at the higher surface heat fluxes when (apparently) the evaporation-condensation process is the dominant mode of heat transfer from the heat source to the heat sink, there exists an optimum water level in the annular region between the heater and stainless steel pipe that maximizes the heat transfer from heat source to heat sink. Indeed, as noted above and in Chapter 5, for the two water masses investigated, the smaller water mass had higher heat transfer coefficients than the larger water mass at the higher surface heat fluxes. Thus, it is recommended that the experiments discussed in Chapter 5 concerning the water-vacuum setups be repeated for different water heights (at the higher surface heat fluxes).

The last recommendation concerning the water thermal switch involves acquiring performance data under the mode of operation that would probably be employed in usage of the water thermal switch. Specifically, thus far, all the performance data acquired has been with the water present in the annular region from the start of the test. Thus, as the heater power was increased from zero watts to full power, smooth transition of the physics governing the heat transfer process from the heat source to the heat sink was allowed. However, in application of this thermal switch, the water will not be introduced into the volume between the heat source and heat sink until the heat source overheats. At this point of water release, the water will be much cooler than the heat source. Hence, problems associated with quenching, such as vapor blanketing and thermal stressing of the physical components, may arise. Thus, it is recommended that experiments be performed to investigate potential problems associated with this mode of thermal switch operation.

Finally, one practical application of the water thermal switch to CANDU reactors is suggested, as shown in Figure 6.2. This simple design would allow calandria water to enter the

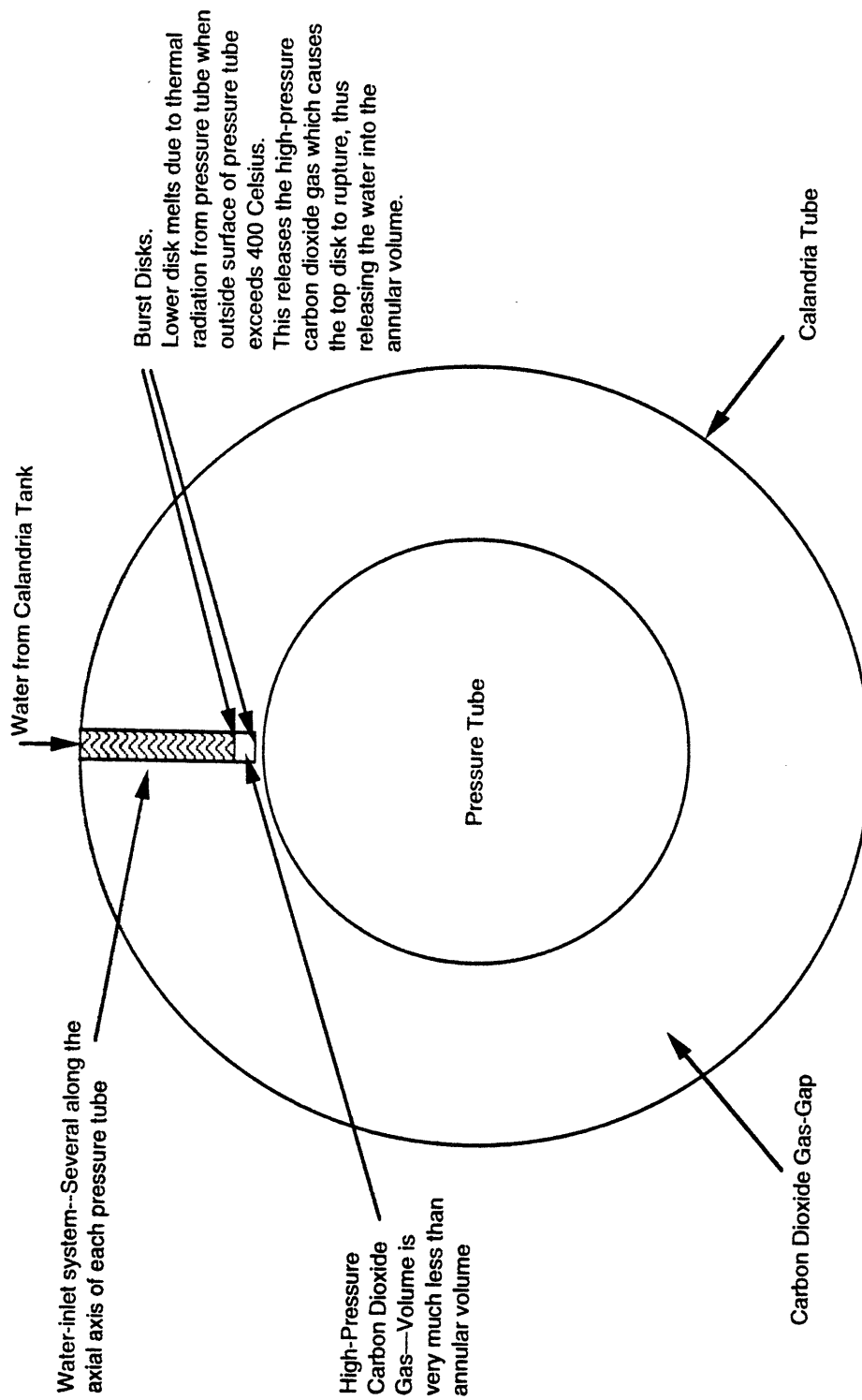


Figure 6.2. Potential Water Thermal Switch in CANDU Reactor

gas-gap to provide thermal switch action following LOCA, before damage to the pressure tube results. Work by another student at MIT also suggests that this might prevent extensive fuel failure (Mattingly, MIT Nuclear Engineering Dept, SM 1995). The above device could be tested in the experimental apparatus described in Chapter 5.

Appendix A

Raw and Reduced Data of Dissociation and Recombination Experiments

Dissociation/Recombination Experimental Results for Magnesium Carbonate (Figure 4.2)

Temperature of MgCO ₃ (Kelvin)	Total Pressure of Test Cavity (psig)	Background Pressure of Test Cavity (psig)	Net Pressure of Test Cavity (psig) Fig 4.2
200.00	-14.675	-14.700	-14.675
250.00	-14.300	-14.697	-14.303
300.00	-13.400	-14.685	-13.415
350.00	-12.450	-14.668	-12.482
400.00	-10.750	-14.651	-10.799
450.00	-7.400	-14.630	-7.470
500.00	2.000	-14.608	1.908
450.00	1.800	-14.605	1.705
400.00	0.800	-14.603	0.703
350.00	-0.100	-14.603	-0.197
300.00	-1.300	-14.603	-1.397

Dissociation/Recombination Experimental Results for Lead Carbonate (Figure 4.3)

Temperature of PbCO ₃ (Kelvin)	Total Pressure of Test Cavity (psig)	Background Pressure of Test Cavity (psig)	Net Pressure of Test Cavity (psig) Fig 4.3
200.00	-14.700	-14.700	-14.700
250.00	-13.600	-14.697	-13.603
300.00	-7.850	-14.685	-7.865
350.00	-3.450	-14.668	-3.482
400.00	0.300	-14.651	0.251
350.00	-0.500	-14.648	-0.552
300.00	-1.400	-14.648	-1.452
250.00	-2.400	-14.648	-2.452
200.00	-3.400	-14.648	-3.452

**Recombination Experimental Results with Increased Surface Area
of MgO and a 19-Hour Hold at 300°C (Figure 4.4)**

Temperature of MgCO ₃ (Kelvin)	Total Pressure of Test Cavity (psig)	Background Pressure of Test Cavity (psig)	Net Pressure of Test Cavity (psig) Fig 4.4
200.00	-14.677	-14.700	-14.677
250.00	-14.302	-14.697	-14.305
300.00	-13.400	-14.685	-13.415
350.00	-12.447	-14.668	-12.479
400.00	-10.749	-14.651	-10.798
450.00	-7.405	-14.630	-7.475
500.00	2.003	-14.608	1.911
450.00	1.798	-14.605	1.703
400.00	0.801	-14.603	0.704
350.00	-0.102	-14.603	-0.199
300.00	-1.296	-14.603	-1.393
300.00	-2.700	-14.603	-2.797

**Recombination Experimental Results with Increased Recombination Sites
of MgO and a Nineteen-Hour Hold at 300°C (Figure 4.5)**

Temperature of MgCO ₃ (Kelvin)	Total Pressure of Test Cavity (psig)	Background Pressure of Test Cavity (psig)	Net Pressure of Test Cavity (psig) Fig 4.5
200.00	-14.674	-14.700	-14.674
250.00	-14.299	-14.697	-14.302
300.00	-13.402	-14.685	-13.417
350.00	-12.449	-14.668	-12.481
400.00	-10.747	-14.651	-10.796
450.00	-7.402	-14.630	-7.472
500.00	2.001	-14.608	1.909
450.00	1.502	-14.605	1.407
400.00	-0.300	-14.603	-0.397
350.00	-2.200	-14.603	-2.297
300.00	-4.200	-14.603	-4.297
300.00	-7.000	-14.603	-7.097

Dissociation Results of Reconstituted Magnesium Carbonate (Figure 4.8)

Temperature of MgCO ₃ (Kelvin)	Total Pressure of Test Cavity (psig)	Background Pressure of Test Cavity (psig)	Net Pressure of Test Cavity (psig) Fig 4.8
325.00	-14.600	-14.700	-14.600
350.00	-14.100	-14.697	-14.103
400.00	-4.500	-14.685	-4.515
425.00	1.724	-14.680	17.220
400.00	15.900	-14.675	15.875
375.00	14.800	-14.675	14.775
350.00	13.300	-14.675	13.275
325.00	11.800	-14.675	11.775
300.00	10.400	-14.675	10.375
275.00	9.000	-14.675	8.975
250.00	7.800	-14.675	7.775

Appendix B

Components and Vendors Employed

Below are listed the main parts of the three experimental setups discussed in Chapters Four and Five. Reading horizontally, the part is given first, followed by the vendor's part number (where applicable), and then the vendor's name and telephone number.

Heat-Transfer-Coefficient Experiment

K-type Thermocouple	CAIN-116U-30	Omega Eng; 1-800-622-2378
Calibration of HP-3852A Data Acquisition Unit		Hewlett-Packard; 1-201-586-5400
Wick Material	ZYF100 18"X24"X0.100"	Zircar Products Inc.; 1-914-651-4481
Needle Valve	SS-6BK-TW	Cambridge Valve and Fitting; 1-617-272-8270
Socket Weld Gland	SS-4-VCR-3	Cambridge Valve and Fitting; 1-617-272-8270
Female Nut	SS-4-VCR-1	Cambridge Valve and Fitting; 1-617-272-8270
Male Nut	SS-4-VCR-4	Cambridge Valve and Fitting; 1-617-272-8270
Union Tee, 0.25"	SS-4-TSW-3	Cambridge Valve and Fitting; 1-617-272-8270
Close Coupling-- Double Female	SS-4-WVCR-6-DF	Cambridge Valve and Fitting; 1-617-272-8270
Whitey 60 Series Ball Valve	SS-62TF4	Cambridge Valve and Fitting; 1-617-272-8270
Whitey 40 Series Ball Valve	SS-43VCR4	Cambridge Valve and Fitting; 1-617-272-8270
3.375" Blank Conflat Flange	954-5185	Varian; 1-800-882-7426
Metal VCR Gasket	SS-4-VCR-2	Cambridge Valve and Fitting; 1-617-272-8270
Copper Gaskets for 3.375" Flange	953-5013	Varian; 1-800-882-7426
Copper Gaskets for 8.000" Flange	953-5017	Varian; 1-800-882-7426
Nut/Bolt Set for 3.375" Flange	953-5012	Varian; 1-800-882-7426
Nut/Bolt Set for 8.000" Flange	953-5022	Varian; 1-800-882-7426

Nonrotatable Flange Blank, 2.75"	110008	MDC Vacuum Products; 1-800-443-8817
Tygon Tubing	190750	MIT Stock Room 3-1881
500 cc Stainless Steel 304 Graduated Measure		McMaster-Carr; 1-908-329-3200
Thick-walled (0.095") 0.375" Tubing		All Stainless; 1-617-749-7100
Tote Drum, Stainless Steel, 58 Gallon, I.D.=24", H=30", 16 Gauge	4562T25	McMaster-Carr; 1-908-329-3200
CO ₂ Pressure Regulator	8H-320	Matheson Instruments; 1-800-732-0340
Stainless Steel 316 Tubing 0.375" I.D., 0.035" Wall	0.375-TCC-316-035	Harbor Controls; 1-508-453-2323
Half-Nipple, Stainless Steel, 6" I.D., 8" Conflat Flange, 2 ft long, 0.083" Wall	5000-MSP-A3391	Varian; 1-800-882-7426
Nipple, Stainless Steel, 2" I.D., 2.25" O.D., 27 inches long with 3.375" Conflat Flange	5000-MSP-A3640	Varian; 1-800-882-7246
Conflat Flange, Stainless Steel, 8" O.D., Blank	954-5087	Varian; 1-800-882-7246
Vacuum Pump, 6 cfm Yellow Jacket	model number 93460	United Refrigeration 1-617-395-8100
OFHC Copper Gaskets	191994	MDC Vacuum Products; 1-800-443-8817
Dodecagon (12-Point) Head Sets for Thru-Hole Flanges	190040	MDC Vacuum Products; 1-800-443-8817
Stainless Steel 316 Tubing 0.25" O.D., 0.035" Wall	0.25-SCI-3161-035	Harbor Controls; 1-508-453-2323
Insulating Sleeves		High Temp Insulation; 1-805-484-2774
Female Connector Converts male NPT thread to metal gasket face seal	SS-4-WVCR-7-4	Cambridge Valve and Fitting; 1-617-272-8270
Kwik Flange to 0.50" Female NPT	731006	MDC Vacuum Products; 1-800-443-8817
Kwik Flange, Blank	712001	MDC Vacuum Products; 1-800-443-8817
Precision Compound Gauge 6-inches, 30/0/15 Hg/PSI	AS800274	Davis Instruments; 1-800-368-2516
Heater, 48" long, 1.00" diam. 18" active heater length, 5000 watts K-Type Ungrounded Thermocouples		Watlow; 1-314-878-4600

Molecular Water Sieve with Del-Seal 2.75" O.D. Flanges	431006	MDC Vacuum Products; 1-800-443-8817
Two-Piece Coaxial Foreline Trap	433006	MDC Vacuum Products; 1-800-443-8817
Stainless Steel Sieve Element	433051	MDC Vacuum Products; 1-800-443-8817
Kwik-Flange to Swagelok Adapter	414013	MDC Vacuum Products; 1-800-443-8817
PVC Hose Adapter	736002	MDC Vacuum Products; 1-800-443-8817
Centering Ring Assembly	710001	MDC Vacuum Products; 1-800-443-8817
Hinged Clamps	701001	MDC Vacuum Products; 1-800-443-8817
Voltmeter, 0-150 Volts	250-344-PZPZ	Calibron Instruments; 1-617-894-6440
Ammeter, 0-20 Amps	250-340-NGNG	Calibron Instruments; 1-617-894-6440
MACOR Cylinders	Ceramic Products; 1-201-947-0336	
Double Female Union	SS-4-VCR-6-DF	Cambridge Valve and Fitting; 1-617-272-8270
Silicon Carbide (16 grit)	4780A34	McMaster-Carr; 1-908-329-3200
Machining	Signet Tool and Engineering	1-617-233-0830
Welding and Machining	Ramsey Welding	1-617-933-4900

Dissociation/Recombination Experiment

Male Socket Weld Gland	SS-4-VCO-3	Cambridge Valve and Fitting; 1-617-272-8270
Female Nut	SS-4-VCO-4	Cambridge Valve and Fitting; 1-617-272-8270
Union Tee, 0.25"	SS-4-TSW-3	Cambridge Valve and Fitting; 1-617-272-8270
Close Coupling-- Double Female	SS-4-WVCR-6-DF	Cambridge Valve and Fitting; 1-617-272-8270
Whitey 40 Series Ball Valve	SS-43VCO4	Cambridge Valve and Fitting; 1-617-272-8270
Compact In-Line Filter	SS-4F-VCR-2	Cambridge Valve and Fitting; 1-617-272-8270
Stainless Steel 316 Tubing 0.25" O.D., 0.035" Wall	0.25-SCI-316I-035	Harbor Controls; 1-508-453-2323
Magnesium Hydroxide	I-4005	ChemService; 1-800-452-9994
Magnesium Carbonate	I-3960	ChemService; 1-800-452-9994
Lead Carbonate	I-3430	ChemService; 1-800-452-9994
Convectron Vacuum Gauge (Low Pressure Gauge)	275185	Granville-Phillips Co.; 1-303-443-7660
Acetone AR(REAG)	290111	MIT Bldg 18 Chemical Supplies; 3-1425
Ethyl Alcohol 200 Absol.	290730	MIT Bldg 18 Chemical Supplies; 3-1425
A286 SS Washer	AN 960 C416	National Aircraft of New Jersey; 1-201-472-2300
Conflat Flange SS-316 2.75"O.D., 1.5"I.D.	959-5071	Varian; 1-800-882-7246
Fel-Pro Lubricant	953-0031	Varian; 1-800-882-7246
A286 SS Bolts, 12 Point 0.75" Thread, 1.00" long	MS 9557-14	Saturn Fasteners Inc.; 1-800-947-9414 or Askew Hardware & Supply; 1-213-727-7772
High-Pressure Gauge	Ti9675	Davis Instruments; 1-800-368-2516
Scoopula, Stainless Steel	172000	MIT Stock Room 3-1881
Forceps Cover Glass, Bent Tip	151400	MIT Stock Room 3-1881
Forceps Sharp Point	151540	MIT Stock Room 3-1881
Spatula, Monel	173580	MIT Stock Room 3-1881
Welding and Machining	Ramsey Welding	1-617-933-4900

Experiment for Combining Moist CO₂ with MgO

Red Silicon Tubing, 0.25" I.D., 0.125" Wall	190180	MIT Stock Room 3-1881
Pyrex Filtering Flask 500 ml	149000	MIT Stock Room 3-1881
Flexible Teflon Tubing 0.25" O.D., 0.1875" I.D.	190195	MIT Stock Room 3-1881
Crystal Dish 100X50 mm	142660	MIT Stock Room 3-1881
Solid Rubber Stopper #15	178360	MIT Stock Room 3-1881
Solid Rubber Stopper #7	178160	MIT Stock Room 3-1881
Stainless Steel Swagelok Union 0.25"	200580	MIT Stock Room 3-1881
Pyrex Glass Tubing 3 mm	187940	MIT Stock Room 3-1881

Appendix C

Mass Calculations for Dissociation Experiment

Below are delineated the theory and calculations required to determine the mass needed of the dissociating chemical to provide 1 atm of pressure in the test cavity. (The theory was acquired from the book *University Chemistry 3rd Edition* by Bruce Mahan, 1975, Addison-Wesley Publisher.)

$$G = H - TS = E + PV - TS \quad (C.1)$$

$$dG = dE + PdV + VdP - TdS - SdT \quad (C.2)$$

But for a situation in which only pressure-volume work can be done,

$$dE = dq - PdV \quad (C.3)$$

so,

$$dG = dq + VdP - TdS - SdT \quad (C.4)$$

Equating TdS and dq then gives

$$dG = VdP - SdT \quad (C.5)$$

For a pressure change at constant temperature

$$dG = VdP \quad (C.6)$$

In the following discussion, quantities that apply to one mole of material will be italicized, as in

$V = (RT/P) dP$. Then for one mole of ideal gas,

$$dG = (RT/P) dP \quad (C.7)$$

Let us integrate this expression taking as one limit of pressure $P^\circ = 1$ atm, the standard pressure. Then the corresponding limit for G will be G° , the standard free energy of one mole of ideal gas.

We get

$$G - G^\circ = RT \ln(P/P^\circ) = RT \ln P \quad (\text{C.8})$$

where G is the molar free energy at any pressure P (in atm) and G° is the standard free energy. If, instead of 1 mole, n moles are considered, we get

$$nG = nG^\circ + nRT \ln P \quad (\text{C.9})$$

The next step is to calculate ΔG for the general reaction between ideal gases



$$aA(P_A) + bB(P_B) = cC(P_C) + dD(P_D) \quad (\text{C.11})$$

where P_A and P_B are the pressures of the reactants and P_C and P_D are the pressures of the products. We have

$$\Delta G = \sum G(\text{products}) - \sum G(\text{reactants}) \quad (\text{C.12})$$

$$= cG(C) + dG(D) - aG(A) - bG(B) \quad (\text{C.13})$$

$$= [cG^\circ(C) + dG^\circ(D) - aG^\circ(A) - bG^\circ(B)] \\ + cRT \ln P_C + dRT \ln P_D - aRT \ln P_A - bRT \ln P_B \quad (\text{C.14})$$

The bracketed terms are equal to ΔG° , and the remaining terms can be combined to give

$$\Delta G = \Delta G^\circ + RT \ln[(P_C)^c (P_D)^d / (P_A)^a (P_B)^b] \quad (\text{C.15})$$

This equation relates the free-energy change for any ideal gas reaction involving arbitrary pressures of reactants and products to the standard free-energy change and the pressure of the reagents.

Suppose that the pressures are those that exist when reactants and products are in equilibrium with each other. Then $\Delta G = 0$, since the initial and final states are in equilibrium, and

$$0 = \Delta G^\circ + RT \ln[(P_C)^c(P_D)^d/(P_A)^a(P_B)^b]_{eq} \quad (C.16)$$

For the reaction



since CO_2 is the only gaseous product or reactant

$$\Delta G^\circ = -RT \ln P \quad P = \text{pressure of CO}_2$$

	ΔH_f° (kcal/mole)	ΔG° (kcal/mole)
MgO	-143.8	-136.1
CO ₂	-94.1	-94.3
MgCO ₃	-266.0	-246.0

$$\Delta H_f^\circ (\text{products}) - \Delta H_f^\circ (\text{reactants}) = 28.1 \text{ kcal/mole} \quad (C.18)$$

$$\Delta G^\circ (\text{products}) - \Delta G^\circ (\text{reactants}) = 15.6 \text{ kcal/mole} \quad (C.19)$$

So,

$$\Delta G^\circ = -RT \ln P \longrightarrow P_0 = \exp[-\Delta G^\circ/RT_0] \quad (C.20)$$

$$P_0 = \exp [-(15.6 \text{ kcal/mole})/((0.001987 \text{ kcal/mole K})(298 \text{ K}))] = \exp[-26.346] \quad (C.21)$$

In general, ΔH_f varies very little as T increases. Hence, we can estimate the pressure using

$$\begin{aligned} P &= P_0 \exp[(\Delta H_f^\circ/RT_0)(1 - T_0/T)] \\ &= \exp[-26.346] \exp \{ [28.1 \text{ kcal/mole}/((0.001987 \text{ kcal/mole K})(298 \text{ K}))] \} \end{aligned}$$

$$\begin{aligned} & \{1 - (298 \text{ K})/T\} \\ & = \exp[21.110 - 47.456 (298/T)] \end{aligned} \quad (\text{C.22})$$

Thus, $T = (47.456)(298)/(21.110 - \ln P)$ where P is in atm and T is in Kelvin. Hence for a final cavity pressure of 1 atm, $T = 669.91 \text{ K} = 396.76^\circ\text{C}$. Therefore,

$$\begin{aligned} n/V &= P/RT \\ &= 1 \text{ atm}/[(0.08206 \text{ liter-atm/mole K})(669.91 \text{ K})] \\ &= 1.819 \times 10^{-2} \text{ mole/liter} \\ &= 18.19 \text{ mole/m}^3 \end{aligned} \quad (\text{C.23})$$

The volume of the test cavity is $5.23 \times 10^{-4} \text{ m}^3$. Thus, the number of moles of CO_2 needed is

$$n = (18.19 \text{ mole/m}^3)(5.23 \times 10^{-4} \text{ m}^3) = 9.51 \times 10^{-3} \text{ moles} \quad (\text{C.24})$$

The chemical equation $\text{MgCO}_3 (\text{s}) \rightarrow \text{MgO} (\text{s}) + \text{CO}_2 (\text{g})$ tells us that for each mole of MgCO_3 dissociated, 1 mole of MgO is produced and 1 mole of CO_2 is produced. Therefore, 9.51×10^{-3} moles of MgCO_3 are to be placed in the test cavity. The molecular weight of MgCO_3 is 84.32 gm/mole. Thus, assuming no CO_2 losses, 0.80 grams of MgCO_3 are needed to pressurize the test cavity to $P = 1 \text{ atm}$ at 396.76°C .

Appendix D

Computer Program

The subject computer program, which incorporated the raw data reduction algorithm, is versatile in handling different experimental situations. Required inputs are status of each thermocouple (i.e., on or off), thermocouple readings, power input to the heater, number of annular finite elements between the opposite-end thermocouples on the stainless steel pipe, and left axial boundary and right axial boundary over which the thermal switch heat transfer coefficient is to be calculated. Once the computer code is given this data, it provides, between the axial boundaries specified, the axial temperature distribution of the surface of the heater, the axial temperature distribution of the inside surface of the stainless steel pipe, the axial thermal switch heat transfer coefficient distribution, and the average thermal switch heat transfer coefficient. The next two pages show the two pages that appear on the computer screen for the data input and the results obtained. Following these input/output pages, the computer code, written in C, is printed.

Data Entry Panel

1 Pipe Thermocouple

105 9100

2 Pipe Thermocouple

174 0100

3 Pipe Thermocouple

126 0100

4 Pipe Thermocouple

126 1200

5 Pipe Thermocouple

118 7200

6 Pipe Thermocouple

127 0300

7 Pipe Thermocouple

127 9100

8 Pipe Thermocouple

105 9100

9 Pipe Thermocouple

38 1400

10 Pipe Thermocouple

37 2300

11 Pipe Thermocouple

37 7200

12 Pipe Thermocouple

38 7400

13 Pipe Thermocouple

37 9300

14 Pipe Thermocouple

38 0500

Load Input

Save Input

Enter & Return

Return


```

#include "novak.h"
#include "novout.h"
#include "hp3852a.h"
#include "C:\LW\INCLUDE\lwsystem.h"
#include "C:\LW\INCLUDE\utility.h"
#include "C:\LW\INCLUDE\gpib.h"
#include "C:\LW\INCLUDE\gpib4882.h"
#include "C:\LW\INCLUDE\formatio.h"
#include "C:\LW\INCLUDE\userint.h"
#include "C:\LW\INCLUDE\graphics.h"
#include "C:\LW\INCLUDE\analysis.h"
#include "C:\LW\INCLUDE\vx1.h"
#include "C:\LW\INCLUDE\dataacq.h"
#include "C:\LW\INCLUDE\rs232.h"
#define KAH 4.611e-3 // Product of Thermal Conductivity and Cross Sectional Ar
#define PIPECONST 8.6466e-4
#define pi 3.14159267

int GetTemperatures(int*StateH,int*StateP,double*HeaterThermTemp,double*PipeThermTemp);
void PopupScreen(char *Title,double *Array,double *AxPosition,int Resolution);
/*= STATIC VARIABLE DECLARATIONS =====*/

static int panelHandle[7];
static int eventPanelID[2];
static int eventControl[2];
static int loopDoneFlag[2];
static int menuBarHandle;

void main()
{
int FileStatus,Type,status=0;
int Resolution=512,i,lbpt,rbpt,lbht,rbht;
int ActiveHeaterTherm=8,ActivePipeTherm=6,StateH[8],StateP[6],j;
double start=6,finish=24,posit; //start location in inches
double dx,*AxPosition,HeaterThermTemp[8],PipeThermTemp[6],xh[8],xp[6],Position[8];
double *splineh,*splines,*qr,*PipeTemp,*WallTemp,*HeatTemp,*U;
double Umean,RightBoundHT,LeftBoundHT,RightBoundPT,LeftBoundPT;
double Qh=1.0;
double Dh=2.5349e-2; //Heater Diameter in meters
char outfile[80],txt[80],Title[80];
FILE *fp;
panelHandle[MAIN] = LoadPanel ("novak.uir", MAIN);
panelHandle[ENTER] = LoadPanel ("novak.uir", ENTER);
HidePanel(panelHandle[ENTER]);
DisplayPanel (panelHandle[MAIN]);
menuBarHandle = LoadMenuBar("novak.uir", MENU);

AxPosition=(double *) malloc (Resolution*sizeof(double));
splineh=(double *) malloc (Resolution*sizeof(double));
splines=(double *) malloc (Resolution*sizeof(double));
qr=(double *) malloc (Resolution*sizeof(double));
PipeTemp=(double *) malloc (Resolution*sizeof(double));
WallTemp=(double *) malloc (Resolution*sizeof(double));
HeatTemp=(double *) malloc (Resolution*sizeof(double));
U=(double *) malloc (Resolution*sizeof(double));
if (U==NULL) {
MessagePopup("Out of Memory");
exit(0);
}
Position[0]=xh[0]=5.828125; //These are the thermocouple posit

```

```

Position[1]=xh[1]=xp[0]=7.265625;
Position[2]=xh[2]=xp[1]=9.968750;
Position[3]=xh[3]=xp[2]=12.984375;
Position[4]=xh[4]=xp[3]=16.203125;
Position[5]=xh[5]=xp[4]=19.531250;
Position[6]=xh[6]=xp[5]=22.718750;
Position[7]=xh[7]=xp[6]=24.156250;

dx=(finish-start)/Resolution;
for (i=0;i<Resolution;i++) AxPosition[i]=dx*i+start;

GetCtrlVal(panelHandle[MAIN],MAIN_RBHT,&posit);
rbht=1*(posit-start)/dx;
GetCtrlVal(panelHandle[MAIN],MAIN_LBHT,&posit);
lbht=1*(posit-start)/dx;
GetCtrlVal(panelHandle[MAIN],MAIN_RBPT,&posit);
rbpt=1*(posit-start)/dx;
GetCtrlVal(panelHandle[MAIN],MAIN_LBPT,&posit);
lbpt=1*(posit-start)/dx;

U[0]=U[Resolution]=0;

// ConfigureAxes(panelHandle[MAIN],MAIN_GRAPHPIPE,0,xp[0],xp[5],-1,0,0);
// Turn all thermocouples on and set them to 70 deg
for (i=0;i<8;i++) {StateH[i]=1;HeaterThermTemp[i]=90.0;}
for (i=0;i<6;i++) {StateP[i]=1;PipeThermTemp[i]=70.0;}

status=GetTemperatures(StateH,StateP,HeaterThermTemp,PipeThermTemp,&Acti
loopDoneFlag[0] = 0;
while (!loopDoneFlag[0]) {
    if (status) {
        DeletePlots(panelHandle[MAIN],MAIN_GRAPHHEATER);
        DeletePlots(panelHandle[MAIN],MAIN_GRAPHPIPE);
        DeletePlots(panelHandle[MAIN],MAIN_COEFFICIENT);

        Spline(xh,HeaterThermTemp,ActiveHeaterTherm,0,0,splineh)
        for (i=0;i<Resolution;i++) (SpInterp(xh,HeaterThermTemp,

        Spline(xp,PipeThermTemp,ActivePipeTherm,0,0,splinep);
        for (i=0;i<Resolution;i++) (SpInterp(xp,PipeThermTemp,sp

        for (i=1;i<Resolution-1;i++) (qr[i]=dx/(finish-start)*Qh

        Mean(&U[lbht],rbht-lbht,&Umean);
        SetCtrlVal(panelHandle[MAIN],MAIN_UAVE,Umean);
// PlotLine(panelHandle[MAIN],MAIN_COEFFICIENT,
        PlotXY(panelHandle[MAIN],MAIN_COEFFICIENT, &AxPosition[1]
        PlotXY(panelHandle[MAIN],MAIN_GRAPHHEATER, &AxPosition[He
        PlotXY(panelHandle[MAIN],MAIN_GRAPHPIPE, &AxPosition[lbp
        PlotXY(panelHandle[MAIN],MAIN_GRAPHPIPE, &AxPosition[lbp
        status=0;
    }
    GetUserEvent (0, &eventPanelID[0], &eventControl[0]);
    if (eventPanelID[0] == panelHandle[MAIN]) {
        switch (eventControl[0]) {

            case MAIN_SWITCH:
                status=GetTemperatures(StateH,StateP,Hea

```

```

        break;

case MAIN_RBHT:
    GetCtrlVal(panelHandle[MAIN],MAIN_RBHT,&
        rbht=1*(RightBoundHT-start)/dx;
    break;
case MAIN_LBHT:
    GetCtrlVal(panelHandle[MAIN],MAIN_LBHT,&
        lbht=1*(LeftBoundHT-start)/dx;
    break;
case MAIN_RBPT:
    GetCtrlVal(panelHandle[MAIN],MAIN_RBPT,&
        rbpt=1*(RightBoundPT-start)/dx;
    break;
case MAIN_LBPT:
    GetCtrlVal(panelHandle[MAIN],MAIN_LBPT,&
        lbpt=1*(LeftBoundPT-start)/dx;
    break;

case MAIN_HEAT:
    GetCtrlVal(panelHandle[MAIN],MAIN_HEAT,&
        break;

case MAIN_RESOLUTION:
    GetCtrlVal(panelHandle[MAIN],MAIN_RESOLU
    free(AxPosition);free(splineh);free(spli
    free(WallTemp);free(HeatTemp);free(U);
    AxPosition=(double *) malloc (Resolution
    splineh=(double *) malloc (Resolution*si
    splinep=(double *) malloc (Resolution*si
    qr=(double *) malloc (Resolution*sizeof(
    PipeTemp=(double *) malloc (Resolution*s
    WallTemp=(double *) malloc (Resolution*s
    HeatTemp=(double *) malloc (Resolution*s
    U=(double *) malloc (Resolution*sizeof(d
    dx=(finish-start)/Resolution;
    GetCtrlVal(panelHandle[MAIN],MAIN_RBHT,&
        rbht=1*(posit-start)/dx;
    GetCtrlVal(panelHandle[MAIN],MAIN_LBHT,&
        lbht=1*(posit-start)/dx;
    GetCtrlVal(panelHandle[MAIN],MAIN_RBPT,&
        rbpt=1*(posit-start)/dx;
    GetCtrlVal(panelHandle[MAIN],MAIN_LBPT,&
        lbpt=1*(posit-start)/dx;
    for (i=0;i<Resolution;i++) AxPosition[i]
    U[0]=U[Resolution]=0;
    break;

case MAIN_SAVE:
    GetCtrlVal(panelHandle[MAIN],MAIN_TYPE,&
    switch (Type) {
        case 0:
            for (i=0;i<Resolution;i+
                fprintf(fp,"%g "
                fprintf(fp,"\n")
            }
            break;
        case 1:
            for (i=0;i<Resolution;i+
                fprintf(fp,"%g "

```

```

        fprintf(fp, "\n")
    }
    break;
case 2:
    for (i=0; i<Resolution; i++)
        fprintf(fp, "%g "
                fprintf(fp, "\n")
    }
    break;
case 3:
    for (i=0; i<Resolution; i++)
        fprintf(fp, "%g "
                fprintf(fp, "\n")
    }
    break;
case 4:
    for (i=0; i<Resolution; i++)
        fprintf(fp, "%g "
                fprintf(fp, "\n")
    }
    break;
case 5:
    fprintf(fp, "%g ", U);
    fprintf(fp, "\n");
    break;
}
break;

case MAIN_COEFFICIENT:
    sprintf(Title, "Heat Transfer Coefficient
    PopupScreen(Title, U, AxPosition, Resolutio
    break;
case MAIN_GRAPHHEATER:
    sprintf(Title, "Heater Temperature");
    PopupScreen(Title, HeatTemp, AxPosition, Re
    break;
case MAIN_GRAPHPIPE:
    sprintf(Title, "Pipe Temperature");
    PopupScreen(Title, PipeTemp, AxPosition, Re
    break;

case MAIN_SWITCH:
    GetCtrlVal(panelHandle[MAIN], MAIN_SWITCH
    break;

    )
}

if (eventPanelID[0] == menuBarHandle)
    switch (eventControl[0]) {
        case MENU_FILE:
            FileStatus=FileSelectPopup ("", "*.mat", "
            if (FileStatus) {
                fclose(fp);
                fp=fopen(outfile, "w+");
            }
            break;
        case MENU_QUIT:
    }
}

```

```

                                exit (0);
                                break;
                                )
                                )
                                )
int GetTemperatures(StateH,StateP,HeaterThermTemp,PipeThermTemp,APT,AHT,xh,xp,Po
int
    *StateH;
int
    *StateP;
double *HeaterThermTemp;
double *PipeThermTemp;
int
    *AHT;
int
    *APT;
double *xh;
double *xp;
double *Position;
{
int i,j,status=0,NumHeat=8,NumPipe=6;
int ActiveHeaterTherm=*AHT,ActivePipeTherm=*APT;

InstallPopup(panelHandle[ENTER]);
i=0;
if (StateH[0]) {SetCtrlVal(panelHandle[ENTER],ENTER_HEATTEMP1,HeaterTher
if (StateH[1]) {SetCtrlVal(panelHandle[ENTER],ENTER_HEATTEMP2,HeaterTher
if (StateH[2]) {SetCtrlVal(panelHandle[ENTER],ENTER_HEATTEMP3,HeaterTher
if (StateH[3]) {SetCtrlVal(panelHandle[ENTER],ENTER_HEATTEMP4,HeaterTher
if (StateH[4]) {SetCtrlVal(panelHandle[ENTER],ENTER_HEATTEMP5,HeaterTher
if (StateH[5]) {SetCtrlVal(panelHandle[ENTER],ENTER_HEATTEMP6,HeaterTher
if (StateH[6]) {SetCtrlVal(panelHandle[ENTER],ENTER_HEATTEMP7,HeaterTher
if (StateH[7]) {SetCtrlVal(panelHandle[ENTER],ENTER_HEATTEMP8,HeaterTher
i=0;
if (StateP[0]) {SetCtrlVal(panelHandle[ENTER],ENTER_PIPETEMP1,PipeThermT
if (StateP[1]) {SetCtrlVal(panelHandle[ENTER],ENTER_PIPETEMP2,PipeThermT
if (StateP[2]) {SetCtrlVal(panelHandle[ENTER],ENTER_PIPETEMP3,PipeThermT
if (StateP[3]) {SetCtrlVal(panelHandle[ENTER],ENTER_PIPETEMP4,PipeThermT
if (StateP[4]) {SetCtrlVal(panelHandle[ENTER],ENTER_PIPETEMP5,PipeThermT
if (StateP[5]) {SetCtrlVal(panelHandle[ENTER],ENTER_PIPETEMP6,PipeThermT
loopDoneFlag[1]=0;
while (!loopDoneFlag[1]) {
    GetPopupEvent (0, &eventControl[1]);
    switch (eventControl[1]) {
        case ENTER_TH1:
            GetCtrlVal(panelHandle[ENTER],ENTER_TH1,&StateH[
            if (StateH[0]) {SetInputMode(panelHandle[ENTER],
            else {SetInputMode(panelHandle[ENTER],ENTER_HEAT
            j=0;
            for (i=0;i<NumHeat;i++) {
                if (StateH[i]) {
                    xh[j]=Position[i];
                    j++;
                }
            }
            break;

        case ENTER_TH2:
            GetCtrlVal(panelHandle[ENTER],ENTER_TH2,&StateH[
            if (StateH[1]) {SetInputMode(panelHandle[ENTER],
            else {SetInputMode(panelHandle[ENTER],ENTER_HEAT
            j=0;
            for (i=0;i<NumHeat;i++) {

```

```

        if (StateH[i]) {
            xh[j]=Position[i];
            j++;
        }
    }
    break;

case ENTER_TH3:
    GetCtrlVal(panelHandle[ENTER],ENTER_TH3,&StateH[
    if (StateH[2]) {SetInputMode(panelHandle[ENTER],
    else {SetInputMode(panelHandle[ENTER],ENTER_HEAT
    j=0;
    for (i=0;i<NumHeat;i++) {
        if (StateH[i]) {
            xh[j]=Position[i];
            j++;
        }
    }
    break;

case ENTER_TH4:
    GetCtrlVal(panelHandle[ENTER],ENTER_TH4,&StateH[
    if (StateH[3]) {SetInputMode(panelHandle[ENTER],
    else {SetInputMode(panelHandle[ENTER],ENTER_HEAT
    j=0;
    for (i=0;i<NumHeat;i++) {
        if (StateH[i]) {
            xh[j]=Position[i];
            j++;
        }
    }
    break;

case ENTER_TH5:
    GetCtrlVal(panelHandle[ENTER],ENTER_TH5,&StateH[
    if (StateH[4]) {SetInputMode(panelHandle[ENTER],
    else {SetInputMode(panelHandle[ENTER],ENTER_HEAT
    j=0;
    for (i=0;i<NumHeat;i++) {
        if (StateH[i]) {
            xh[j]=Position[i];
            j++;
        }
    }
    break;

case ENTER_TH6:
    GetCtrlVal(panelHandle[ENTER],ENTER_TH6,&StateH[
    if (StateH[5]) {SetInputMode(panelHandle[ENTER],
    else {SetInputMode(panelHandle[ENTER],ENTER_HEAT
    j=0;
    for (i=0;i<NumHeat;i++) {
        if (StateH[i]) {
            xh[j]=Position[i];
            j++;
        }
    }
    break;

case ENTER_TH7:

```

```

GetCtrlVal(panelHandle[ENTER],ENTER_TH7,&StateH[
if (StateH[6]) {SetInputMode(panelHandle[ENTER],
else {SetInputMode(panelHandle[ENTER],ENTER_HEAT
j=0;
for (i=0;i<NumHeat;i++) {
    if (StateH[i]) {
        xh[j]=Position[i];
        j++;
    }
}
break;

case ENTER_TH8:
GetCtrlVal(panelHandle[ENTER],ENTER_TH8,&StateH[
if (StateH[7]) {SetInputMode(panelHandle[ENTER],
else {SetInputMode(panelHandle[ENTER],ENTER_HEAT
j=0;
for (i=0;i<NumHeat;i++) {
    if (StateH[i]) {
        xh[j]=Position[i];
        j++;
    }
}
break;

case ENTER_TP1:
GetCtrlVal(panelHandle[ENTER],ENTER_TP1,&StateP[
if (StateP[0]) {SetInputMode(panelHandle[ENTER],
else {SetInputMode(panelHandle[ENTER],ENTER_PIPE
j=0;
for (i=0;i<NumPipe;i++) {
    if (StateP[i]) {
        xp[j]=Position[i+1];
        j++;
    }
}
break;

case ENTER_TP2:
GetCtrlVal(panelHandle[ENTER],ENTER_TP2,&StateP[
if (StateP[1]) {SetInputMode(panelHandle[ENTER],
else {SetInputMode(panelHandle[ENTER],ENTER_PIPE
j=0;
for (i=0;i<NumPipe;i++) {
    if (StateP[i]) {
        xp[j]=Position[i+1];
        j++;
    }
}
break;

case ENTER_TP3:
GetCtrlVal(panelHandle[ENTER],ENTER_TP3,&StateP[
if (StateP[2]) {SetInputMode(panelHandle[ENTER],
else {SetInputMode(panelHandle[ENTER],ENTER_PIPE
j=0;
for (i=0;i<NumPipe;i++) {
    if (StateP[i]) {
        xp[j]=Position[i+1];
        j++;
    }
}

```



```

    }
    }
    break;

case ENTER_TP4:
    GetCtrlVal(panelHandle[ENTER],ENTER_TP4,&StateP[
    if (StateP[3]) {SetInputMode(panelHandle[ENTER],
    else {SetInputMode(panelHandle[ENTER],ENTER_PIPE
    j=0;
    for (i=0;i<NumPipe;i++) {
        if (StateP[i]) {
            xp[j]=Position[i+1];
            j++;
        }
    }
    break;

case ENTER_TP5:
    GetCtrlVal(panelHandle[ENTER],ENTER_TP5,&StateP[
    if (StateP[4]) {SetInputMode(panelHandle[ENTER],
    else {SetInputMode(panelHandle[ENTER],ENTER_PIPE
    j=0;
    for (i=0;i<NumPipe;i++) {
        if (StateP[i]) {
            xp[j]=Position[i+1];
            j++;
        }
    }
    break;

case ENTER_TP6:
    GetCtrlVal(panelHandle[ENTER],ENTER_TP6,&StateP[
    if (StateP[5]) {SetInputMode(panelHandle[ENTER],
    else {SetInputMode(panelHandle[ENTER],ENTER_PIPE
    j=0;
    for (i=0;i<NumPipe;i++) {
        if (StateP[i]) {
            xp[j]=Position[i+1];
            j++;
        }
    }
    break;

case ENTER_RETURN:
    RemovePopup(0);
    loopDoneFlag[1]++;
    status=0;
    break;

case ENTER_ENTER:
    i=0;
    if (StateH[0]) {GetCtrlVal(panelHandle[ENTER],EN
    if (StateH[1]) {GetCtrlVal(panelHandle[ENTER],EN
    if (StateH[2]) {GetCtrlVal(panelHandle[ENTER],EN
    if (StateH[3]) {GetCtrlVal(panelHandle[ENTER],EN
    if (StateH[4]) {GetCtrlVal(panelHandle[ENTER],EN
    if (StateH[5]) {GetCtrlVal(panelHandle[ENTER],EN
    if (StateH[6]) {GetCtrlVal(panelHandle[ENTER],EN
    if (StateH[7]) {GetCtrlVal(panelHandle[ENTER],EN

```

```

        i=0;
        if (StateP[0]) (GetCtrlVal(panelHandle[ENTER],EN
        if (StateP[1]) (GetCtrlVal(panelHandle[ENTER],EN
        if (StateP[2]) (GetCtrlVal(panelHandle[ENTER],EN
        if (StateP[3]) (GetCtrlVal(panelHandle[ENTER],EN
        if (StateP[4]) (GetCtrlVal(panelHandle[ENTER],EN
        if (StateP[5]) (GetCtrlVal(panelHandle[ENTER],EN
        RemovePopup(0);
        loopDoneFlag[1]++;
        status=1;
        break;
    )
}

    *AHT=ActiveHeaterTherm;
    *APT=ActivePipeTherm;
    return(status);
}

void PopupScreen(Title,Array,AxPosition,Resolution)
char *Title;
double *Array;
double *AxPosition;
int Resolution;
{
    int status;
    int eventControl,loopDoneFlag=0,panelHandle;
    panelHandle = LoadPanel ("novout.uir", GRAPHS);
    HidePanel (panelHandle);
    InstallPopup(panelHandle);
    SetGraphAttribute(panelHandle,GRAPHS_GRAPH,0,Title);
    PlotXY(panelHandle,GRAPHS_GRAPH,AxPosition,Array,Resolution,4,4,0,0,0,1)

    while (!loopDoneFlag) {
        GetPopupEvent (0, &eventControl);
        switch (eventControl) {
            case GRAPHS_PRINT:
                status=OutputGraph(-1,"",1,panelHandle,GRAPHS_GR
                break;
            case GRAPHS_RETURN:
                loopDoneFlag++;
                break;
        }
    }
    RemovePopup(0);
    UnloadPanel(panelHandle);
}

```

Appendix E

Raw and Reduced Data of Heat Transfer Coefficient Experiments

D) Particle Bed Thermal Switch

Raw Data
Particle Bed (Silicon Carbide Particles) and
Carbon Dioxide Gas (1 atm) - - On-Mode
Heater Power Input = 106.50 watts
Temperatures = °C

Heater Thermocouple #1	79.12
Heater Thermocouple #2	110.62
Heater Thermocouple #3	135.64
Heater Thermocouple #4	144.27
Heater Thermocouple #5	151.01
Heater Thermocouple #6	151.21
Heater Thermocouple #7	128.06
Heater Thermocouple #8	97.39

Pipe Thermocouple #1	22.88
Pipe Thermocouple #2	23.22
Pipe Thermocouple #3	23.14
Pipe Thermocouple #4	23.03
Pipe Thermocouple #5	23.04
Pipe Thermocouple #6	22.97

Raw Data
Particle Bed (Silicon Carbide Particles) and
Carbon Dioxide Gas (1 atm)- -On-Mode
Heater Power Input = 295.00 watts
Temperatures = °C

Heater Thermocouple #1	157.93
Heater Thermocouple #2	224.29
Heater Thermocouple #3	269.52
Heater Thermocouple #4	284.15
Heater Thermocouple #5	297.39
Heater Thermocouple #6	299.74
Heater Thermocouple #7	255.71
Heater Thermocouple #8	185.72

Pipe Thermocouple #1	31.62
Pipe Thermocouple #2	32.20
Pipe Thermocouple #3	32.19
Pipe Thermocouple #4	32.13
Pipe Thermocouple #5	31.75
Pipe Thermocouple #6	31.75

Raw Data
Particle Bed (Silicon Carbide Particles) and
Carbon Dioxide Gas (1 atm)- -On-Mode
Heater Power Input = 616.85 watts
Temperatures = °C

Heater Thermocouple #1	243.20
Heater Thermocouple #2	346.53
Heater Thermocouple #3	404.47
Heater Thermocouple #4	422.12
Heater Thermocouple #5	442.01
Heater Thermocouple #6	451.33
Heater Thermocouple #7	394.26
Heater Thermocouple #8	271.53

Pipe Thermocouple #1	38.56
Pipe Thermocouple #2	39.59
Pipe Thermocouple #3	39.26
Pipe Thermocouple #4	39.12
Pipe Thermocouple #5	38.40
Pipe Thermocouple #6	38.39

**Particle Bed Thermal Switch - - On-Mode
Reduced Data - - Figure 5.15**

Heater Power Input Watts	Heater Surface Flux kw/(m ²)	Heat Transfer Coefficient w/(m ² K)	Temp Diff between Heater Surface and Inside Surface of Stainless Steel Pipe Kelvin
0.00	0.00	0.00	0.00
106.50	2.92	23.74	122.92
295.00	8.09	31.84	254.01
616.85	16.91	43.98	384.41

Raw Data
Particle Bed (Silicon Carbide Particles) and
Vacuum (2.59 torr) - - Off-Mode
Heater Power Input = 106.50 watts
Temperatures = °C

Heater Thermocouple #1	96.79
Heater Thermocouple #2	138.96
Heater Thermocouple #3	180.29
Heater Thermocouple #4	196.01
Heater Thermocouple #5	202.40
Heater Thermocouple #6	197.71
Heater Thermocouple #7	161.42
Heater Thermocouple #8	121.06

Pipe Thermocouple #1	22.01
Pipe Thermocouple #2	22.15
Pipe Thermocouple #3	22.23
Pipe Thermocouple #4	22.14
Pipe Thermocouple #5	21.96
Pipe Thermocouple #6	21.89

Raw Data
Particle Bed (Silicon Carbide Particles) and
Vacuum (2.59 torr) - - Off-Mode
Heater Power Input = 295.00 watts
Temperatures = °C

Heater Thermocouple #1	202.87
Heater Thermocouple #2	298.42
Heater Thermocouple #3	384.72
Heater Thermocouple #4	414.12
Heater Thermocouple #5	429.78
Heater Thermocouple #6	419.50
Heater Thermocouple #7	341.68
Heater Thermocouple #8	242.54

Pipe Thermocouple #1	26.52
Pipe Thermocouple #2	26.91
Pipe Thermocouple #3	27.08
Pipe Thermocouple #4	27.00
Pipe Thermocouple #5	26.55
Pipe Thermocouple #6	26.44

**Particle Bed Thermal Switch- -Off-Mode
Reduced Data- -Figure 5.15**

Heater Power Input Watts	Heater Surface Flux kw/(m ²)	Heat Transfer Coefficient w/(m ² K)	Temp Diff between Heater Surface and Inside Surface of Stainless Steel Pipe Kelvin
0.00	0.00	0.00	0.00
106.50	2.92	16.49	177.05
295.00	8.09	20.66	391.40

Particle Bed On-Mode/Off-Mode Heat Transfer Coefficient Ratio

Reduced Data - - Figure 5.16

Temp Diff between Heater Surface and Inside Surface of Stainless Steel Pipe Kelvin	On-Mode Heat Transfer Coefficient w/(m ² K)	Off-Mode Heat Transfer Coefficient w/(m ² K)	On-Mode/Off-Mode Heat Transfer Coefficient Ratio
0.00	0.00	0.00	1.00
25.00	7.00	3.20	2.19
50.00	12.80	5.80	2.21
100.00	21.20	10.80	1.96
150.00	26.30	14.70	1.79
200.00	29.30	17.60	1.66
250.00	31.60	19.10	1.65
300.00	34.60	19.80	1.75
350.00	39.20	20.60	1.90
391.40	44.90	20.66	2.17

II) Wick Thermal Switch

Raw Data

Wick (Zirconium Oxide Felt) + Water (184.5 g) +

Vacuum (1.65 torr) - -On-Mode

Heater Power Input = 57.20 watts

Temperatures = °C

Heater Thermocouple #1	27.88
Heater Thermocouple #2	30.45
Heater Thermocouple #3	32.37
Heater Thermocouple #4	31.54
Heater Thermocouple #5	29.73
Heater Thermocouple #6	29.69
Heater Thermocouple #7	29.67
Heater Thermocouple #8	27.51

Pipe Thermocouple #1	22.57
Pipe Thermocouple #2	22.58
Pipe Thermocouple #3	22.57
Pipe Thermocouple #4	22.65
Pipe Thermocouple #5	22.66
Pipe Thermocouple #6	22.68

Raw Data

Wick (Zirconium Oxide Felt) + Water (184.5 g) +

Vacuum (1.65 torr) - - On-Mode

Heater Power Input = 105.00 watts

Temperatures = °C

Heater Thermocouple #1	30.87
Heater Thermocouple #2	34.20
Heater Thermocouple #3	34.68
Heater Thermocouple #4	31.23
Heater Thermocouple #5	32.53
Heater Thermocouple #6	33.57
Heater Thermocouple #7	34.60
Heater Thermocouple #8	30.05

Pipe Thermocouple #1	25.26
Pipe Thermocouple #2	23.12
Pipe Thermocouple #3	23.18
Pipe Thermocouple #4	23.22
Pipe Thermocouple #5	23.26
Pipe Thermocouple #6	23.29

Raw Data

Wick (Zirconium Oxide Felt) + Water (184.5 g) +

Vacuum (1.65 torr)- - -On-Mode

Heater Power Input = 290.00 watts

Temperatures = °C

Heater Thermocouple #1	36.43
Heater Thermocouple #2	38.40
Heater Thermocouple #3	42.82
Heater Thermocouple #4	39.88
Heater Thermocouple #5	37.78
Heater Thermocouple #6	52.11
Heater Thermocouple #7	50.46
Heater Thermocouple #8	35.49

Pipe Thermocouple #1	28.76
Pipe Thermocouple #2	28.94
Pipe Thermocouple #3	26.19
Pipe Thermocouple #4	26.11
Pipe Thermocouple #5	26.36
Pipe Thermocouple #6	27.36

Raw Data

Wick (Zirconium Oxide Felt) + Water (184.5 g) +

Vacuum (1.65 torr)- -On-Mode

Heater Power Input = 613.20 watts

Temperatures = °C

Heater Thermocouple #1	46.15
Heater Thermocouple #2	49.81
Heater Thermocouple #3	60.74
Heater Thermocouple #4	57.08
Heater Thermocouple #5	167.63
Heater Thermocouple #6	153.48
Heater Thermocouple #7	102.01
Heater Thermocouple #8	50.28

Pipe Thermocouple #1	34.43
Pipe Thermocouple #2	34.16
Pipe Thermocouple #3	33.89
Pipe Thermocouple #4	32.35
Pipe Thermocouple #5	32.23
Pipe Thermocouple #6	34.61

Raw Data

Wick (Zirconium Oxide Felt) + Water (184.5 g) +

Vacuum (1.65 torr)- - -On-Mode

Heater Power Input = 890.00 watts

Temperatures = °C

Heater Thermocouple #1	57.89
Heater Thermocouple #2	125.37
Heater Thermocouple #3	324.21
Heater Thermocouple #4	318.14
Heater Thermocouple #5	276.74
Heater Thermocouple #6	222.02
Heater Thermocouple #7	150.42
Heater Thermocouple #8	60.07

Pipe Thermocouple #1	40.76
Pipe Thermocouple #2	40.98
Pipe Thermocouple #3	40.97
Pipe Thermocouple #4	40.51
Pipe Thermocouple #5	39.57
Pipe Thermocouple #6	41.21

Raw Data

Wick (Zirconium Oxide Felt) + Water (184.5 g) +

Vacuum (1.65 torr) - - On-Mode

Heater Power Input = 1206.40 watts

Temperatures = °C

Heater Thermocouple #1	71.33
Heater Thermocouple #2	104.35
Heater Thermocouple #3	377.96
Heater Thermocouple #4	382.16
Heater Thermocouple #5	332.26
Heater Thermocouple #6	255.24
Heater Thermocouple #7	173.34
Heater Thermocouple #8	73.65

Pipe Thermocouple #1	53.76
Pipe Thermocouple #2	53.58
Pipe Thermocouple #3	53.81
Pipe Thermocouple #4	53.89
Pipe Thermocouple #5	52.45
Pipe Thermocouple #6	53.04

Raw Data

Wick (Zirconium Oxide Felt) + Water (184.5 g) +

Vacuum (1.65 torr)- - -On-Mode

Heater Power Input = 1584.00 watts

Temperatures = °C

Heater Thermocouple #1	84.03
Heater Thermocouple #2	193.44
Heater Thermocouple #3	457.18
Heater Thermocouple #4	457.60
Heater Thermocouple #5	402.40
Heater Thermocouple #6	309.35
Heater Thermocouple #7	245.73
Heater Thermocouple #8	86.36

Pipe Thermocouple #1	58.44
Pipe Thermocouple #2	58.40
Pipe Thermocouple #3	58.26
Pipe Thermocouple #4	59.59
Pipe Thermocouple #5	57.43
Pipe Thermocouple #6	58.18

Raw Data

Wick (Zirconium Oxide Felt) + Water (184.5 g) +

Vacuum (1.65 torr)- -On-Mode

Heater Power Input = 1921.25 watts

Temperatures = °C

Heater Thermocouple #1	94.29
Heater Thermocouple #2	229.66
Heater Thermocouple #3	500.25
Heater Thermocouple #4	502.44
Heater Thermocouple #5	446.25
Heater Thermocouple #6	339.51
Heater Thermocouple #7	269.90
Heater Thermocouple #8	94.12

Pipe Thermocouple #1	63.79
Pipe Thermocouple #2	64.68
Pipe Thermocouple #3	63.75
Pipe Thermocouple #4	64.55
Pipe Thermocouple #5	62.38
Pipe Thermocouple #6	62.75

Wick Thermal Switch
Wick-Vacuum-Water- -On-Mode
Reduced Data- -Figure 5.19

Heater Power Input Watts	Heater Surface Flux kw/(m ²)	Heat Transfer Coefficient w/(m ² K)	Temp Diff between Heater Surface and Inside Surface of Stainless Steel Pipe Kelvin
0.00	0.00	0.00	0.00
57.20	1.57	202.66	7.74
105.00	2.88	324.13	8.88
290.00	7.95	596.42	13.33
613.20	16.81	475.63	35.34
890.00	24.40	98.80	246.93
1206.40	33.07	114.31	289.27
1584.00	43.42	125.31	346.49
1921.25	52.66	138.18	381.11

Raw Data

Wick (Zirconium Oxide Felt) + Water (184.5 g) +

Air (Pressure = 1 atm) - - On-Mode

Heater Power Input = 57.20 watts

Temperatures = °C

Heater Thermocouple #1	41.67
Heater Thermocouple #2	56.13
Heater Thermocouple #3	63.87
Heater Thermocouple #4	62.86
Heater Thermocouple #5	59.53
Heater Thermocouple #6	56.78
Heater Thermocouple #7	53.87
Heater Thermocouple #8	48.04

Pipe Thermocouple #1	22.77
Pipe Thermocouple #2	22.80
Pipe Thermocouple #3	22.88
Pipe Thermocouple #4	22.91
Pipe Thermocouple #5	23.16
Pipe Thermocouple #6	23.06

Raw Data

Wick (Zirconium Oxide Felt) + Water (184.5 g) +

Air (Pressure = 1 atm) - - On-Mode

Heater Power Input = 105.00 watts

Temperatures = °C

Heater Thermocouple #1	54.23
Heater Thermocouple #2	76.42
Heater Thermocouple #3	86.80
Heater Thermocouple #4	84.66
Heater Thermocouple #5	78.77
Heater Thermocouple #6	74.33
Heater Thermocouple #7	70.68
Heater Thermocouple #8	61.84

Pipe Thermocouple #1	22.82
Pipe Thermocouple #2	22.88
Pipe Thermocouple #3	22.87
Pipe Thermocouple #4	23.16
Pipe Thermocouple #5	23.51
Pipe Thermocouple #6	23.53

Raw Data

Wick (Zirconium Oxide Felt) + Water (184.5 g) +

Air (Pressure = 1 atm) - - -On-Mode

Heater Power Input = 290.00 watts

Temperatures = °C

Heater Thermocouple #1	86.60
Heater Thermocouple #2	115.09
Heater Thermocouple #3	121.85
Heater Thermocouple #4	118.96
Heater Thermocouple #5	112.78
Heater Thermocouple #6	111.43
Heater Thermocouple #7	109.87
Heater Thermocouple #8	93.30

Pipe Thermocouple #1	31.79
Pipe Thermocouple #2	33.21
Pipe Thermocouple #3	33.18
Pipe Thermocouple #4	33.62
Pipe Thermocouple #5	34.12
Pipe Thermocouple #6	33.53

Raw Data

Wick (Zirconium Oxide Felt) + Water (184.5 g) +

Air (Pressure = 1 atm)- - -On-Mode

Heater Power Input = 613.20 watts

Temperatures = °C

Heater Thermocouple #1	113.91
Heater Thermocouple #2	121.01
Heater Thermocouple #3	128.01
Heater Thermocouple #4	123.12
Heater Thermocouple #5	118.79
Heater Thermocouple #6	127.03
Heater Thermocouple #7	130.98
Heater Thermocouple #8	106.48

Pipe Thermocouple #1	38.14
Pipe Thermocouple #2	37.29
Pipe Thermocouple #3	37.72
Pipe Thermocouple #4	38.74
Pipe Thermocouple #5	37.93
Pipe Thermocouple #6	38.05

Raw Data

Wick (Zirconium Oxide Felt) + Water (184.5 g) +

Air (Pressure = 1 atm) - - On-Mode

Heater Power Input = 898.90 watts

Temperatures = °C

Heater Thermocouple #1	121.49
Heater Thermocouple #2	128.35
Heater Thermocouple #3	137.26
Heater Thermocouple #4	130.87
Heater Thermocouple #5	125.27
Heater Thermocouple #6	137.12
Heater Thermocouple #7	147.39
Heater Thermocouple #8	118.68

Pipe Thermocouple #1	51.21
Pipe Thermocouple #2	47.39
Pipe Thermocouple #3	47.35
Pipe Thermocouple #4	50.90
Pipe Thermocouple #5	47.33
Pipe Thermocouple #6	46.88

Raw Data

Wick (Zirconium Oxide Felt) + Water (184.5 g) +

Air (Pressure = 1 atm) - - -On-Mode

Heater Power Input = 1216.80 watts

Temperatures = °C

Heater Thermocouple #1	127.47
Heater Thermocouple #2	134.33
Heater Thermocouple #3	145.76
Heater Thermocouple #4	137.45
Heater Thermocouple #5	130.11
Heater Thermocouple #6	146.53
Heater Thermocouple #7	160.33
Heater Thermocouple #8	122.98

Pipe Thermocouple #1	56.04
Pipe Thermocouple #2	48.96
Pipe Thermocouple #3	48.17
Pipe Thermocouple #4	55.52
Pipe Thermocouple #5	48.66
Pipe Thermocouple #6	48.97

Raw Data

Wick (Zirconium Oxide Felt) + Water (184.5 g) +

Air (Pressure = 1 atm) - - On-Mode

Heater Power Input = 1614.00 watts

Temperatures = °C

Heater Thermocouple #1	135.54
Heater Thermocouple #2	144.27
Heater Thermocouple #3	155.63
Heater Thermocouple #4	145.89
Heater Thermocouple #5	136.64
Heater Thermocouple #6	160.72
Heater Thermocouple #7	175.91
Heater Thermocouple #8	128.14

Pipe Thermocouple #1	64.48
Pipe Thermocouple #2	57.96
Pipe Thermocouple #3	54.48
Pipe Thermocouple #4	63.03
Pipe Thermocouple #5	53.47
Pipe Thermocouple #6	53.56

Raw Data

Wick (Zirconium Oxide Felt) + Water (184.5 g) +

Air (Pressure = 1 atm) - - On-Mode

Heater Power Input = 1891.50 watts

Temperatures = °C

Heater Thermocouple #1	142.93
Heater Thermocouple #2	154.31
Heater Thermocouple #3	171.06
Heater Thermocouple #4	159.21
Heater Thermocouple #5	143.20
Heater Thermocouple #6	175.11
Heater Thermocouple #7	188.02
Heater Thermocouple #8	134.25

Pipe Thermocouple #1	75.77
Pipe Thermocouple #2	67.73
Pipe Thermocouple #3	63.83
Pipe Thermocouple #4	76.84
Pipe Thermocouple #5	63.60
Pipe Thermocouple #6	64.69

Wick Thermal Switch
Wick-Air-Water - - -On-Mode
Reduced Data - - -Figure 5.19

Heater Power Input Watts	Heater Surface Flux kw/(m ²)	Heat Transfer Coefficient w/(m ² K)	Temp Diff between Heater Surface and Inside Surface of Stainless Steel Pipe Kelvin
0.00	0.00	0.00	0.00
57.20	1.57	42.15	37.21
105.00	2.88	50.67	56.81
290.00	7.95	99.14	80.18
613.20	16.81	203.88	82.44
898.90	24.64	312.37	78.88
1216.80	33.35	406.72	82.01
1614.00	44.24	535.51	82.61
1891.50	51.85	641.16	80.86

Raw Data

**Wick (Zirconium Oxide Felt) +
Vacuum (1.65 torr)- - Off-Mode
Heater Power Input = 57.20 watts**

Temperatures = °C

Heater Thermocouple #1	114.17
Heater Thermocouple #2	167.41
Heater Thermocouple #3	235.00
Heater Thermocouple #4	260.07
Heater Thermocouple #5	265.08
Heater Thermocouple #6	253.58
Heater Thermocouple #7	219.44
Heater Thermocouple #8	191.27

Pipe Thermocouple #1	22.09
Pipe Thermocouple #2	22.20
Pipe Thermocouple #3	22.21
Pipe Thermocouple #4	22.21
Pipe Thermocouple #5	22.20
Pipe Thermocouple #6	22.10

Raw Data
Wick (Zirconium Oxide Felt) +
Vacuum (1.65 torr)- - Off-Mode
Heater Power Input = 105.00 watts
Temperatures = °C

Heater Thermocouple #1	179.86
Heater Thermocouple #2	268.59
Heater Thermocouple #3	370.93
Heater Thermocouple #4	404.18
Heater Thermocouple #5	408.31
Heater Thermocouple #6	387.02
Heater Thermocouple #7	325.50
Heater Thermocouple #8	269.52

Pipe Thermocouple #1	21.98
Pipe Thermocouple #2	22.17
Pipe Thermocouple #3	22.29
Pipe Thermocouple #4	22.32
Pipe Thermocouple #5	22.25
Pipe Thermocouple #6	22.09

Raw Data

Wick (Zirconium Oxide Felt) +

Vacuum (1.65 torr) - - Off-Mode

Heater Power Input = 188.00 watts

Temperatures = °C

Heater Thermocouple #1	264.12
Heater Thermocouple #2	393.89
Heater Thermocouple #3	528.09
Heater Thermocouple #4	565.84
Heater Thermocouple #5	567.77
Heater Thermocouple #6	534.77
Heater Thermocouple #7	440.04
Heater Thermocouple #8	343.20

Pipe Thermocouple #1	25.56
Pipe Thermocouple #2	25.91
Pipe Thermocouple #3	26.11
Pipe Thermocouple #4	26.29
Pipe Thermocouple #5	26.06
Pipe Thermocouple #6	25.70

**Wick Thermal Switch
Wick-Vacuum - - Off-Mode
Reduced Data - - Figure 5.19**

Heater Power Input Watts	Heater Surface Flux kw/(m ²)	Heat Transfer Coefficient w/(m ² K)	Temp Diff between Heater Surface and Inside Surface of Stainless Steel Pipe Kelvin
0.00	0.00	0.00	0.00
57.20	1.43	6.02	237.10
105.00	2.74	7.11	385.72
188.00	4.92	9.30	528.50

Raw Data

**Wick (Zirconium Oxide Felt) +
Air (Pressure = 1 atm)- - -Off-Mode
Heater Power Input = 57.20 watts
Temperatures = °C**

Heater Thermocouple #1	91.03
Heater Thermocouple #2	137.95
Heater Thermocouple #3	192.85
Heater Thermocouple #4	210.92
Heater Thermocouple #5	212.17
Heater Thermocouple #6	198.91
Heater Thermocouple #7	164.65
Heater Thermocouple #8	136.22

Pipe Thermocouple #1	22.39
Pipe Thermocouple #2	22.50
Pipe Thermocouple #3	22.61
Pipe Thermocouple #4	22.66
Pipe Thermocouple #5	22.66
Pipe Thermocouple #6	22.54

Raw Data

**Wick (Zirconium Oxide Felt) +
Air (Pressure = 1 atm) - - Off-Mode
Heater Power Input = 105.00 watts
Temperatures = °C**

Heater Thermocouple #1	138.16
Heater Thermocouple #2	213.85
Heater Thermocouple #3	297.28
Heater Thermocouple #4	321.97
Heater Thermocouple #5	323.50
Heater Thermocouple #6	303.85
Heater Thermocouple #7	248.42
Heater Thermocouple #8	198.68

Pipe Thermocouple #1	23.02
Pipe Thermocouple #2	23.35
Pipe Thermocouple #3	23.34
Pipe Thermocouple #4	23.39
Pipe Thermocouple #5	23.20
Pipe Thermocouple #6	23.17

Raw Data

**Wick (Zirconium Oxide Felt) +
Air (Pressure = 1 atm)- -Off-Mode
Heater Power Input = 290.00 watts
Temperatures = °C**

Heater Thermocouple #1	269.40
Heater Thermocouple #2	422.96
Heater Thermocouple #3	561.29
Heater Thermocouple #4	594.73
Heater Thermocouple #5	596.73
Heater Thermocouple #6	567.50
Heater Thermocouple #7	468.61
Heater Thermocouple #8	352.91

Pipe Thermocouple #1	25.62
Pipe Thermocouple #2	26.29
Pipe Thermocouple #3	26.38
Pipe Thermocouple #4	26.59
Pipe Thermocouple #5	25.93
Pipe Thermocouple #6	25.56

**Wick Thermal Switch
Wick-Air - -Off-Mode
Reduced Data - -Figure 5.19**

Heater Power Input Watts	Heater Surface Flux kw/(m ²)	Heat Transfer Coefficient w/(m ² K)	Temp Diff between Heater Surface and Inside Surface of Stainless Steel Pipe Kelvin
0.00	0.00	0.00	0.00
57.20	1.46	7.85	185.43
105.00	2.73	9.27	293.96
290.00	7.79	13.97	557.80

Wick Thermal Switch On-Mode/Off-Mode Heat Transfer Coefficient Ratio

Reduced Data - - Figure 5.20

Temp Diff between Heater Surface and Inside Surface of Stainless Steel Pipe Kelvin	On-Mode Heat Transfer Coefficient w/(m ² K) Wick- Vacuum-Water	Off-Mode Heat Transfer Coefficient w/(m ² K) Wick-Vacuum	On-Mode/Off-Mode Heat Transfer Coefficient Ratio
0.00	0.00	0.00	1.00
7.74	202.66	0.37	541.15
8.88	324.13	0.43	756.73
13.33	596.42	0.64	939.22
35.34	475.63	1.58	300.21
60.00	385.00	2.51	153.37
100.00	268.00	3.73	71.76
140.00	180.00	4.66	38.60
180.00	125.00	5.35	23.36
220.00	99.00	5.85	16.92
246.93	98.80	6.11	16.17
289.27	114.31	6.43	17.77
346.49	125.31	6.81	18.40
381.11	138.18	7.07	19.55

Wick Thermal Switch On-Mode/Off-Mode Heat Transfer Coefficient Ratio

Reduced Data - - Figure 5.21

Temp Diff between Heater Surface and Inside Surface of Stainless Steel Pipe Kelvin	On-Mode Heat Transfer Coefficient w/(m ² K) Wick-Vacuum-Water	Off-Mode Heat Transfer Coefficient w/(m ² K) Wick-Air	On-Mode/Off-Mode Heat Transfer Coefficient Ratio
0.00	0.00	0.00	1.00
7.74	202.66	0.54	372.88
8.88	324.13	0.62	521.43
13.33	596.42	0.92	647.18
35.34	475.63	2.30	206.88
60.00	385.00	3.64	105.71
100.00	268.00	5.42	49.49
140.00	180.00	6.76	26.65
180.00	125.00	7.74	16.15
220.00	99.00	8.44	11.73
246.93	98.80	8.80	11.23
289.27	114.31	9.22	12.39
346.49	125.31	9.71	12.91
381.11	138.18	10.02	13.79

Wick Thermal Switch On-Mode/Off-Mode Heat Transfer Coefficient Ratio

Reduced Data - - Figure 5.20

Temp Diff between Heater Surface and Inside Surface of Stainless Steel Pipe Kelvin	On-Mode Heat Transfer Coefficient w/(m ² K) Wick-Air-Water	Off-Mode Heat Transfer Coefficient w/(m ² K) Wick-Vacuum	On-Mode/Off-Mode Heat Transfer Coefficient Ratio
0.00	0.00	0.00	1.00
37.21	42.15	1.66	25.40
56.81	50.67	2.40	21.13
80.17	99.14	3.17	31.29
82.44	203.88	3.24	62.98
78.88	312.37	3.13	99.84
82.01	406.72	3.22	126.16
82.61	535.51	3.24	165.17
80.86	641.16	3.19	201.04

Wick Thermal Switch On-Mode/Off-Mode Heat Transfer Coefficient Ratio

Reduced Data - - Figure 5.21

Temp Diff between Heater Surface and Inside Surface of Stainless Steel Pipe Kelvin	On-Mode Heat Transfer Coefficient w/(m ² K) Wick-Air-Water	Off-Mode Heat Transfer Coefficient w/(m ² K) Wick-Air	On-Mode/Off-Mode Heat Transfer Coefficient Ratio
0.00	0.00	0.00	1.00
37.21	42.15	2.41	17.50
56.81	50.67	3.48	14.56
80.17	99.14	4.60	21.57
82.44	203.88	4.70	43.42
78.88	312.37	4.54	68.83
82.01	406.72	4.68	86.98
82.61	535.51	4.70	113.88
80.86	641.16	4.63	138.60

III) Water Thermal Switch

Raw Data

**311.6 Grams of Water +
 Vacuum (1.65 torr) - - On-Mode
 Heater Power Input = 57.20 watts
 Temperatures = °C**

Heater Thermocouple #1	29.93
Heater Thermocouple #2	33.66
Heater Thermocouple #3	34.85
Heater Thermocouple #4	34.46
Heater Thermocouple #5	34.66
Heater Thermocouple #6	36.01
Heater Thermocouple #7	35.04
Heater Thermocouple #8	29.75

Pipe Thermocouple #1	23.07
Pipe Thermocouple #2	23.08
Pipe Thermocouple #3	23.11
Pipe Thermocouple #4	23.08
Pipe Thermocouple #5	23.04
Pipe Thermocouple #6	23.09

Raw Data
311.6 Grams of Water +
Vacuum (1.65 torr) - -On-Mode
Heater Power Input = 105.00 watts
Temperatures = °C

Heater Thermocouple #1	35.39
Heater Thermocouple #2	41.36
Heater Thermocouple #3	43.38
Heater Thermocouple #4	43.16
Heater Thermocouple #5	42.95
Heater Thermocouple #6	45.58
Heater Thermocouple #7	44.38
Heater Thermocouple #8	35.19

Pipe Thermocouple #1	23.47
Pipe Thermocouple #2	23.46
Pipe Thermocouple #3	23.53
Pipe Thermocouple #4	23.55
Pipe Thermocouple #5	23.48
Pipe Thermocouple #6	23.54

Raw Data

311.6 Grams of Water +

Vacuum (1.65 torr)- -On-Mode

Heater Power Input = 290.00 watts

Temperatures = °C

Heater Thermocouple #1	47.60
Heater Thermocouple #2	57.55
Heater Thermocouple #3	65.49
Heater Thermocouple #4	65.61
Heater Thermocouple #5	67.47
Heater Thermocouple #6	71.96
Heater Thermocouple #7	68.63
Heater Thermocouple #8	48.62

Pipe Thermocouple #1	26.14
Pipe Thermocouple #2	26.25
Pipe Thermocouple #3	26.22
Pipe Thermocouple #4	26.28
Pipe Thermocouple #5	26.10
Pipe Thermocouple #6	26.15

Raw Data

**311.6 Grams of Water +
Vacuum (1.65 torr) - -On-Mode
Heater Power Input = 613.20 watts
Temperatures = °C**

Heater Thermocouple #1	53.56
Heater Thermocouple #2	60.02
Heater Thermocouple #3	72.69
Heater Thermocouple #4	66.06
Heater Thermocouple #5	67.64
Heater Thermocouple #6	76.47
Heater Thermocouple #7	70.46
Heater Thermocouple #8	51.82

Pipe Thermocouple #1	32.96
Pipe Thermocouple #2	32.80
Pipe Thermocouple #3	32.77
Pipe Thermocouple #4	32.40
Pipe Thermocouple #5	32.05
Pipe Thermocouple #6	32.55

Raw Data

**311.6 Grams of Water +
Vacuum (1.65 torr)- - On-Mode
Heater Power Input = 898.90 watts
Temperatures = °C**

Heater Thermocouple #1	62.07
Heater Thermocouple #2	69.39
Heater Thermocouple #3	80.87
Heater Thermocouple #4	73.34
Heater Thermocouple #5	67.95
Heater Thermocouple #6	89.56
Heater Thermocouple #7	85.25
Heater Thermocouple #8	59.46

Pipe Thermocouple #1	40.09
Pipe Thermocouple #2	39.20
Pipe Thermocouple #3	39.43
Pipe Thermocouple #4	39.55
Pipe Thermocouple #5	39.15
Pipe Thermocouple #6	38.09

Raw Data

**311.6 Grams of Water +
Vacuum (1.65 torr)- -On-Mode
Heater Power Input = 1206.40 watts
Temperatures = °C**

Heater Thermocouple #1	74.35
Heater Thermocouple #2	83.07
Heater Thermocouple #3	95.70
Heater Thermocouple #4	86.49
Heater Thermocouple #5	78.82
Heater Thermocouple #6	103.63
Heater Thermocouple #7	102.97
Heater Thermocouple #8	71.83

Pipe Thermocouple #1	51.22
Pipe Thermocouple #2	49.50
Pipe Thermocouple #3	50.73
Pipe Thermocouple #4	53.06
Pipe Thermocouple #5	50.04
Pipe Thermocouple #6	51.05

Raw Data

311.6 Grams of Water +

Vacuum (1.65 torr)- -On-Mode

Heater Power Input = 1602.65 watts

Temperatures = °C

Heater Thermocouple #1	82.51
Heater Thermocouple #2	93.61
Heater Thermocouple #3	108.62
Heater Thermocouple #4	98.49
Heater Thermocouple #5	87.60
Heater Thermocouple #6	119.29
Heater Thermocouple #7	119.84
Heater Thermocouple #8	78.43

Pipe Thermocouple #1	54.62
Pipe Thermocouple #2	55.23
Pipe Thermocouple #3	57.24
Pipe Thermocouple #4	58.30
Pipe Thermocouple #5	55.44
Pipe Thermocouple #6	56.82

Raw Data

311.6 Grams of Water +

Vacuum (1.65 torr)- -On-Mode

Heater Power Input = 1914.00 watts

Temperatures = °C

Heater Thermocouple #1	89.96
Heater Thermocouple #2	103.31
Heater Thermocouple #3	122.34
Heater Thermocouple #4	108.24
Heater Thermocouple #5	94.29
Heater Thermocouple #6	126.90
Heater Thermocouple #7	134.03
Heater Thermocouple #8	85.25

Pipe Thermocouple #1	60.59
Pipe Thermocouple #2	59.88
Pipe Thermocouple #3	61.18
Pipe Thermocouple #4	61.57
Pipe Thermocouple #5	58.27
Pipe Thermocouple #6	59.91

Water Thermal Switch
311.6 Grams of Water and Vacuum (1.65 torr) - -On-Mode
Reduced Data - -Figure 5.26

Heater Power Input Watts	Heater Surface Flux kw/(m ²)	Heat Transfer Coefficient w/(m ² K)	Temp Diff between Heater Surface and Inside Surface of Stainless Steel Pipe Kelvin
0.00	0.00	0.00	0.00
57.20	1.57	137.81	11.38
105.00	2.88	148.85	19.34
290.00	7.95	199.56	39.83
613.20	16.81	479.96	35.02
898.90	24.64	761.37	32.36
1206.40	33.07	1046.09	31.61
1602.65	43.93	1223.81	35.90
1914.00	52.46	1311.99	39.99

Raw Data

311.6 Grams of Water +

Air (Pressure = 1 atm)- -On-Mode

Heater Power Input = 57.20 watts

Temperatures = °C

Heater Thermocouple #1	31.33
Heater Thermocouple #2	37.08
Heater Thermocouple #3	38.65
Heater Thermocouple #4	38.24
Heater Thermocouple #5	38.30
Heater Thermocouple #6	38.99
Heater Thermocouple #7	37.03
Heater Thermocouple #8	30.78

Pipe Thermocouple #1	21.37
Pipe Thermocouple #2	21.40
Pipe Thermocouple #3	21.40
Pipe Thermocouple #4	21.38
Pipe Thermocouple #5	21.37
Pipe Thermocouple #6	21.38

Raw Data

311.6 Grams of Water +

Air (Pressure = 1 atm)- -On-Mode

Heater Power Input = 105.00 watts

Temperatures = °C

Heater Thermocouple #1	37.91
Heater Thermocouple #2	47.27
Heater Thermocouple #3	49.69
Heater Thermocouple #4	48.93
Heater Thermocouple #5	49.08
Heater Thermocouple #6	50.48
Heater Thermocouple #7	47.49
Heater Thermocouple #8	36.89

Pipe Thermocouple #1	21.17
Pipe Thermocouple #2	21.16
Pipe Thermocouple #3	21.19
Pipe Thermocouple #4	21.21
Pipe Thermocouple #5	21.20
Pipe Thermocouple #6	21.22

Raw Data

311.6 Grams of Water +

Air (Pressure = 1 atm)- -On-Mode

Heater Power Input = 290.00 watts

Temperatures = °C

Heater Thermocouple #1	60.28
Heater Thermocouple #2	77.27
Heater Thermocouple #3	81.69
Heater Thermocouple #4	80.26
Heater Thermocouple #5	80.27
Heater Thermocouple #6	84.48
Heater Thermocouple #7	80.87
Heater Thermocouple #8	57.96

Pipe Thermocouple #1	22.79
Pipe Thermocouple #2	22.86
Pipe Thermocouple #3	22.94
Pipe Thermocouple #4	22.99
Pipe Thermocouple #5	22.92
Pipe Thermocouple #6	22.98

Raw Data

**311.6 Grams of Water +
Air (Pressure = 1 atm)- - On-Mode
Heater Power Input = 613.20 watts**

Temperatures = °C

Heater Thermocouple #1	86.09
Heater Thermocouple #2	110.82
Heater Thermocouple #3	120.97
Heater Thermocouple #4	118.35
Heater Thermocouple #5	117.67
Heater Thermocouple #6	127.04
Heater Thermocouple #7	123.35
Heater Thermocouple #8	84.56

Pipe Thermocouple #1	25.79
Pipe Thermocouple #2	25.90
Pipe Thermocouple #3	26.15
Pipe Thermocouple #4	25.96
Pipe Thermocouple #5	25.91
Pipe Thermocouple #6	26.06

Raw Data

311.6 Grams of Water +

Air (Pressure = 1 atm)- -On-Mode

Heater Power Input = 895.00 watts

Temperatures = °C

Heater Thermocouple #1	106.80
Heater Thermocouple #2	138.17
Heater Thermocouple #3	154.25
Heater Thermocouple #4	151.07
Heater Thermocouple #5	149.61
Heater Thermocouple #6	162.09
Heater Thermocouple #7	157.80
Heater Thermocouple #8	107.05

Pipe Thermocouple #1	33.58
Pipe Thermocouple #2	33.73
Pipe Thermocouple #3	33.64
Pipe Thermocouple #4	34.07
Pipe Thermocouple #5	33.74
Pipe Thermocouple #6	33.73

Raw Data

311.6 Grams of Water +

Air (Pressure = 1 atm)- -On-Mode

Heater Power Input = 1206.40 watts

Temperatures = °C

Heater Thermocouple #1	121.12
Heater Thermocouple #2	159.62
Heater Thermocouple #3	180.79
Heater Thermocouple #4	178.12
Heater Thermocouple #5	176.96
Heater Thermocouple #6	194.57
Heater Thermocouple #7	187.44
Heater Thermocouple #8	124.26

Pipe Thermocouple #1	40.93
Pipe Thermocouple #2	41.60
Pipe Thermocouple #3	41.83
Pipe Thermocouple #4	42.07
Pipe Thermocouple #5	41.72
Pipe Thermocouple #6	41.91

Raw Data

311.6 Grams of Water +

Air (Pressure = 1 atm)- - -On-Mode

Heater Power Input = 1596.00 watts

Temperatures = °C

Heater Thermocouple #1	135.85
Heater Thermocouple #2	179.30
Heater Thermocouple #3	207.46
Heater Thermocouple #4	203.77
Heater Thermocouple #5	204.48
Heater Thermocouple #6	225.84
Heater Thermocouple #7	217.54
Heater Thermocouple #8	136.42

Pipe Thermocouple #1	52.37
Pipe Thermocouple #2	53.52
Pipe Thermocouple #3	53.12
Pipe Thermocouple #4	54.41
Pipe Thermocouple #5	52.97
Pipe Thermocouple #6	54.77

Raw Data

311.6 Grams of Water +

Air (Pressure = 1 atm)- - On-Mode

Heater Power Input = 1914.00 watts

Temperatures = °C

Heater Thermocouple #1	145.13
Heater Thermocouple #2	186.06
Heater Thermocouple #3	221.69
Heater Thermocouple #4	218.22
Heater Thermocouple #5	218.67
Heater Thermocouple #6	243.38
Heater Thermocouple #7	233.41
Heater Thermocouple #8	141.22

Pipe Thermocouple #1	60.16
Pipe Thermocouple #2	60.40
Pipe Thermocouple #3	60.69
Pipe Thermocouple #4	62.63
Pipe Thermocouple #5	62.14
Pipe Thermocouple #6	62.09

Water Thermal Switch
311.6 Grams of Water and Air (1.0 atm)- -On-Mode

Reduced Data- -Figure 5.26

Heater Power Input Watts	Heater Surface Flux kw/(m ²)	Heat Transfer Coefficient w/(m ² K)	Temp Diff between Heater Surface and Inside Surface of Stainless Steel Pipe Kelvin
0.00	0.00	0.00	0.00
57.20	1.57	94.52	16.60
105.00	2.88	105.20	27.36
290.00	7.95	140.76	56.47
613.20	16.81	184.73	90.99
895.00	24.53	212.96	115.20
1206.40	33.07	246.42	134.19
1596.00	43.75	294.13	148.73
1914.00	52.46	338.41	155.03

Raw Data

**628.1 Grams of Water +
Vacuum (1.65 torr)- - On-Mode
Heater Power Input = 57.20 watts**

Temperatures = °C

Heater Thermocouple #1	25.93
Heater Thermocouple #2	27.69
Heater Thermocouple #3	28.40
Heater Thermocouple #4	27.73
Heater Thermocouple #5	27.22
Heater Thermocouple #6	28.50
Heater Thermocouple #7	28.38
Heater Thermocouple #8	25.84

Pipe Thermocouple #1	21.39
Pipe Thermocouple #2	21.41
Pipe Thermocouple #3	21.43
Pipe Thermocouple #4	21.45
Pipe Thermocouple #5	21.40
Pipe Thermocouple #6	21.40

Raw Data

628.1 Grams of Water +

Vacuum (1.65 torr) - - On-Mode

Heater Power Input = 105.00 watts

Temperatures = °C

Heater Thermocouple #1	29.76
Heater Thermocouple #2	32.57
Heater Thermocouple #3	33.87
Heater Thermocouple #4	32.69
Heater Thermocouple #5	31.73
Heater Thermocouple #6	34.17
Heater Thermocouple #7	33.94
Heater Thermocouple #8	29.57

Pipe Thermocouple #1	21.89
Pipe Thermocouple #2	21.88
Pipe Thermocouple #3	22.04
Pipe Thermocouple #4	22.02
Pipe Thermocouple #5	21.91
Pipe Thermocouple #6	21.95

Raw Data

628.1 Grams of Water +

Vacuum (1.65 torr)- -On-Mode

Heater Power Input = 290.00 watts

Temperatures = °C

Heater Thermocouple #1	45.03
Heater Thermocouple #2	50.66
Heater Thermocouple #3	54.05
Heater Thermocouple #4	50.98
Heater Thermocouple #5	48.45
Heater Thermocouple #6	54.91
Heater Thermocouple #7	54.63
Heater Thermocouple #8	44.78

Pipe Thermocouple #1	27.54
Pipe Thermocouple #2	27.51
Pipe Thermocouple #3	27.71
Pipe Thermocouple #4	27.90
Pipe Thermocouple #5	27.47
Pipe Thermocouple #6	27.56

Raw Data

**628.1 Grams of Water +
 Vacuum (1.65 torr)- -On-Mode
 Heater Power Input = 616.85 watts
 Temperatures = °C**

Heater Thermocouple #1	65.80
Heater Thermocouple #2	74.33
Heater Thermocouple #3	80.71
Heater Thermocouple #4	75.08
Heater Thermocouple #5	70.30
Heater Thermocouple #6	82.15
Heater Thermocouple #7	82.18
Heater Thermocouple #8	65.25

Pipe Thermocouple #1	37.04
Pipe Thermocouple #2	37.63
Pipe Thermocouple #3	37.33
Pipe Thermocouple #4	38.11
Pipe Thermocouple #5	37.16
Pipe Thermocouple #6	37.22

Raw Data

**628.1 Grams of Water +
 Vacuum (1.65 torr) - - On-Mode
 Heater Power Input = 890.00 watts
 Temperatures = °C**

Heater Thermocouple #1	79.33
Heater Thermocouple #2	90.05
Heater Thermocouple #3	99.10
Heater Thermocouple #4	91.41
Heater Thermocouple #5	84.68
Heater Thermocouple #6	101.03
Heater Thermocouple #7	101.50
Heater Thermocouple #8	78.47

Pipe Thermocouple #1	41.30
Pipe Thermocouple #2	41.82
Pipe Thermocouple #3	42.81
Pipe Thermocouple #4	42.84
Pipe Thermocouple #5	41.25
Pipe Thermocouple #6	42.31

Raw Data

**628.1 Grams of Water +
Vacuum (1.65 torr)- - On-Mode
Heater Power Input = 1206.40 watts
Temperatures = °C**

Heater Thermocouple #1	85.84
Heater Thermocouple #2	91.25
Heater Thermocouple #3	104.82
Heater Thermocouple #4	95.22
Heater Thermocouple #5	87.19
Heater Thermocouple #6	106.72
Heater Thermocouple #7	102.63
Heater Thermocouple #8	78.80

Pipe Thermocouple #1	47.47
Pipe Thermocouple #2	47.11
Pipe Thermocouple #3	48.53
Pipe Thermocouple #4	47.87
Pipe Thermocouple #5	47.61
Pipe Thermocouple #6	46.73

Raw Data

**628.1 Grams of Water +
Vacuum (1.65 torr)- - On-Mode
Heater Power Input = 1596.00 watts
Temperatures = °C**

Heater Thermocouple #1	92.12
Heater Thermocouple #2	100.21
Heater Thermocouple #3	114.72
Heater Thermocouple #4	101.96
Heater Thermocouple #5	93.67
Heater Thermocouple #6	118.33
Heater Thermocouple #7	115.38
Heater Thermocouple #8	83.79

Pipe Thermocouple #1	54.62
Pipe Thermocouple #2	55.97
Pipe Thermocouple #3	56.27
Pipe Thermocouple #4	56.14
Pipe Thermocouple #5	54.23
Pipe Thermocouple #6	53.76

Raw Data

628.1 Grams of Water +

Vacuum (1.65 torr)- -On-Mode

Heater Power Input = 1899.50 watts

Temperatures = °C

Heater Thermocouple #1	100.48
Heater Thermocouple #2	110.67
Heater Thermocouple #3	127.26
Heater Thermocouple #4	113.27
Heater Thermocouple #5	102.53
Heater Thermocouple #6	130.97
Heater Thermocouple #7	128.36
Heater Thermocouple #8	91.80

Pipe Thermocouple #1	61.07
Pipe Thermocouple #2	63.36
Pipe Thermocouple #3	63.66
Pipe Thermocouple #4	65.18
Pipe Thermocouple #5	61.34
Pipe Thermocouple #6	60.92

Water Thermal Switch
628.1 Grams of Water and Vacuum (1.65 torr) - -On-Mode
Reduced Data- - -Figure 5.26

Heater Power Input Watts	Heater Surface Flux kw/(m ²)	Heat Transfer Coefficient w/(m ² K)	Temp Diff between Heater Surface and Inside Surface of Stainless Steel Pipe Kelvin
0.00	0.00	0.00	0.00
57.20	1.57	257.55	6.09
105.00	2.88	278.83	10.32
290.00	7.95	356.31	22.31
616.85	16.91	476.40	35.49
890.00	24.40	528.84	46.13
1206.40	33.07	753.60	43.88
1596.00	43.75	1032.26	42.38
1899.50	52.07	1185.52	43.92

Raw Data

628.1 Grams of Water +

Air (Pressure = 1 atm)- - -On-Mode

Heater Power Input = 57.20 watts

Temperatures = °C

Heater Thermocouple #1	26.81
Heater Thermocouple #2	28.51
Heater Thermocouple #3	29.21
Heater Thermocouple #4	28.62
Heater Thermocouple #5	28.12
Heater Thermocouple #6	29.40
Heater Thermocouple #7	29.19
Heater Thermocouple #8	26.62

Pipe Thermocouple #1	22.11
Pipe Thermocouple #2	22.12
Pipe Thermocouple #3	22.13
Pipe Thermocouple #4	22.12
Pipe Thermocouple #5	22.11
Pipe Thermocouple #6	22.13

Raw Data

628.1 Grams of Water +

Air (Pressure = 1 atm) - - On-Mode

Heater Power Input = 105.00 watts

Temperatures = °C

Heater Thermocouple #1	30.11
Heater Thermocouple #2	32.96
Heater Thermocouple #3	34.22
Heater Thermocouple #4	33.10
Heater Thermocouple #5	32.19
Heater Thermocouple #6	34.62
Heater Thermocouple #7	34.30
Heater Thermocouple #8	29.86

Pipe Thermocouple #1	21.99
Pipe Thermocouple #2	21.98
Pipe Thermocouple #3	22.07
Pipe Thermocouple #4	22.08
Pipe Thermocouple #5	22.02
Pipe Thermocouple #6	22.00

Raw Data

**628.1 Grams of Water +
Air (Pressure = 1 atm) - - On-Mode
Heater Power Input = 290.00 watts**

Temperatures = °C

Heater Thermocouple #1	42.76
Heater Thermocouple #2	48.57
Heater Thermocouple #3	51.87
Heater Thermocouple #4	48.99
Heater Thermocouple #5	46.52
Heater Thermocouple #6	52.99
Heater Thermocouple #7	52.48
Heater Thermocouple #8	42.14

Pipe Thermocouple #1	24.00
Pipe Thermocouple #2	24.11
Pipe Thermocouple #3	24.10
Pipe Thermocouple #4	24.11
Pipe Thermocouple #5	24.03
Pipe Thermocouple #6	24.05

Raw Data

628.1 Grams of Water +

Air (Pressure = 1 atm)- - -On-Mode

Heater Power Input = 613.20 watts

Temperatures = °C

Heater Thermocouple #1	61.11
Heater Thermocouple #2	70.34
Heater Thermocouple #3	76.79
Heater Thermocouple #4	71.17
Heater Thermocouple #5	66.42
Heater Thermocouple #6	78.80
Heater Thermocouple #7	78.35
Heater Thermocouple #8	59.99

Pipe Thermocouple #1	28.76
Pipe Thermocouple #2	28.97
Pipe Thermocouple #3	28.94
Pipe Thermocouple #4	29.08
Pipe Thermocouple #5	28.82
Pipe Thermocouple #6	28.92

Raw Data

628.1 Grams of Water +

Air (Pressure = 1 atm)- - On-Mode

Heater Power Input = 890.00 watts

Temperatures = °C

Heater Thermocouple #1	77.64
Heater Thermocouple #2	89.04
Heater Thermocouple #3	97.89
Heater Thermocouple #4	90.22
Heater Thermocouple #5	83.71
Heater Thermocouple #6	100.66
Heater Thermocouple #7	100.32
Heater Thermocouple #8	76.19

Pipe Thermocouple #1	36.34
Pipe Thermocouple #2	36.40
Pipe Thermocouple #3	36.41
Pipe Thermocouple #4	36.67
Pipe Thermocouple #5	36.78
Pipe Thermocouple #6	36.54

Raw Data

628.1 Grams of Water +

Air (Pressure = 1 atm) - - On-Mode

Heater Power Input = 1206.40 watts

Temperatures = °C

Heater Thermocouple #1	95.14
Heater Thermocouple #2	108.61
Heater Thermocouple #3	119.97
Heater Thermocouple #4	110.20
Heater Thermocouple #5	101.83
Heater Thermocouple #6	123.45
Heater Thermocouple #7	123.35
Heater Thermocouple #8	92.91

Pipe Thermocouple #1	44.80
Pipe Thermocouple #2	44.75
Pipe Thermocouple #3	45.36
Pipe Thermocouple #4	45.60
Pipe Thermocouple #5	45.43
Pipe Thermocouple #6	45.27

Raw Data

628.1 Grams of Water +

Air (Pressure = 1 atm)- - -On-Mode

Heater Power Input = 1596.00 watts

Temperatures = °C

Heater Thermocouple #1	113.01
Heater Thermocouple #2	128.04
Heater Thermocouple #3	141.63
Heater Thermocouple #4	129.89
Heater Thermocouple #5	119.63
Heater Thermocouple #6	145.37
Heater Thermocouple #7	145.06
Heater Thermocouple #8	109.81

Pipe Thermocouple #1	55.68
Pipe Thermocouple #2	55.86
Pipe Thermocouple #3	55.85
Pipe Thermocouple #4	56.50
Pipe Thermocouple #5	55.63
Pipe Thermocouple #6	56.27

Raw Data

628.1 Grams of Water +

Air (Pressure = 1 atm)- - -On-Mode

Heater Power Input = 1905.44 watts

Temperatures = °C

Heater Thermocouple #1	122.48
Heater Thermocouple #2	138.42
Heater Thermocouple #3	154.70
Heater Thermocouple #4	141.28
Heater Thermocouple #5	129.71
Heater Thermocouple #6	158.68
Heater Thermocouple #7	157.90
Heater Thermocouple #8	118.73

Pipe Thermocouple #1	58.43
Pipe Thermocouple #2	57.54
Pipe Thermocouple #3	57.80
Pipe Thermocouple #4	58.02
Pipe Thermocouple #5	57.62
Pipe Thermocouple #6	58.37

Water Thermal Switch
628.1 Grams of Water and Air (1.0 atm)- - On-Mode
Reduced Data- - Figure 5.26

Heater Power Input Watts	Heater Surface Flux kw/(m ²)	Heat Transfer Coefficient w/(m ² K)	Temp Diff between Heater Surface and Inside Surface of Stainless Steel Pipe Kelvin
0.00	0.00	0.00	0.00
57.20	1.57	249.42	6.29
105.00	2.88	269.32	10.69
290.00	7.95	331.77	23.96
613.20	16.81	416.51	40.36
890.00	24.40	477.62	51.08
1206.40	33.07	538.99	61.35
1596.00	43.75	631.42	69.28
1905.44	52.23	667.43	78.25

Raw Data

Vacuum (1.65 torr)- - Off-Mode

Heater Power Input = 57.20 watts

Temperatures = °C

Heater Thermocouple #1	115.18
Heater Thermocouple #2	164.71
Heater Thermocouple #3	224.31
Heater Thermocouple #4	245.25
Heater Thermocouple #5	249.96
Heater Thermocouple #6	239.51
Heater Thermocouple #7	209.41
Heater Thermocouple #8	183.31

Pipe Thermocouple #1	22.14
Pipe Thermocouple #2	22.30
Pipe Thermocouple #3	22.32
Pipe Thermocouple #4	22.34
Pipe Thermocouple #5	22.26
Pipe Thermocouple #6	22.24

Raw Data

Vacuum (1.65 torr) - - Off-Mode

Heater Power Input = 105.00 watts

Temperatures = °C

Heater Thermocouple #1	183.72
Heater Thermocouple #2	263.16
Heater Thermocouple #3	346.04
Heater Thermocouple #4	370.50
Heater Thermocouple #5	375.29
Heater Thermocouple #6	360.25
Heater Thermocouple #7	314.55
Heater Thermocouple #8	268.41

Pipe Thermocouple #1	23.12
Pipe Thermocouple #2	23.42
Pipe Thermocouple #3	23.50
Pipe Thermocouple #4	23.56
Pipe Thermocouple #5	23.50
Pipe Thermocouple #6	23.25

Raw Data

**Vacuum (1.65 torr) - - Off-Mode
Heater Power Input = 290.00 watts**

Temperatures = °C

Heater Thermocouple #1	321.70
Heater Thermocouple #2	452.72
Heater Thermocouple #3	551.56
Heater Thermocouple #4	571.14
Heater Thermocouple #5	575.17
Heater Thermocouple #6	555.26
Heater Thermocouple #7	485.77
Heater Thermocouple #8	387.59

Pipe Thermocouple #1	27.59
Pipe Thermocouple #2	28.41
Pipe Thermocouple #3	28.60
Pipe Thermocouple #4	28.85
Pipe Thermocouple #5	28.63
Pipe Thermocouple #6	27.92

**Water Thermal Switch
Vacuum (1.65 torr) - - Off-Mode
Reduced Data - - Figure 5.26**

Heater Power Input Watts	Heater Surface Flux kw/(m ²)	Heat Transfer Coefficient w/(m ² K)	Temp Diff between Heater Surface and Inside Surface of Stainless Steel Pipe Kelvin
0.00	0.00	0.00	0.00
57.20	1.46	6.54	222.65
105.00	2.74	7.99	342.88
290.00	7.90	14.77	534.90

Raw Data

Air (Pressure = 1 atm) - - Off-Mode

Heater Power Input = 57.20 watts

Temperatures = °C

Heater Thermocouple #1	85.22
Heater Thermocouple #2	125.01
Heater Thermocouple #3	167.51
Heater Thermocouple #4	180.88
Heater Thermocouple #5	184.09
Heater Thermocouple #6	177.81
Heater Thermocouple #7	157.88
Heater Thermocouple #8	138.47

Pipe Thermocouple #1	22.42
Pipe Thermocouple #2	22.64
Pipe Thermocouple #3	22.65
Pipe Thermocouple #4	22.81
Pipe Thermocouple #5	22.74
Pipe Thermocouple #6	22.58

Raw Data

Air (Pressure = 1 atm) - - Off-Mode

Heater Power Input = 105.00 watts

Temperatures = °C

Heater Thermocouple #1	132.53
Heater Thermocouple #2	197.66
Heater Thermocouple #3	261.74
Heater Thermocouple #4	279.72
Heater Thermocouple #5	283.91
Heater Thermocouple #6	274.31
Heater Thermocouple #7	242.89
Heater Thermocouple #8	208.66

Pipe Thermocouple #1	24.45
Pipe Thermocouple #2	24.92
Pipe Thermocouple #3	24.96
Pipe Thermocouple #4	25.24
Pipe Thermocouple #5	25.15
Pipe Thermocouple #6	24.77

Raw Data

Air (Pressure = 1 atm)- - Off-Mode

Heater Power Input = 290.00 watts

Temperatures = °C

Heater Thermocouple #1	251.64
Heater Thermocouple #2	377.08
Heater Thermocouple #3	475.18
Heater Thermocouple #4	494.27
Heater Thermocouple #5	498.67
Heater Thermocouple #6	481.77
Heater Thermocouple #7	420.67
Heater Thermocouple #8	334.12

Pipe Thermocouple #1	26.98
Pipe Thermocouple #2	27.99
Pipe Thermocouple #3	28.08
Pipe Thermocouple #4	28.50
Pipe Thermocouple #5	28.20
Pipe Thermocouple #6	27.66

**Table
Raw Data**

**Air (Pressure = 1 atm) - - Off-Mode
Heater Power Input = 382.80 watts**

Temperatures = °C

Heater Thermocouple #1	303.49
Heater Thermocouple #2	448.99
Heater Thermocouple #3	550.64
Heater Thermocouple #4	568.25
Heater Thermocouple #5	572.88
Heater Thermocouple #6	554.66
Heater Thermocouple #7	487.95
Heater Thermocouple #8	380.80

Pipe Thermocouple #1	33.26
Pipe Thermocouple #2	34.55
Pipe Thermocouple #3	34.42
Pipe Thermocouple #4	34.84
Pipe Thermocouple #5	34.52
Pipe Thermocouple #6	33.84

Water Thermal Switch

Air (1.0 atm) - -Off-Mode

Reduced Data- - -Figure 5.26

Heater Power Input Watts	Heater Surface Flux kw/(m ²)	Heat Transfer Coefficient w/(m ² K)	Temp Diff between Heater Surface and Inside Surface of Stainless Steel Pipe Kelvin
0.00	0.00	0.00	0.00
57.20	1.49	9.55	156.24
105.00	2.78	11.07	251.57
290.00	7.91	17.17	460.85
382.80	10.51	19.93	527.23

Water Thermal Switch On-Mode/Off-Mode Heat Transfer Coefficient Ratio

Reduced Data- - Figure 5.27

Temp Diff between Heater Surface and Inside Surface of Stainless Steel Pipe Kelvin	On-Mode Heat Transfer Coefficient w/(m ² K) 311.6 Grams of Water and Vacuum	Off-Mode Heat Transfer Coefficient w/(m ² K) Vacuum (1.65 torr)	On-Mode/Off-Mode Heat Transfer Coefficient Ratio
0.00	0.00	0.00	1.00
11.38	137.81	0.64	215.04
19.34	148.85	1.06	140.18
39.83	199.56	2.05	97.35
35.02	479.96	1.83	262.27
32.36	761.37	1.71	446.45
31.61	1046.09	1.67	626.47
35.90	1223.81	1.87	654.26
39.99	1311.99	2.06	637.85

Water Thermal Switch On-Mode/Off-Mode Heat Transfer Coefficient Ratio

Figure 5.28

Temp Diff between Heater Surface and Inside Surface of Stainless Steel Pipe Kelvin	On-Mode Heat Transfer Coefficient w/(m ² K) 311.6 Grams of Water and Vacuum	Off-Mode Heat Transfer Coefficient w/(m ² K) Air (1.0 atm)	On-Mode/Off-Mode Heat Transfer Coefficient Ratio
0.00	0.00	0.00	1.00
11.38	137.81	1.35	102.33
19.34	148.85	2.20	67.53
39.83	199.56	4.12	48.41
35.02	479.96	3.71	129.46
32.36	761.37	3.47	219.47
31.61	1046.09	3.40	307.61
35.90	1223.81	3.78	323.38
39.99	1311.99	4.14	317.26

Water Thermal Switch On-Mode/Off-Mode Heat Transfer Coefficient Ratio

Reduced Data - - Figure 5.27

Temp Diff between Heater Surface and Inside Surface of Stainless Steel Pipe Kelvin	On-Mode Heat Transfer Coefficient w/(m ² K) 311.6 Grams of Water and Air	Off-Mode Heat Transfer Coefficient w/(m ² K) Vacuum (1.65 torr)	On-Mode/Off-Mode Heat Transfer Coefficient Ratio
0.00	0.00	0.00	1.00
16.60	94.52	0.92	102.83
27.36	105.20	1.46	71.81
56.47	140.76	2.76	51.07
90.99	184.73	3.98	46.45
115.20	212.96	4.66	45.68
134.19	246.42	5.11	48.18
148.73	294.13	5.42	54.30
155.03	338.41	5.54	61.11

Water Thermal Switch On-Mode/Off-Mode Heat Transfer Coefficient Ratio

Reduced Data- - -Figure 5.28

Temp Diff between Heater Surface and Inside Surface of Stainless Steel Pipe Kelvin	On-Mode Heat Transfer Coefficient w/(m ² K) 311.6 Grams of Water and Air	Off-Mode Heat Transfer Coefficient w/(m ² K) Air (1.0 atm)	On-Mode/Off-Mode Heat Transfer Coefficient Ratio
0.00	0.00	0.00	1.00
16.60	94.52	1.92	49.33
27.36	105.20	3.00	35.03
56.47	140.76	5.40	26.05
90.99	184.73	7.41	24.91
115.20	212.96	8.41	25.32
134.19	246.42	9.01	27.35
148.73	294.13	9.38	31.35
155.03	338.41	9.53	35.52

Water Thermal Switch On-Mode/Off-Mode Heat Transfer Coefficient Ratio

Reduced Data - - Figure 5.27

Temp Diff between Heater Surface and Inside Surface of Stainless Steel Pipe Kelvin	On-Mode Heat Transfer Coefficient w/(m ² K) 628.1 Grams of Water and Vacuum	Off-Mode Heat Transfer Coefficient w/(m ² K) Vacuum (1.65 torr)	On-Mode/Off-Mode Heat Transfer Coefficient Ratio
0.00	0.00	0.00	1.00
6.09	257.55	0.35	738.63
10.32	278.83	0.58	478.13
22.31	356.31	1.21	293.60
35.49	476.40	1.85	257.26
46.13	528.84	2.33	227.27
43.88	753.60	2.23	338.03
42.38	1032.26	2.16	477.15
43.92	1185.52	2.23	531.38

Water Thermal Switch On-Mode/Off-Mode Heat Transfer Coefficient Ratio

Reduced Data - - Figure 5.28

Temp Diff between Heater Surface and Inside Surface of Stainless Steel Pipe Kelvin	On-Mode Heat Transfer Coefficient w/(m ² K) 628.1 Grams of Water and Vacuum	Off-Mode Heat Transfer Coefficient w/(m ² K) Air (1.0 atm)	On-Mode/Off-Mode Heat Transfer Coefficient Ratio
0.00	0.00	0.00	1.00
6.09	257.55	0.74	348.57
10.32	278.83	1.23	227.14
22.31	356.31	2.51	142.10
35.49	476.40	3.75	127.08
46.13	528.84	4.63	114.11
43.88	753.60	4.46	169.14
42.38	1032.26	4.33	238.20
43.92	1185.52	4.46	265.90

Water Thermal Switch On-Mode/Off-Mode Heat Transfer Coefficient Ratio

Reduced Data - - Figure 5.27

Temp Diff between Heater Surface and Inside Surface of Stainless Steel Pipe Kelvin	On-Mode Heat Transfer Coefficient w/(m ² K) 628.1 Grams of Water and Air (10 atm)	Off-Mode Heat Transfer Coefficient w/(m ² K) Vacuum (1.65 torr)	On-Mode/Off-Mode Heat Transfer Coefficient Ratio
0.00	0.00	0.00	1.00
6.29	249.42	0.36	693.22
10.69	269.32	0.60	446.61
23.96	331.77	1.30	255.90
40.36	416.51	2.07	200.88
51.08	477.62	2.54	188.32
61.35	538.99	2.95	182.82
69.28	631.42	3.25	194.53
78.25	667.43	3.56	187.35

Water Thermal Switch On-Mode/Off-Mode Heat Transfer Coefficient Ratio

Reduced Data - - Figure 5.28

Temp Diff between Heater Surface and Inside Surface of Stainless Steel Pipe Kelvin	On-Mode Heat Transfer Coefficient w/(m ² K) 628.1 Grams of Water and Air (10 atm)	Off-Mode Heat Transfer Coefficient w/(m ² K) Air (1.0 atm)	On-Mode/Off-Mode Heat Transfer Coefficient Ratio
0.00	0.00	0.00	1.00
6.29	249.42	0.76	327.25
10.69	269.32	1.27	212.28
23.96	331.77	2.67	124.17
40.36	416.51	4.17	99.97
51.08	477.62	5.01	95.27
61.35	538.99	5.74	93.93
69.28	631.42	6.24	101.12
78.25	667.43	6.76	98.67